PB94-193745

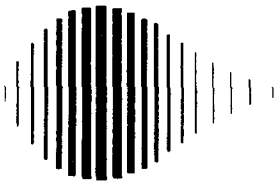

NATIONAL CENTER FOR EARTHQUAKE
ENGINEERING RESEARCH
State University of New York at Buffalo

Seismic Isolation of Multi-Story Frame Structures Using Spherical Sliding Isolation Systems

by

T.M. Al-Hussaini, V.A. Zayas and M.C. Constantinou
State University of New York at Buffalo
Department of Civil Engineering
Buffalo, New York 14260

Technical Report NCEER-94-0007

March 17, 1994

This research was conducted at the State University of New York at Buffalo and was partially supported by the National Science Foundation under Grant No. BCS 90-25010 and the New York State Science and Technology Foundation under Grant No. NEC-91029.

NOTICE

This report was prepared by the State University of New York at Buffalo as a result of research sponsored by the National Center for Earthquake Engineering Research (NCEER) through grants from the National Science Foundation, the New York State Science and Technology Foundation, and other sponsors. Neither NCEER, associates of NCEER, its sponsors, the State University of New York at Buffalo, nor any person acting on their behalf:

a. makes any warranty, express or implied, with respect to the use of any information, apparatus, method, or process disclosed in this report or that such use may not infringe upon privately owned rights; or

b. assumes any liabilities of whatsoever kind with respect to the use of, or the damage resulting from the use of, any information, apparatus, method or process disclosed in this report.

Any opinions, findings, and conclusions or recommendations expressed in this publication are those of the author(s) and do not necessarily reflect the views of NCEER, the National Science Foundation, the New York State Science and Technology Foundation, or other sponsors.

PB94-193745

Seismic Isolation of Multi-Story Frame Structures Using Spherical Sliding Isolation Systems

by

T.M. Al-Hussaini[1], V.A. Zayas[1] and M.C. Constantinou[2]

March 17, 1994

Technical Report NCEER-94-0007

NCEER Task Number 90-2101

NSF Master Contract Number BCS 90-25010

NYSSTF Grant Number NEC-91029
and
NSF Grant Number ISI-8921115

1 Engineer, Earthquake Protection Systems, Inc.
2 Associate Professor, Department of Civil Engineering, State University of New York at Buffalo

NATIONAL CENTER FOR EARTHQUAKE ENGINEERING RESEARCH
State University of New York at Buffalo
Red Jacket Quadrangle, Buffalo, NY 14261

PREFACE

The National Center for Earthquake Engineering Research (NCEER) was established to expand and disseminate knowledge about earthquakes, improve earthquake-resistant design, and implement seismic hazard mitigation procedures to minimize loss of lives and property. The emphasis is on structures in the eastern and central United States and lifelines throughout the country that are found in zones of low, moderate, and high seismicity.

NCEER's research and implementation plan in years six through ten (1991-1996) comprises four interlocked elements, as shown in the figure below. Element I, Basic Research, is carried out to support projects in the Applied Research area. Element II, Applied Research, is the major focus of work for years six through ten. Element III, Demonstration Projects, have been planned to support Applied Research projects, and will be either case studies or regional studies. Element IV, Implementation, will result from activity in the four Applied Research projects, and from Demonstration Projects.

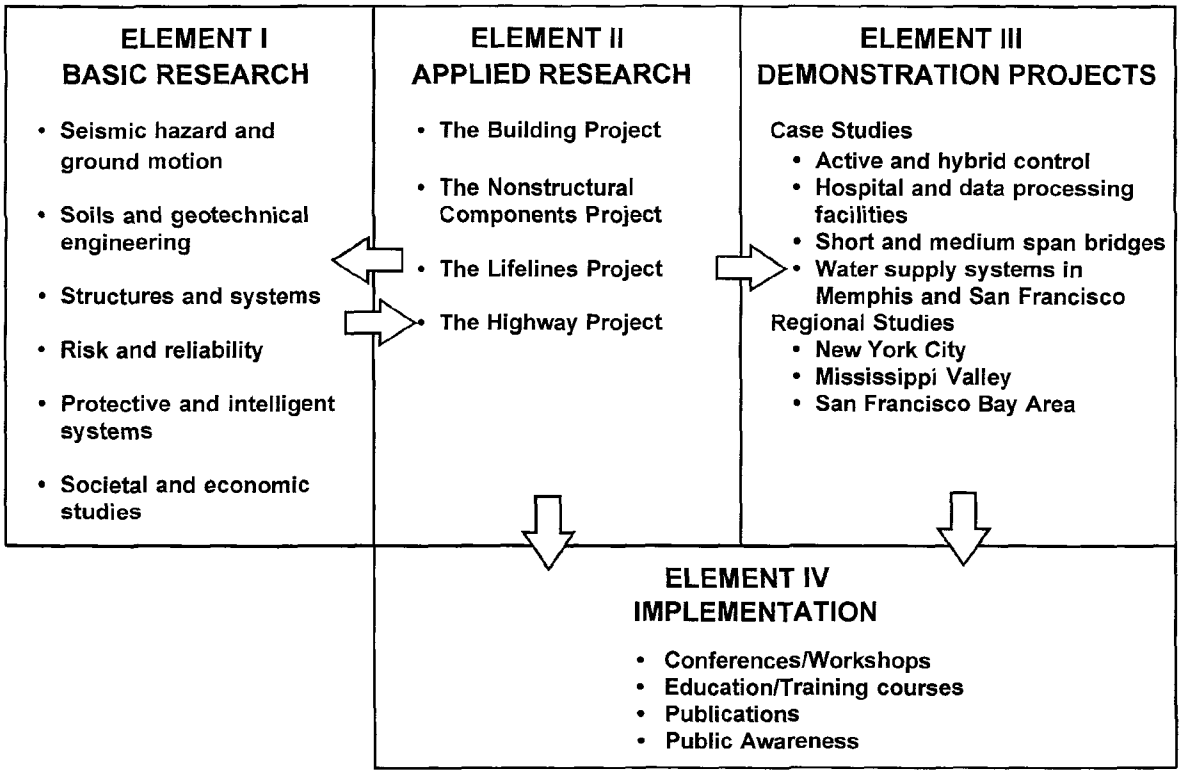

Research in the **Building Project** focuses on the evaluation and retrofit of buildings in regions of moderate seismicity. Emphasis is on lightly reinforced concrete buildings, steel semi-rigid frames, and masonry walls or infills. The research involves small- and medium-scale shake table tests and full-scale component tests at several institutions. In a parallel effort, analytical models and computer programs are being developed to aid in the prediction of the response of these buildings to various types of ground motion.

Two of the short-term products of the **Building Project** will be a monograph on the evaluation of lightly reinforced concrete buildings and a state-of-the-art report on unreinforced masonry.

The **protective and intelligent systems program** constitutes one of the important areas of research in the **Building Project**. Current tasks include the following:

1. Evaluate the performance of full-scale active bracing and active mass dampers already in place in terms of performance, power requirements, maintenance, reliability and cost.
2. Compare passive and active control strategies in terms of structural type, degree of effectiveness, cost and long-term reliability.
3. Perform fundamental studies of hybrid control.
4. Develop and test hybrid control systems.

This report documents experimental and analytical results pertaining to the application of a spherical sliding isolation system to multi-story frame structures. As a collaborative effort between NCEER and Earthquake Protective Systems, Inc., shaking table tests were carried out on two building frames with a variety of isolator installation configurations. Analytical models were developed which accurately predict the response of the isolation system and structural response characteristics. Results show that the isolation system provides the desired reductions in story shears and story drifts.

ABSTRACT

Experimental and analytical results are presented from shake table tests conducted on six and seven story framed building models. The models are seismically isolated using a spherical sliding isolation system, known as Friction Pendulum System (FPS). The models include moment and braced frames, with different isolator installation configurations, including isolators installed directly at the bases of the first story columns, and isolators installed below a rigid diaphragm base. In all cases, the isolators reduce structure shear forces and inter story drifts in the multi-story building models by factors of 4 to 6, allowing the upper structural system to remain elastic during severe earthquake loadings.

The installation of the isolators at the bases of the individual first story columns, as compared to beneath a rigid diaphragm base, does not significantly affect the behavior of the isolation system. The articulated joint of the Friction Pendulum isolators accommodates the required joint rotations with no affect on the isolator properties. Relative differences in displacements which occur in the isolators have no measurable effect on the overall response of the isolation system or upper story response. Local variation of vertical loads on the isolators does not have any measurable effect on the overall response of the isolation system or the upper structure story shears and drifts. Local uplift of individual isolators within the structural frame does not have any measurable effect on the overall response of the isolation system or the upper structure story shears and drifts. The use of displacement restraints, or displacement limits, were observed to be an effective means to limit isolator displacements, and insure isolator stability, in the event of extreme seismic events significantly exceeding the design event.

The shear stiffness of the framing in the isolation story affects the upper story shears and drifts. Analytical models which include the flexibility of the framing in the isolation story accurately predict the response of the isolation system and upper structure shears and drifts. The response of the first three modes of the upper structure fully accounts for the response of the experimentally observed structure shears and drifts, with differences of typically less than 1% as compared to the experimental results. Consistent results are achieved in the isolation system response throughout the test program which included over 60 seismic tests.

ACKNOWLEDGMENTS

This research was conducted as a collaborative effort between Earthquake Protection Systems, Inc. with funding by the National Science Foundation, Grant No. ISI-8921115 and the Department of Civil Engineering , State University of New York at Buffalo with funding by the National Center for Earthquake Engineering Research, Contract No. 902101. The support of the National Science Foundation and the National Center For Earthquake Engineering Research which encourage collaborative industry and university research, is greatly appreciated. The opinions, findings, conclusions and recommendations expressed in this report, however, are those of the authors and do not necessarily reflect the views of the National Science Foundation or the National Center for Earthquake Engineering Research.

The expert assistance of Stanley Low (Earthquake Protection Systems, San Francisco, CA), Alloua Kartoum (Imbsen & Associates, Sacramento, CA) and Mark Pitman (National Center for Earthquake Engineering Research, Buffalo, NY) during the design, assembly and testing of the experimental models is very much appreciated.

TABLE OF CONTENTS

TABLE OF CONTENTS (cont'd)

LIST OF FIGURES

LIST OF FIGURES (Cont'd)

LIST OF FIGURES (Cont'd)

LIST OF FIGURES (Cont'd)

LIST OF FIGURES (Cont'd)

LIST OF FIGURES (Cont'd)

LIST OF FIGURES (Cont'd)

LIST OF FIGURES (Cont'd)

LIST OF TABLES

SECTION 1

INTRODUCTION

1.1 Research Program

The research reported herein contains technical information on the application of sliding isolators that use spherical surfaces in multi-story framed buildings for protection against earthquake ground shaking. For the purpose of this research the Friction Pendulum System (FPS) was selected as an example of spherical sliding isolation system. Shake table tests of 6 and 7-story quarter scale building models were conducted at the National Center for Earthquake Engineering Research, at the State University of New York at Buffalo. This research was part of an extensive series of test programs launched with the following objectives: to establish experimentally the effectiveness of the FPS isolators to a wide range of earthquake loading conditions and superstructure types; and to develop analytical models that can accurately predict the response of base-isolated structures using the FPS system. Experimental results have demonstrated a high degree of consistency in the behavior of the FPS isolators throughout the test programs and have been a strong basis for the practical application of these isolators in real structures.

1.2 Overview of Seismic Isolation

Seismic isolation is based on the principle of uncoupling a building (or other structure) from the damaging effects of ground motion by providing additional flexibility and energy dissipation capability through the addition of specially designed isolators between the foundation and the superstructure. The lateral flexibility of the isolators shift the natural period of the isolated structure beyond the predominant periods of earthquakes and thus reduces the inertia forces on the structure. The energy dissipation capacity or damping in the isolators restrict the displacement at the isolator level within desirable limits.

The practical application of the seismic isolation concept became a reality only recently. The first isolated building in the United States was constructed in 1985. Seismic isolators in use at the current time may be grouped into two groups: (i) elastomeric isolation systems and (ii) sliding isolation systems. The Friction Pendulum isolator is a sliding isolation system (Zayas et al., 1987), where the weight of the structure is supported on spherical sliding interfaces (usually steel-teflon type interfaces), that slide relative to each other when the ground motion exceeds a certain threshold level. Energy dissipation is achieved by friction during sliding motion.

Recentering of the isolator to its original position takes place through gravitational action by sliding along the spherical interface.

1.3 Experimental Work on FPS Isolators

With the objective of verifying the suitability of the Friction Pendulum Isolator for various practical applications, an extensive series of test programs have been carried out since 1986. Tests have been carried out at both the Earthquake Engineering Research Center (EERC), University of California at Berkeley and the National Center for Earthquake Engineering Research (NCEER), State University of New York at Buffalo. Testing objectives have included investigating the individual FPS isolator response as well as earthquake simulation tests on the shake table for structures supported on FPS isolators. The following is a brief description of each test performed so far:

1986 Compression-Shear Testing of Model Isolators at EERC (Zayas et al., 1987)
This was the inaugural testing on the FPS isolator, after the isolator had been patented by its inventor. A series of tests were carried out to verify the predicted FPS isolator properties. Compression-shear tests were performed on quarter-scale FPS bearings having a natural period of one second.

1986 Shake Table Test of 2-Story Steel Frame at EERC (Zayas et al., 1987)
With the isolator properties established from earlier tests, shake table tests were performed with the objective of investigating the behavior and response of FPS-isolated frame structure exhibiting a wide range of stiffness and plan eccentricities. A two-story steel frame test structure was tested which modeled full size buildings with natural periods ranging from 0.3 to 3.0 seconds. Torsional eccentricities of up to 45%, and mass variations of up to 100%, were tested by varying mass amounts, mass locations and column stiffness. Quantifiable and predictable bearing behavior was reported in addition to significant reductions in superstructure shears, deformations as well as torsional uncoupling.

1989 Compression-Shear Test of Model Isolators at EERC (Zayas et al., 1989)
The purpose of these tests was to verify the performance and properties of bearings constructed to deliver low dynamic friction coefficients at high velocities. Model FPS bearings were subjected to compression-shear testing with velocities of up to 20 inches per second. Coefficients of dynamic friction below 0.05 were reported over the entire velocity range for typical bearing pressures.

1989 Shake Table Test of 6-Story Steel Frame at NCEER (Mokha et al., 1990, 1991)

The purpose of the second series of shake table tests was to investigate the behavior and response of FPS isolators within a realistic multi-story structural model having a large overturning aspect ratio. A quarter scale six-story steel moment frame model was tested on FPS isolators installed below a rigid-base diaphragm. Two different FPS isolators were used in the structure that gave two different friction values of 0.075 and 0.095. Under moderate to severe level ground motions, no uplift of the bearings occurred despite the model's large overturning aspect ratio, and residual post-earthquake bearing deformations were negligible. It was also reported that the isolated structure could sustain, while elastic, a peak ground acceleration of six to eight times larger than that it could sustain under fixed-base conditions.

1990 Compression-Shear Test of Full-Size Isolators at EERC (Zayas and Low, 1991)

These bearing tests represented the first compression-shear testing of full-sized FPS isolators prior to their practical installation. The bearings were two second period prototype isolators which were eventually used in the seismic retrofitting of a four story apartment frame building in San Francisco, damaged by the 1989 Loma Prieta Earthquake. Isolators were installed at the base of columns at ground level. It was reported that for the Design Earthquake, the isolators would reduce the drift in the superstructure by 90%, and the ductility demand by 80%.

1990 Shake Table Test of Rigid Slab Bridge at NCEER (Constantinou and Kartoum, 1993)

The purpose of this series of shake table tests was to investigate the response of FPS isolators on a stiffer class of superstructure, that is a rigid slab bridge. Quarter scale model bearings having a natural period of one second were used.

1991 Shake Table Test of 7-Story Steel Frame at NCEER (this report)

Shake table tests were performed on a quarter scale seven story steel frame with various braced and unbraced configurations. Instead of having a rigid base above the FPS isolators, the isolators were placed directly at the base of individual columns. The FPS isolators used had a friction value of 0.06. The focus of this report is on this test program.

1992 Shake Table Test of Highway Bridge on Flexible Piers at NCEER (Constantinou et al., 1993)

As part of the NCEER-Taisei Corporation collaborative research program, this series of shake table tests investigated the response of FPS isolators on a highway bridge mode which included

pier flexibility. The model bearings were located between the top of the pier and the bridge deck.

1992 Shake Table Test of Unreinforced Masonry Infill Panel Structures Using Full Size Isolators at EERC (Piepenbrock et al., 1993)

Shake table tests on unreinforced masonry infill panel structures, isolated by full size FPS bearings were conducted. Two types of masonry infill panels were used: unreinforced brick masonry, which typified mid to high-rise constructions before 1930, and granite masonry representative of historic buildings constructed earlier. The main purpose of this research was to perform a comparative investigation of the isolated and non-isolated (fixed-base) response of non-ductile, drift-sensitive structures. Among other important goals were to test for the first time the effectiveness of full size FPS bearings on the shake table and to evaluate the torsional response of a highly eccentric superstructure.

1993 Compression-Shear Test of Full-Size Isolators at EERC (Zayas et al., 1993)

These bearing tests represent an extensive testing program for prototype bearings to be used for the seismic isolation of the U.S. Court of Appeals Building in San Francisco. Full size FPS isolators having a period of 2.75 secs were subjected to a comprehensive matrix of compression-shear tests in a specially designed test machine. Compression loading varying from 44 kips to 1275 kips have been used. The effects of sliding velocities varying from 0.1 inch/sec to 20 inch/sec on full size FPS isolators have also been studied.

1.4 Practical Applications of FPS Isolators in Multi-Story Buildings

Thirty two FPS isolators were used in the seismic retrofitting of a four story apartment building in San Francisco shown in figure 1-1. This building is the first building in San Francisco and Northern California to be seismically isolated. The original building was severely damaged during the 1989 Loma Prieta Earthquake, which caused a lateral lean and structural drift of approximately two feet at the garage level. A new steel moment frame was erected to accommodate the garage space, which supported the three stories of wooden frame apartment above. The isolators were placed at the bases of steel columns, in between the column base plates and the foundation as shown in figure 1-2. It may be noted that the isolation system lacks a rigid basemat above the isolators. Dynamic analyses (Zayas and Low, 1991) showed that for the design earthquake, the isolators reduced the ductility demand in the upper structure from 38.4 for the non-isolated building to 1.0 for the isolated building. The cost of the isolators and seismic gap details was approximately 10% of the total repair costs.

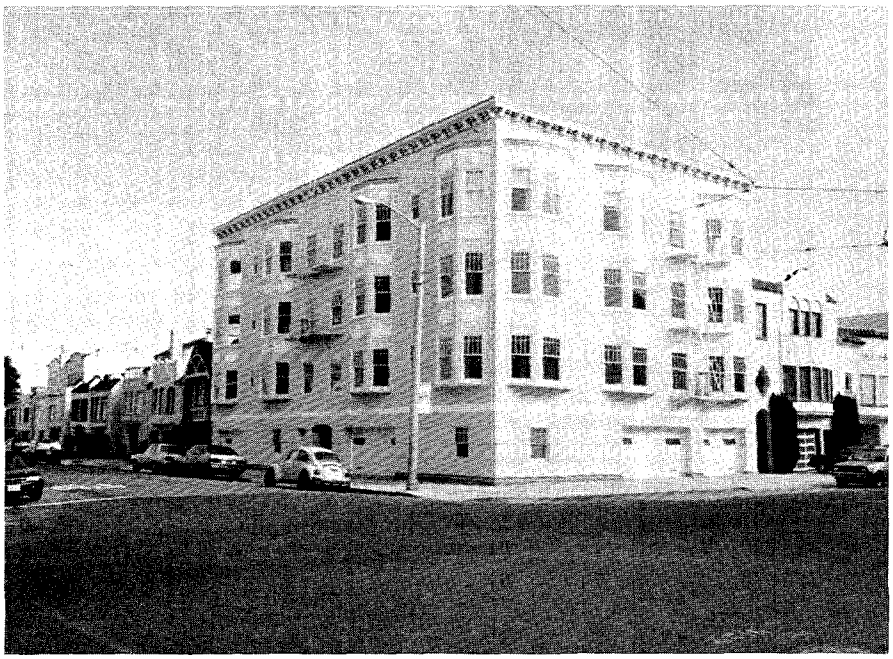

FIGURE 1-1 Hawley Apartments, San Francisco (32 FPS Isolators)

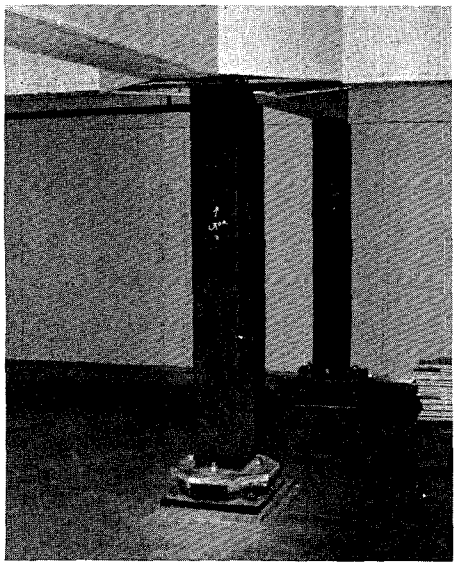

FIGURE 1-2 FPS Isolators Installed at Column Base, Hawley Apartments.

The U.S. Court of Appeals in San Francisco is an application of FPS isolators in a large government building. Figure 1-3 shows this historic building with its exquisite exterior decorations. The seismic upgrade of the 350,000 square feet U.S. Court of Appeals building includes the installation of 256 FPS isolators. To date this is the largest building in the U.S. to be seismically isolated. The building is a five story, 80 feet tall structure with a steel frame which supports unreinforced granite and brick masonry panel walls. Analysis (Amin et al., 1992) showed that use of the FPS isolators cause reductions in the peak structure shear and peak interstory drift by factors of 4.5 and 6.2 respectively for a 475-year event return period earthquake. Isolators will be installed at the base of existing steel columns with a new concrete jacket and shoring beam (used for supporting column load while the column is cut) cast around the column as shown in figure 1-4. This arrangement is equivalent to having a rigid base just above the isolation system. The seismic isolation scheme achieves the life-safety criteria, and simultaneously protects the ornate architectural finishes in the event of a severe earthquake.

1.5 Scope of Current Study

This report contains experimental and analytical studies on seismic isolation of multi-story frame buildings using the Friction Pendulum System. Most of the work presented herein is related to the shake table testing of a series of 7-story frames at NCEER. Figure 1-5 is a photograph of one of the 7-story test structures on the shake table. This test structure is a quarter scale model which represents a section in the weak direction of a typical steel frame building. FPS isolators are installed at the base of individual columns. Figure 1-6 shows a close-up-view of the FPS isolator installation at the column base. This test program was an extension of the 1989 test program (Mokha et al., 1990) on a 6-story moment frame, supported on rigid beams with four FPS isolators below the rigid beams. Figure 1-7 presents a schematic sketch of the 6-story test structure with three bays.

The 7-story frame was formed by removing the rigid base of the 6-story moment frame, and adding an additional story of beams and columns in its place with FPS isolators at the column bases. The objective of the two test programs were to study the effectiveness of FPS isolators on multi-story frame structures with different structural configurations having large overturning effects. The bottom story of the seven story test structure with the isolators at the column bases is defined as the "isolation system" or "isolation story". Braces were added to achieve four different structural configurations:

FIGURE 1-3 U.S. Court of Appeals, San Francisco (256 FPS Isolators)

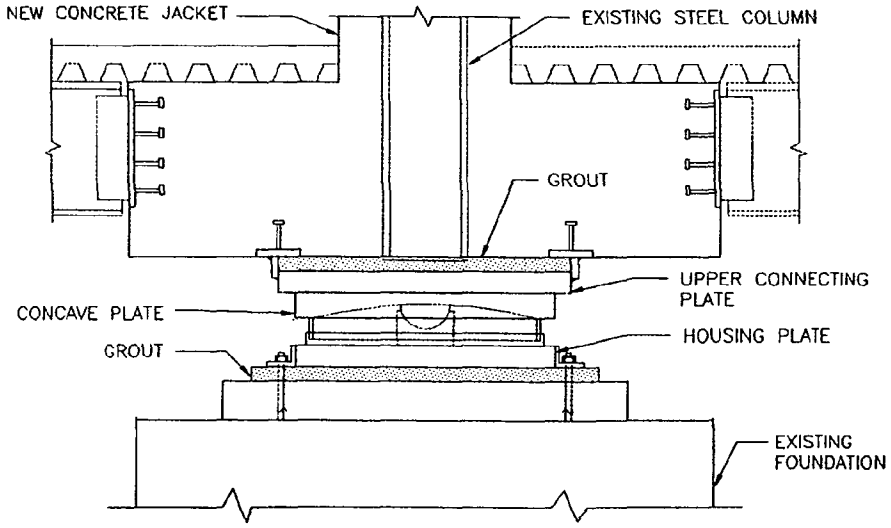

FIGURE 1-4 Isolator Installation Details, U.S. Court of Appeals

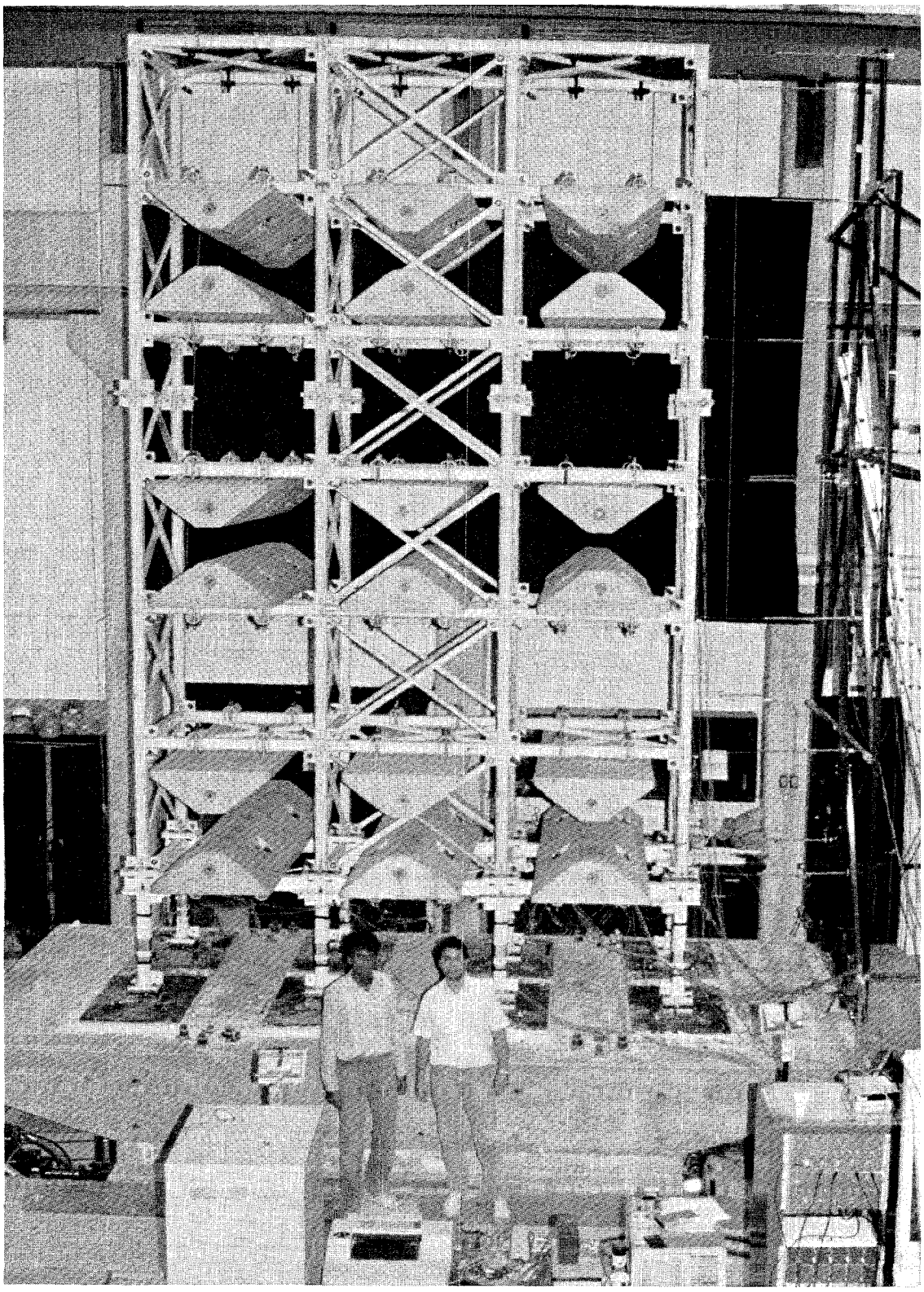

FIGURE 1-5 Photograph of 7-Story Test Frame on Shake Table

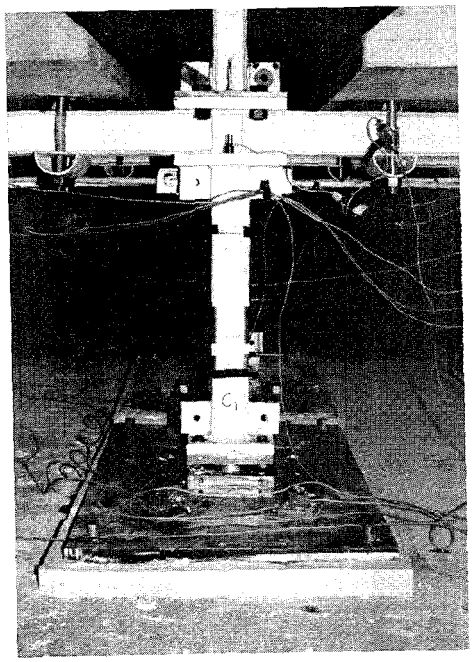

FIGURE 1-6 Close-up View of Isolator Installed at Column Base of 7 Story Frame

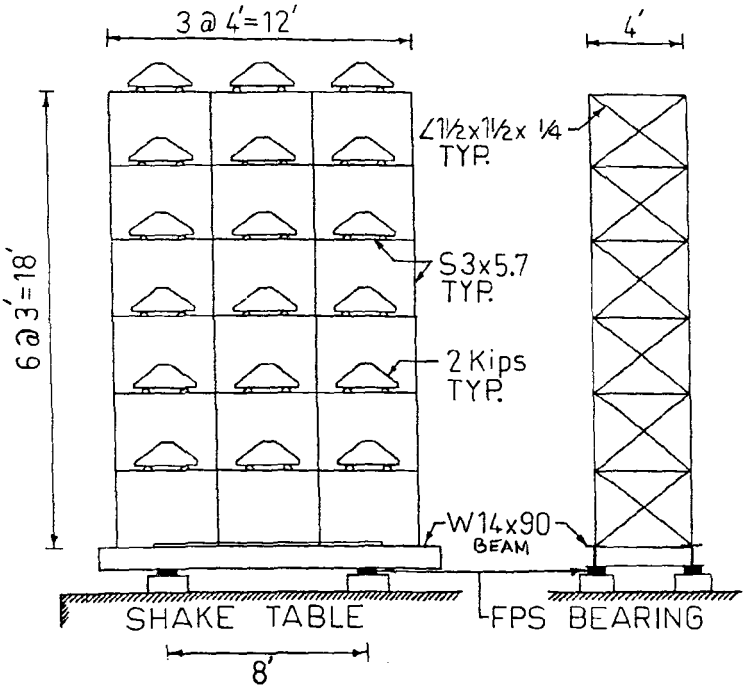

FIGURE 1-7 Schematic Diagram of Six Story Test Frame (after Mokha et al., 1990)

(i) Moment frame with unbraced isolation system (MFUIS)
(ii) Moment frame with braced isolation system, including bracing the column bases (MFBIS)
(iii) Braced frame (braces added in center bay only) with unbraced isolation system (BFUIS)
(iv) Braced frame with braced isolation system (BFBIS).

Figure 1-8 shows schematic diagrams of the four structure configurations. Tests were also conducted on non-isolated (fixed-base) moment frame (MFF) by locking the FPS bearings for comparison with the isolated moment frame (MFUIS). Several moderate and severe ground motions, representing a variety of site conditions were used. Comparison was also done with respect to the experimental results (Mokha et al., 1990) from the 6-story frame test to study the influence of installing the FPS isolators below a rigid base in contrast to installing the isolators directly at the base of individual columns.

An analytical model, involving a rigorous mathematical solution method, has been developed to predict the earthquake response of the 7-story test structure. In addition, dynamic analysis software for three-dimensional base isolated structures such as 3D-BASIS (Nagarajaiah et al., 1989), currently in use by seismic isolation consultants, has also been used for comparison with experimental results. Comparisons with isolator response and superstructure response is presented to validate the analytical procedures for multi-story frame structures. Experimental structure responses have been investigated in detail. Modal decomposition of the structure response is done to quantify the contributions from the different structure modes to the observed structure response.

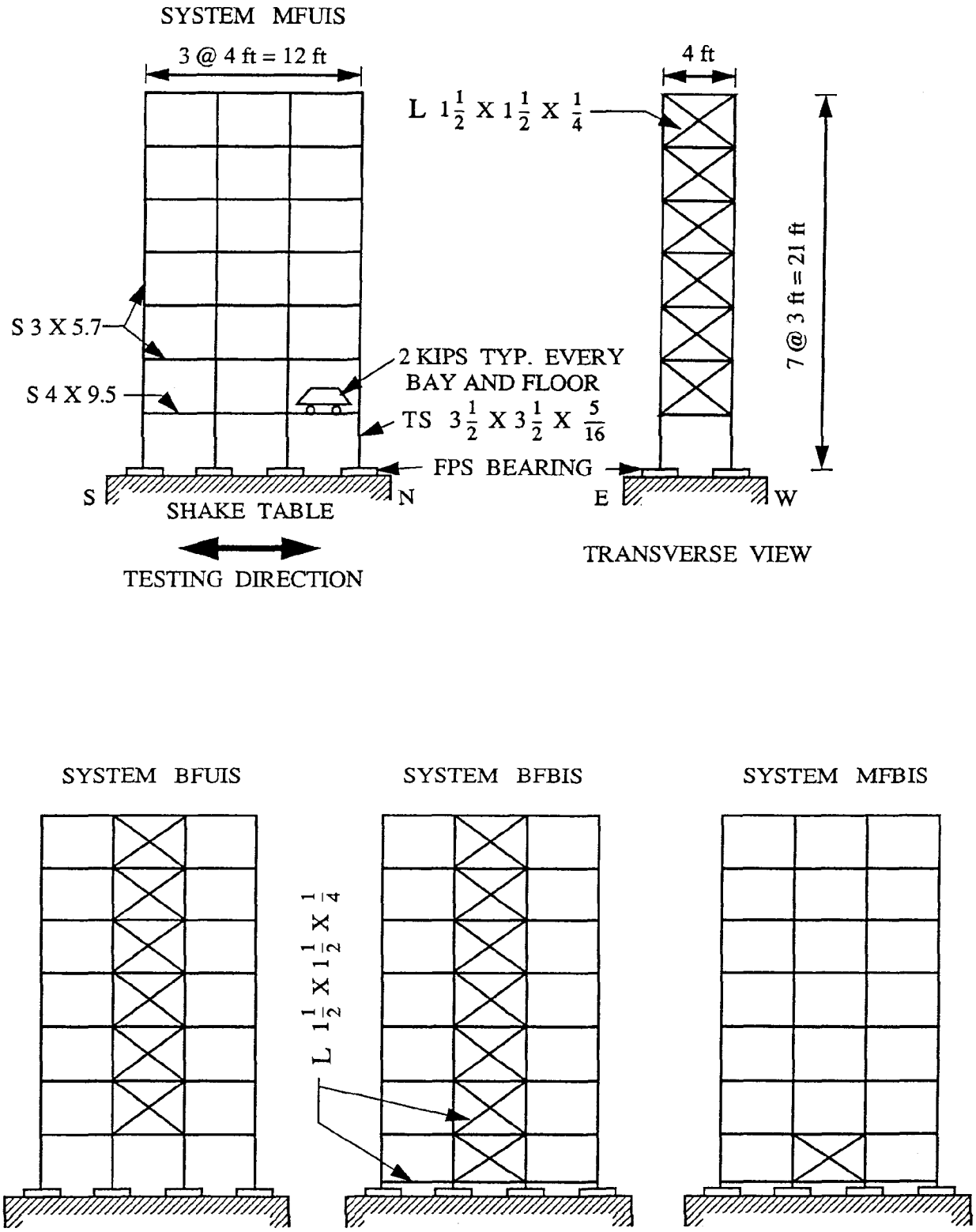

FIGURE 1-8 Schematic Diagram of Different Structural Configurations of Seven Story Test Frame

SECTION 2

RESPONSE OF ISOLATION SYSTEM

2.1 Description of Isolation System

Friction Pendulum (FPS) Isolators are steel bearings. The FPS isolator has two parts, one part containing an articulated slider, the other part with a concave sliding surface. Figure 2-1 shows a photograph of the isolator, while figure 2-2 shows the two components separated. The side of the stainless steel slider in contact with the concave surface is faced with a high load capacity, low friction bearing material composite. The spherical cavity housing the articulated slider is also surfaced with the low friction bearing material. The concave sliding surface is stainless steel. As the slider slides over the concave spherical surface, causing the supported mass to rise, the gravitational force component parallel to the surface acts as the restoring force. This restoring force provides the stiffness of the FPS isolator during sliding motion. The friction force between the slider bearing material and the concave surface determines the friction damping of the isolator.

The seismic isolation system below the 7-story test structure consisted of eight FPS isolators installed at the base of eight columns, as depicted in figure 1-8. The bearings were installed with the concave surface facing down. The height to width aspect ratio of the structure was 2.0. Large overturning moment effects were induced on the FPS bearings, under strong lateral shaking. For some severe motions, the fluctuations in the vertical bearing loads caused by the overturning moments were large enough to reduce the bearing load to zero, and cause local bearing uplifts.

The FPS isolator used in the test had a period of 1 second, simulating a prototype isolator of 2 seconds period. Figure 2-3 shows a section of the FPS isolator. The size of the bearing is 8 inches square and 3 inches high. The radius of curvature of the concave surface is 9.75 inches. The isolator is designed to provide a maximum allowable bearing displacement of 2 inches. If the earthquake demands require a larger bearing displacement, the housing column containing the slider is engaged by the circular retainer ring of the isolator.

2.2 Non-linear Model for Isolation System

The shear force mobilized at each FPS isolator during sliding motion is given by

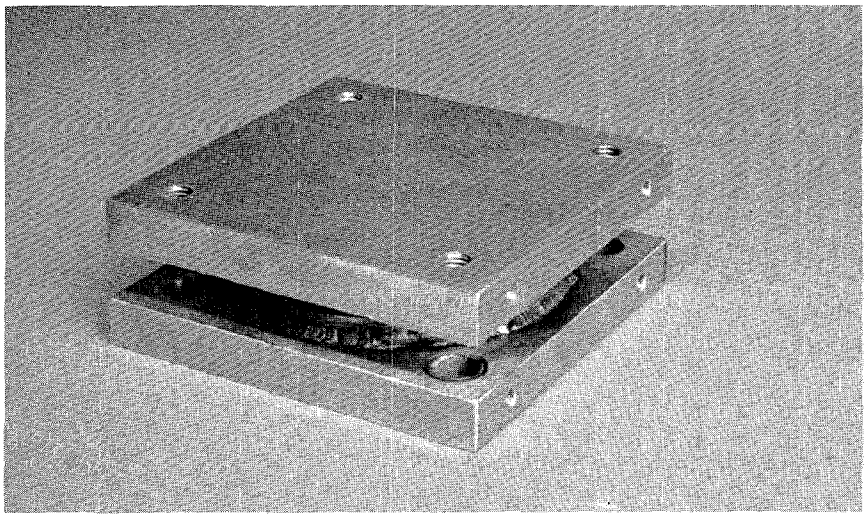

FIGURE 2-1 Photograph of Friction Pendulum Bearing

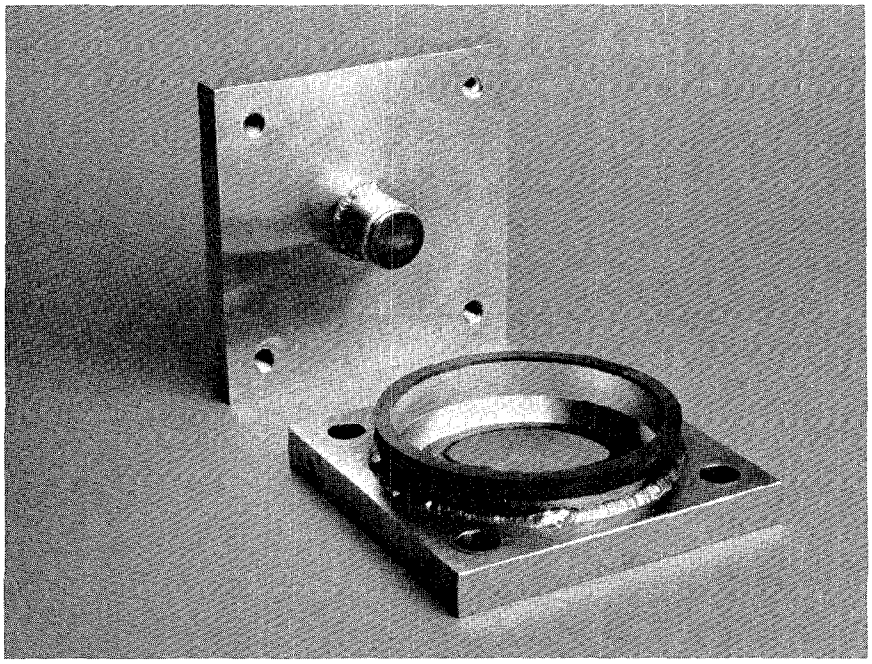

FIGURE 2-2 Internal Components of Friction Pendulum Bearing

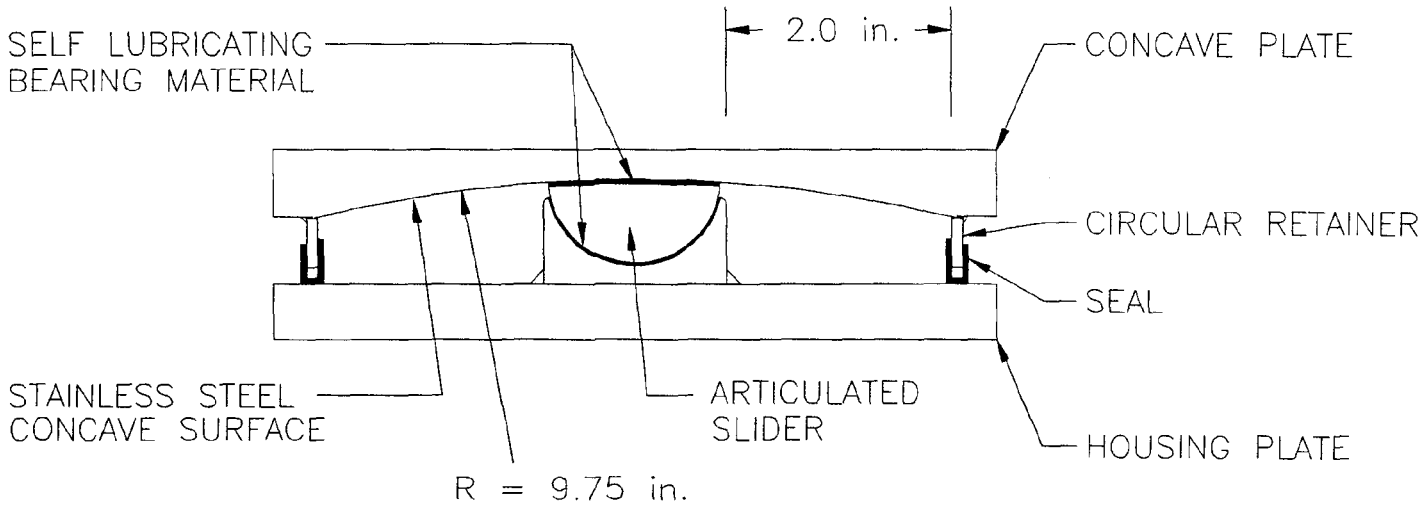

FIGURE 2-3 Cross-Sectional View of the Model FPS Isolator

$$F_i = \left(\frac{W_i}{R}\right)U + \mu W_i sgn(\dot{U}) \tag{2.1}$$

where, W_i is the vertical load on the *ith* bearing, R is the radius of curvature, μ is the coefficient of sliding friction and U is the bearing displacement. Dot represents differentiation with respect to time and the index i represents the *ith* FPS bearing.

The first term in equation (2.1) is the isolator restoring force, discussed in the previous section. The stiffness W_i/R determines the slope of the force-displacement relationship during sliding motion. This corresponds to an isolator period of

$$T = 2\pi\sqrt{(R/g)}. \tag{2.2}$$

The isolator period is in fact the period of a pendulum of length R with small angular displacements, indicating that the fundamental concept of the system is based on the principles of pendulum motion. It should be noted that the isolator period is independent of the mass of the supported structure. This facilitates practical applications and any desired period can be obtained by simply varying the radius of curvature. The second term in equation (2.1) is the friction force between the slider and sliding surface. The coefficient of friction μ is a function of the sliding velocity $\dot{U}$ and bearing pressure P. The friction-velocity relationship, as determined by Constantinou et al. (1990) is given by

$$\mu = f_{\max} - (f_{\max} - f_{\min})\exp\left(-a|\dot{U}|\right) \tag{2.3}$$

where f_{max} and f_{min} are the maximum and minimum mobilized friction coefficients respectively and 'a' is a parameter which controls the variation of friction with velocity. The friction increases swiftly from f_{min} to f_{max} in the low velocity range (usually within 2 inch/sec) and thereafter remains constant at higher velocities. The friction coefficient decreases with increasing pressure and stabilizes at pressures greater than about 20 ksi.

The isolation system response for the 7-story test structure is represented by the base shear force versus isolation system displacement plot. The base shear is the total shear force developed above the bearing level in the isolation system. The base shear is normalized with respect to the total structure weight to portray a coefficient that is somewhat representative of

the effective horizontal acceleration (in g's) of the test structure. The isolation system displacement is the horizontal displacement of the 1st floor with respect to the table.

Figure 2-4 shows a typical isolation system response plot from the shake table test of the 7-story moment frame (MFUIS). It represents the overall hysteretic (energy dissipation) behavior of the entire isolation system during a particular earthquake. "Yielding", which in this case is sliding, starts when the shear force exceeds the friction coefficient times the weight. Once the bearing starts sliding, the shear force increases as the bearing slides up the concave surface and vice-versa. The steep part of the force-displacement curve that represents pre-yielding movement corresponds to the stiffness of the columns in the isolation story. The flexibility of all eight columns in the isolation story determines the slope of this part, which was found to be about 95 kip/inch, the total weight ($W = \sum_{i=1}^{8} W_i$) of the structure being 47.5 kips. The slant part represents the isolation system stiffness and is found to be very close to the combined theoretical stiffness (W/R=47.5/9.75=4.87 kip/inch) of all the FPS isolators. To be exact, the theoretical stiffness should be the combined stiffness of the eight FPS isolators and the isolation story columns, acting in series. However, the contribution of column flexibility to the slope of this part is relatively small and may be disregarded.

The energy dissipation occurring in the isolators during the shake table motion is represented by the area enclosed by the hysteresis loops. The hysteresis loop is ideally a parallelogram. Half the vertical thickness of the parallelogram should be equal to the "yield" or friction force μW, where μ is the coefficient of friction. Accordingly, the effective friction coefficient may be stated to be equal to the area of the loop divided by $2DW$, where D is the length parameter shown in figure 2-4. The friction coefficient based on the largest hysteresis loop of figure 2-4 is 0.06. It should be noted that this value is actually equal to the parameter f_{max} in the model of equation (2.2) when considering the contribution from all eight bearings. The average pressure on the eight bearings was about 18 ksi.

2.3 Experimental Results

2.3.1 Test Program

The four structural configurations of the 7-story frame have already been discussed in section 1.4 and graphically presented in figure 1-8. Necessary floor loads have been simulated by adding 6 kips of concrete blocks (2 kips each bay) at each floor level. Assuming that the mass

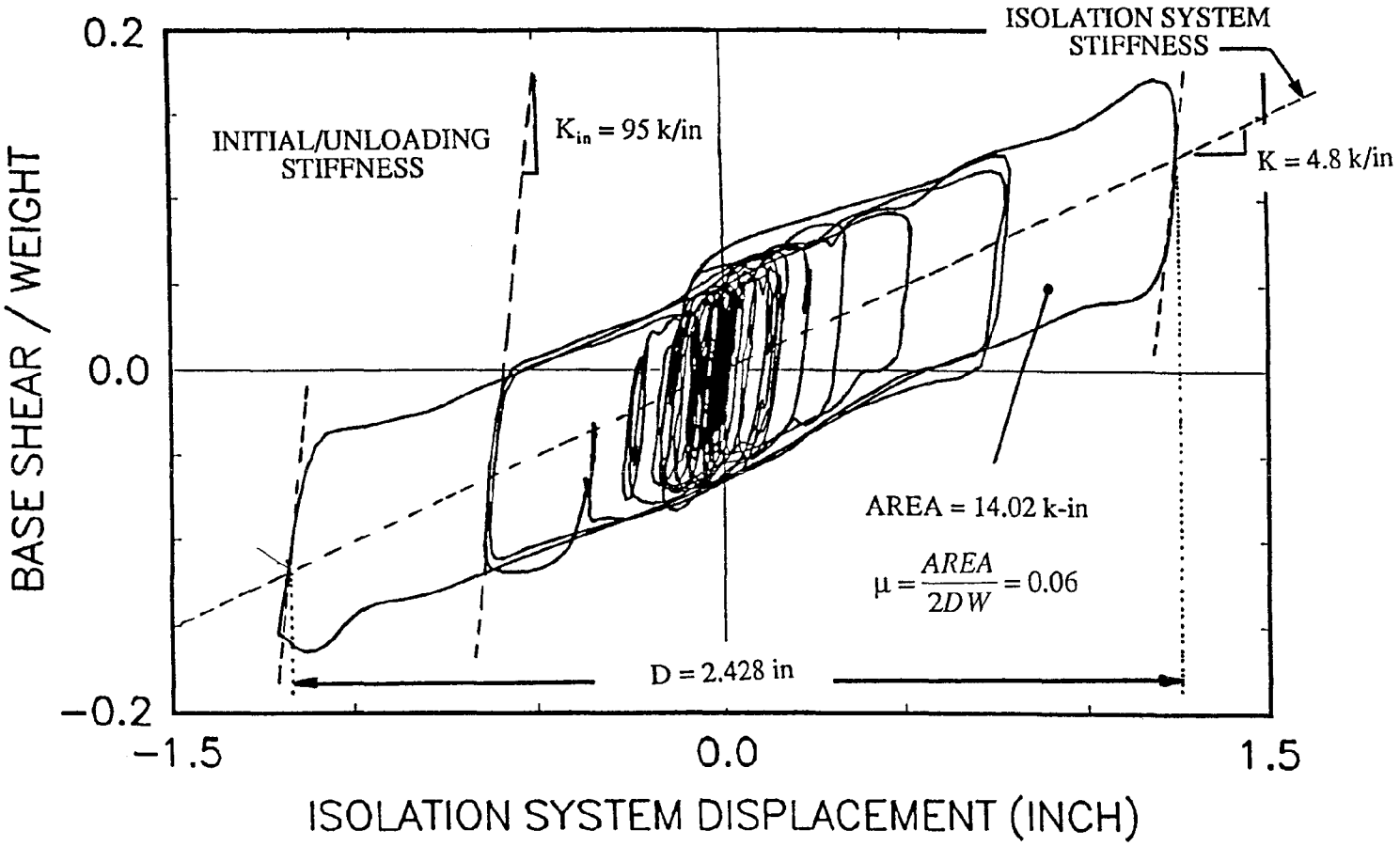

FIGURE 2-4 Isolation System Response Showing Pre-yielding and Post-yielding Stiffness, and Effective Friction

of the model structure can be concentrated at the different floor levels, the following lumped mass distribution is achieved: 6.4 kips in 7th floor, 6.7 kips each in 2nd to 6th floors and 7.6 kips in the 1st floor. The acceleration of these masses result in shear forces along the structure height. The structure is intended to be symmetric about the central vertical axis, in both East-West and North-South planes.

The basic instrumentation consisted of accelerometers and displacement transducers to measure the horizontal accelerations and displacement (with respect to a stationary reference frame) of the frame (at different floor levels) and the shake table. At the 1st, 4th and 7th floor, displacement transducers and accelerometers were provided at both the eastern and western corners, to detect torsional motion, if any of the structure. Additional accelerometers were installed to measure the vertical acceleration of the frame and the shake table. Two displacement transducers were installed to measure the relative displacement of one exterior column bearing and one interior column bearing, with respect to the table. All eight columns in the isolation story were calibrated with strain gauge load cells to measure the column shears. The overall instrumentation of the test structure is shown in figure 2-5. All electronically measured responses were transmitted almost instantaneously via an advanced data acquisition system and stored in the computer hard disk.

During the 1989 6-story frame test, identification tests were carried out on the shake table to determine the dynamic characteristics of the 6-story moment frame under non-isolated (fixed-base) condition. The non-isolated condition was achieved by locking the side plates of the FPS isolators thereby joining the two parts that are otherwise free to slide relative to each other. A banded white noise of 0.04g peak acceleration with frequency content in the range of 0-50 Hz was used as the input motion of the shake table. The structural parameters were obtained from the absolute acceleration transfer functions of the different floors using modal identification techniques (Reinhorn et al., 1989). Table 2-I presents the natural frequencies, damping ratio and mode shapes for the different modes (Mokha et al., 1990). The fundamental frequency of the 6-story frame was 2.34 Hz. Analytically obtained frequencies and mode shapes, using the commercially available software "GTSTRUDL", are also listed in parenthesis in the same table. There is a good agreement between the experimental and analytical results, results however indicate that the structure is actually slightly stiffer than what the theory predicts.

The 7-story frame can be considered as an extension of this 6-story frame with the addition of an isolation system beneath. Analysis and studies done later will show that the 7-story frame

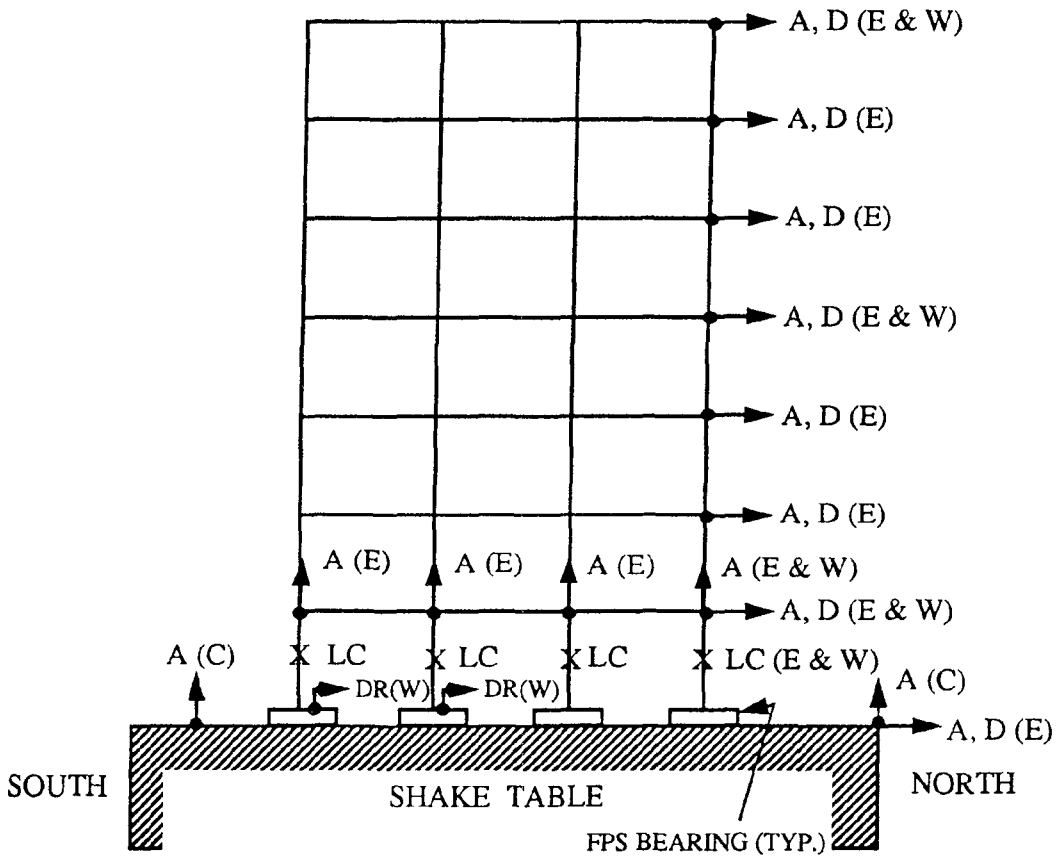

A : ACCELEROMETER

D : DISPLACEMENT TRANSDUCER (ABS. DISPL. WRT FIXED FRAME)

DR : DISPLACEMENT TRANSDUCER (RELATIVE DISPL. WRT TABLE)

LC : SHEAR FORCE LOAD CELL (E & W)

E : EAST W : WEST C : CENTER

FIGURE 2-5 Instrumentation Diagram for the 7-Story Test Frame

can be modelled as a 6-story frame on top of a separately modelled isolation story, in which the dynamic properties of the 6-story frame are explicitly used.

TABLE 2-I Dynamic Characteristics of Six Story Moment Frame under Fixed-Base Conditions (after Mokha et al., 1990)
Note: values in parenthesis are analytical

Mode (1)	Frequency Hz (2)	Damping Ratio (3)	Mode Shape (4)					
			Floor 1	Floor 2	Floor 3	Floor 4	Floor 5	Floor 6 (top)
1	2.34 (2.14)	0.0142	0.214 (0.164)	0.437 (0.395)	0.632 (0.611)	0.797 (0.791)	0.921 (0.923)	1 (1)
2	7.76 (7.72)	0.0204	0.563 (0.520)	1 (1)	0.900 (0.956)	0.326 (0.386)	-0.423 (-0.401)	-0.997 (-0.996)
3	13.28 (12.04)	0.0235	0.822 (0.804)	0.750 (0.863)	-0.248 (-0.230)	-1 (-1)	-0.435 (-0.383)	0.850 (0.817)
4	19.04 (17.98)	0.0155	1 (1)	-0.010 (0.104)	-0.827 (-0.996)	0.283 (0.240)	0.639 (0.908)	-0.461 (-0.619)
5	24.80 (24.02)	0.0059	0.739 (1)	-0.851 (-0.769)	0.229 (-0.027)	0.708 (0.805)	-1 (-0.946)	0.425 (0.397)
6	28.92 (28.82)	0.0086	0.515 (0.679)	-0.850 (-0.919)	1 (1)	-0.902 (-0.879)	0.605 (0.580)	-0.209 (-0.196)

During the 1991 7-story frame test, identification tests were also conducted on the moment frame (MFUIS) and braced frame (BFUIS) structure under non-isolated conditions. Let these non-isolated (fixed base) structures be identified as MFF and BFF respectively. Table 2-II presents experimental frequencies and mode shapes for the moment frame MFF. Identification of the 7th mode was not clear and is therefore omitted from the table. The experimentally determined fundamental frequency was 2.2 Hz., which is slightly less than that of the 6-story

frame due to the flexibility of the additional isolation story. Visual observation during the test suggested that with the side plates locking the FPS isolators, the isolators are laterally restrained, but rotationally flexible achieving a pinned (hinge) support. Analytical results obtained with the structural analysis software "ETABS", are presented for the laterally fixed base case assuming fully pinned column bases. Comparison of analytical mode shapes with the experimental results reveal similar mode shapes. The analytical natural frequencies are, however, slightly lower than the experimental frequencies. Thus, the structure is actually slightly stiffer than the theoretical structure as was the case with the 6 story model.

TABLE 2-II Dynamic Characteristics of 7-Story Moment Frame

Experimental :

Mode	Frequency (Hz.)	Mode Shapes						
		Floor 1	Floor 2	Floor 3	Floor 4	Floor 5	Floor 6	Floor 7
1	2.2	0.138	0.289	0.479	0.675	0.822	0.914	1
2	7.2	-0.373	-0.755	-1	-0.798	-0.193	0.467	0.918
3	12.4	0.473	0.844	0.708	-0.513	-1	-0.197	0.812
4	19.4	-0.837	-0.932	0.653	1	-0.742	-0.967	0.704
5	24.4	1	0.542	-0.948	0.493	0.346	-0.896	0.471
6	29.4	-0.868	0.538	0.033	-0.755	1	-0.7	0.363
7	31	-	-	-	-	-	-	-

Analytical :

Mode	Frequency (Hz.)	Mode Shapes						
		Floor 1	Floor 2	Floor 3	Floor 4	Floor 5	Floor 6	Floor 7
1	2.0	0.138	0.32	0.519	0.696	0.84	0.942	1
2	6.1	-0.461	-0.879	-1	-0.703	-0.105	0.542	0.984
3	10.4	0.814	1	0.194	-0.808	-0.951	-0.08	0.93
4	15.1	-1	-0.396	0.95	0.56	-0.853	-0.698	0.81
5	20.1	0.924	-0.452	-0.728	0.92	0.132	-1	0.595
6	25.0	-0.785	1	-0.445	-0.38	0.969	-0.947	0.395
7	28.5	0.484	-0.863	1	-0.987	0.822	-0.527	0.184

For the braced frame BFF we were unable to properly identify the mode shapes in the identification tests. The braces were not functioning properly, the reason probably being significant slippage at the brace joints due to oversized bolt holes in the braces. The resulting structure had a much smaller stiffness than what theory predicted. The first two natural frequencies of the braced frame were determined to be 3.0 Hz. and 10.6 Hz. respectively.

Shake table motions having a variety of frequency content and amplitude were applied to the test structures in the direction shown in figure 1-4. These included moderate and severe ground motions representing near fault pulses, deep soil sites and rock sites. The isolated structures were subjected to motions far exceeding design basis earthquakes, with peak ground accelerations as high as 0.77g. The earthquake motions are expressed as a percentage of the actual record. Examples of very severe motions used are El Centro S00E 220%, Pacoima S74W 100%, Taft N21E 400%, Miyagi-Ken-Oki EW 500% etc. Long period motion such as the Japanese Hachinohe NS has also been applied. Table 2-III presents a list of the earthquake motions applied. More information on the testing program and table motion characteristics is presented in Section 3.

Table 2-III List of Earthquake Motions Used in 1991 7-Story Frame Test

EQ. No.	Earthquake Name	Record Description	Magnitude
1	El Centro S00E	Imperial Valley, May 18, 1940 Component S00E	6.7
2	Taft N21E	Kern County, July 21, 1952 Component N21E	7.2
3	Pacoima S74W	San Fernando, Feb. 9, 1971 Component S74W	6.4
4	Pacoima S16E	San Fernando, Feb. 9, 1971 Component S16E	6.4
5	Hachinohe NS	Tokachi-Oki Earthquake, Japan, May 16, 1968 Component NS	7.9
6	Miyagi-Ken-Oki EW	Tohoku Univ., Sendai, Japan, June 12, 1978 Component EW	7.4
7	Caltrans Rock 1	Artificial motion, rock sites in California by CalTrans (PGA = 0.6g)	
8	Caltrans Rock 2	Artificial motion, rock sites in California by CalTrans (PGA = 0.6g)	
9	Caltrans Alluvium 1	Artificial motion, 10-80 ft. alluvium sites in California by CalTrans (PGA = 0.6g)	

All ground motions were time compressed by a factor of 2 to satisfy similitude requirements of the quarter scale model. Figures 2-6 to 2-14 present recorded time histories of the shake table motion for the different earthquakes. Response spectra of these motions (for 5% damping) are also presented in these figures.

An additional test was done to study the case where the vertical component of motion was applied simultaneously with the horizontal component. A limited number of tests were also performed on the fixed-base moment frame structure (MFF) to permit comparison between isolated and non-isolated structure. Different strengths of the El Centro S00E, Taft N21E and Hachinohe NS were applied, taking care that the structure remained elastic at all times.

2.3.2 Isolator Response

The response of the isolators is presented as a combination of two graphs as follows: (i) time-histories of the isolation system displacement, interior bearing displacement and exterior bearing displacement all on one graph, and (ii) overall hysteretic response of the isolation system.

The basic moment frame structure MFUIS (see Section 1.4) is considered as our primary focus and results are presented in figures 2-15 to 2-24 for several moderate and severe earthquake motions. For the other three structure configurations (MFBIS, BFUIS, BFBIS), results are presented (figures 2-25 to 2-36) for a few selected cases of strong motions.

Study of the displacement time histories show that the peak bearing displacements are slightly smaller than the peak isolation system displacement, the difference simply being the deformation in the individual isolation story columns. For the braced isolation system (MFBIS, BFBIS), the interior and exterior bearing displacements are essentially the same due to the horizontal bracing of the column bases. All the floor levels including the 1st floor level are rigid in their own plane. Hence, for the unbraced isolation system (MFUIS, BFUIS) the interior and exterior bearing displacements are slightly different, as allowed by the individual column flexure and rotation at column base. The bearing displacements reached their full displacement capacity of 2 inches in some of the tests, such as for El Centro S00E 220%.

The shape of the hysteresis loops, in general, suggest that they may be idealized as parallelograms, indicating a bilinear force-displacement relationship. The base shear force is computed by summing the inertia forces due to the accelerating floor masses.

Base-shear coefficients normally ranged between 0.1 to 0.28, depending on the motion. Only for certain special cases, the base shear coefficient reached values as high as 0.47. This occurred for cases where the bearing reached its displacement restraint. This special aspect will be addressed later in another section. It may also be noted that the base shear was also determined from the column shears measured directly by the strain gauge load cells, for the unbraced isolation system case (structures MFUIS, BFUIS). It is found that both methods of computing base shear agree very well thereby verifying the reliability of the lumped mass model and accelerometer readings. Furthermore, the characteristics of the hysteresis loops in the entire test series remained consistent implying that the stiffness and friction properties of the FPS isolator did not change even after such a large number of tests on the same isolators.

The influence of the various structural configurations on the peak isolation system responses is studied. Considering the 6-story frame (1989 test) and the 7-story frame (1991 test), we have the following three configurations for a 6-story moment frame with:

(i) A rigid base supported by isolators
(ii) An additional isolation story with isolators at base of unbraced columns
(iii) An additional isolation story with isolators at base of braced columns.

For the braced frame structure, we had the later two configurations only.

Figures 2-37 and 2-38 present the effect of bracing the isolation story on the isolation system displacement for moment frame and braced frame, respectively. Results for a selected group of four strong ground motions are presented. There is no significant difference between the braced and unbraced isolation story.

Figures 2-39 and 2-40 present the effects of the different isolation story configurations, including the rigid base case, on the peak individual bearing displacement for moment frame and braced frame respectively. Differences between the isolator responses of braced and unbraced isolation systems are relatively small, and are simply due to differences in stiffness of the isolation story framing. The case of rigid base for the moment frame (figure 2-39) represents magnitudes close to the frame with an additional isolation story. It needs to be noted that in addition to the difference in the structural configuration, there is difference in the isolator properties with the 6-story rigid base case representing 0.075 friction, while the 7-story cases represent 0.06 friction.

Figures 2-41 and 2-42 show the effects of different structural configurations on the base shear. The difference between the different configurations is relatively small, even though the friction for the 6-story rigid base frame is different from the 7-story frame. Differences in the responses between the rigid base and framed isolator stories are fully accounted for by the differences in isolator function, and the differences in isolation story stiffness. Analytical models incorporating these differences (presented later) were able to accurately predict the responses of all structural configurations tested.

Simple comparison between the braced frame versus moment frame response indicates that the base shear has a general tendency of being the same or a little greater for the braced frame due to its greater stiffness. The maximum variation was found to be 18%. As a result, the isolation system displacement response is also about the same or slightly larger for the braced frame. The only exception was observed in the long period motion of Hachinohe NS, where the braced frame base shear was about 14% smaller than the moment frame shear. The braced frame was not as stiff as it was intended to be due to elongated bolt hole connections. Nevertheless, the braced frame was a stiffer structure with an experimentally determined natural frequency of about 3 Hz., compared to 2.2 Hz. for the moment frame under fixed-base (non-isolated) conditions.

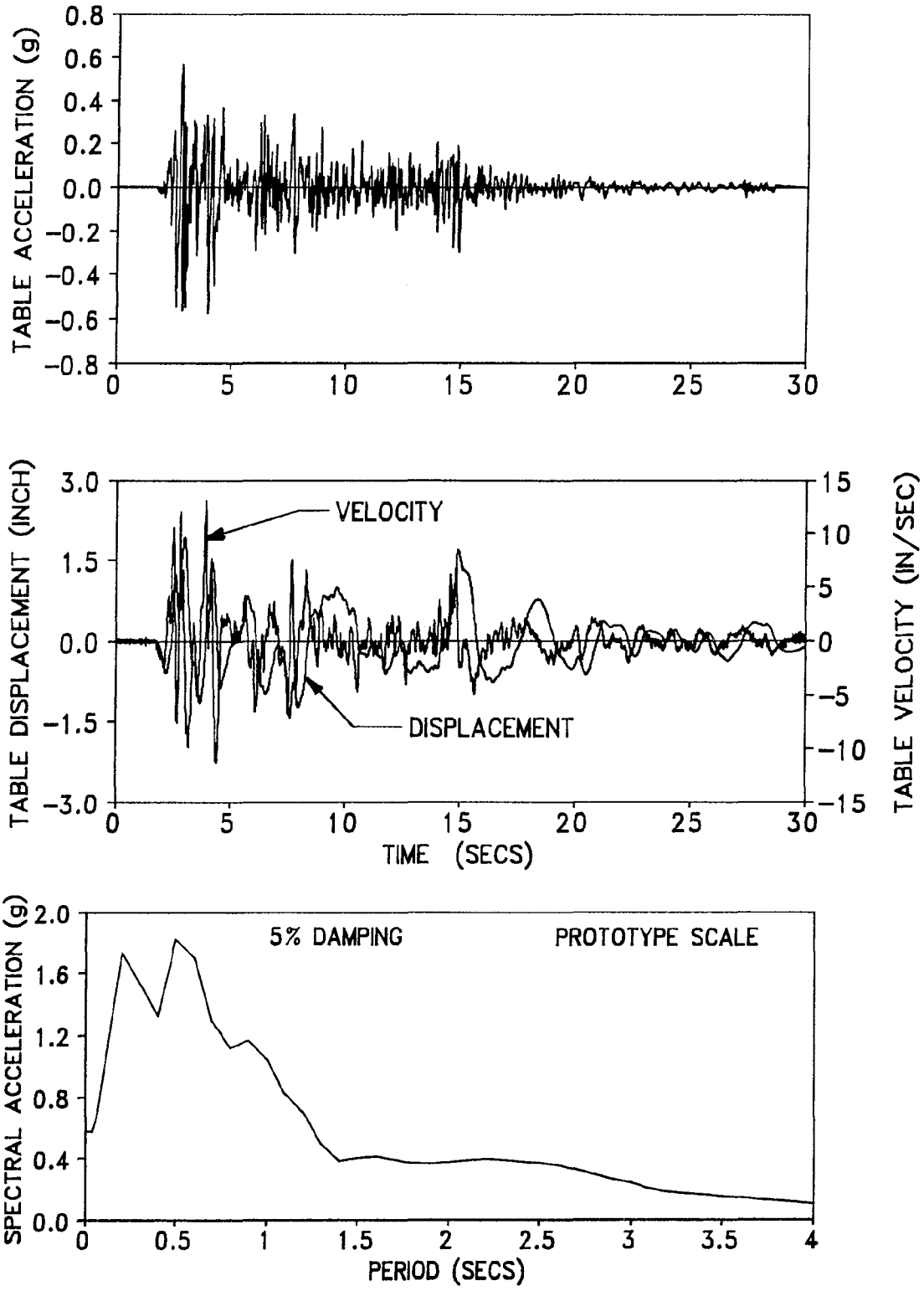

FIGURE 2-6 Time History Records and Response Spectrum of Shake Table Motion for El Centro S00E 200%

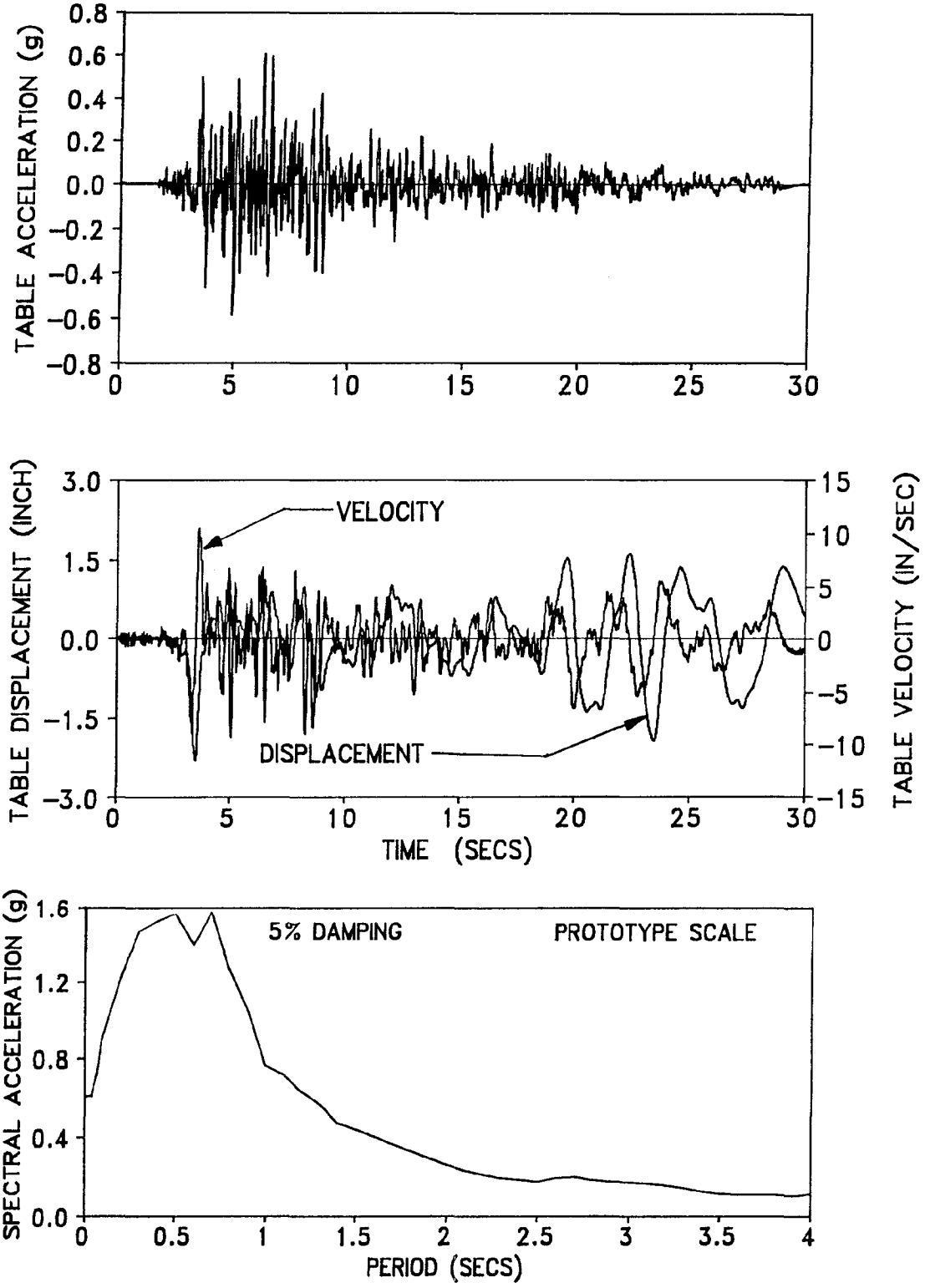

FIGURE 2-7 Time History Records and Response Spectrum of Shake Table Motion for Taft N21E 300%

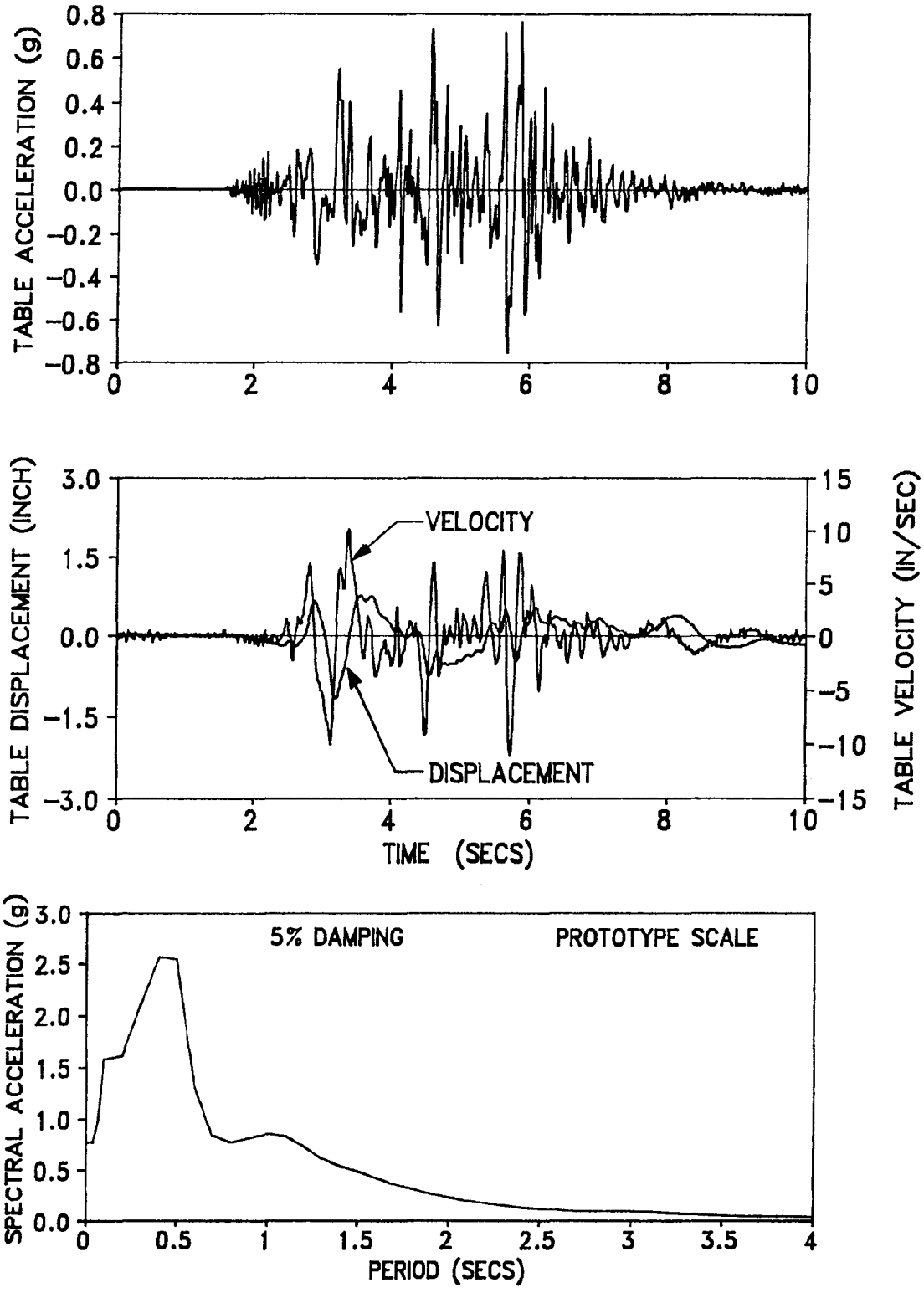

FIGURE 2-8 Time History Records and Response Spectrum of Shake Table Motion for Pacoima S74W 100%

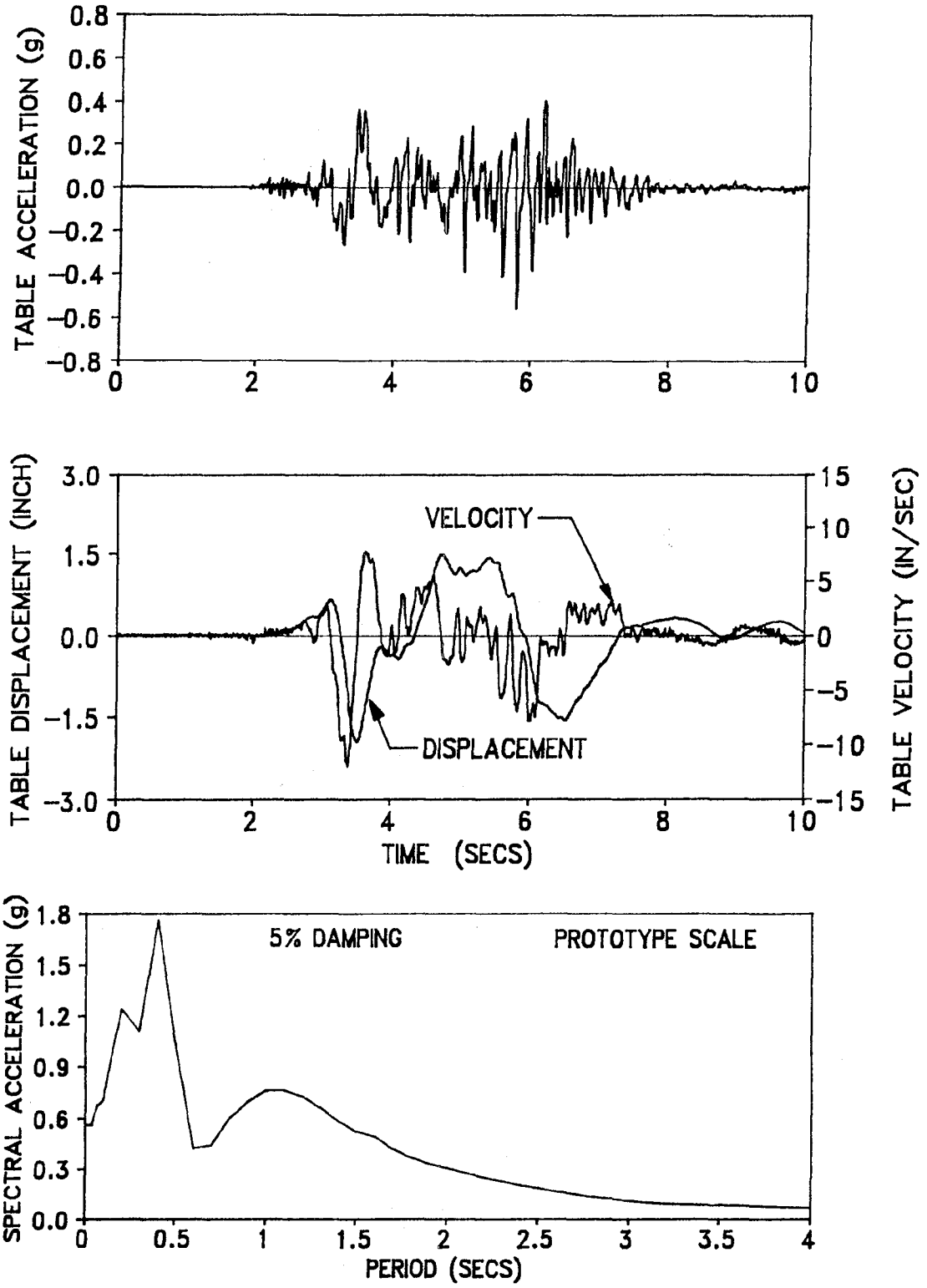

FIGURE 2-9 Time History Records and Response Spectrum of Shake Table Motion for Pacoima S16E 60%

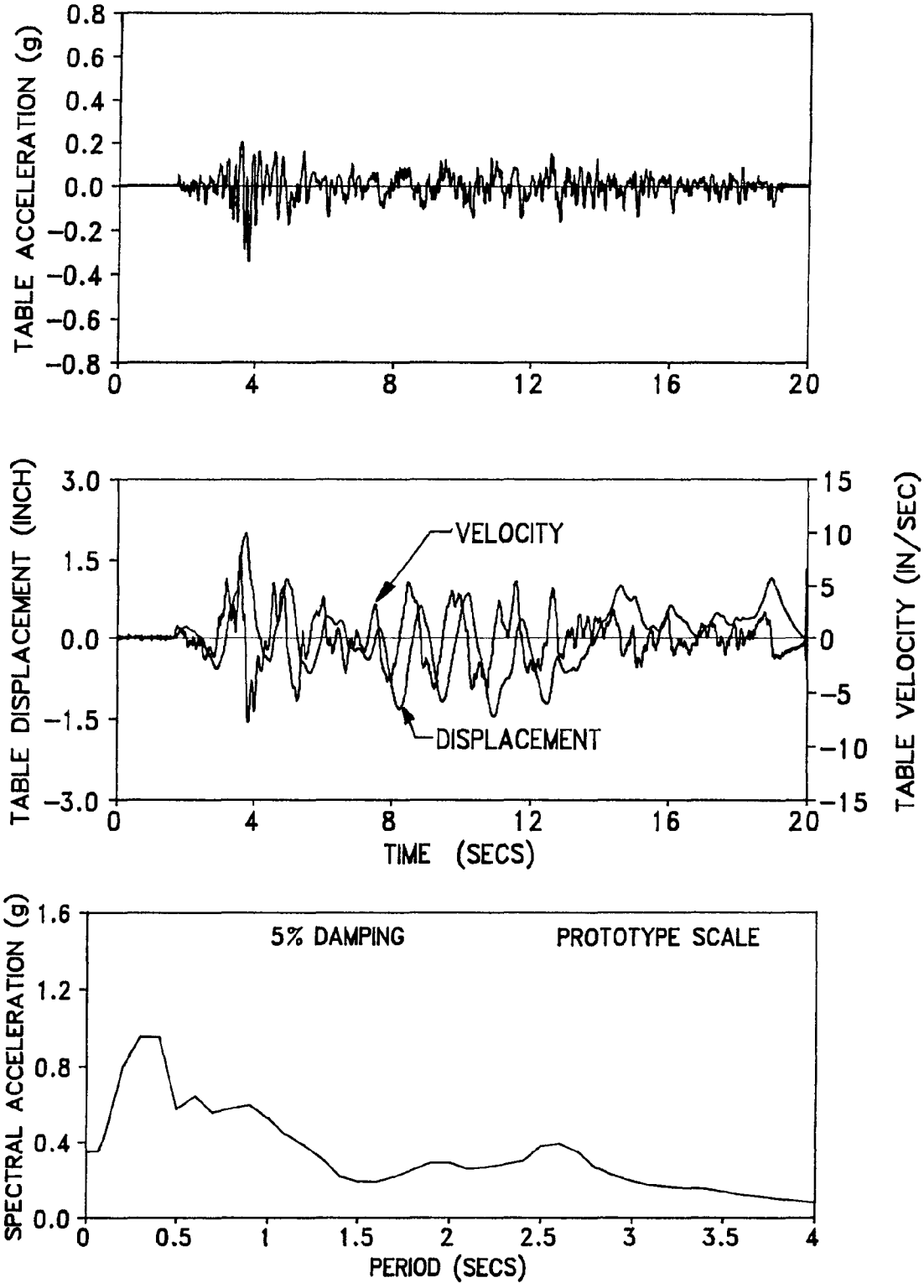

FIGURE 2-10 Time History Records and Response Spectrum of Shake Table Motion for Hachinohe NS 150%

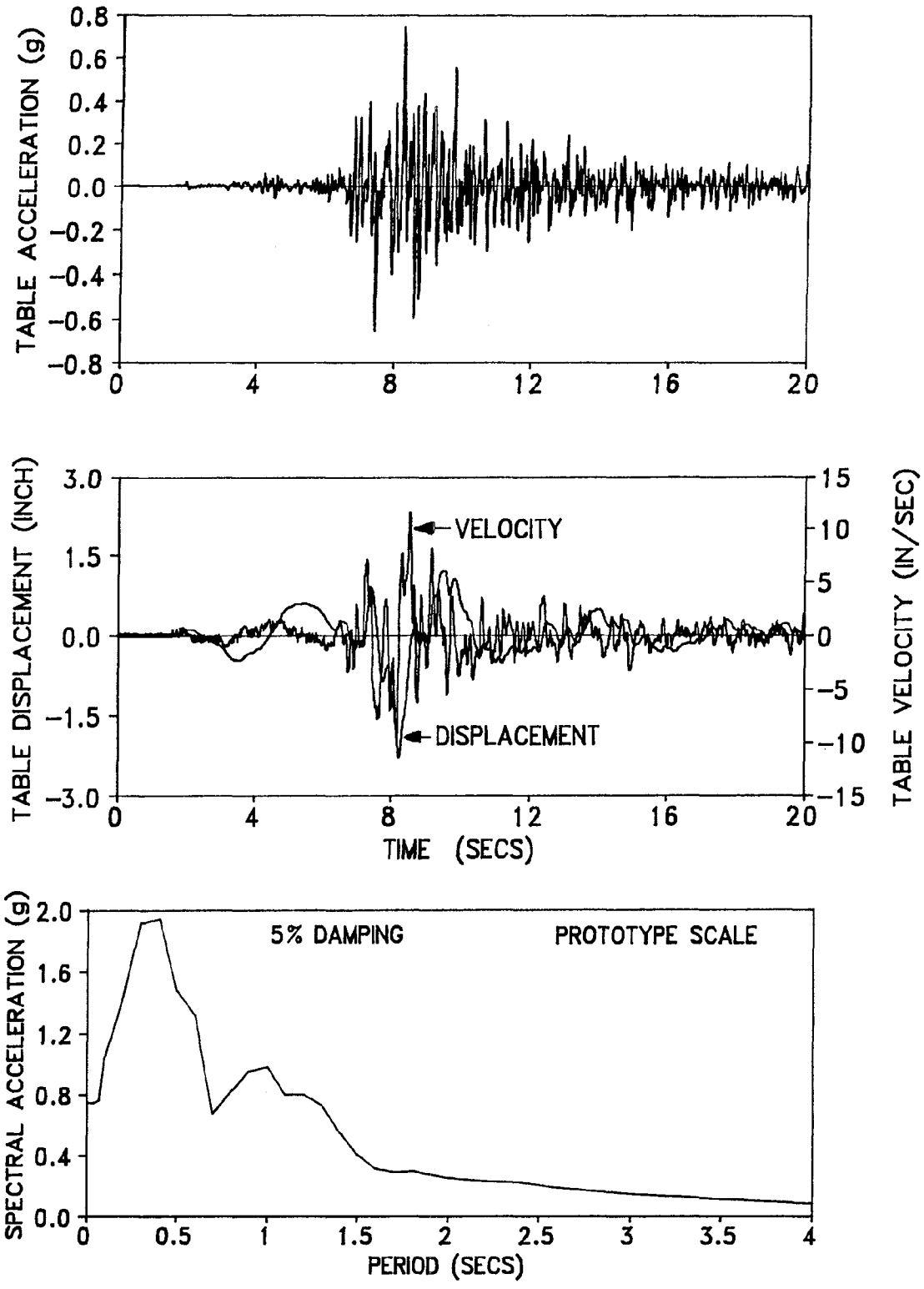

FIGURE 2-11 Time History Records and Response Spectrum of Shake Table Motion for Miyagi-Ken-Oki 500%

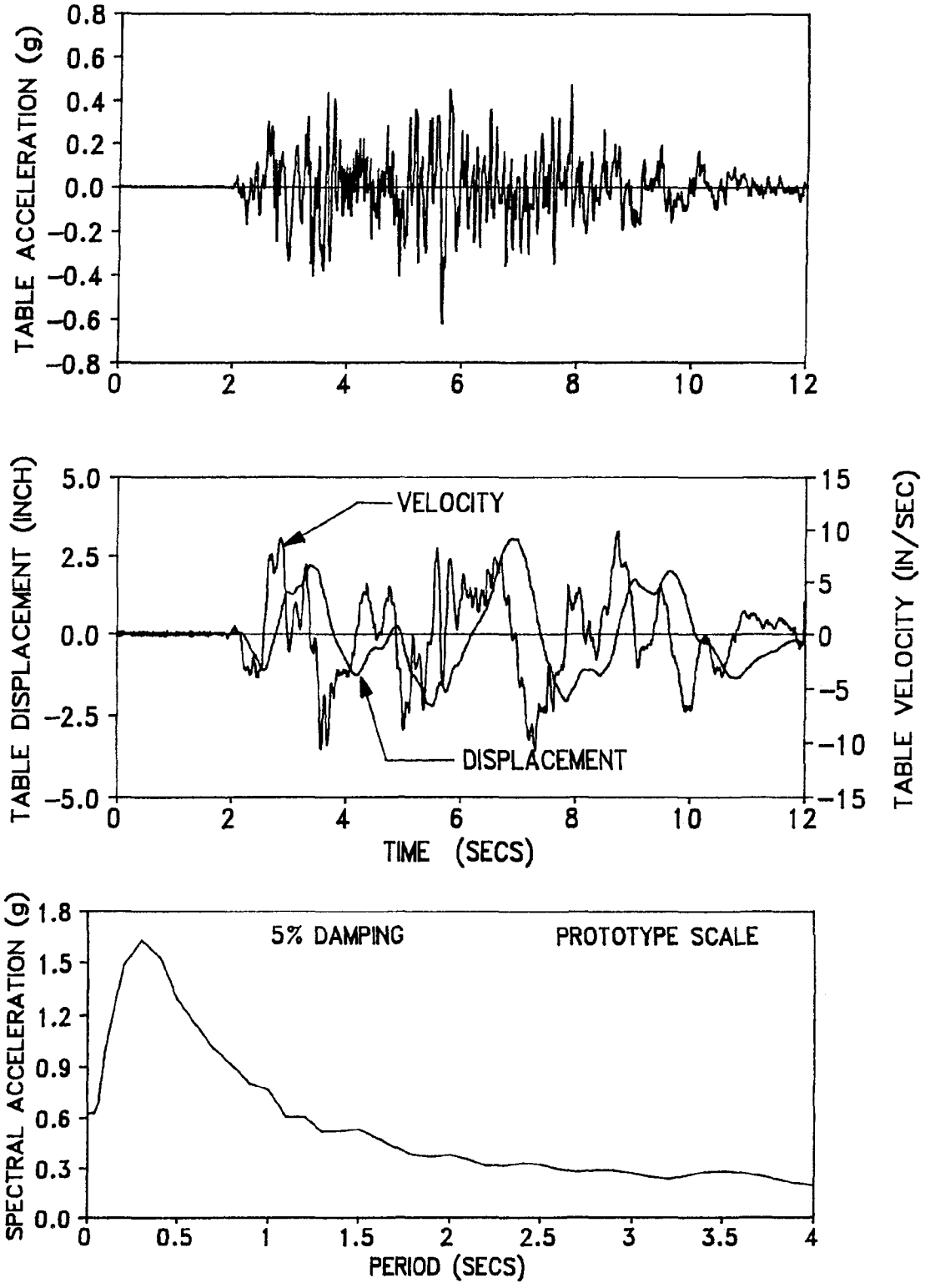

FIGURE 2-12 Time History Records and Response Spectrum of Shake Table Motion for CalTrans Rock.1 100%

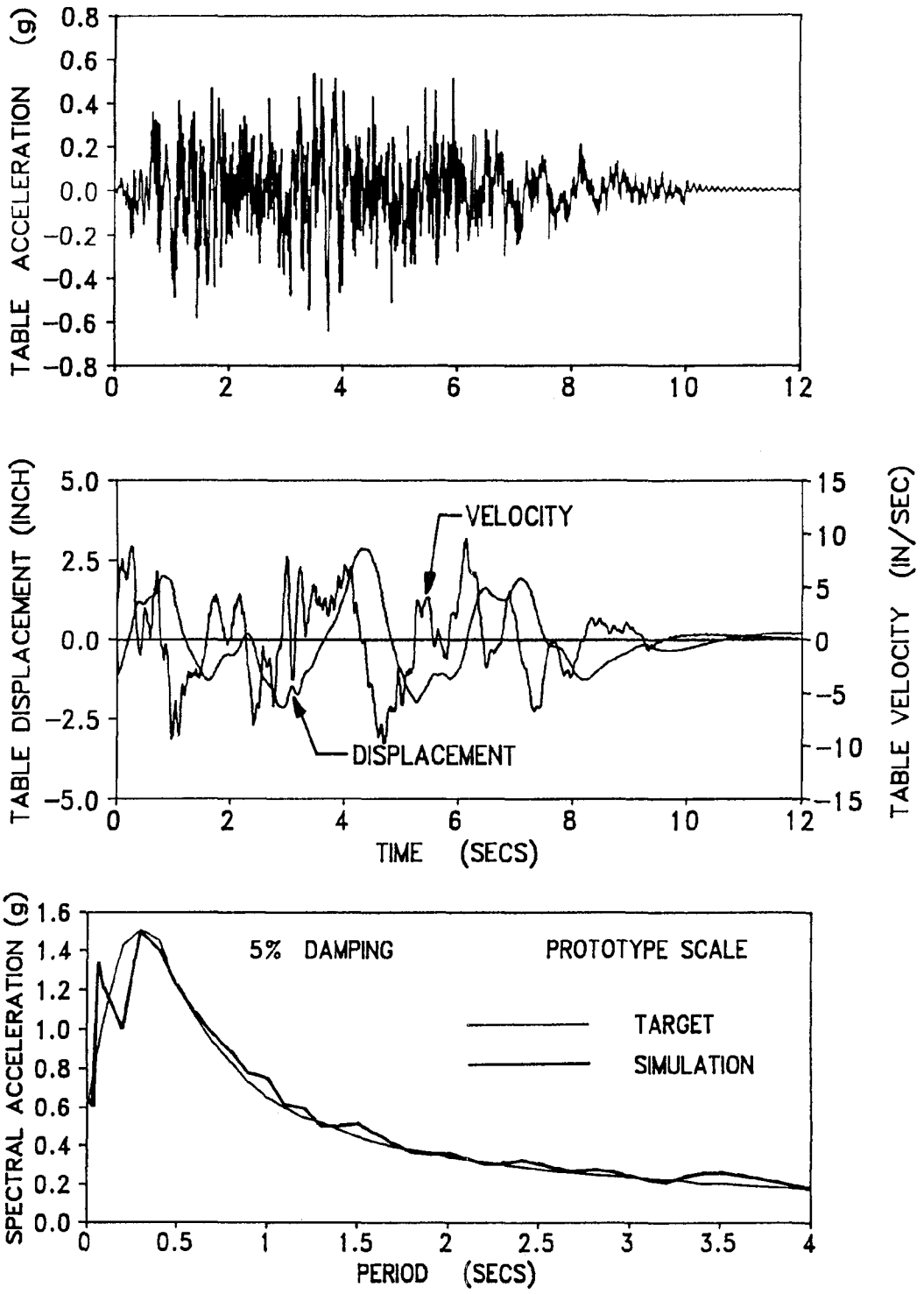

FIGURE 2-13 Time History Records and Response Spectrum of Shake Table Motion for CalTrans Rock.2 100%

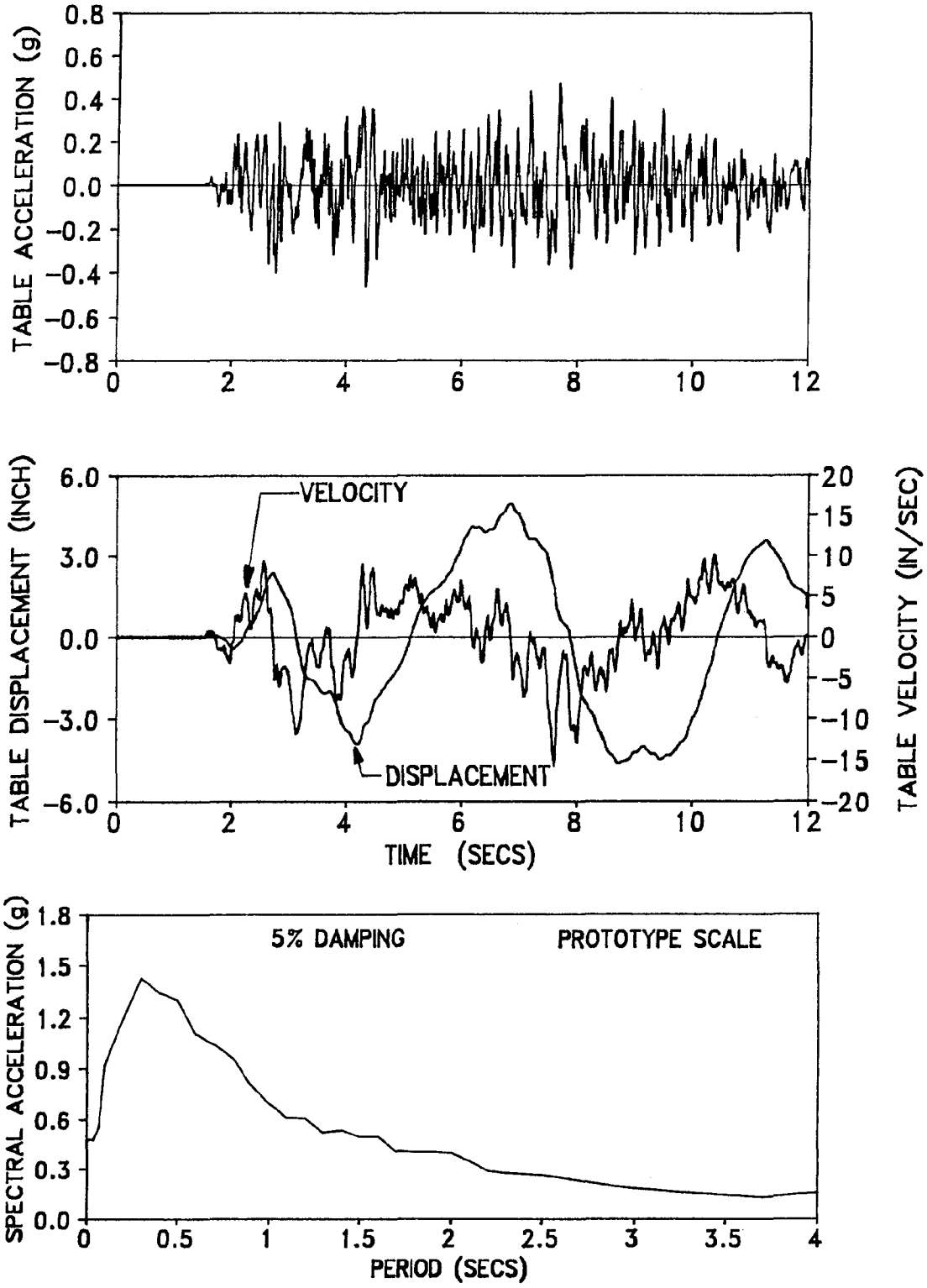

FIGURE 2-14 Time History Records and Response Spectrum of Shake Table Motion for CalTrans Alluvium.1 75%

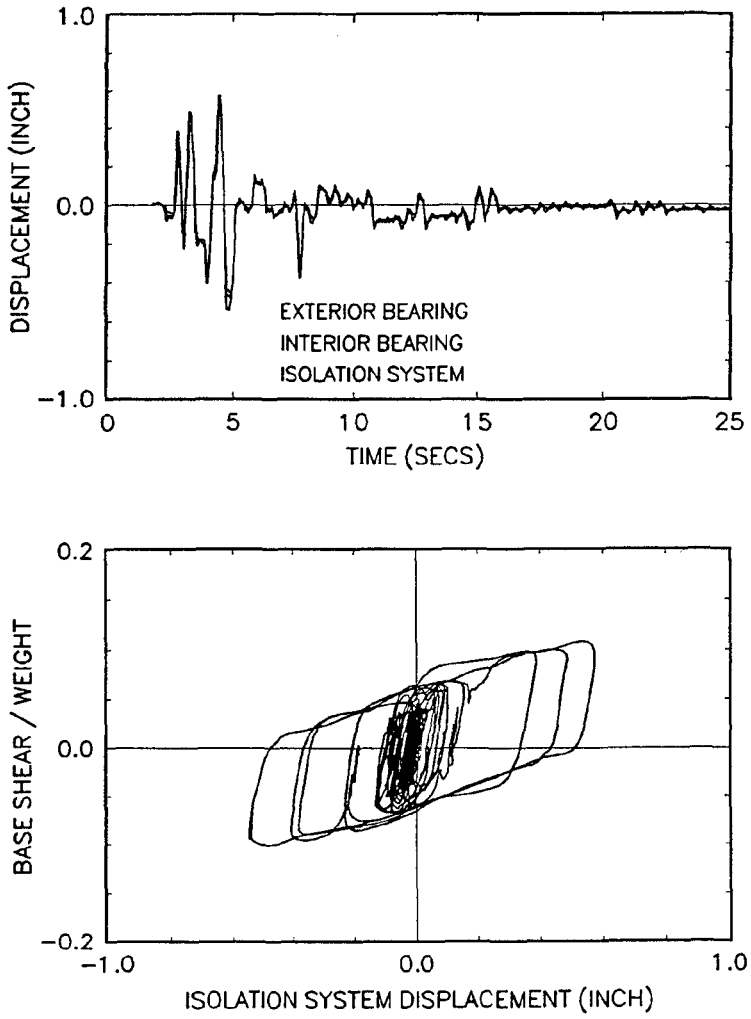

FIGURE 2-15 Isolation System Response for MFUIS for El Centro S00E 100%

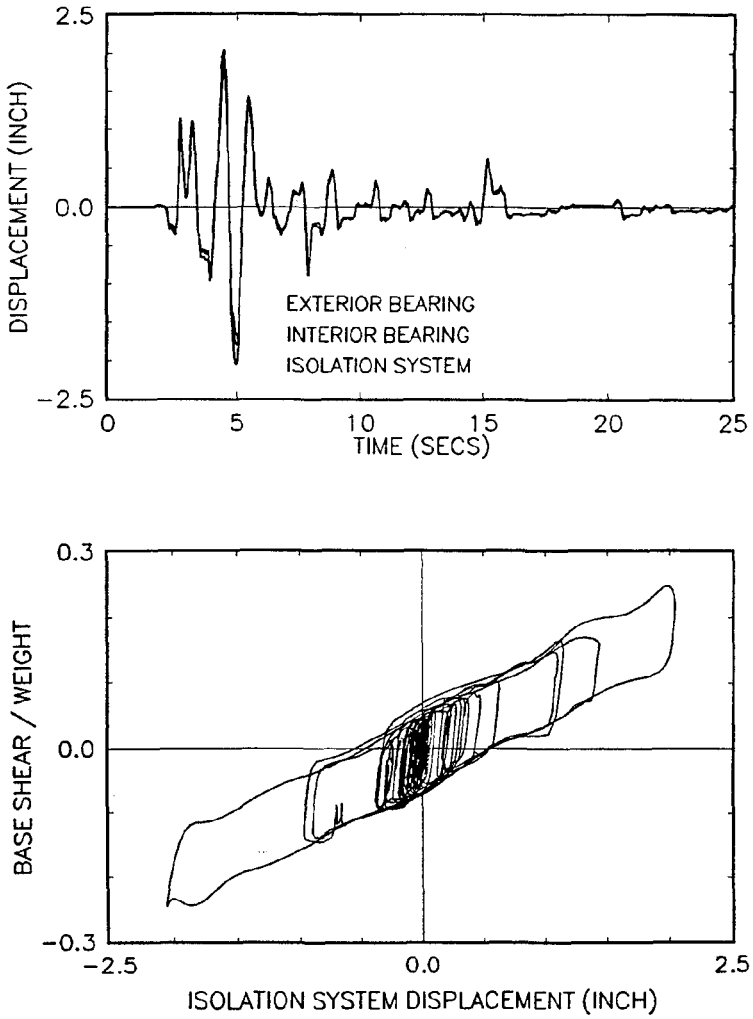

FIGURE 2-16 Isolation System Response for MFUIS for El Centro S00E 200%

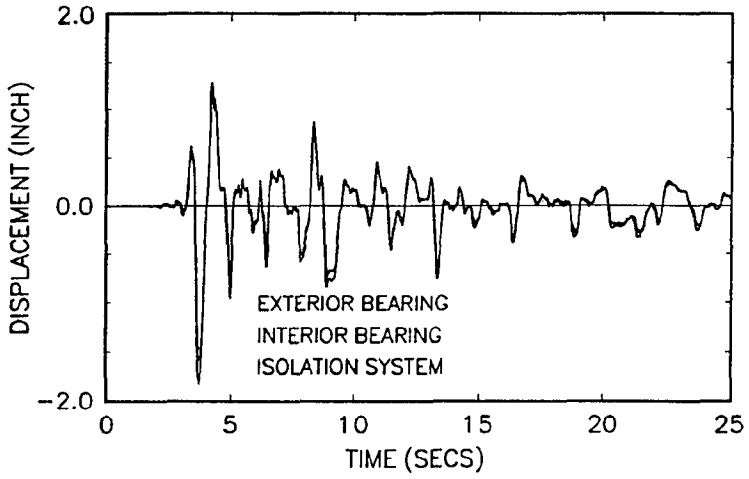

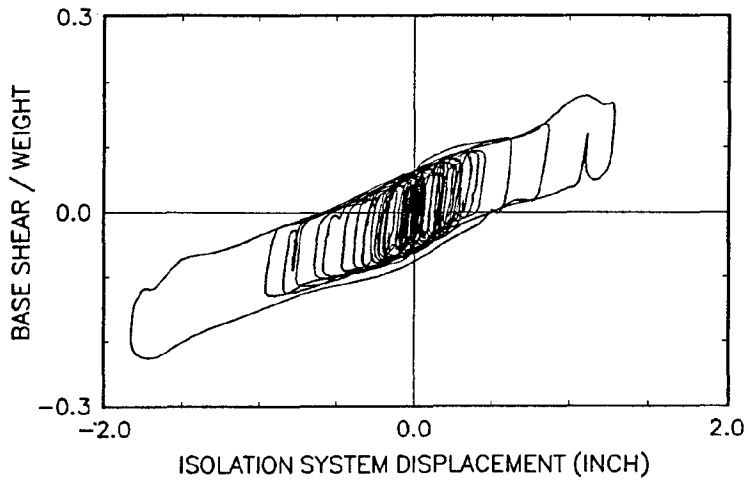

FIGURE 2-17 Isolation System Response for MFUIS for Taft N21E 400%

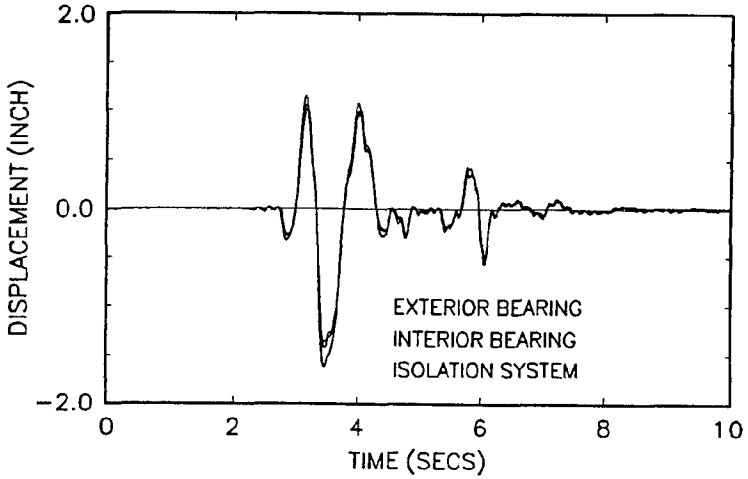

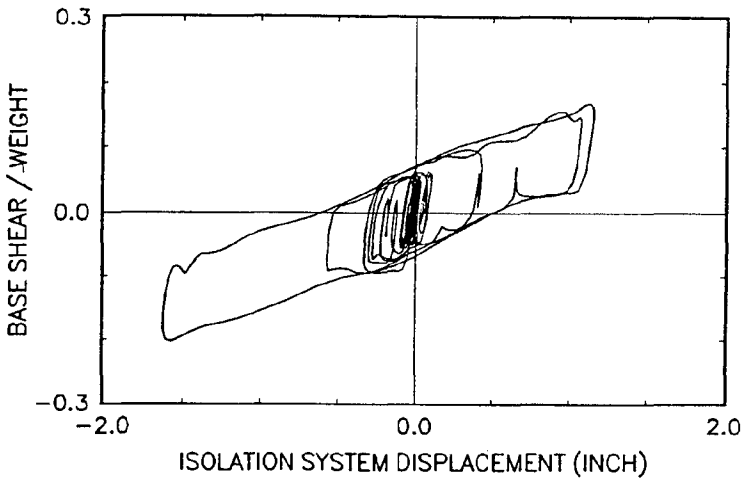

FIGURE 2-18 Isolation System Response for MFUIS for Pacoima S74W 100%

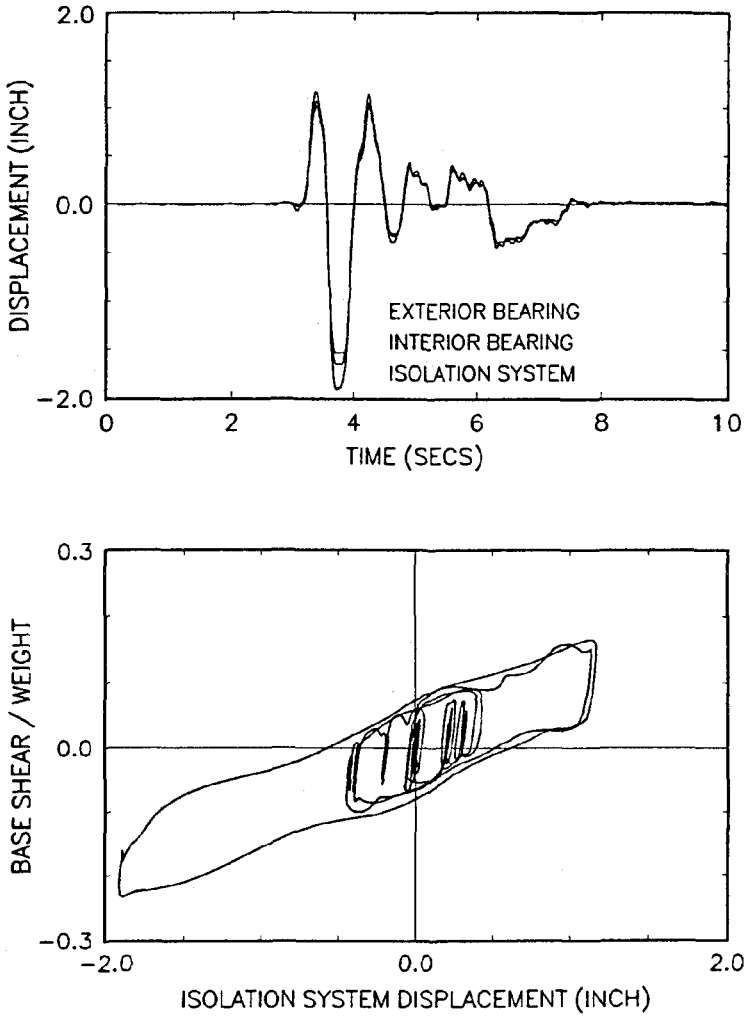

FIGURE 2-19 Isolation System Response for MFUIS for Pacoima S16E 60%

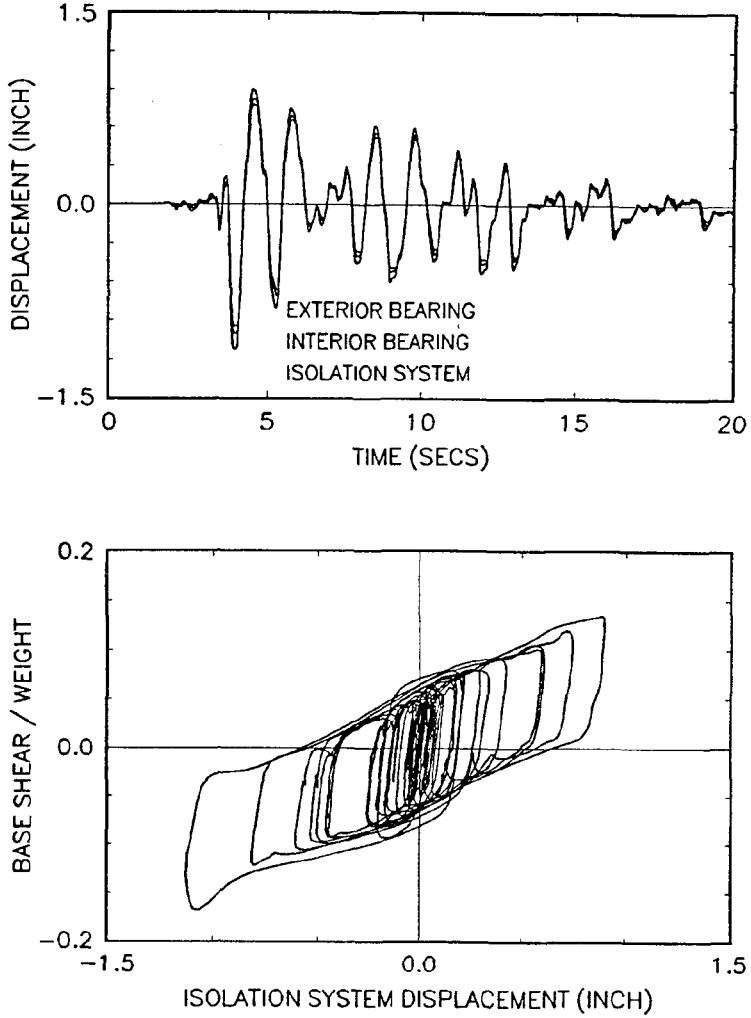

FIGURE 2-20 Isolation System Response for MFUIS for Hachinohe NS 150%

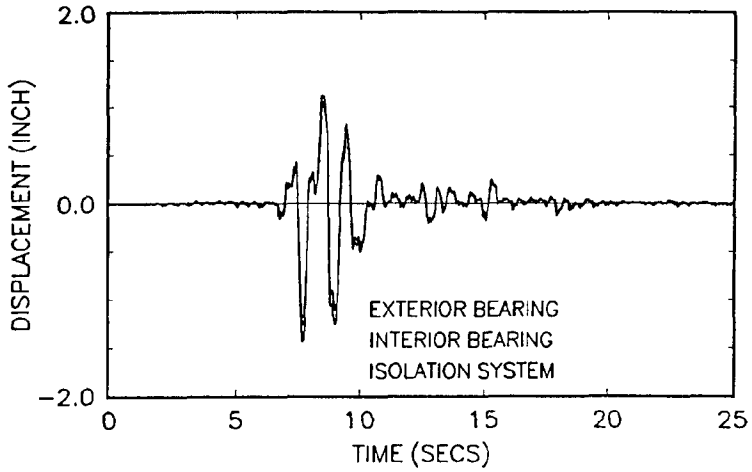

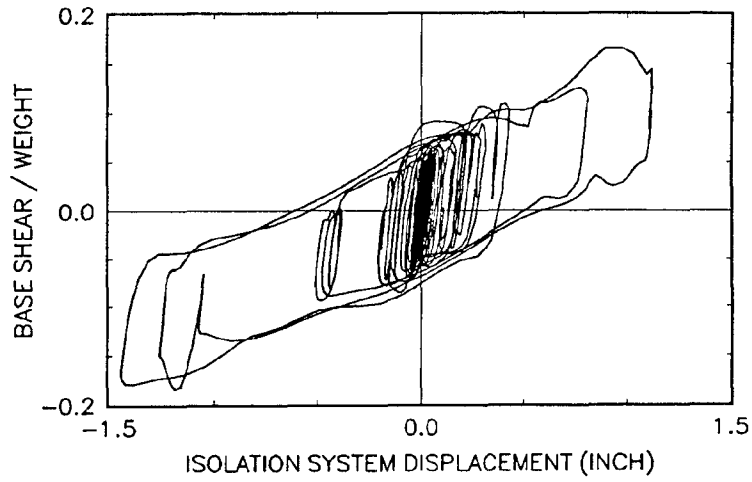

FIGURE 2-21 Isolation System Response for MFUIS for Miyagi-Ken-Oki EW 500%

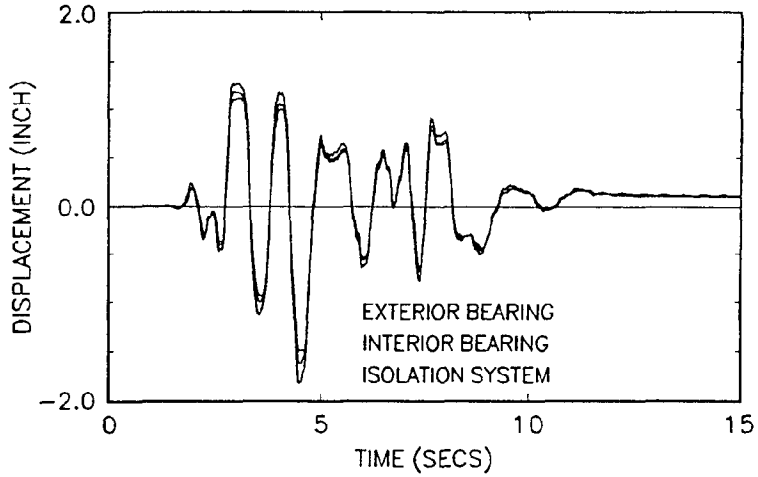

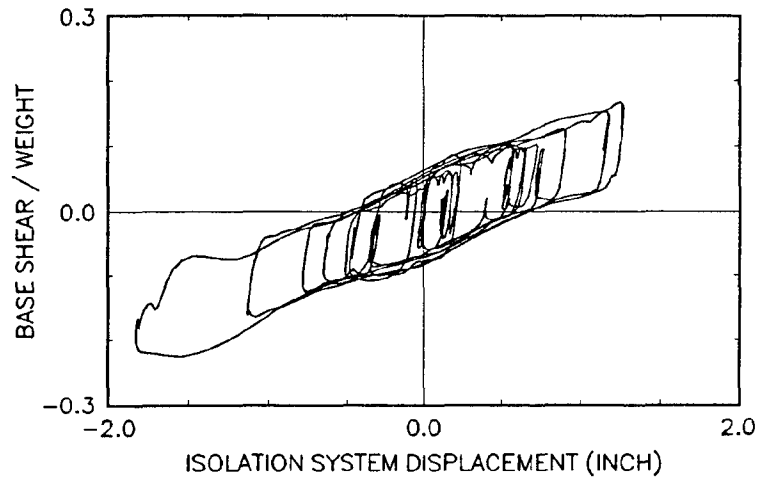

FIGURE 2-22 Isolation System Response for MFUIS for CalTrans Rock.1 100%

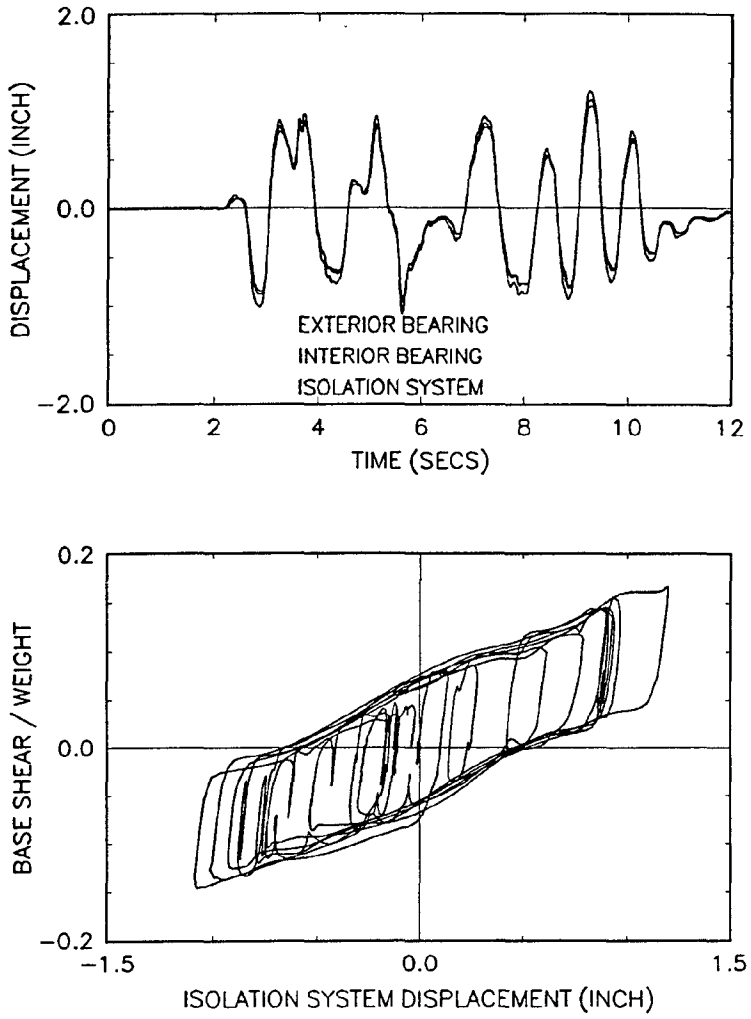

FIGURE 2-23 Isolation System Response for MFUIS for CalTrans Rock.2 100%

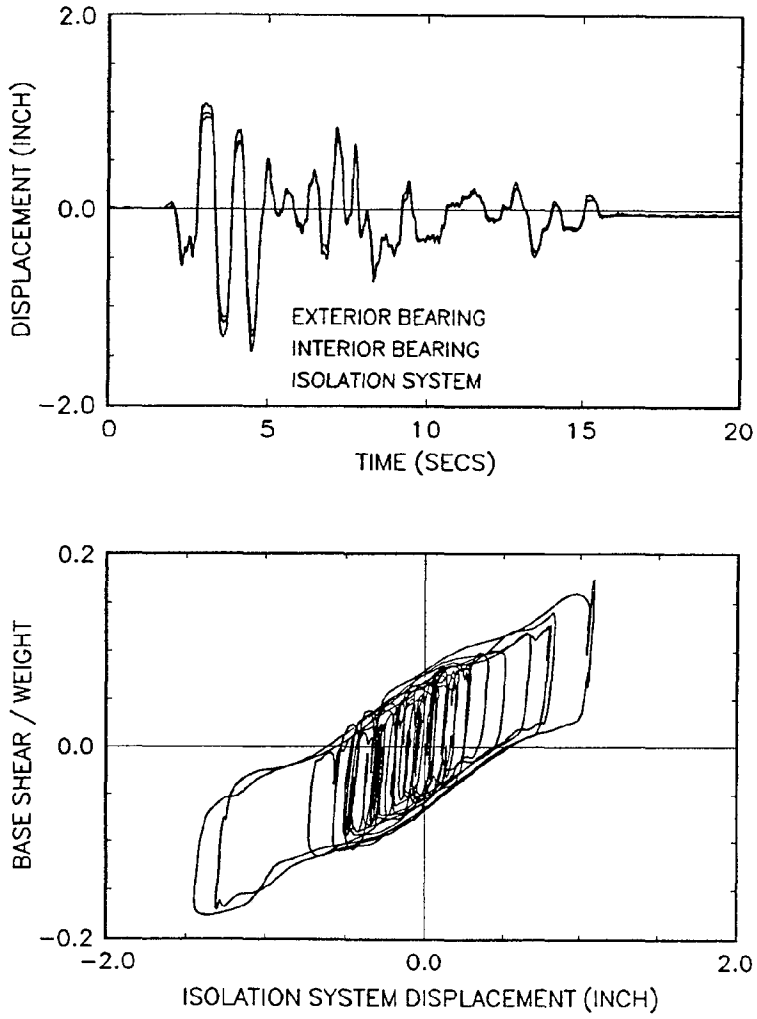

FIGURE 2-24 Isolation System Response for MFUIS for CalTrans Alluvium.1 75%

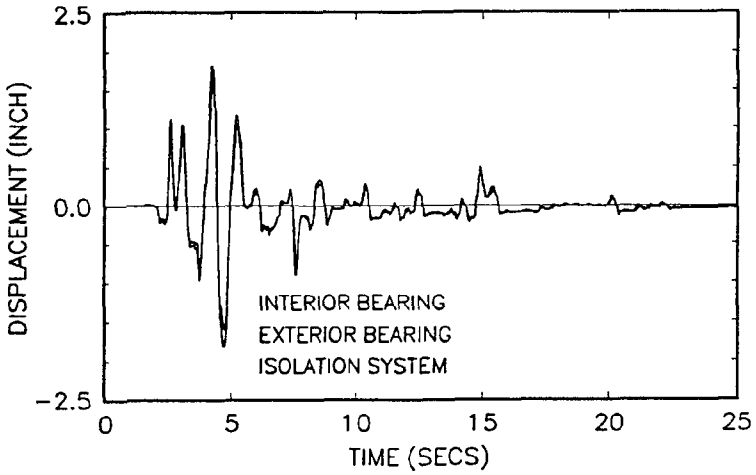

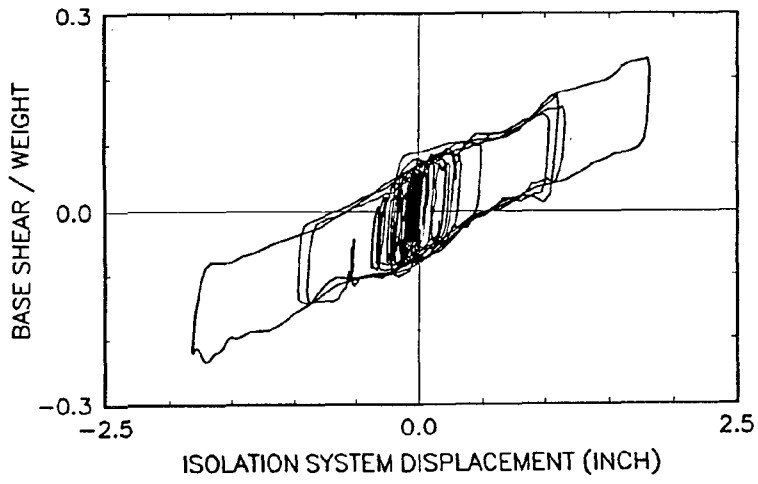

FIGURE 2-25 Isolation System Response for MFBIS for El Centro S00E 200%

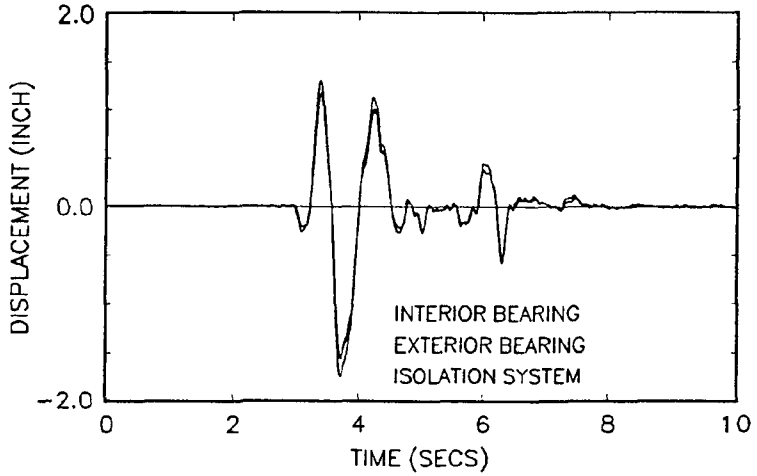

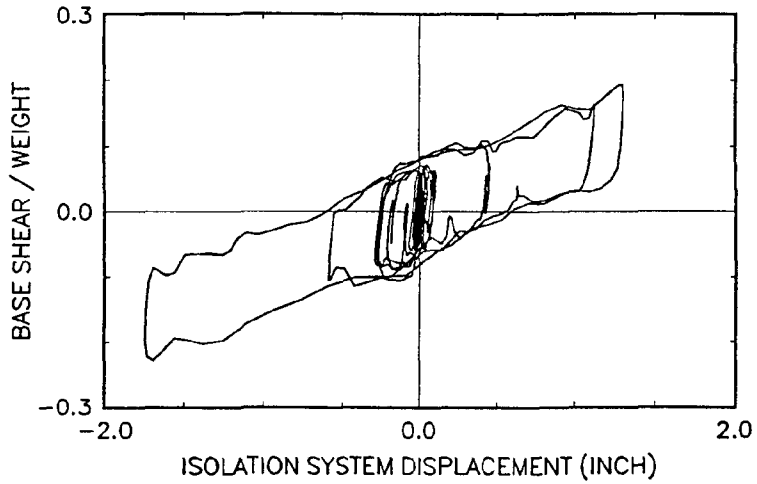

FIGURE 2-26 Isolation System Response for MFBIS for Pacoima S74W 100%

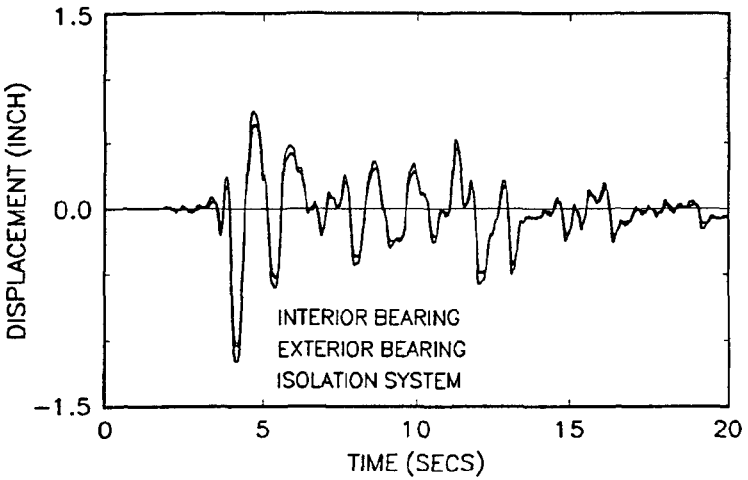

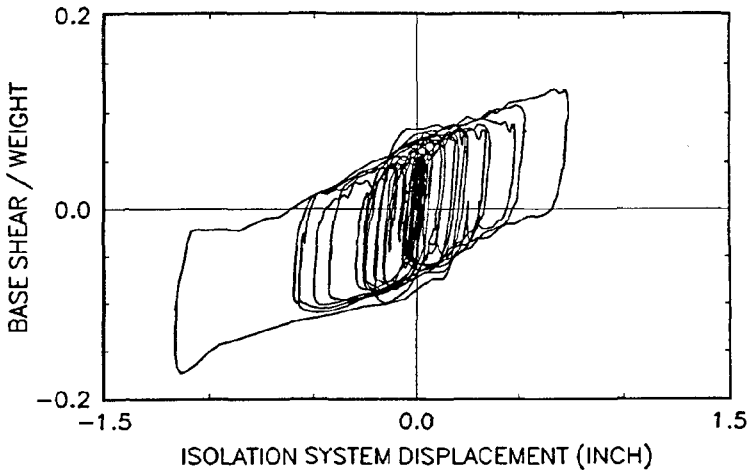

FIGURE 2-27 Isolation System Response for MFBIS for Hachinohe NS 150%

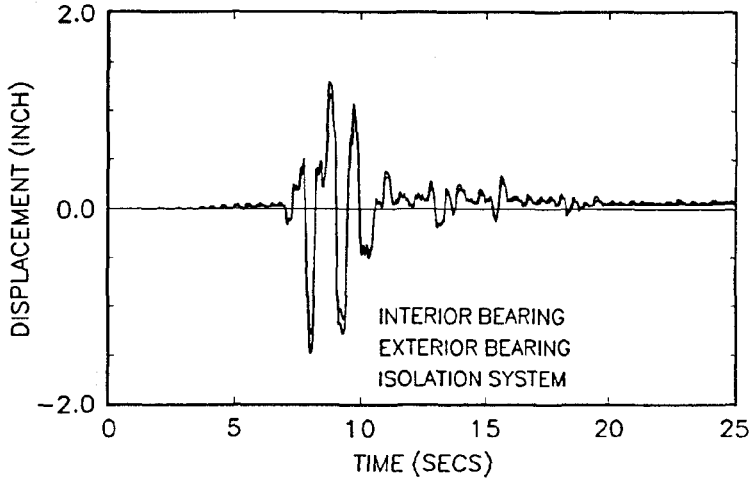

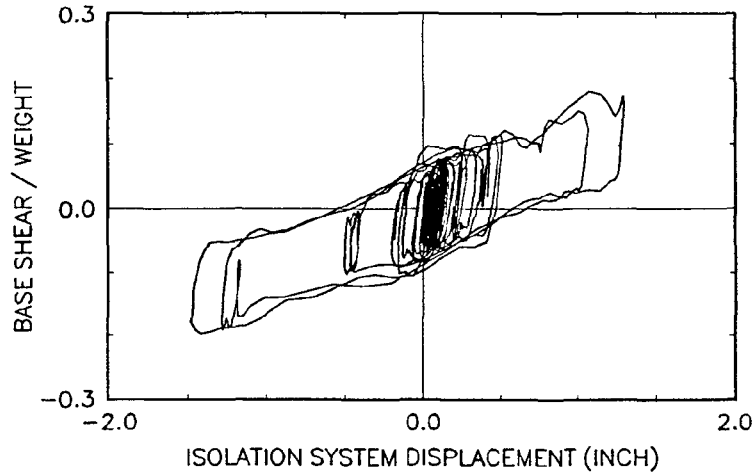

FIGURE 2-28 Isolation System Response for MFBIS for Miyagi-Ken-Oki EW 500%

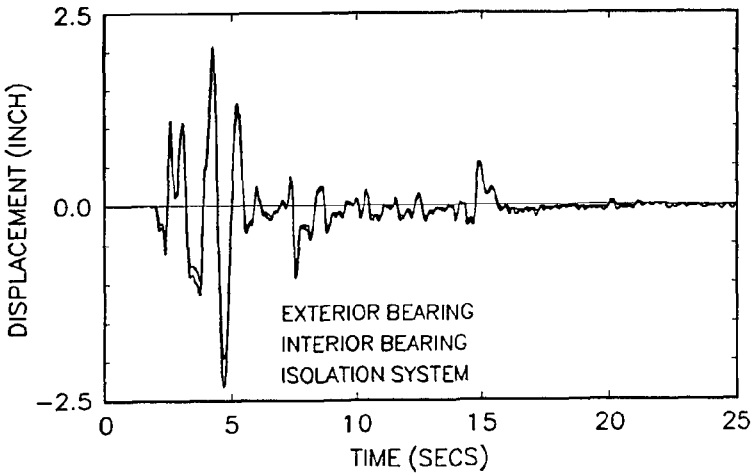

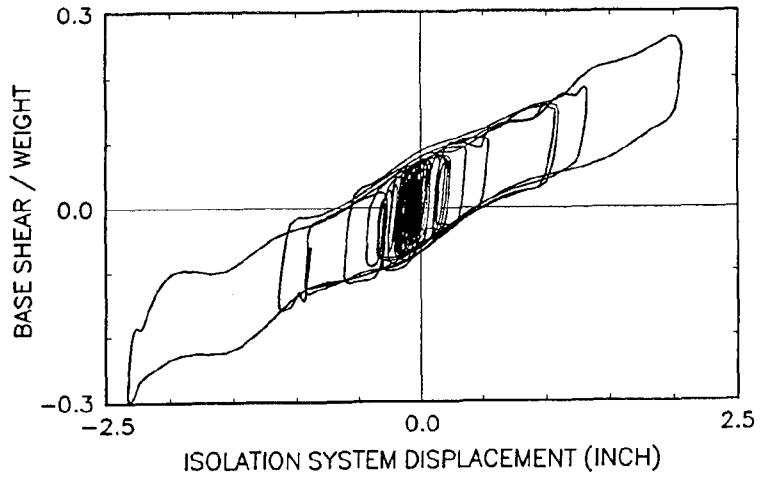

FIGURE 2-29 Isolation System Response for BFUIS for El Centro S00E 200%

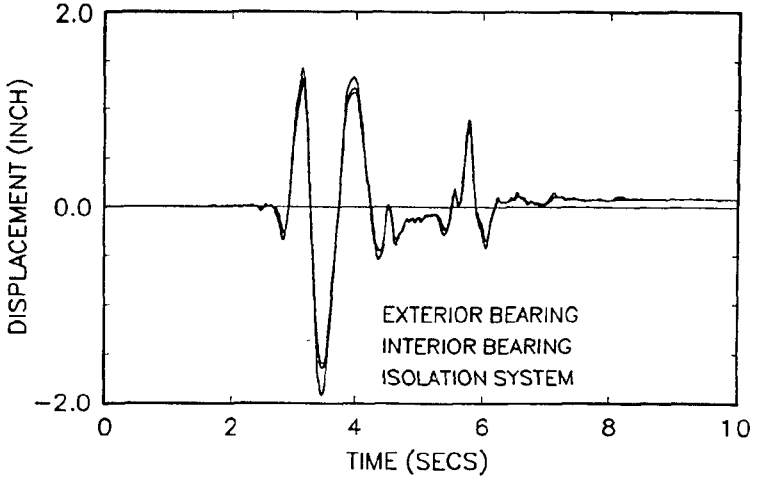

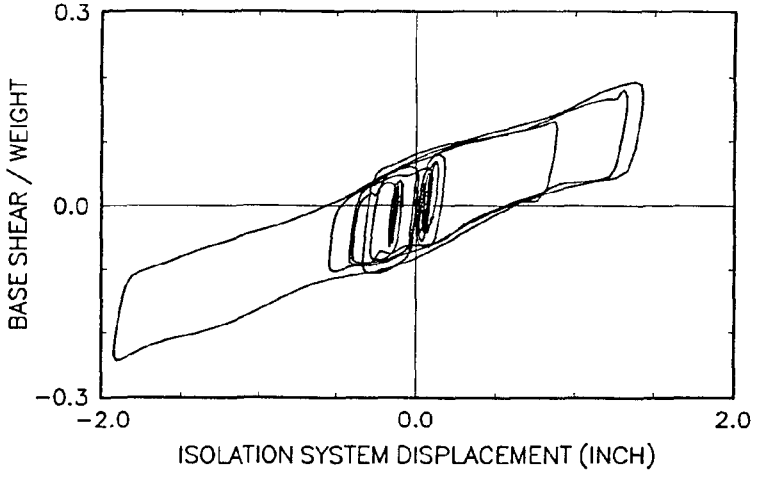

FIGURE 2-30 Isolation System Response for BFUIS for Pacoima S74W 100%

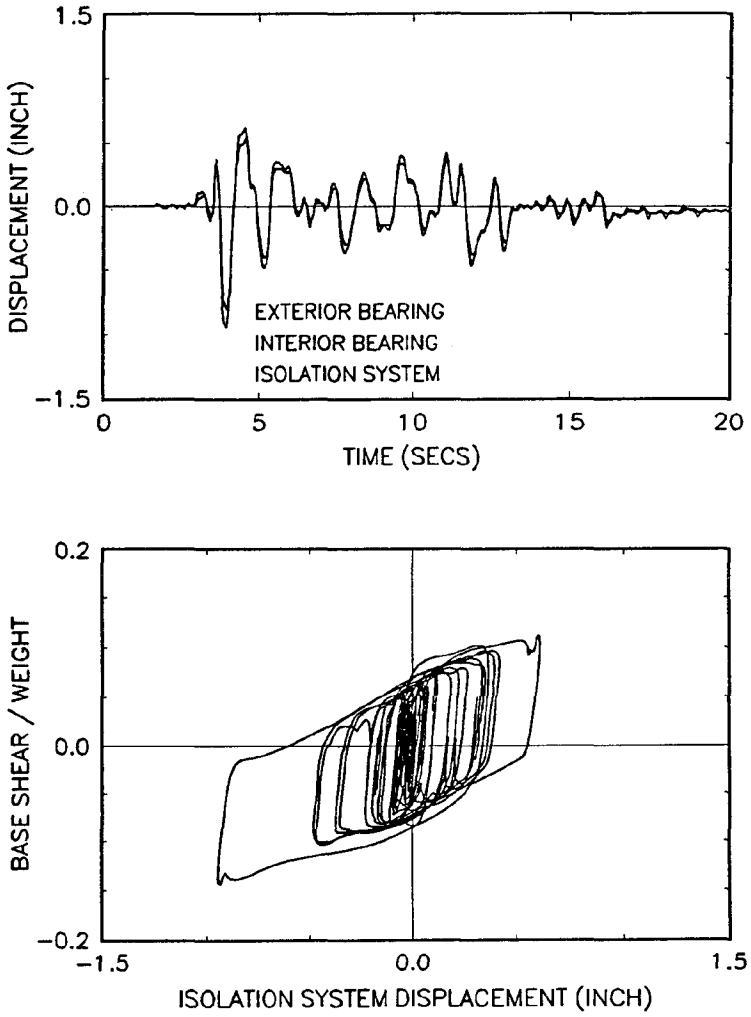

FIGURE 2-31 Isolation System Response for BFUIS for Hachinohe NS 150%

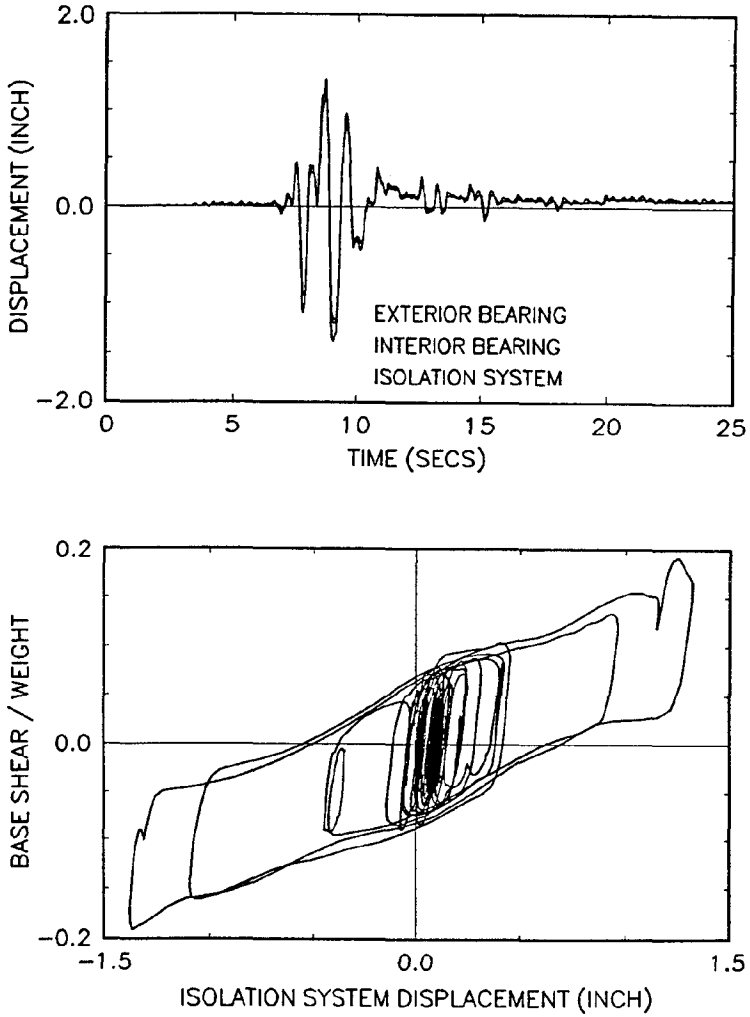

FIGURE 2-32 Isolation System Response for BFUIS for Miyagi-Ken-Oki EW 500%

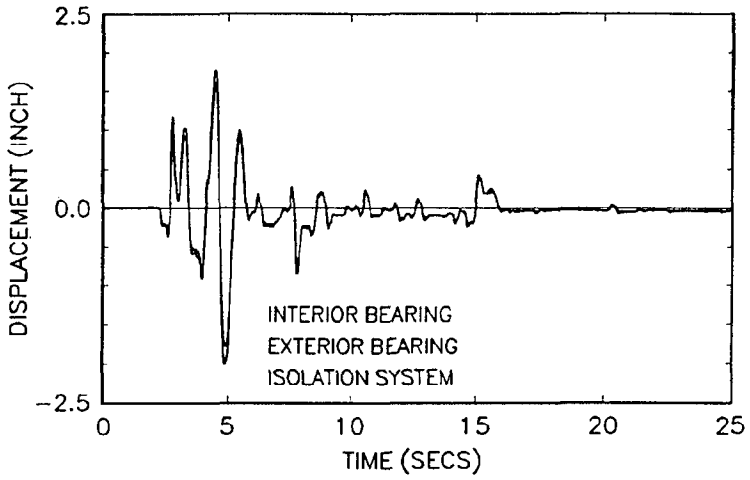

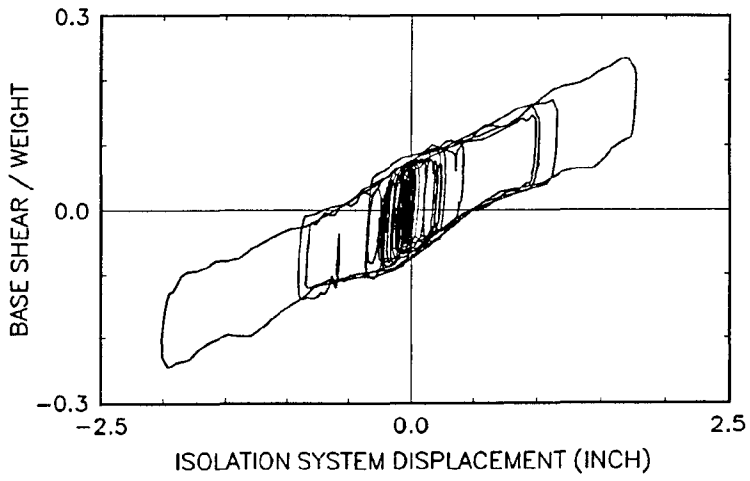

FIGURE 2-33 Isolation System Response for BFBIS for El Centro S00E 200%

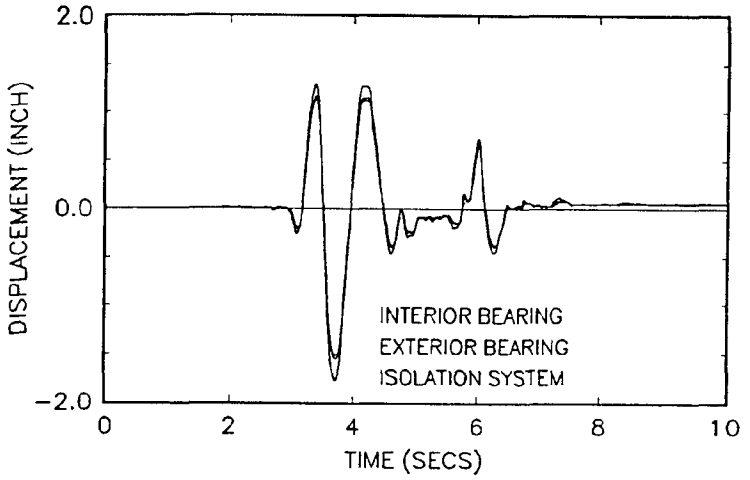

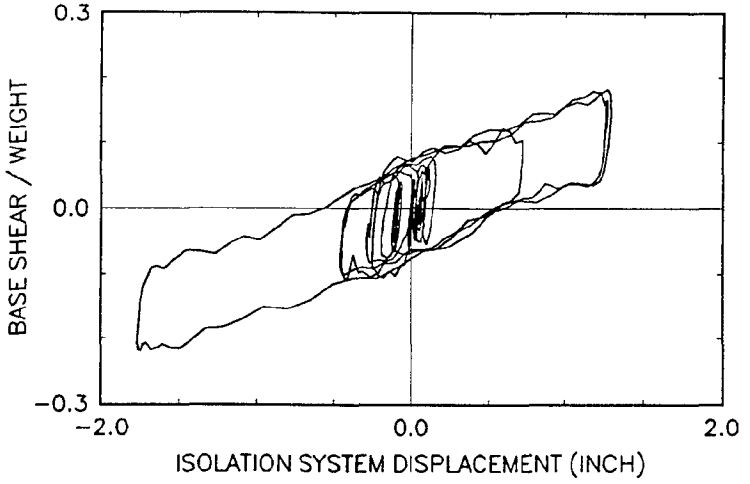

FIGURE 2-34 Isolation System Response for BFBIS for Pacoima S74W 100%

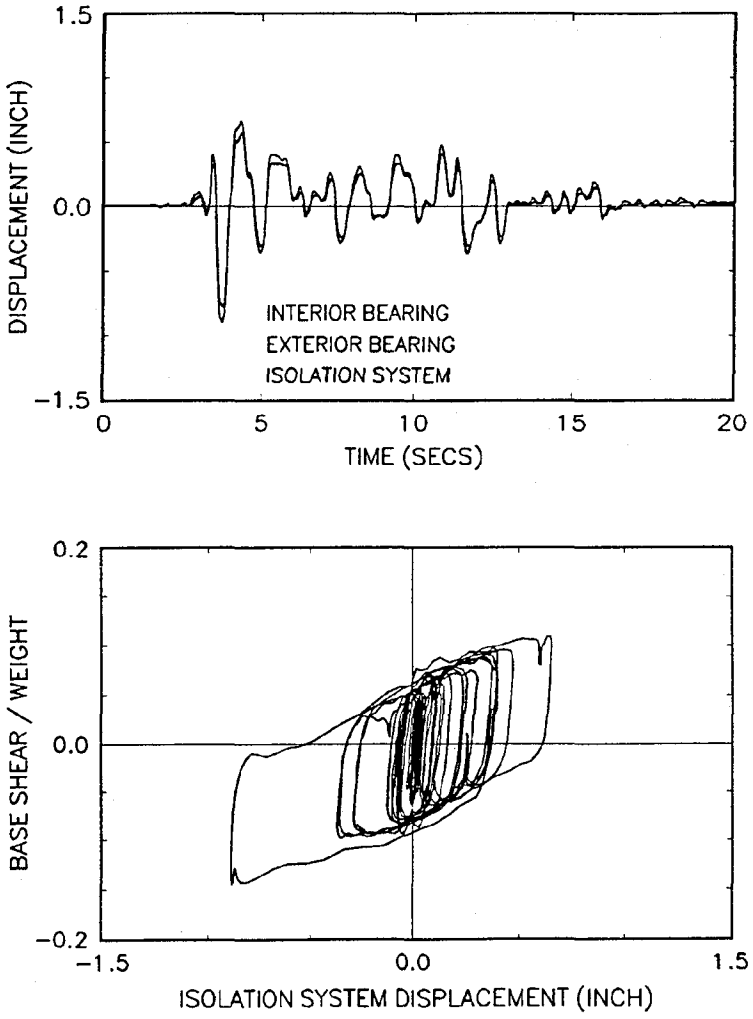

FIGURE 2-35 Isolation System Response for BFBIS for Hachinohe NS 150%

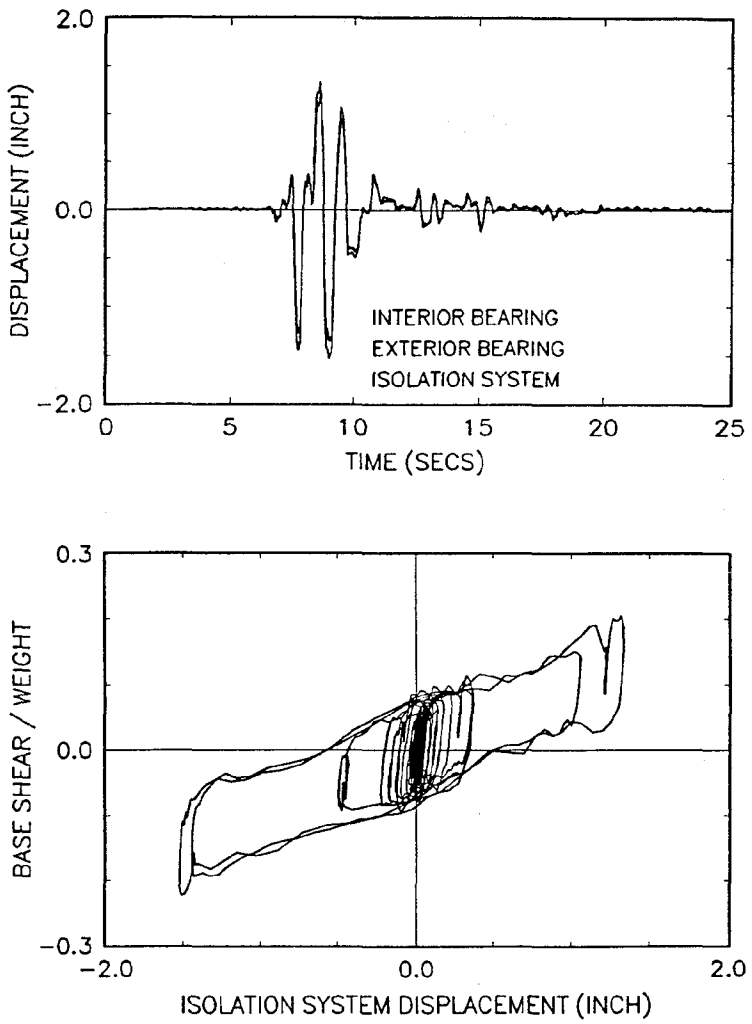

FIGURE 2-36 Isolation System Response for BFBIS for Miyagi-Ken-Oki EW 500%

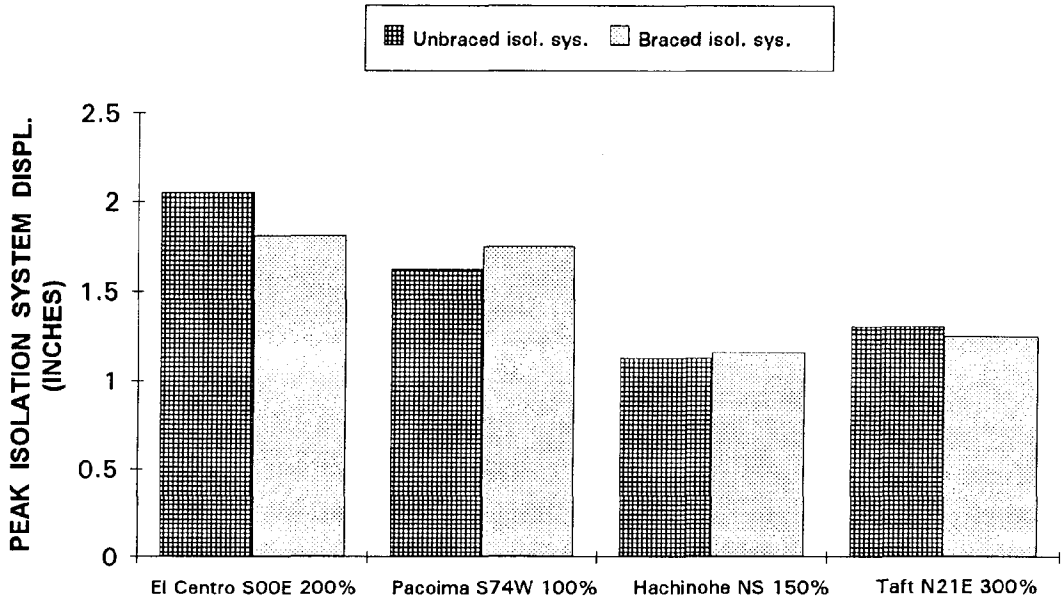

FIGURE 2-37 Comparison of Isolation System Displacement in Moment Frames for Braced and Unbraced Isolation Story

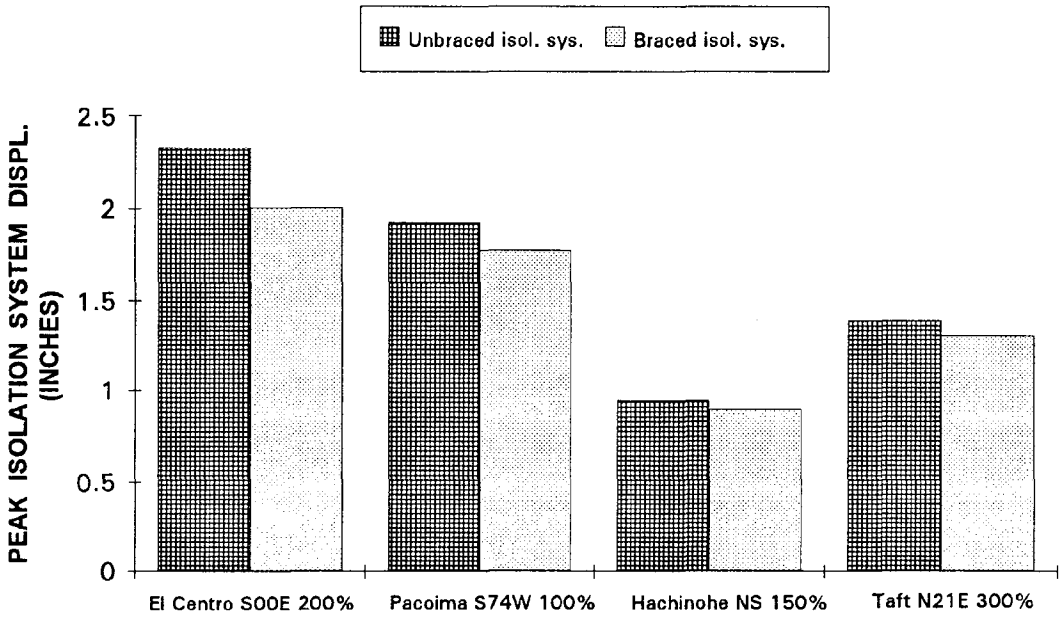

FIGURE 2-38 Comparison of Isolation System Displacement in Braced Frames for Braced and Unbraced Isolation Story

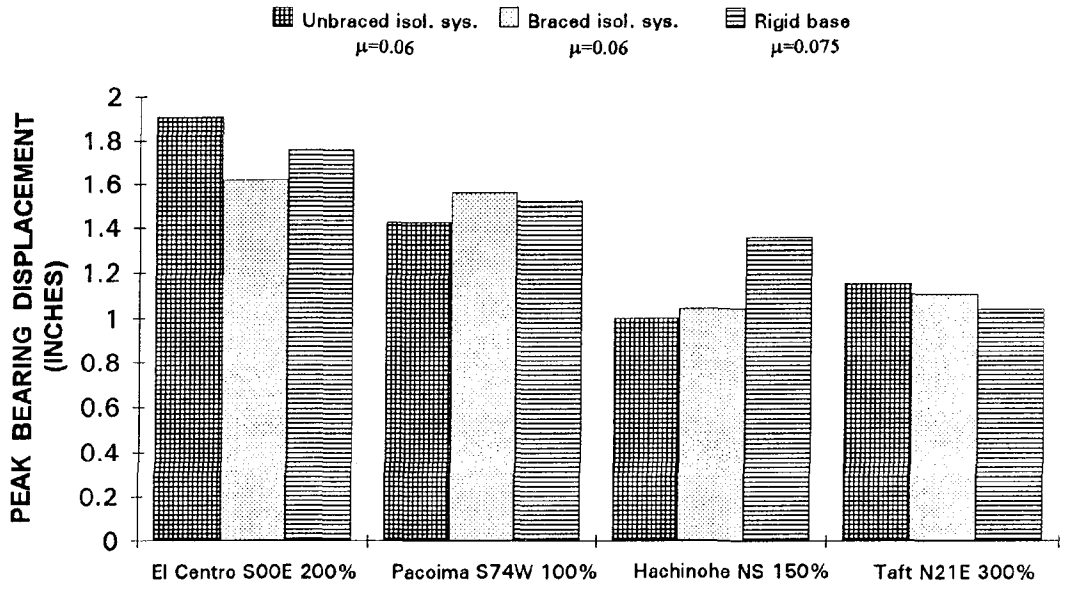

FIGURE 2-39 Comparison of Individual Isolator Displacement in Moment Frames for Three Different Isolation System Configurations

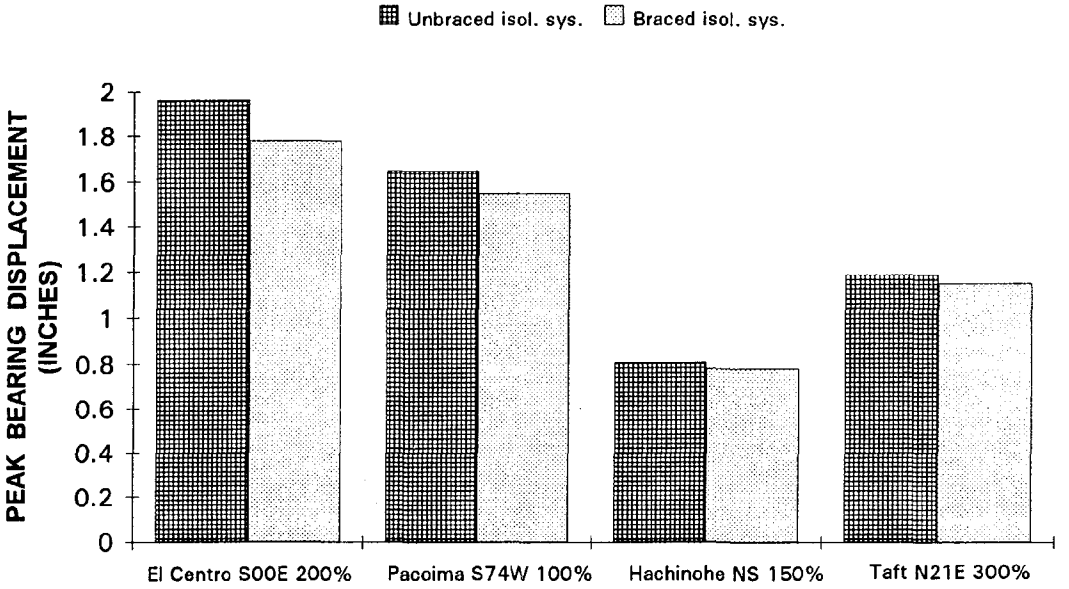

FIGURE 2-40 Comparison of Individual Isolator Displacement in Braced Frames for Braced and Unbraced Isolation Story

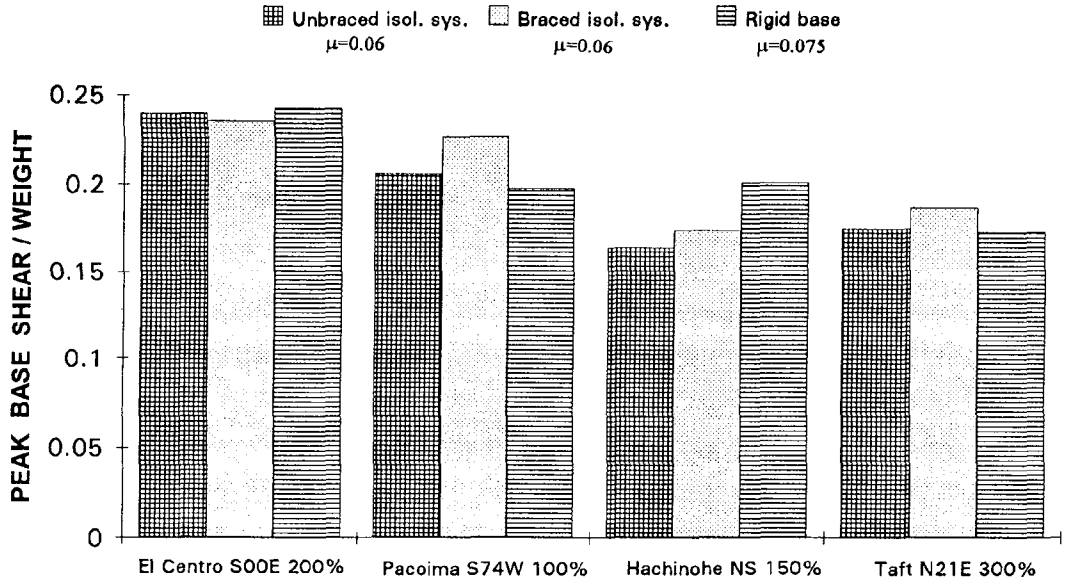

FIGURE 2-41 Comparison of Base Shear in Moment Frames for Three Different Isolation System Configurations

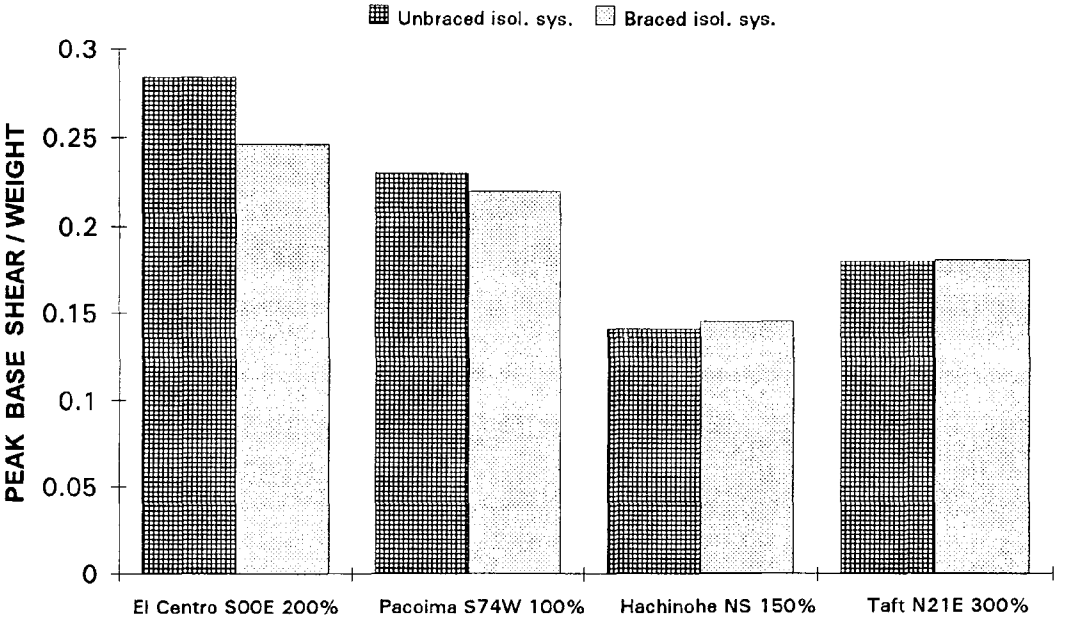

FIGURE 2-42 Comparison of Base Shear in Braced Frames for Braced and Unbraced Isolation Story

SECTION 3

RESPONSE OF ISOLATED STRUCTURE

3.1 Comparison of Response of Isolated and Non-isolated Structure

Shake table tests have been performed on the non-isolated fixed base moment frame (MFF) for comparison with the isolated moment frame (MFUIS). The same earthquake record is used but at different strength levels, such that the structure drifts remain within elastic limits at all times. Table 3-I presents the response in the case of three different earthquakes El Centro S00E, Taft N21E and Hachinohe NS. The strength of the earthquake expressed as a percentage of the actual record that results in comparable structure shear forces and story drifts is listed in the table. It can be seen that the effect of 35% El-Centro on the non-isolated structure is about the same as that of 200% El-Centro on the isolated structure. All comparisons show that the isolated structure can withstand earthquake shaking 4 to 6 times stronger than the non-isolated structure, while remaining within its elastic drift limit. The bottom story drift is expressed with respect to the exterior and interior column base. This isolation story drift for the isolated structure is much larger than its counterpart, because the column bottom is free to slide and rotate and is not fixed to the table as in the fixed base structure.

Response spectra of floor accelerations, normalized with respect to the peak ground spectral acceleration, for the non-isolated and isolated moment frame are presented in figures 3-1 and 3-2 respectively. The acceleration spectra are computed from experimental records time scaled up by a factor of two, in order to represent prototype conditions. For the non-isolated frame El Centro 35% is presented, while for the isolated moment frame El Centro 200% is presented, since they result in comparable structure shear forces and story drifts. Normalized spectral accelerations for the 1st floor, 3rd floor and the 7th floor are presented, along with the normalized spectrum for the ground (table) motion.

The non-isolated structure has floor response spectra much higher than the ground motion spectra. Amplification of accelerations is observed in the floors with increased height. The peak spectral values in the upper floors correspond to the fundamental period (0.91 sec) of the prototype structure. For the non-isolated structure, the peak floor spectral acceleration is about 8 times greater than the peak ground spectral acceleration, and occurs at the building's natural period, indicating that substantial dynamic amplification effects have occurred. On the

TABLE 3-I Comparison between Non-isolated and Isolated Moment Frame

Story	Non-isolated (MFF) El Centro S00E 35%		Isolated (MFUIS) El Centro S00E 200%		Non-isolated (MFF) Taft N21E 75%		Isolated (MFUIS) Taft N21E 300%		Non-isolated (MFF) Hachinohe NS 35%		Isolated (MFUIS) Hachinohe NS 150%	
	Shear / Weight	Drift / Height (%)	Shear / Weight	Drift / Height (%)	Shear / Weight	Drift / Height (%)	Shear / Weight	Drift / Height (%)	Shear / Weight	Drift / Height (%)	Shear / Weight	Drift / Height (%)
7	0.077	0.231	0.083	0.318	0.06	0.187	0.065	0.194	0.038	0.123	0.058	0.154
6	0.138	0.339	0.143	0.42	0.111	0.278	0.097	0.267	0.073	0.174	0.086	0.194
5	0.181	0.387	0.159	0.453	0.147	0.34	0.127	0.316	0.099	0.218	0.1	0.22
4	0.21	0.458	0.168	0.501	0.184	0.401	0.141	0.358	0.118	0.26	0.124	0.288
3	0.218	0.46	0.206	0.569	0.212	0.463	0.148	0.364	0.133	0.293	0.132	0.29
2	0.22	0.361	0.226	0.435	0.224	0.36	0.149	0.264	0.145	0.227	0.152	0.24
1	0.235	0.281 (Ex) 0.284 (In)	0.24	1.396 (Ex) 0.875 (In)	0.235	0.328 (Ex) 0.294 (In)	0.175	0.753 (Ex) 0.519 (In)	0.153	0.215 (Ex) 0.232 (In)	0.164	0.611 (Ex) 0.438 (In)

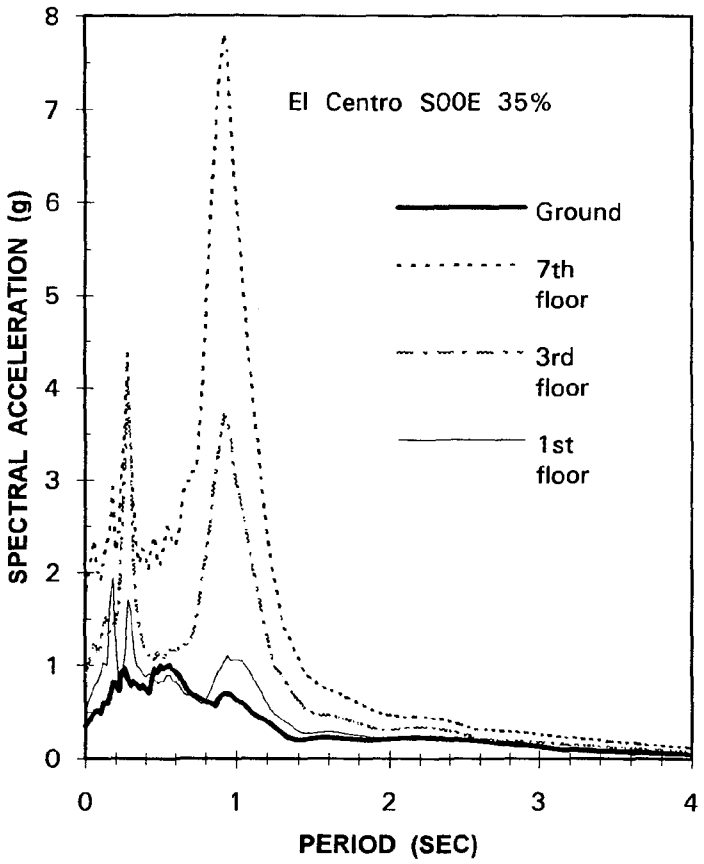

FIGURE 3-1 Response Spectra for Floor Acceleration in Non-Isolated Moment Frame (MFF)

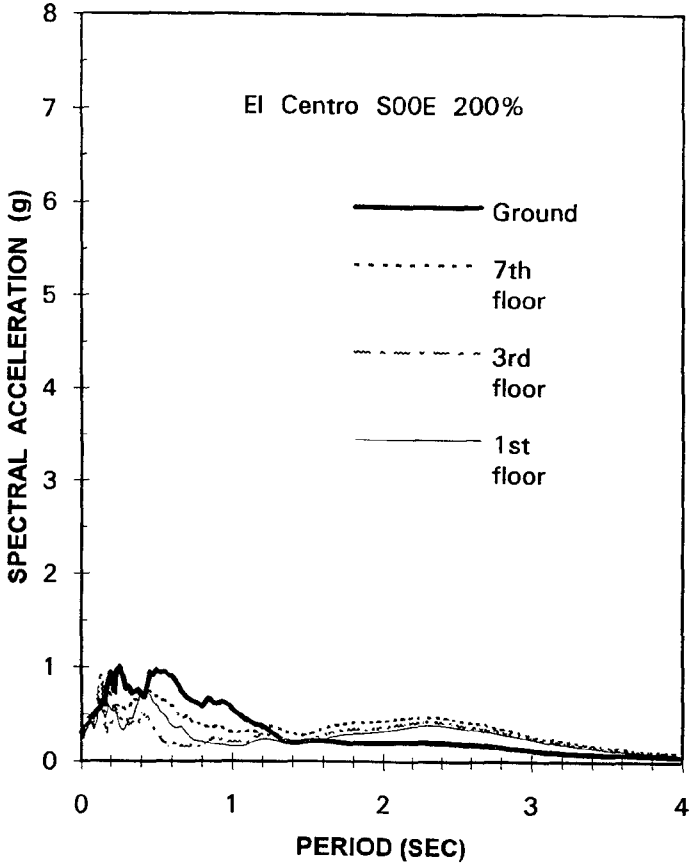

FIGURE 3-2 Response Spectra for Floor Acceleration in Isolated Moment Frame (MFUIS)

other hand, for the isolated structure, the peak floor spectral acceleration is about the same or lower than the peak ground spectra and occurs within the dominant period range of the ground motion. For the non-isolated structure, it is observed that the floor spectral accelerations exceed the ground spectral accelerations at all periods. For the isolated structure, it is observed that at periods greater than 1.4 seconds, the floor spectral accelerations exceed the ground spectral acceleration, and are about the same strength as the floor spectra of the non-isolated structure. Therefore, the isolation system significantly reduced the floor accelerations for periods in the range of the natural periods of the non-isolated structure. On the other hand, for periods approaching and exceeding the isolated structure period, the isolation system did not significantly affect the floor spectral accelerations.

3.2 Response of Upper Structure

In this section, an overall picture of the response of the upper structure (stories 2 to 7) above the isolation story will be presented. Table 3-II presents the list of the principal response quantities of the first story and upper stories for different shake table motions. Also included are table motion characteristics such as peak table acceleration, velocity and displacement. This list represents the non-isolated moment frame MFF and the different structural configurations of the isolated 7-story frame. The results are listed in the same chronological order as the tests were performed. The maximum upper story shear (in stories 2 to 7) and the maximum upper story drift (presented as a percentage of the story height) are presented. The story at which these maxima occur is listed in parenthesis. Peak responses for the floor accelerations, story shears, story drifts in the different floors and stories of the structure as well as peak bearing displacements and isolation system displacement are listed for a few selected cases in Table 3-III.

When over viewing all structure configurations, the maximum upper story shear is observed to occur in the 2nd, 3rd and 4th story, while the maximum story drift is found to occur in the 3rd or 4th story. Story drifts were naturally smaller for the braced frame when compared to the moment frame. However, they were not as small as theoretically obtained, since the braces were only partially effective (section 2.3.1). Similarly, story shears were higher for the braced frame when compared to the moment frame, but not as high as theoretically obtained since the braces were only partially effective. The maximum upper story shear coefficient (normalized with respect to structure weight) ranges usually from 0.1 to 0.24. Extreme loading cases where the earthquake strength significantly exceeded the design earthquake, and the displacement restraint was engaged, are marked with an asterisk, and discussed in detail in Section 5.

TABLE 3-II Summary of Experimental Results Showing Table Motion Characteristics and Peak Structure Response (Value in parenthesis is story at which peak value was recorded)

Excitation	Structure Isolation System	Table Motion			First Story Shear / Weight	Upper Story Shear / Weight	Upper Story Drift / Height (%)	Isolation System Displ. (inch)	Residual Bearing Displ. (inch)
		Accel. (g)	Vel. (in/sec)	Displ. (in)					
El Centro S00E 35%	MF-FIXED	0.11	2.57	0.34	0.235	0.22 (2)	0.460 (3)		
Taft N21E 75%	MF-FIXED	0.11	2.1	0.45	0.235	0.224 (2)	0.463 (3)		
Hachinohe NS 35%	MF-FIXED	0.09	1.9	0.49	0.153	0.145 (2)	0.293 (3)		
El Centro S00E 100%	MFUIS	0.29	6.27	0.96	0.106	0.11 (2,4)	0.245 (4)	0.57	0.006
El Centro S00E 150%	MFUIS	0.44	9.77	1.43	0.17	0.164 (2)	0.347 (3)	1.261	0.006
El Centro S00E 175%	MFUIS	0.51	11.33	1.67	0.207	0.194 (2)	0.437 (3)	1.626	0.006
El Centro S00E 200%	MFUIS	0.58	13.07	1.93	0.24	0.226 (2)	0.569 (3)	2.053	0
Taft N21E 200%	MFUIS	0.31	5.27	1.16	0.124	0.107 (2)	0.218 (4)	0.788	0.012
Taft N21E 300%	MFUIS	0.46	7.84	1.74	0.175	0.149 (2)	0.364 (3)	1.309	0.017
Taft N21E 400%	MFUIS	0.6	10.5	2.32	0.218	0.196 (3)	0.546 (3)	1.828	0.012
Pacoima S74W 50%	MFUIS	0.42	5.63	0.58	0.116	0.124 (4)	0.250 (4)	0.743	0.012
Pacoima S74W 75%	MFUIS	0.62	8.1	0.86	0.159	0.176 (4)	0.354 (4)	1.168	0.006
Pacoima S74W 100%	MFUIS	0.76	11.07	1.17	0.206	0.2 (4)	0.438 (4)	1.626	0.006
Pacoima S16E 50%	MFUIS	0.45	10.03	1.63	0.194	0.182 (3)	0.472 (3)	1.577	0.011
Pacoima S16E 60%	MFUIS	0.56	11.98	1.96	0.228	0.223 (3)	0.612 (3)	1.917	0.006
Pacoima S16E 60%	MFUIS	0.55	12.16	1.96	0.226	0.221 (3)	0.608 (3)	1.918	0.006
Hachinohe NS 100%	MFUIS	0.24	5.38	1.33	0.128	0.128 (2)	0.227 (3)	0.819	0.04
Hachinohe NS 150%	MFUIS	0.35	8.1	1.99	0.164	0.152 (2)	0.290 (3)	1.13	0.039
Miyagi-Ken-Oki EW 300%	MFUIS	0.45	7.03	1.43	0.119	0.149 (2)	0.315 (4)	0.73	0.023
Miyagi-Ken-Oki EW 500%	MFUIS	0.74	11.54	2.3	0.181	0.180 (2)	0.451 (4)	1.441	0.018
Caltrans 0.6g Rock 1 50%	MFUIS	0.28	5.89	2.43	0.113	0.110 (2)	0.218 (4)	0.579	0.08
Caltrans 0.6g Rock 1 100%	MFUIS	0.57	11.58	4.84	0.216	0.199 (2)	0.523 (3)	1.828	0.114
Caltrans 0.6g Rock 2 100%	MFUIS	0.62	10.77	3.04	0.161	0.153 (2)	0.302(3)	1.198	0.05
Caltrans 0.6g Alluvium 1 50%	MFUIS	0.31	10.66	3.3	0.115	0.120 (2)	0.215 (3)	0.653	0.08
Caltrans 0.6g Alluvium 1 75%	MFUIS	0.47	15.8	4.92	0.161	0.153 (2)	0.302 (3)	1.448	0.06

TABLE 3-II Summary of Experimental Results Showing Table Motion Characteristics and Peak Structure Response (Contd.)
(Value in parenthesis is story at which peak value was recorded)

Excitation	Structure Isolation System	Table Motion			First Story Shear / Weight	Upper Story Shear / Weight	Upper Story Drift / Height (%)	Isolation System Displ. (inch)	Residual Bearing Displ. (inch)
		Accel. (g)	Vel. (in/sec)	Displ. (in)					
El Centro S00E Hor.-Vert. 100%	MFUIS	0.33	6.44	0.95	0.154	0.137 (2)	0.310 (4)	0.543	0.017
El Centro S00E 205%	MFUIS	0.61	13.67	2.03	0.245	0.232 (2)	0.610 (3)	2.166	0.011
El Centro S00E 220% *	MFUIS	0.64	14.24	2.11	0.266	0.243 (2)	0.669 (3)	2.317	0.006
El Centro S00E 100%	BFUIS	0.31	6.53	1.05	0.112	0.109 (3)	0.106 (4)	0.639	0.06
El Centro S00E 200%	BFUIS	0.58	13.19	1.99	0.284	0.246 (2)	0.418 (3)	2.331	0.017
Taft N21E 300%	BFUIS	0.46	7.82	1.77	0.18	0.155 (2)	0.216 (2)	1.388	0.034
Pacoima S74W 100%	BFUIS	0.48	11.63	1.24	0.23	0.201 (2)	0.325 (3)	1.928	0.075
Pacoima S16E 60%	BFUIS	0.52	12.02	1.97	0.268	0.23 (2)	0.399 (3)	2.312	0.075
Hachinohe NS 150%	BFUIS	0.34	8.12	2	0.141	0.118 (2)	0.186 (3)	0.944	0.04
Miyagi-Ken-Oki EW 500%	BFUIS	0.71	11.69	2.3	0.188	0.177 (2)	0.271 (3)	1.381	0.068
Caltrans 0.6g Rock 1 100%	BFUIS	0.51	11.32	4.84	0.201	0.18 (2)	0.29 (3)	1.696	0.04
Caltrans 0.6g Alluvium 1 75%	BFUIS	0.44	15.64	4.93	0.17	0.153 (2)	0.211 (3,4)	1.186	0.006
El Centro S00E 195%	BFUIS	0.55	12.49	1.89	0.236	0.213 (2)	0.383 (3)	2.071	0.028
El Centro S00E 220% *	BFUIS	0.64	14.5	2.17	0.438	0.359 (2)	0.654 (3)	2.429	0
Miyagi-Ken-Oki EW 100%	BFUIS	0.16	2.37	0.52	0.087	0.090 (3)	0.149 (3)	0.143	0.023
Miyagi-Ken-Oki EW 200%	BFUIS	0.31	4.91	1.02	0.112	0.127 (4)	0.208 (4)	0.509	0.017
Taft N21E 100%	BFUIS	0.15	2.65	0.59	0.088	0.098 (3)	0.171 (3)	0.152	0.017
El Centro S00E 100%	BFBIS	0.32	6.34	0.98	0.113	0.143 (3)	0.232 (3)	0.503	0.045
El Centro S00E 200%	BFBIS	0.58	12.83	1.95	0.246	0.204 (3)	0.393 (3)	2.008	0.033
El Centro S00E 220% *	BFBIS	0.66	14.27	2.14	0.346	0.285 (2)	0.533 (3)	2.325	0.005
Taft N21E 300%	BFBIS	0.46	8.03	1.8	0.181	0.166 (2)	0.317 (3)	1.306	0.011
Pacoima S74W 100%	BFBIS	0.77	11.77	1.23	0.22	0.211 (2)	0.462 (3)	1.774	0.049
Pacoima S16E 60%	BFBIS	0.54	11.94	1.97	0.246	0.234 (2)	0.504 (3)	2.149	0.114
Hachinohe NS 150%	BFBIS	0.32	8.02	2	0.145	0.123 (2)	0.217 (3)	0.893	0.017
El Centro S00E 230% *	BFBIS	0.69	14.97	2.26	0.468	0.376 (2)	0.661 (3)	2.347	0.062

* Displacement restraint engaged

TABLE 3-II Summary of Experimental Results Showing Table Motion Characteristics and Peak Structure Response (Contd.)
(Value in parenthesis is story at which peak value was recorded)

Excitation	Structure Isolation System	Table Motion			First Story Shear Weight	Upper Story Shear Weight	Upper Story Drift Height (%)	Isolation System Displ. (inch)	Residual Bearing Displ. (inch)
		Accel. (g)	Vel. (in/sec)	Displ. (in)					
Miyagi-Ken-Oki EW 500%	BFBIS	0.76	12.54	2.52	0.222	0.196 (4)	0.375 (3)	1.527	0.005
Caltrans 0.6g Rock 1 100%	BFBIS	0.52	11.41	4.83	0.204	0.179 (2)	0.358 (3)	1.558	0.04
Caltrans 0.6g Alluvium 1 75%	BFBIS	0.43	15.6	4.93	0.168	0.155 (2)	0.258 (3)	1.093	0.011
El Centro S00E 100%	MFBIS	0.3	6.47	0.97	0.11	0.136 (4)	0.278 (3,4)	0.498	0.018
El Centro S00E 200%	MFBIS	0.59	13.04	1.94	0.236	0.222 (2)	0.513 (3)	1.813	0.017
Taft N21E 300%	MFBIS	0.45	8.12	1.8	0.187	0.157 (2)	0.346 (4)	1.256	0.022
Pacoima S74W 100%	MFBIS	0.78	11.39	1.23	0.227	0.216 (4)	0.483 (4)	1.753	0.005
Pacoima S16E 60%	MFBIS	0.52	11.98	1.97	0.236	0.211 (3)	0.546 (4)	1.894	0.011
Hachinohe NS 150%	MFBIS	0.35	8.04	2	0.174	0.156 (2)	0.274 (4)	1.165	0.065
Miyagi-Ken-Oki EW 500%	MFBIS	0.81	12.71	2.53	0.198	0.199 (4)	0.471 (4)	1.48	0.073
El Centro S00E 220%	MFBIS	0.64	14.32	2.13	0.271	0.246 (2)	0.617 (3)	2.238	0.02
Miyagi-Ken-Oki EW 200%	MFBIS	0.32	5.01	1.01	0.112	0.135 (2,3)	0.264 (4)	0.456	0.005
Miyagi-Ken-Oki EW 400%	MFBIS	0.66	10.03	2.03	0.164	0.179 (2)	0.422 (4)	1.218	0.005
Taft N21E 200%	MFBIS	0.3	5.36	1.2	0.125	0.114 (2)	0.226 (3)	0.759	0

TABLE 3-III Experimentally Recorded Peak Structure Response

Story or Floor	Structure : MFUIS El Centro S00E 200% Floor Accel. (g)	Shear / Weight	Drift / Height (%)	Structure : MFUIS El Centro S00E 220% * Floor Accel. (g)	Shear / Weight	Drift / Height (%)	Structure : MFUIS Taft N21E 200% Floor Accel. (g)	Shear / Weight	Drift / Height (%)	Structure : MFUIS Taft N21E 400% Floor Accel. (g)	Shear / Weight	Drift / Height (%)
7	0.61	0.083	0.318	0.65	0.088	0.385	0.39	0.053	0.132	0.53	0.071	0.292
6	0.45	0.143	0.42	0.49	0.153	0.488	0.26	0.063	0.17	0.43	0.114	0.375
5	0.38	0.159	0.453	0.43	0.171	0.547	0.26	0.09	0.196	0.34	0.162	0.437
4	0.39	0.168	0.501	0.42	0.181	0.587	0.24	0.094	0.218	0.41	0.188	0.506
3	0.4	0.206	0.569	0.44	0.221	0.669	0.29	0.098	0.203	0.43	0.196	0.546
2	0.39	0.226	0.435	0.42	0.243	0.493	0.23	0.107	0.175	0.46	0.189	0.411
1	0.47	0.24	1.396 (Ex) 0.875 (In)	0.5	0.266	1.681 (Ex) 1.096 (In)	0.28	0.124	0.466 (Ex) 0.349 (In)	0.5	0.218	0.773 (Ex) 1.157 (In)
Table	0.58			0.64			0.31			0.6		
Exterior Bearing Displ. (in)			1.909			2.048			0.648			1.47
Interior Bearing Displ. (in)			1.796			2			0.688			1.59
Isolation System Displ. (in)			2.053			2.317 *			0.788			1.828

* Displacement restraint engaged

TABLE 3-III Experimentally Recorded Peak Structure Response (Contd.)

Story or Floor	Structure : MFUIS Pacoima S74W 50%			Structure : MFUIS Pacoima S74W 100%			Structure : MFUIS Pacoima S16E 60%			Structure : MFUIS Hachinohe NS 150%		
	Floor Accel. (g)	Shear / Weight	Drift / Height (%)	Floor Accel. (g)	Shear / Weight	Drift / Height (%)	Floor Accel. (g)	Shear / Weight	Drift / Height (%)	Floor Accel. (g)	Shear / Weight	Drift / Height (%)
7	0.43	0.058	0.137	0.73	0.098	0.243	0.59	0.08	0.313	0.43	0.058	0.154
6	0.35	0.094	0.208	0.56	0.144	0.328	0.45	0.135	0.42	0.26	0.086	0.194
5	0.28	0.119	0.238	0.45	0.184	0.38	0.39	0.169	0.488	0.36	0.1	0.22
4	0.29	0.124	0.25	0.46	0.2	0.438	0.39	0.205	0.569	0.304	0.124	0.288
3	0.33	0.12	0.239	0.45	0.196	0.41	0.47	0.223	0.612	0.378	0.132	0.29
2	0.35	0.108	0.169	0.62	0.145	0.27	0.42	0.2	0.442	0.27	0.152	0.24
1	0.38	0.116	0.346 (Ex) 0.296 (In)	0.67	0.206	0.84 (Ex) 0.656 (In)	0.52	0.228	1.238 (Ex) 0.845 (In)	0.304	0.164	0.611 (Ex) 0.438 (In)
Table	0.42			0.76			0.56			0.345		
Exterior Bearing Displ. (in)			0.638			1.367			1.533			0.951
Interior Bearing Displ. (in)			0.655			1.423			1.658			1
Isolation System Displ. (in)			0.743			1.626			1.917			1.13

TABLE 3-III Experimentally Recorded Peak Structure Response (Contd.)

Story or Floor	Structure : MFUIS Miyagi-Ken-Oki EW 500% Floor Accel. (g)	Shear / Weight	Drift / Height (%)	Structure : MFUIS Caltrans Rock 1 100% Floor Accel. (g)	Shear / Weight	Drift / Height (%)	Structure : MFUIS Caltrans Rock 2 100% Floor Accel. (g)	Shear / Weight	Drift / Height (%)	Structure : MFUIS Caltrans Alluvium 1 75% Floor Accel. (g)	Shear / Weight	Drift / Height (%)
7	0.69	0.093	0.234	0.58	0.077	0.269	0.48	0.065	0.163	0.49	0.065	0.168
6	0.49	0.15	0.368	0.39	0.126	0.375	0.3	0.095	0.236	0.37	0.093	0.229
5	0.42	0.184	0.399	0.38	0.149	0.354	0.38	0.106	0.237	0.36	0.125	0.229
4	0.45	0.192	0.451	0.44	0.173	0.469	0.4	0.124	0.294	0.33	0.137	0.333
3	0.47	0.179	0.406	0.4	0.193	0.523	0.36	0.139	0.302	0.41	0.157	0.345
2	0.52	0.18	0.333	0.39	0.199	0.408	0.42	0.153	0.262	0.36	0.163	0.286
1	0.57	0.181	0.876 (Ex) 0.602 (In)	0.41	0.216	1.06 (Ex) 0.65 (In)	0.46	0.161	0.573 (Ex) 0.533 (In)	0.43	0.171	0.685 (Ex) 0.514 (In)
Table	0.74			0.57			0.62			0.47		
Exterior Bearing Displ. (in)			1.18			1.498			1.104			1.236
Interior Bearing Displ. (in)			1.261			1.626			1.038			1.302
Isolation System Displ. (in)			1.441			1.828			1.198			1.448

The residual bearing displacement, which is the permanent bearing displacement at the end of the shake table motion, is also presented in table 3-II. In most cases, it was negligibly small. The maximum value was 0.11 inches which was about 5.5% of the bearing displacement capacity. This occurred in a test with artificial earthquake input. Excluding the artificial earthquakes, the maximum residual displacement was 0.075 inches or nearly 4% of the bearing displacement capacity.

The repeatability of structure response can also be studied from the table. Table 3-II lists the same earthquake Pacoima S16E 60% performed twice on the same MFUIS structure. Results are basically the same for the repeated tests. Also El Centro S00E 200% test may be compared with El Centro S00E 205% performed the following day with several tests performed in between. The later produced consistent results showing slightly greater response quantities, indicating that the isolator properties remained unchanged.

The influence of the various structural configurations on the peak superstructure responses is studied. Figures 3-3 and 3-4 show the effect of bracing in the isolation story on the peak upper story shear of a moment frame and braced frame respectively. A selected group of four strong motions is represented.

Using a braced or unbraced isolation story did not significantly affect the isolation bearing response, but did change the stiffness and dynamic characteristics of the structure, and somewhat affect upper story shears and drifts. These effects were accounted for in the analytical models by including the flexibility of the first story framing members (Section 4). However, drift responses in the braced frame were not always consistent because of slipping of the braces due to the elongated holes.

The effects of having a rigid base isolation system (see section 2.3.2), as compared to either a brace or unbraced isolation story are shown in Figure 3-5. The peak upper story drifts are similar for the three isolation system cases, even though the friction values of isolators for the rigid base case was 0.075, as compared to 0.060 for the braced and unbraced isolation system cases. In all cases the behavior of the isolation system and upper structure were consistent with the assumed behavior and could be accurately predicted using analytical models which included the characteristics of the isolation system and upper structure. The installation of the

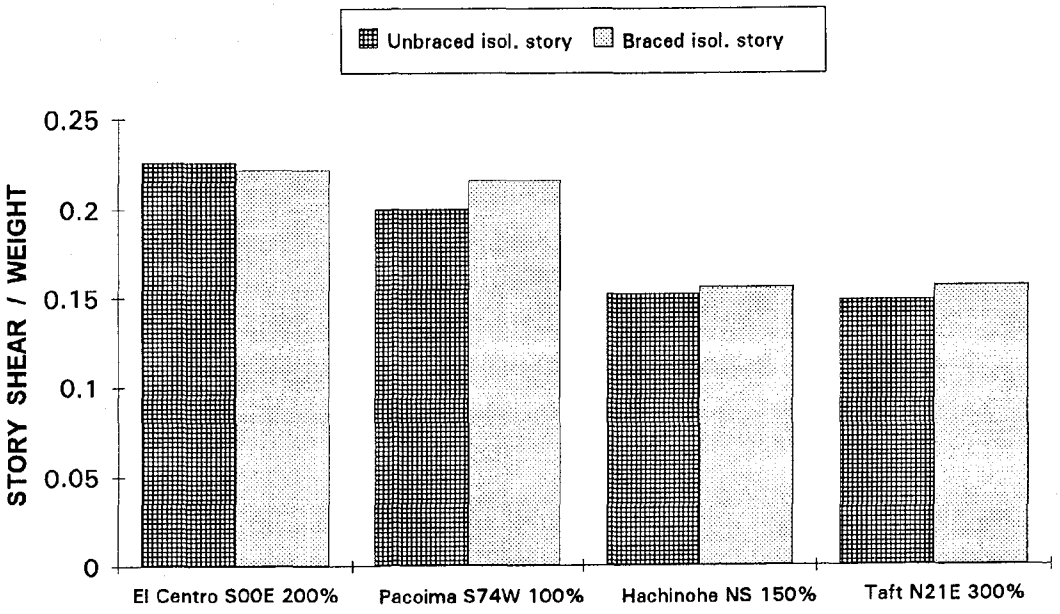

FIGURE 3-3 Comparison of Peak Upper Story Shear in Moment Frame for Braced and Unbraced Isolation Story

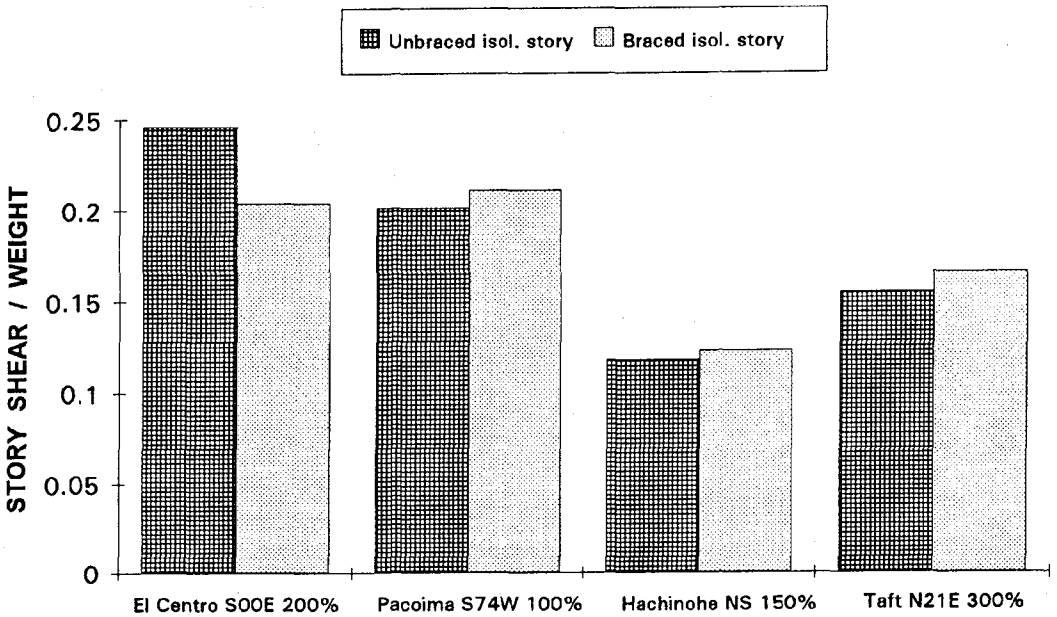

FIGURE 3-4 Comparison of Peak Upper Story Shear in Braced Frame for Braced and Unbraced Isolation Story

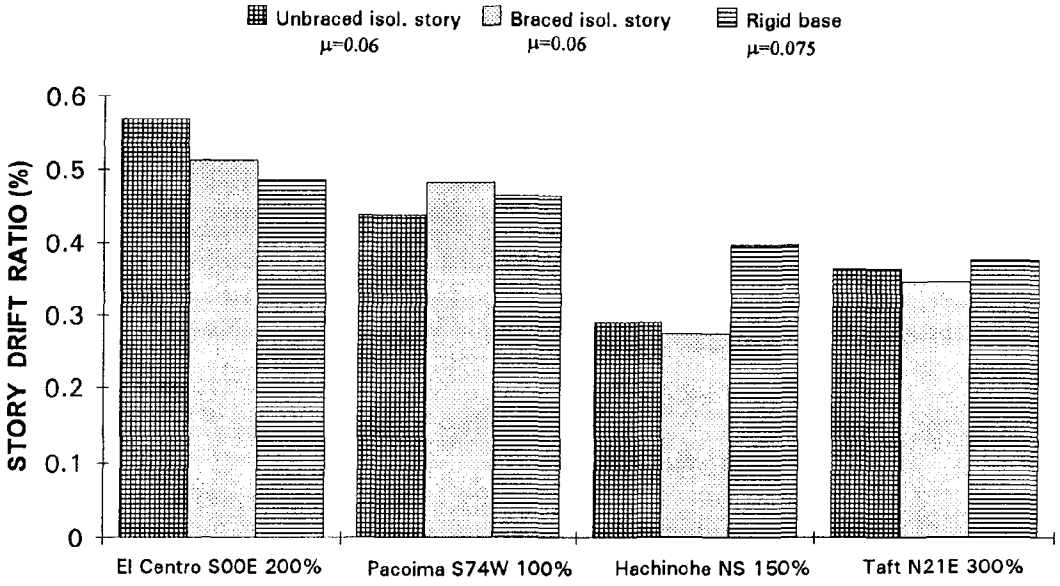

FIGURE 3-5 Comparison of Peak Upper Story Drift in Moment Frame for Different Isolation System Configurations

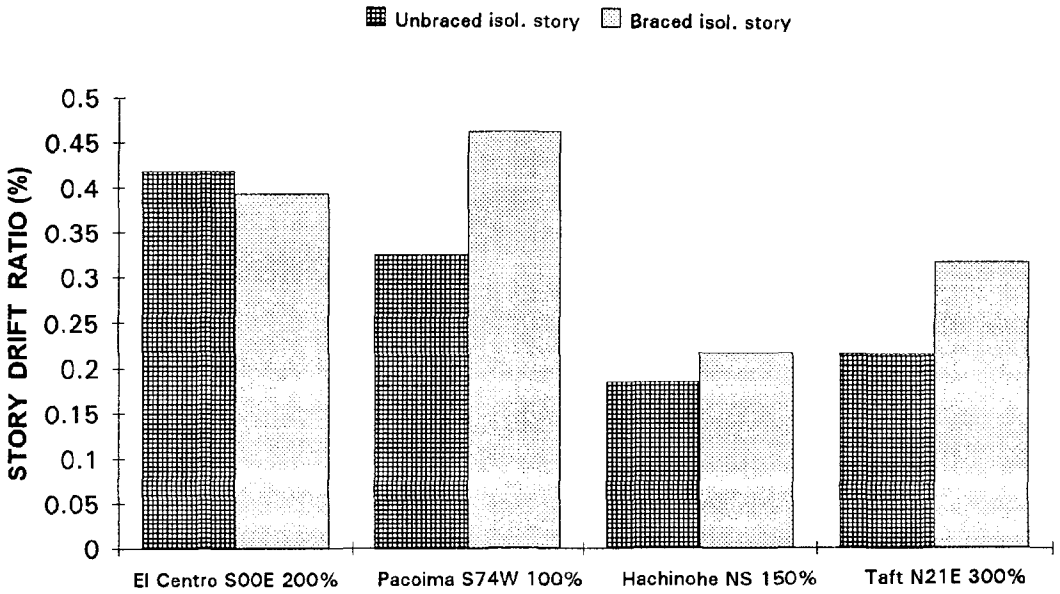

FIGURE 3-6 Comparison of Peak Upper Story Drift in Braced Frame for Braced and Unbraced Isolation Story

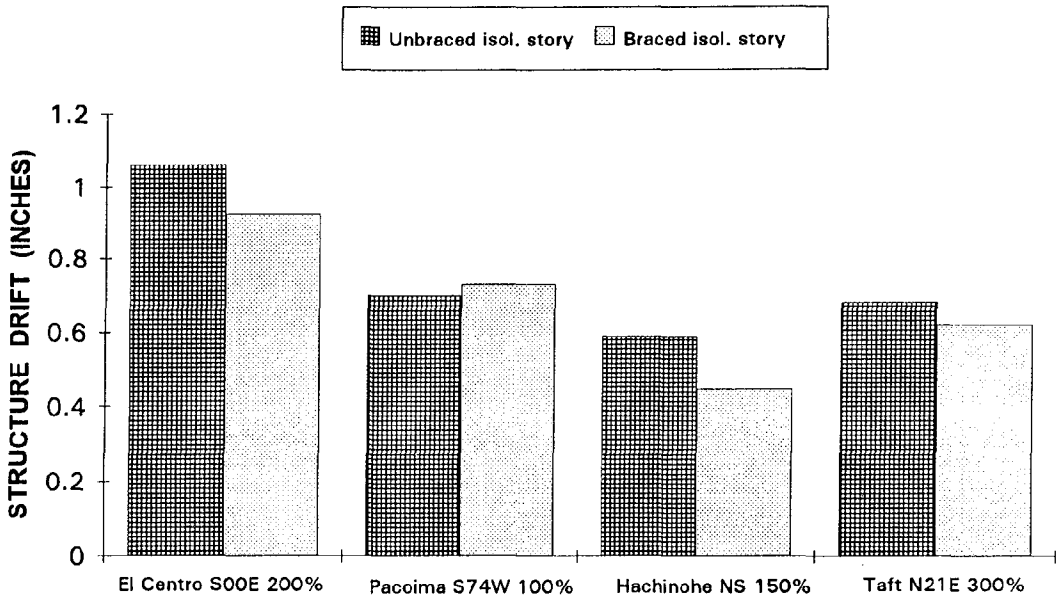

FIGURE 3-7 Comparison of Peak Structure Drift (Displ. of Top Floor wrt. Column Base) in Moment Frame for Braced and Unbraced Isolation Story

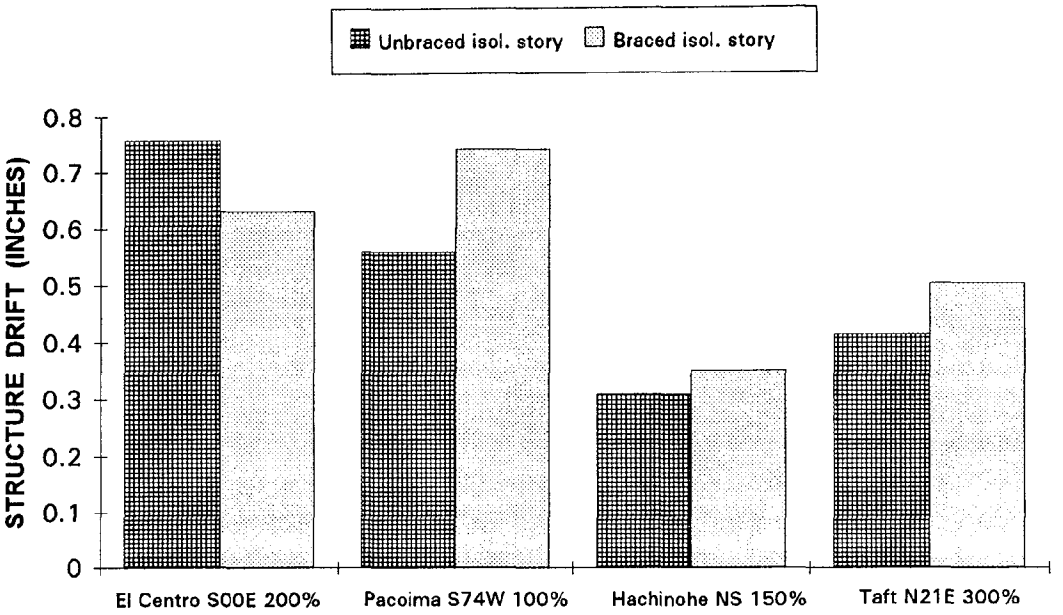

FIGURE 3-8 Comparison of Peak Structure Drift (Displ. of Top Floor wrt. Column Base) in Braced Frame for Braced and Unbraced Isolation Story

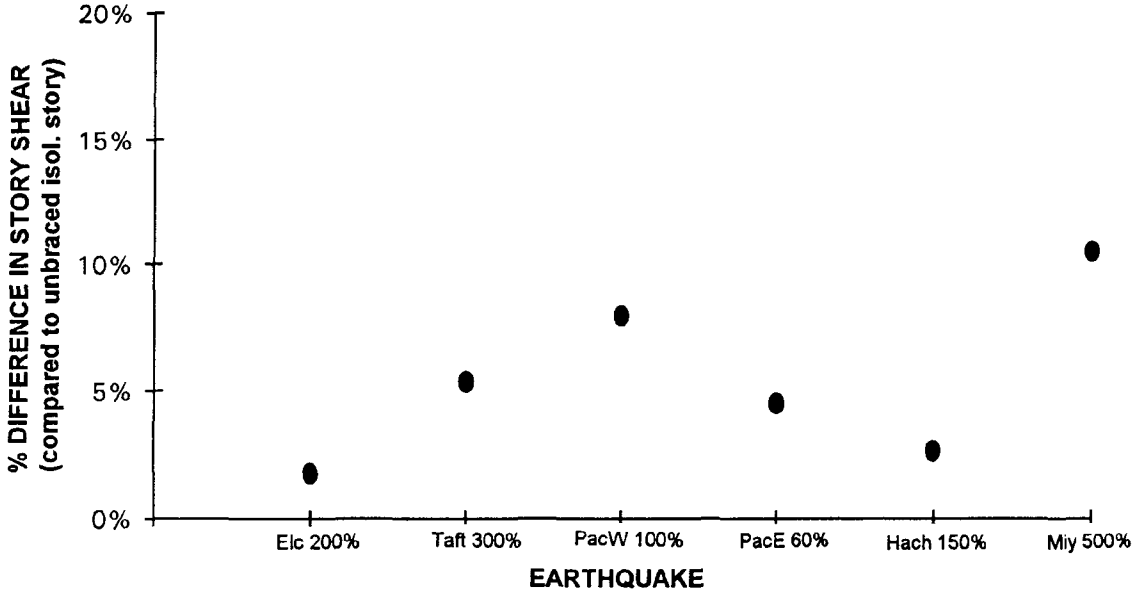

FIGURE 3-9 Effect of Bracing Isolation Story on Peak Story Shear of Moment Frame

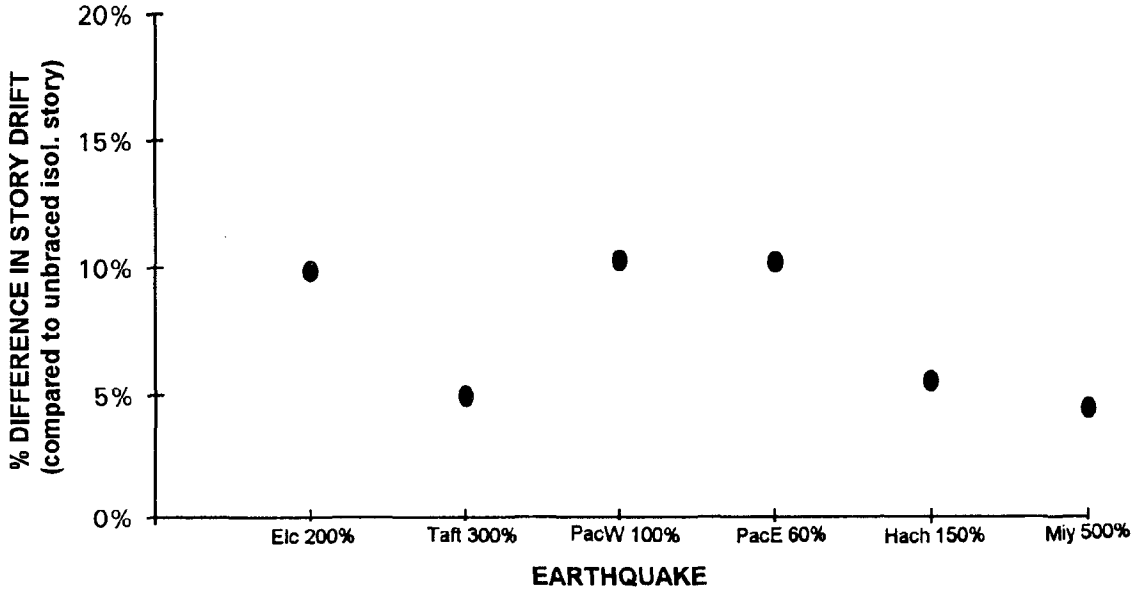

FIGURE 3-10 Effect of Bracing Isolation Story on Peak Inter-Story Drift of Moment Frame

isolators at the bases of the individual first story columns, as compared to beneath a rigid diaphragm base, did not significantly affect the behavior of the isolation bearings or system. The articulated joint of the Friction Pendulum isolators accommodated the required joint rotations with no affect on the isolator properties.

When isolators were installed at the bases of cantilever columns, different isolator displacements were observed at different column locations. The differences in isolator displacements were small in comparison to the total isolator displacements. The relative differences in isolator displacements had no measurable effect on the overall response of the isolation system or the upper story shears and drifts. The differences in displacements were accounted for in analytical models which included the flexibility of the frame members. Bracing the column bases together with horizontal braces achieved equal displacements in the isolators, but did not affect the overall response of the isolation system or the upper structure, or the ability to analytically predict the structure response.

The shears and drifts occurring in the upper structure were affected by the shear stiffness of the framing in the isolation story. The diagonal bracing added to the framing in the isolation story changed the stiffness and dynamic characteristics of structure. Figure 3-5 and 3-6 presents the effect of diagonally bracing the isolation story on the peak upper story drift (braced isolation story versus unbraced isolation story). Figures 3-7 and 3-8 represent the effect of diagonally bracing the isolation story on the peak structure drift. The structure drift (or total structure drift) is defined as the total drift of the structure above the isolation bearings including the flexure of the first story columns. Figures 3-9 and 3-10 summarize the effect of diagonally bracing the isolation story on the story shears and drifts of the moment frame. The difference between the braced and unbraced isolation story is expressed as a percentage of the unbraced results. The differences in the peak story shears and drifts are observed to be about 10% or less. This difference is attributed to the changed stiffness and dynamic characteristics of structure. Analytical models which accounted for the stiffness of the framing in the isolation story were able to account for the observed response of the upper structure and isolation system.

The distribution of lateral displacements along the 7-story frame height for earthquakes El Centro S00E 200% and Hachinohe NS 150% is shown in figures 3-11 and 3-12. The experimental peak story drifts are normalized with respect to the peak total drift, which is the displacement of the structure top with respect to the ground to show the relative amount of the displacement within the isolators. These normalized peak story drifts are accumulated

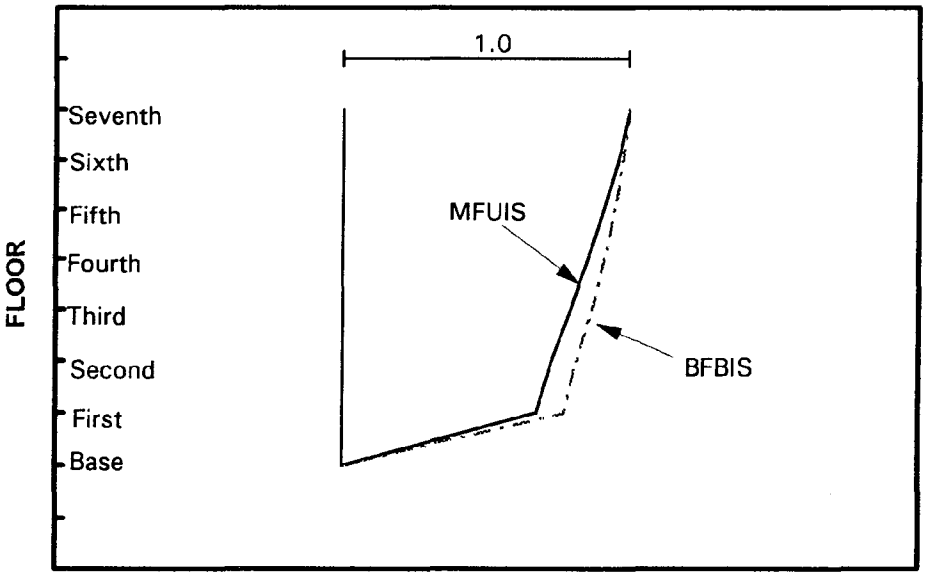

FIGURE 3-11 Distribution of Peak Lateral Displacements along the Structure Height for El Centro S00E 200% Motion

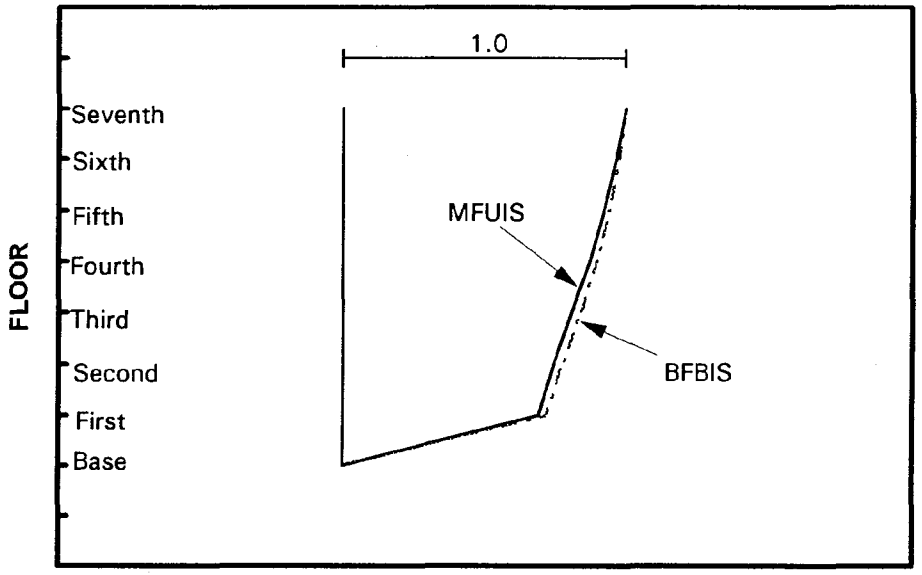

FIGURE 3-12 Distribution of Peak Lateral Displacements along the Structure Height for Hachinohe NS 150% Motion

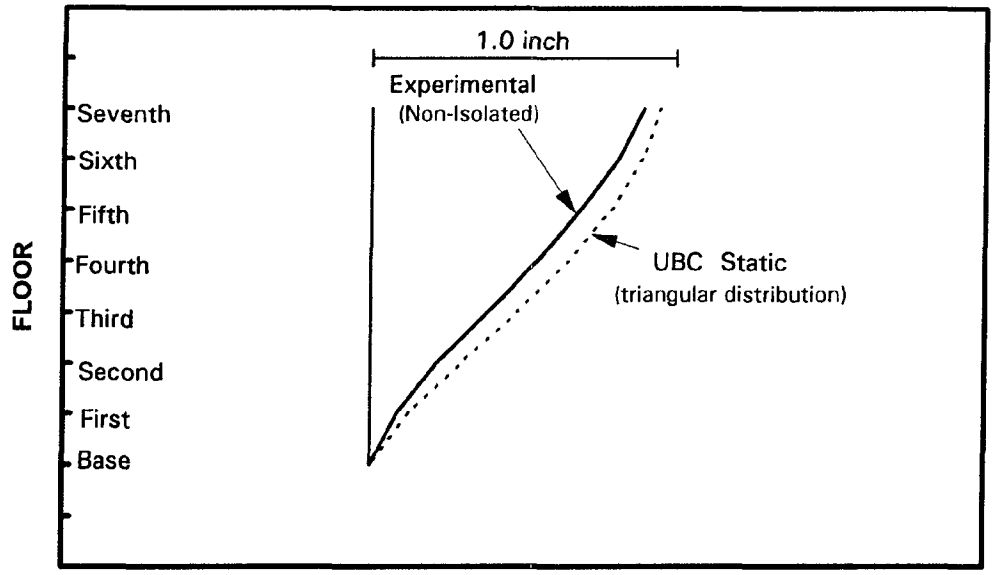

FIGURE 3-13 Comparison of Peak Experimental Lateral Displacements in Non-Isolated MFF with 1991 UBC Static Analysis for El Centro S00E 35%

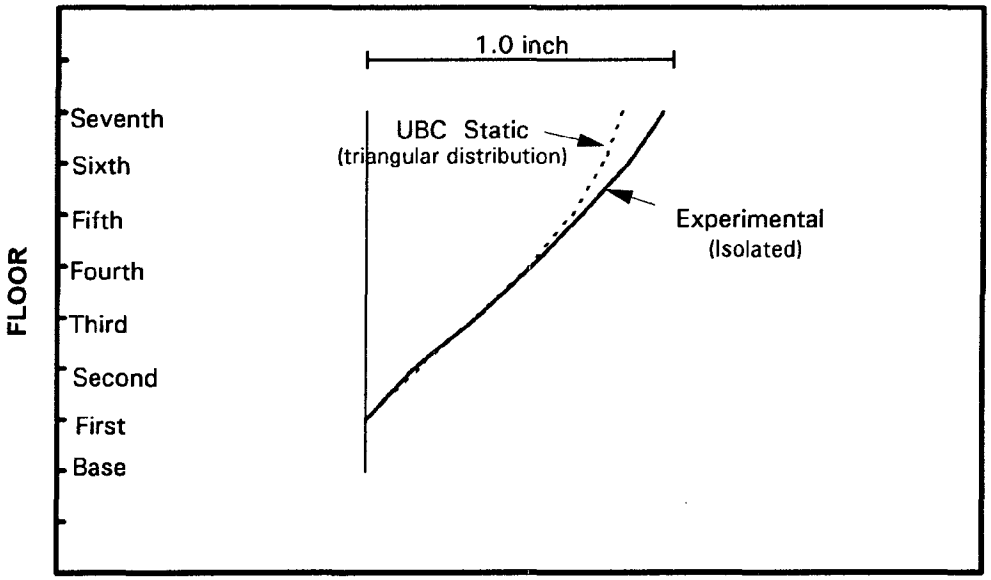

FIGURE 3-14 Comparison of Peak Experimental Lateral Displacements in Isolated MFUIS with 1991 UBC Static Analysis for El Centro S00E 200%

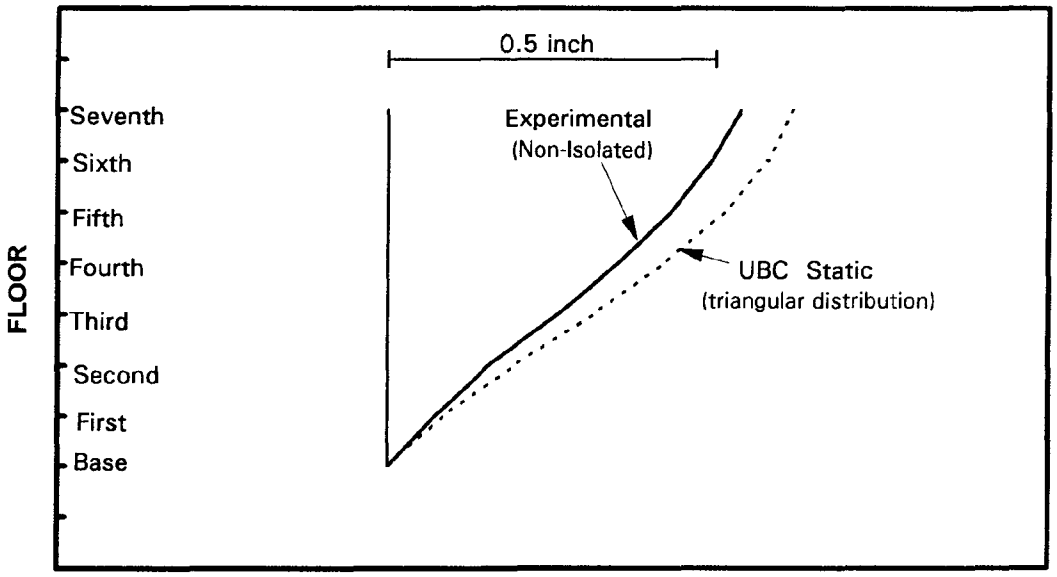

FIGURE 3-15 Comparison of Peak Experimental Lateral Displacements in Non-Isolated MFF with 1991 UBC Static Analysis for Hachinohe NS 35%

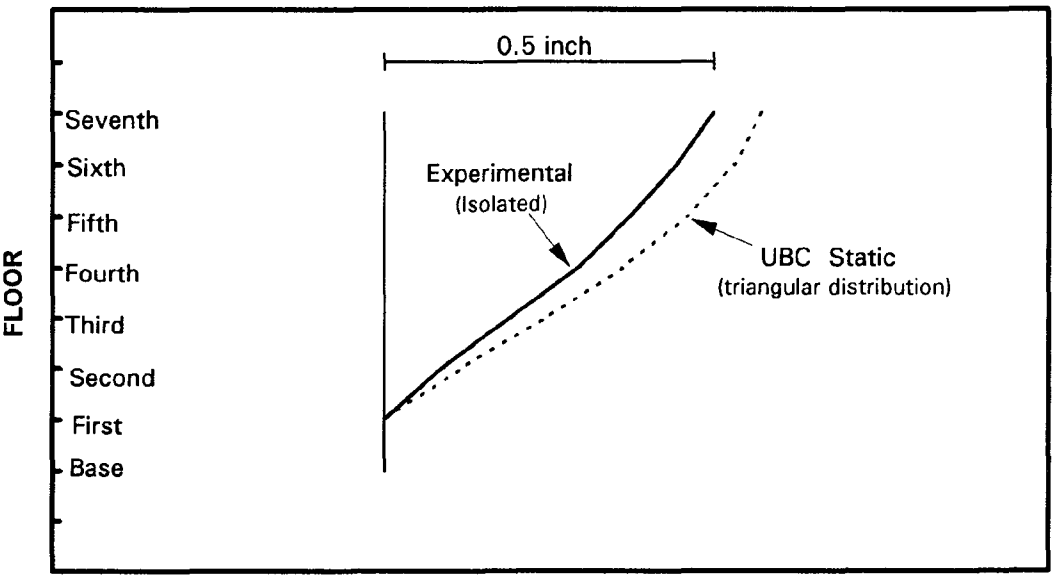

FIGURE 3-16 Comparison of Peak Experimental Lateral Displacements in Isolated MFUIS with 1991 UBC Static Analysis for Hachinohe NS 150%

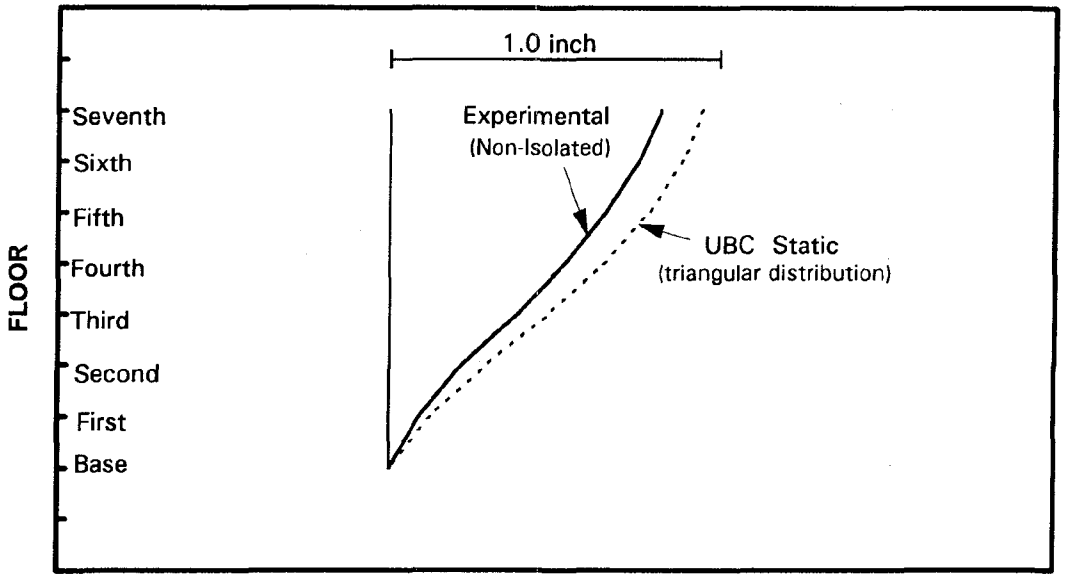

FIGURE 3-17 Comparison of Peak Experimental Lateral Displacements in Non-Isolated MFF with 1991 UBC Static Analysis for Taft N21E 75%

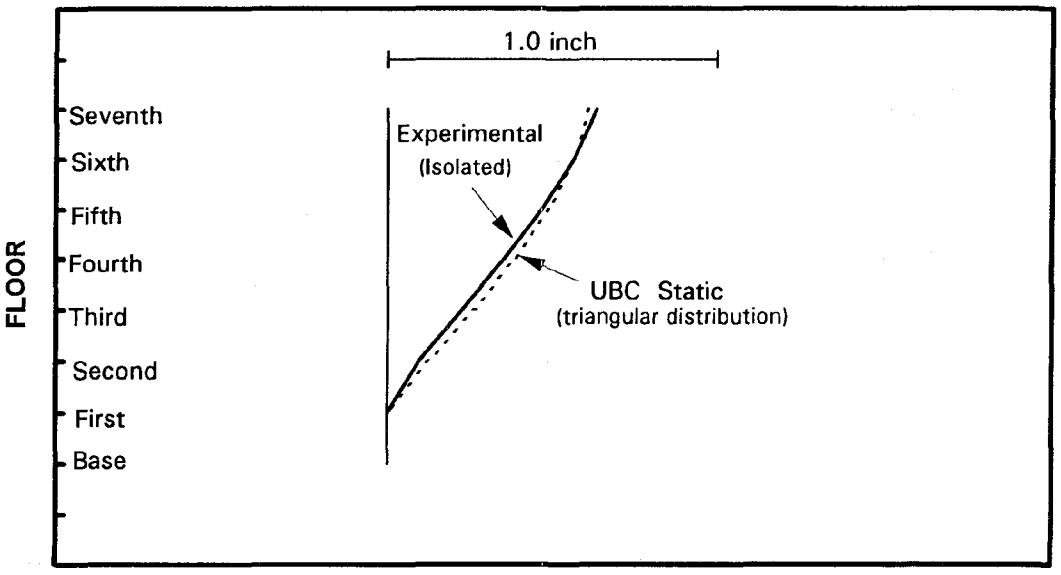

FIGURE 3-18 Comparison of Peak Experimental Lateral Displacements in Isolated MFUIS with 1991 UBC Static Analysis for Taft N21E 300%

along the structure height. The two cases of fully moment frame (MFUIS) and fully braced frame (BFBIS) are presented. The 1st story drift representing the isolation system displacement (bearing displacement plus 1st story column drift) is observed to be a major portion (in the range of 75% to 85%) of the total drift. By absorbing a large part of the total displacement demand within the isolator itself, the structure drifts due to the earthquake are greatly reduced. The braced frame having smaller interstory drifts, naturally results in smaller normalized structure drifts compared to the moment frame as shown in the figures.

Figures 3-13 to 3-18 present comparison of the experimentally measured story drifts for the isolated and non-isolated moment frame with story drifts obtained by using the UBC (Uniform Building Code) static analysis procedures (ICBO, 1991) for seismic design of conventional non-isolated buildings. The UBC drift is calculated assuming a base shear value equal to the measured isolated structure base shear and a triangular distribution of seismic forces along the structure height. Three different earthquake motions were considered. The peak story drifts are accumulated along the structure height to get the structure deflection as shown in the figures. The static lateral drifts due to the static loading specified by UBC are evaluated using the structural analysis software 'ETABS', and these drift values are scaled up or down using the ratio of the experimental base shear to the ETABS calculated base shear. This forms the basis of comparison between the UBC results and the experimental results. For the isolated structure, the isolation story drift is not included in the comparison because it has a very different response than a conventional story. For the non-isolated structure, pinned base supports are assumed for the ETABS model.

From these figures, it can be seen that the experimentally measured story drifts appear to be quite close to the UBC static procedure when the experimentally measured isolated structure base shear is used instead of the UBC specified base shear. Note the earthquake strengths expressed as a percentage of the ground motion records used for the isolated and non-isolated structure. The earthquakes applied to the non-isolated structure were 4 to 6 times stronger than those applied to the non-isolated structure. The isolated structure subjected to these very strong earthquake, reduced the structure drifts by a factor in the range of 4 to 6, and maintaining a drift distribution similar to that occurring in the elastic non-isolated structure when subjected to low strength earthquake ground motions. Thus, since the upper structure remained elastic, the isolated structure responded to very severe earthquake motions similar to the way the non-isolated structure responded to low strength ground motions. If the very severe ground motions had been applied to the non-isolated structure, substantial yielding and

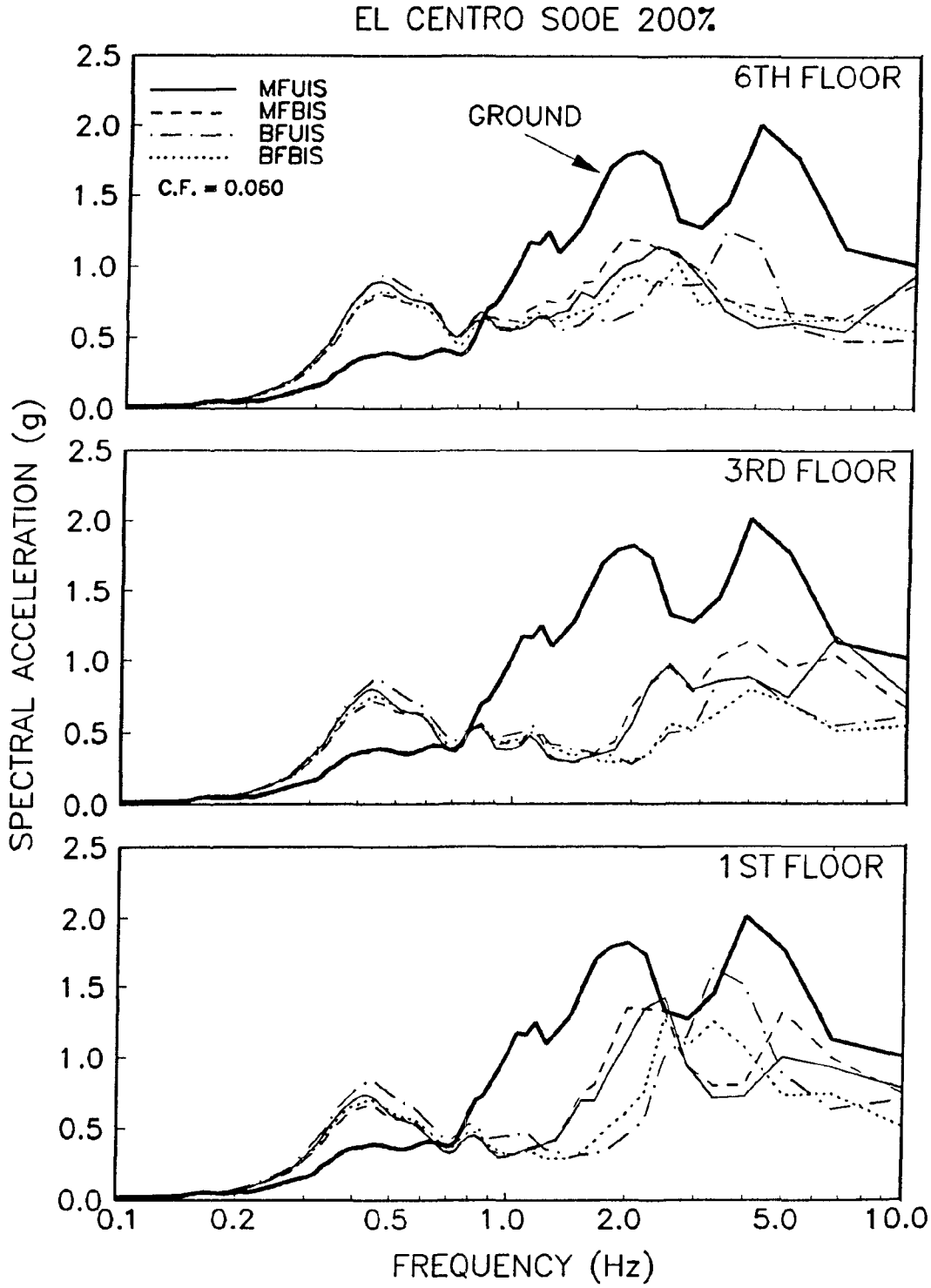

FIGURE 3-19 Response Spectra in Prototype Scale of Different Floor Accelerations in Different Structures for El Centro S00E 200%

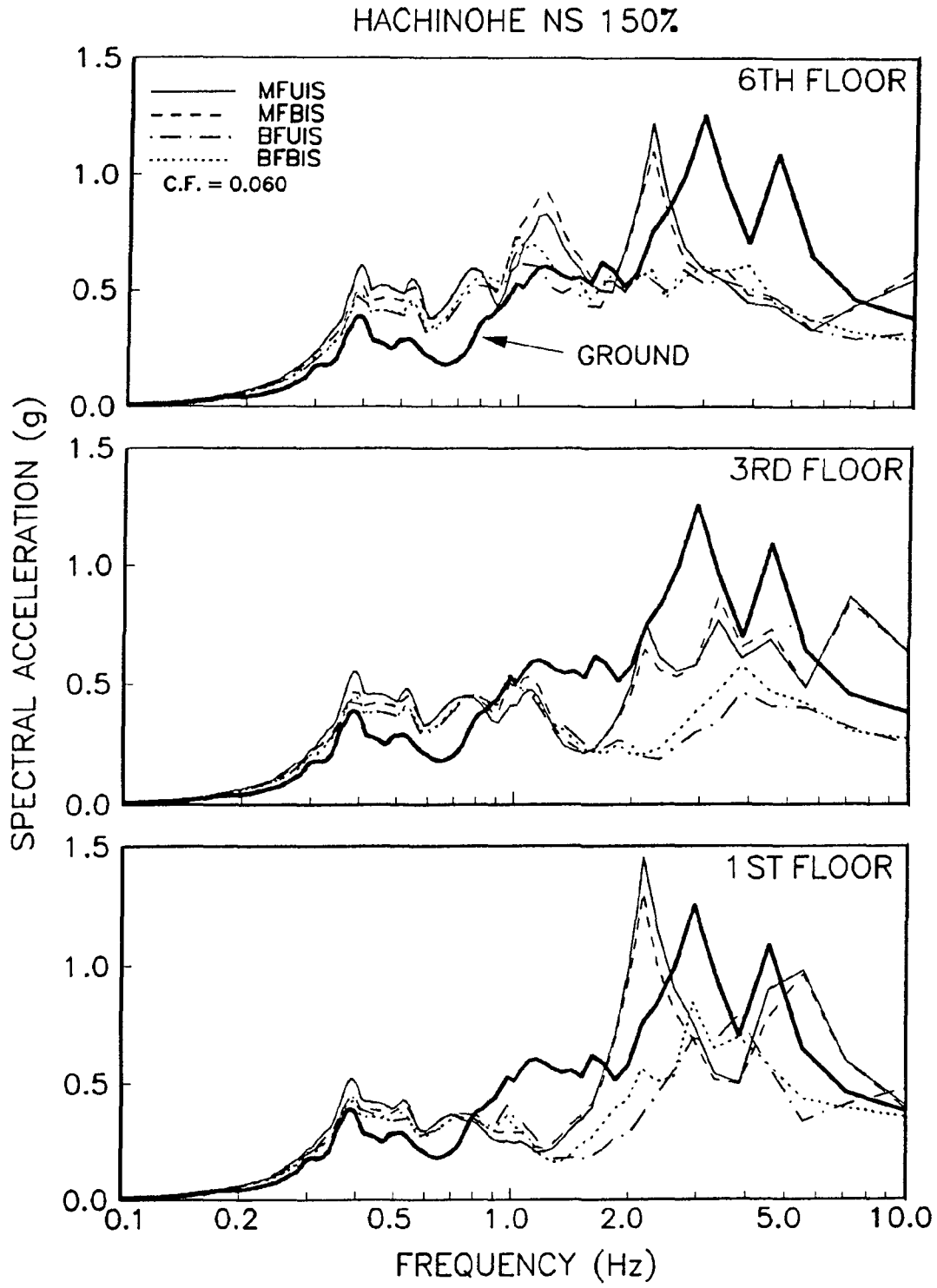

FIGURE 3-20 Response Spectra in Prototype Scale of Different Floor Accelerations in Different Structures for Hachinohe NS 150%

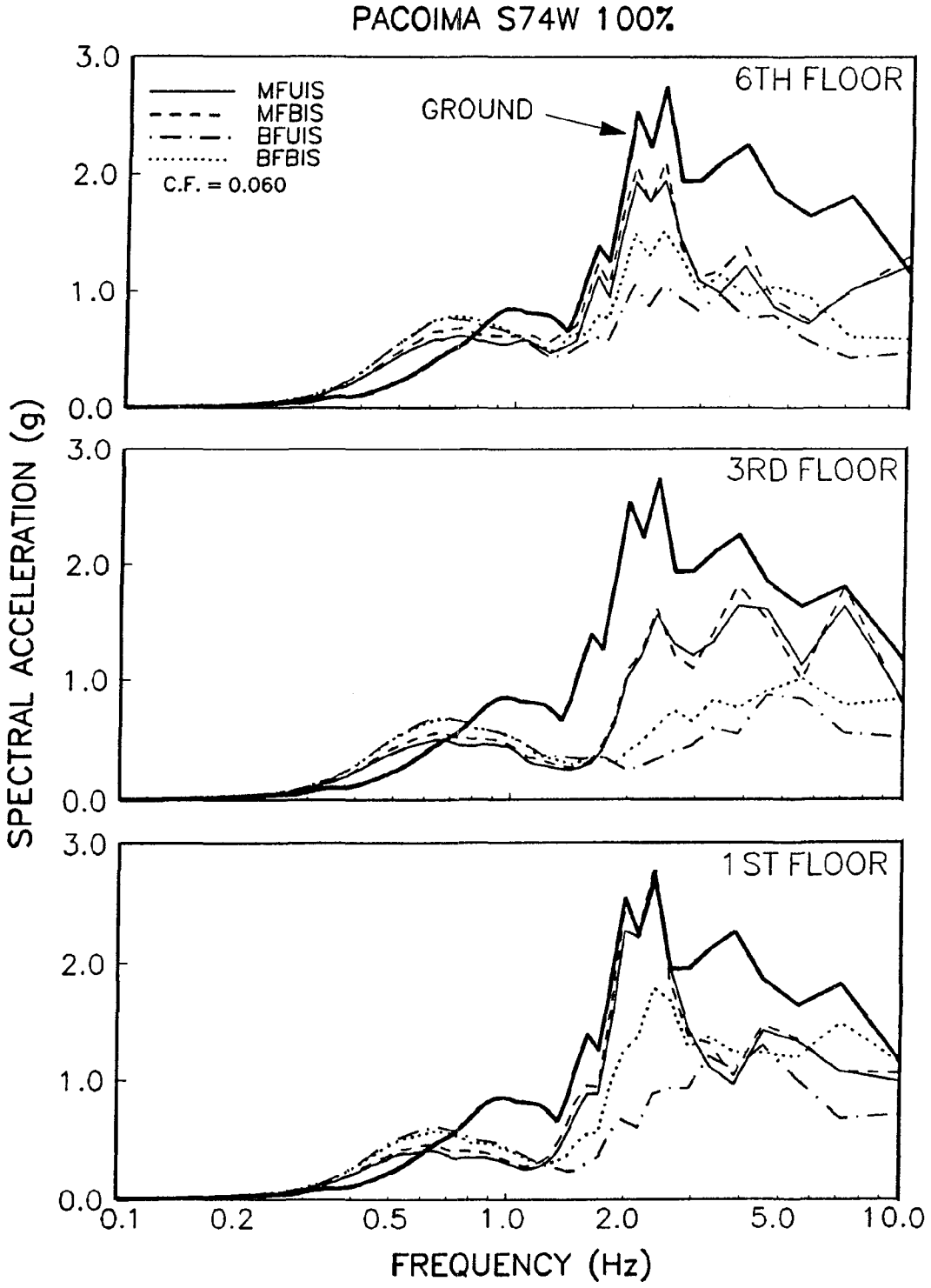

FIGURE 3-21 Response Spectra in Prototype Scale of Different Floor Accelerations in Different Structures for Pacoima S74W 100%

brace buckling would have occurred, and the structure drifts would have been significantly different than those predicted by UBC static procedures.

Figures 3-19 to 3-21 present 5% damped floor acceleration spectra for the severe earthquake motions of El Centro S00E 200%, Hachinohe NS 150% and Pacoima S74W 100%. Floor spectral accelerations for the 1st floor, 3rd floor and the 6th floor are presented, along with the spectrum for the ground motion. All four structural configurations (MFUIS, MFBIS, BFUIS, BFBIS) of the 7-story model are represented. The response spectra are developed from experimental records of the floor accelerations time scaled up by a factor of two, in order to represent prototype conditions. All these floor spectral accelerations of the isolated structures exceed the ground motion spectra at a frequency of around 0.5 Hz, which corresponds to the period of the prototype isolator. At other frequencies, the floor spectra remain about the same or lower than the ground spectra. The figures also reveal that bracing the isolation story did not have a significant effect on the floor response spectra.

Figures 3-22 and 3-23 show the effect of the friction coefficient (in the range of 0.06 to 0.095) on these response spectra. This is done by considering the 7 story moment frame with system (MFBIS) to be structurally close to the 6 story moment frame with a rigid base. The 6th, 3rd and 1st floor of the 7-story model is thus compared with the 5th, 2nd floor and base respectively of the 6-story model. Friction coefficients of 0.075 and 0.095 were used in the 1989 6-story frame tests, while the 7-story frame test results were obtained with bearings having a friction coefficient of 0.06. Comparison of the floor spectra shows that the effect of the friction coefficient on the response spectra is relatively small, with a general tendency of greater response with increased friction. This is in accordance with the experimental observation that an increase in the friction coefficient increases peak floor accelerations.

3.3 Modal Decomposition of Test Structure Response

3.3.1 Floor Acceleration Profile

Figures 3-24 to 3-29 display the floor acceleration profiles along the height of the moment frame MFUIS and the braced frame BFBIS for selected instants of time. In these figures, 'base' refers to the shake table acceleration at those particular instants. Three different motions have been represented. The instants of time chosen correspond to the time of occurrence of the peak floor acceleration, peak base shear, peak overturning moment (about base), peak interstory drift and peak isolation system displacement and are given in the figures. These are

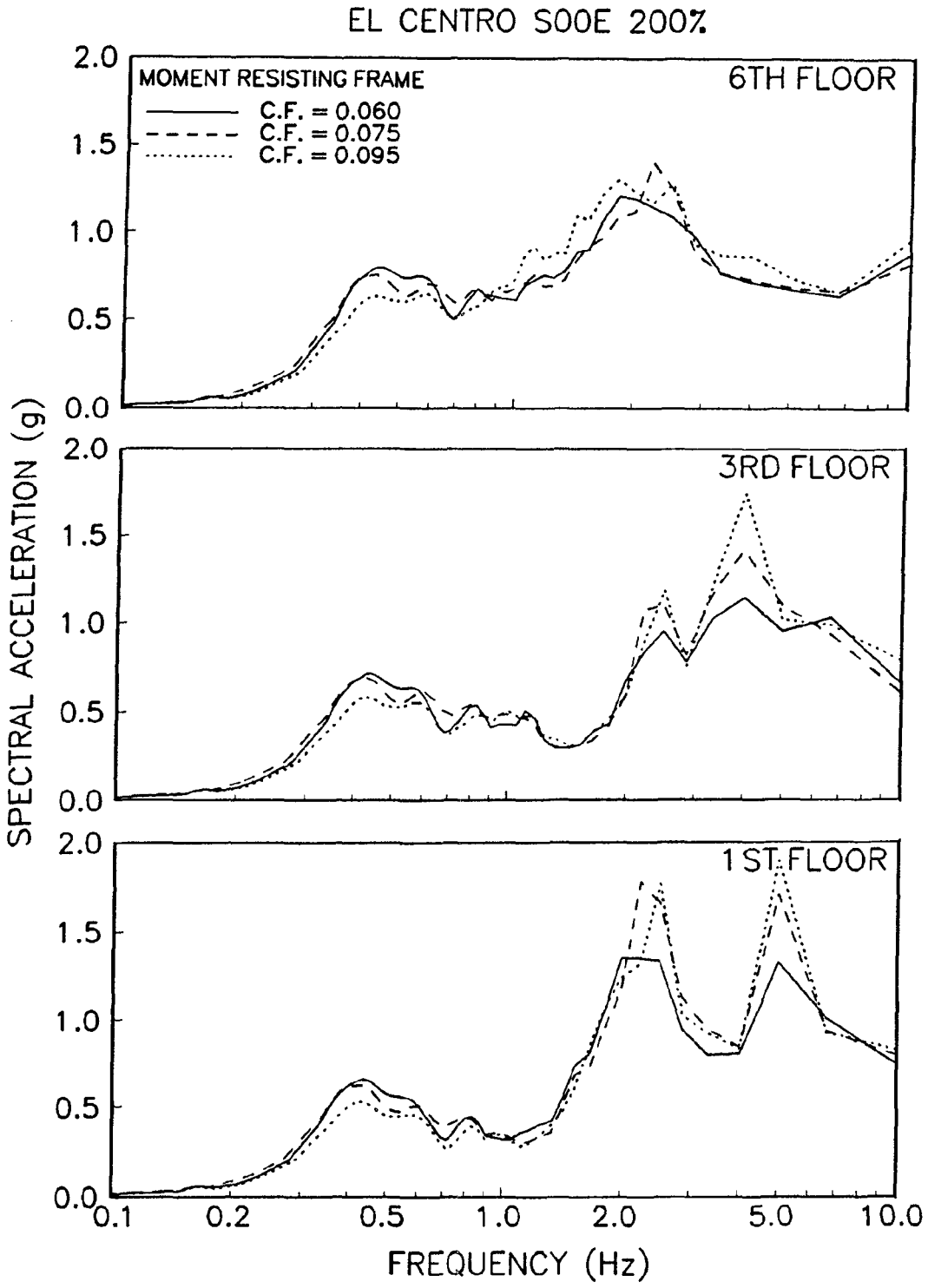

FIGURE 3-22 Effect of Different Friction Coefficients on Floor Response Spectra in Moment Frame for El Centro S00E 200%

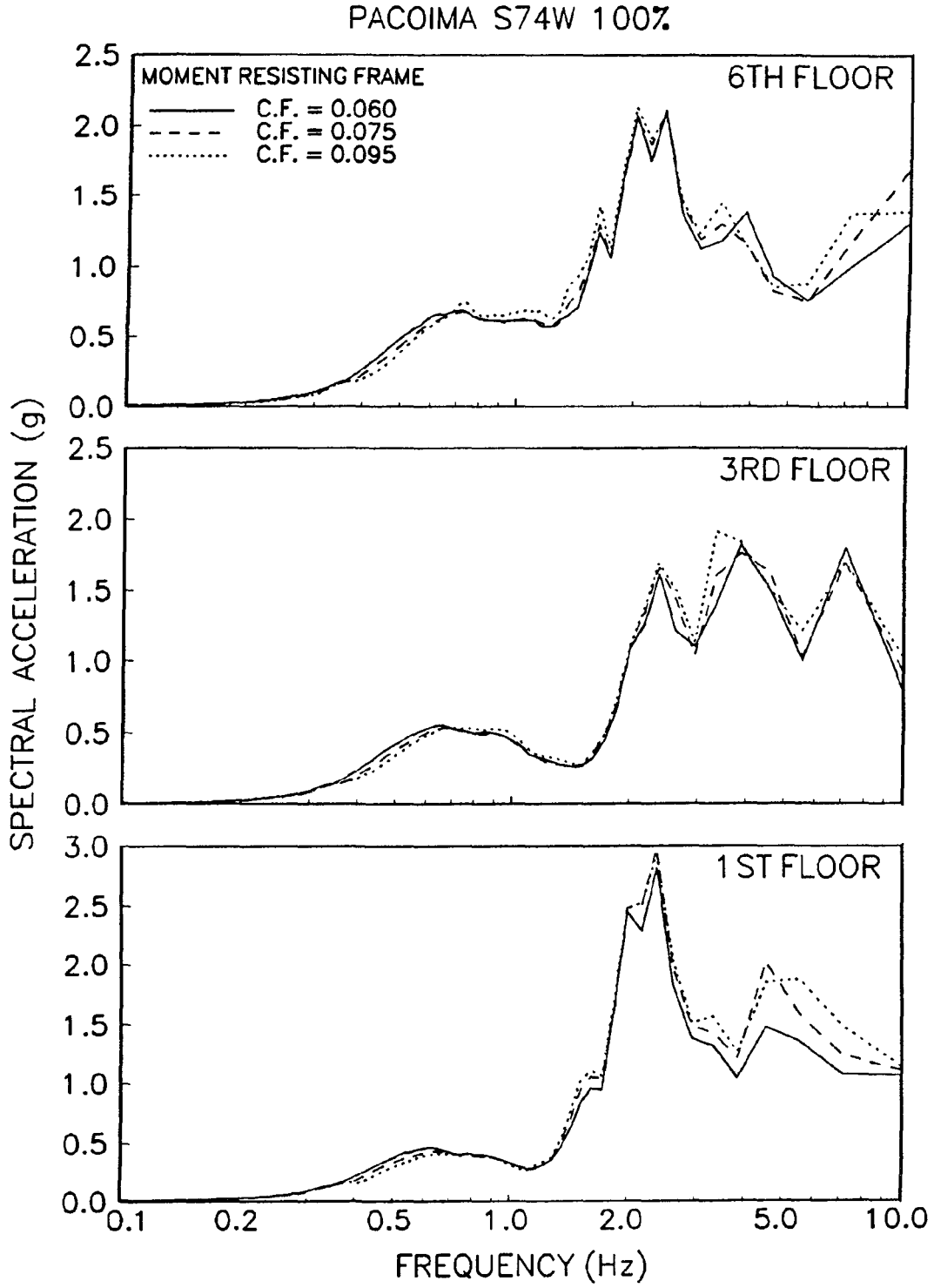

FIGURE 3-23 Effect of Different Friction Coefficients on Floor Response Spectra in Moment Frame for Pacoima S74W 100%

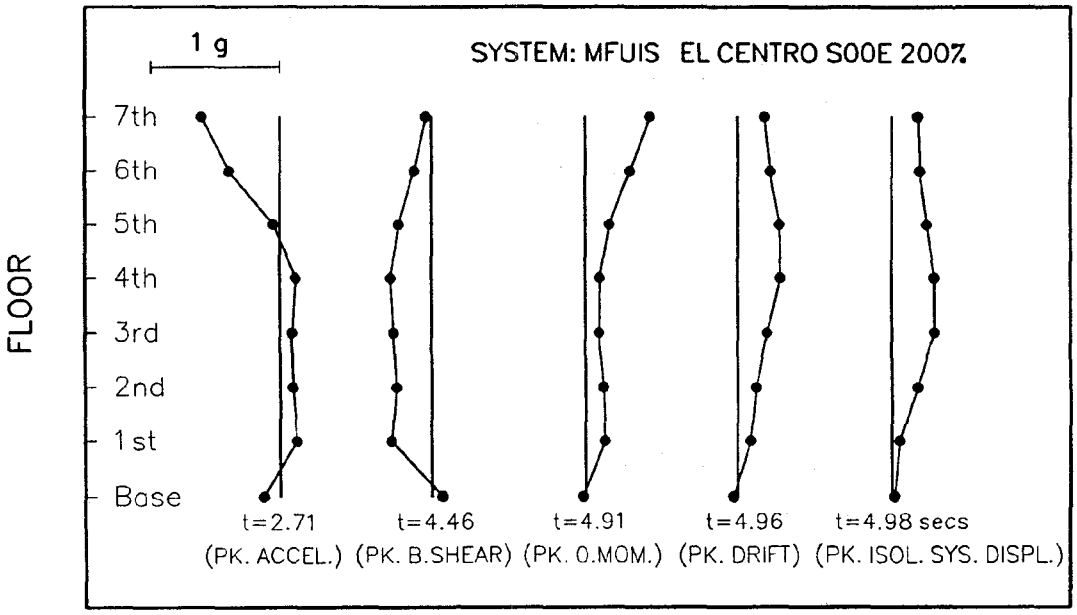

FIGURE 3-24 Floor Acceleration Profiles in Structure MFUIS for El Centro S00E 200%

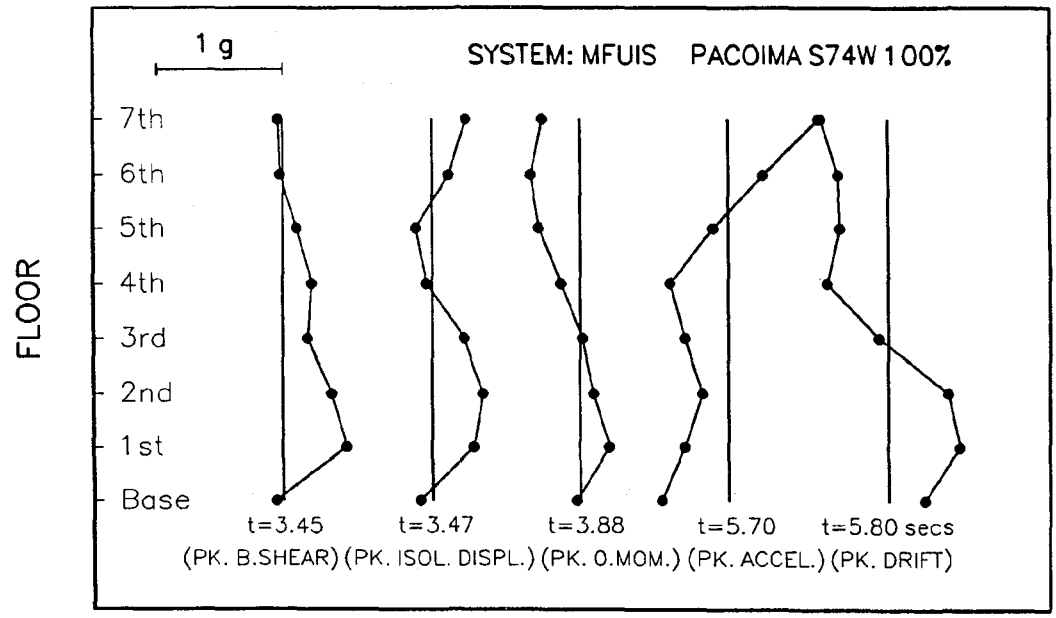

FIGURE 3-25 Floor Acceleration Profiles in Structure MFUIS for Pacoima S74W 100%

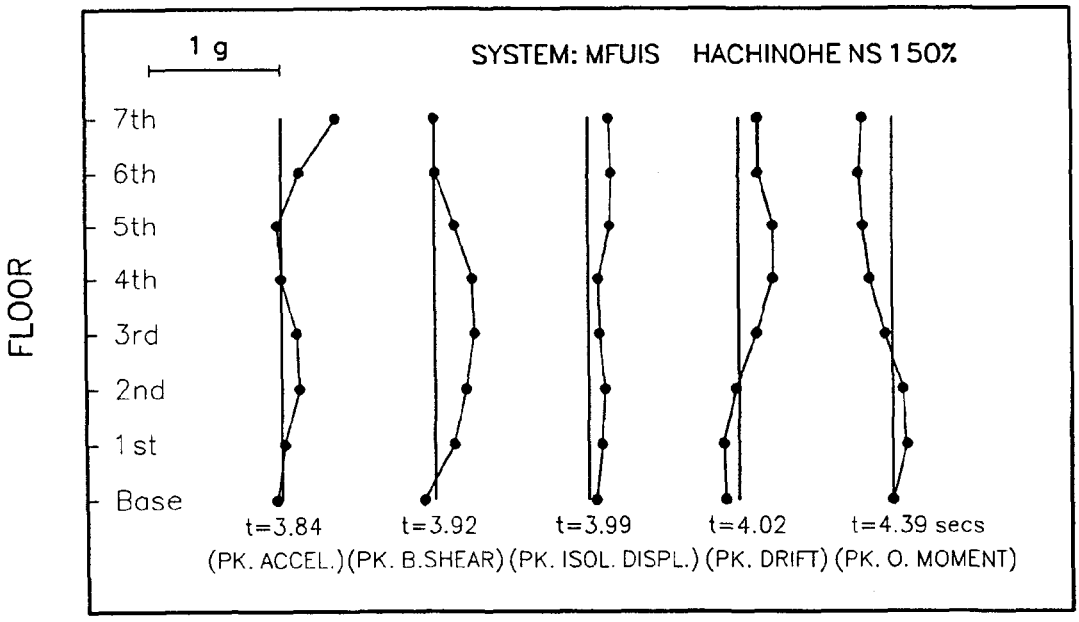

FIGURE 3-26 Floor Acceleration Profiles in Structure MFUIS for Hachinohe NS 150%

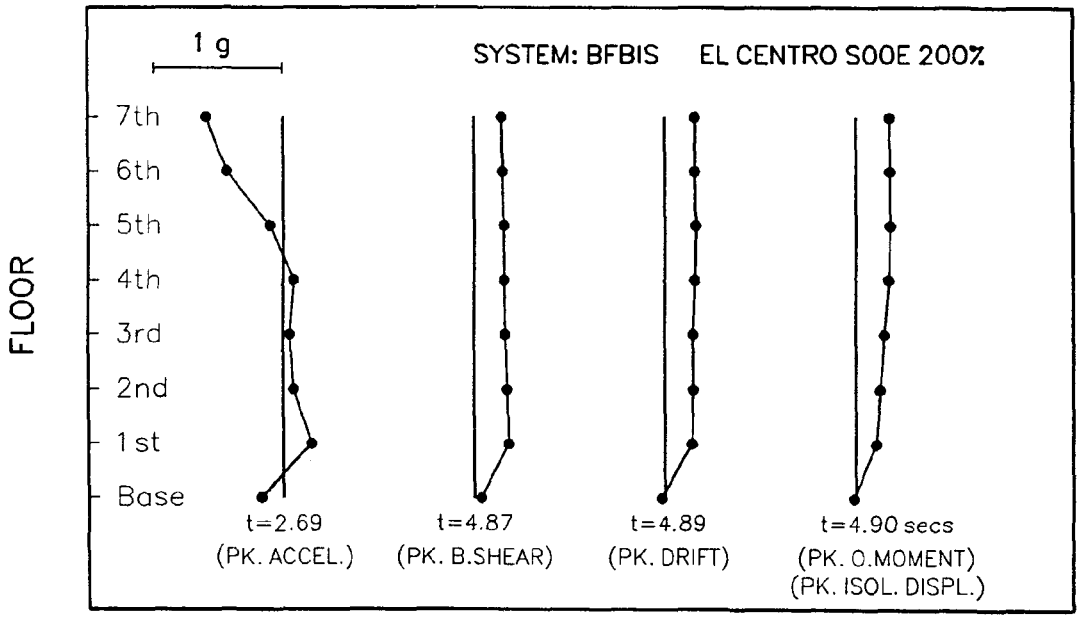

FIGURE 3-27 Floor Acceleration Profiles in Structure BFBIS for El Centro S00E 200%

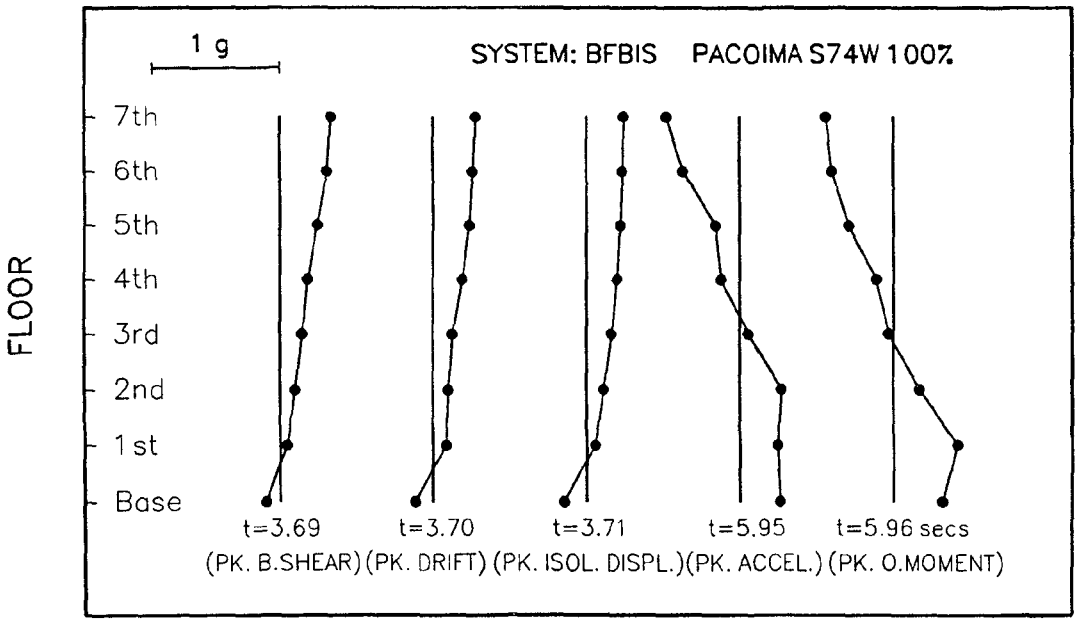

FIGURE 3-28 Floor Acceleration Profiles in Structure BFBIS for Pacoima S74W 100%

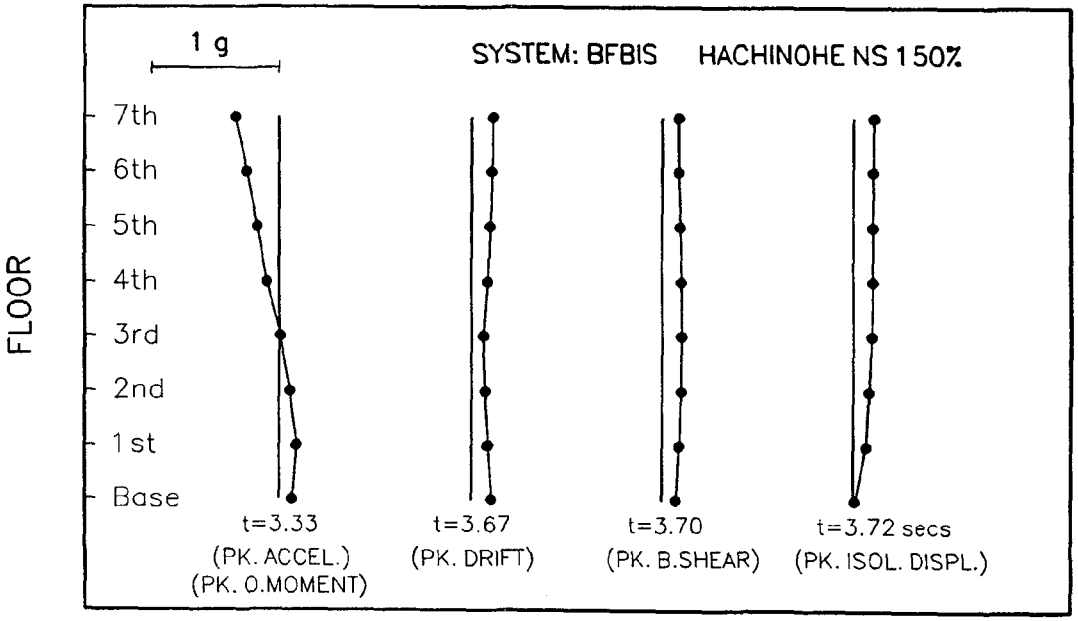

FIGURE 3-29 Floor Acceleration Profiles in Structure BFBIS for Hachinohe NS 150%

the most important structure responses. The overturning moment is the moment about the base of the structure due to the inertia forces.

Figures 3-24 to 3-26 show that, for the moment frame, the second and third mode responses significantly affect the floor acceleration profiles. For the braced frame (figures 3-27 to 3-29) the effects of the second and third modes were not as evident. For the braced frame, slippage at the slotted holes in the braces may have added friction damping to the upper structure, thereby reducing second and third mode participation.

A common observation for both moment and braced frame is that at the time of peak base shear, the floor acceleration profiles tend to follow a first or second mode response, whereas at the time of peak floor acceleration the 2nd and 3rd modes are dominant. At the time of peak floor acceleration, the accelerations occur in opposing directions, and do not significantly affect the structure drifts. As a result, peak floor acceleration is not that significant to the structural response of the frame. These observations are consistent with the ability of the isolated structure to sustain shake table motions 4 to 6 times stronger than the non-isolated structure while remaining elastic. The ability to maintain structure shear and drifts within the elastic range represent the most reliable method of assessing the effectiveness of the isolation system. Similar observations on floor acceleration profiles and there affects on the structural response were also reported by Mokha et al., 1990, from the 1989 6-story moment frame test.

3.3.2 Method of Modal Decomposition

The 7-story structure is modeled as a 6-story upper frame on top of the isolation system, which consist of the FPS bearings together with the first story columns. The modal responses are, therefore, considered with reference to the 6-story upper frame. The lateral behavior of this frame is condensed into a 6 degree of freedom (DOF) lumped mass system with 6 modes. The experimental results are decomposed into the participating modes in order to assess the importance of higher modes. An outline of the method of decomposition is given below.

All displacements and accelerations for the upper 6-story frame are determined relative to the first floor. Let $\{U\}$ and $\{\dot{U}\}$ represent the experimentally obtained relative displacement and acceleration vector for the 6-DOF structure. Hence,

$$\{U\} = [\Phi]\{y\} \tag{3.1}$$

where,
$[\Phi]$ = modal matrix, containing the six mode shapes (known)
$\{y\}$ = modal displacement vector (unknown)

Equation (3.1) is solved as a system of simultaneous algebraic equations for the unknown vector $\{y\}$. Contribution from each mode is then calculated as:

$$\{U\}_i = \{\varphi\}_i y_i \tag{3.2}$$

where, the index *i* represents *ith* mode and $\{\varphi\}_i$ is the *ith* mode shape (ith column of matrix $[\Phi]$).

Displacements (for each mode) given by equation (3.2) are relative to the first floor. The displacement of the first floor (isolation system displacement) is added to the modal displacement (or summation of modal displacements) to obtain the displacement with respect to the shake table. Modal displacements for mode 1, or for modes 1+2, or for modes 1+2+3, are compared against the experimental displacements to observe the number of modes which are required to represent the structure deformation with reasonable accuracy.

Differentiation of equation (3.1) twice with respect to time results in

$$\{\ddot{U}\} = [\Phi]\{\ddot{y}\} \tag{3.3}$$

where,
$\{\ddot{y}\}$ = modal relative acceleration vector (unknown)

The modal contributions to the floor accelerations can then be evaluated in a similar fashion. It is important to note that the modal accelerations are relative to the first floor. The acceleration of the first floor is, thus, added to the modal acceleration (or summation of modal accelerations) to obtain the absolute acceleration. This absolute acceleration of the floors is used in determining the story shear forces. The objective of analyzing the modal participation in the accelerations is to obtain the modal contributions to the story shears.

3.3.3 Modal Decomposition Results

The modal contribution to the story shears and drifts of the isolated structure are studied at different instants of time corresponding to the occurrence of peak response quantities. The modal responses are evaluated for the upper six story frame as outlined in the previous section. Analytical mode shapes have been used, which are presented elsewhere in sections two and four. Results are graphically presented in the form of structure deflection and story shear distribution in figures 3-30 to 3-37. The story drift in the isolation story frame is calculated using the base shear and isolation story stiffness. In these figures, the experimental results (solid line) are compared with the first mode only response (dotted line) and with the combined first three mode response (dotted dashed line). Results are presented here for three selected strong motions for the fully moment frame MFUIS and the fully braced frame BFBIS.

It may be concluded from these figures that consideration of three modes is sufficient to represent the structure response for all cases. For some cases, the motion appears to be dominated by the first mode only. Upon initial observation, it may appear strange that the modal participation is different for the structure deformation and structure shear forces at the same instant of time. The reason for this is that when the 1st floor acceleration is added to the modal accelerations of the different floors to get the absolute acceleration, the modal acceleration values may change substantially with possible change in signs. This leads to a new distribution of modal accelerations and consequently affects the modal participation in the story shears as observed in the figures. Higher modes appear to be more important in the evaluation of the story shears, compared to the structure deflection.

Results are also presented for the non-isolated moment frame MFF in figures 3-36 and 3-37 for two different earthquakes. For the low strength earthquake motions applied, the story drifts and shears closely followed the first mode response. However, for earthquake loading 4 to 6 times stronger as were applied to the isolated structure, it is anticipated that the non-isolated structure drifts and shears would significantly differ from a first mode response.

Figures 3-38 to 3-41 present the percentage error between the modal decomposition and the actual structure response. The peak base shear and the peak structure drift of all four structure configurations of the isolated structure are considered for two different earthquake types El Centro S00E 200% and Hachinohe NS. 150%. The non-isolated structure MFF is included for earthquake El Centro S00E 35% and Hachinohe NS 35%. The percentage error is plotted

against the number of modes considered. The response of the first three modes of the upper structure fully accounted for the response of the experimentally observed structure shears and drifts, with differences of typically less than 1% as compared to the experimental results. The inclusion of only two modes resulted in differences as large as 5%, and the inclusion of only 1 mode resulted in differences as large as 23%. Thus, the response of isolated structures subjected to severe earthquake ground motions can be well represented using only the first few modes of the upper structure.

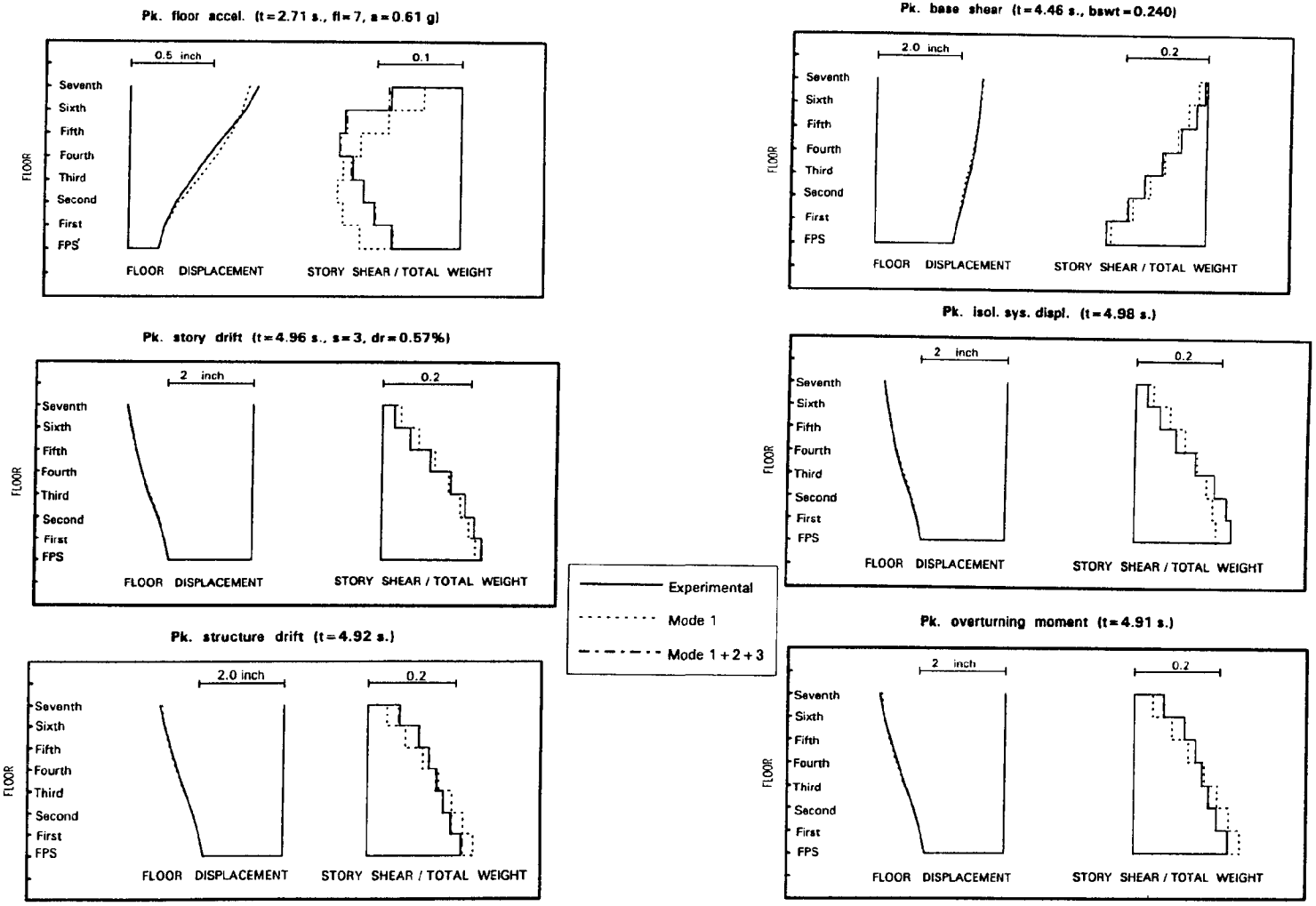

FIGURE 3-30 Modal Participation in Response of Structure MFUIS for El Centro S00E 200% at Different Instants of Time (t=time, s=story, fl=floor, a=acceleration, dr=drift ratio, bswt=base shear/weight)

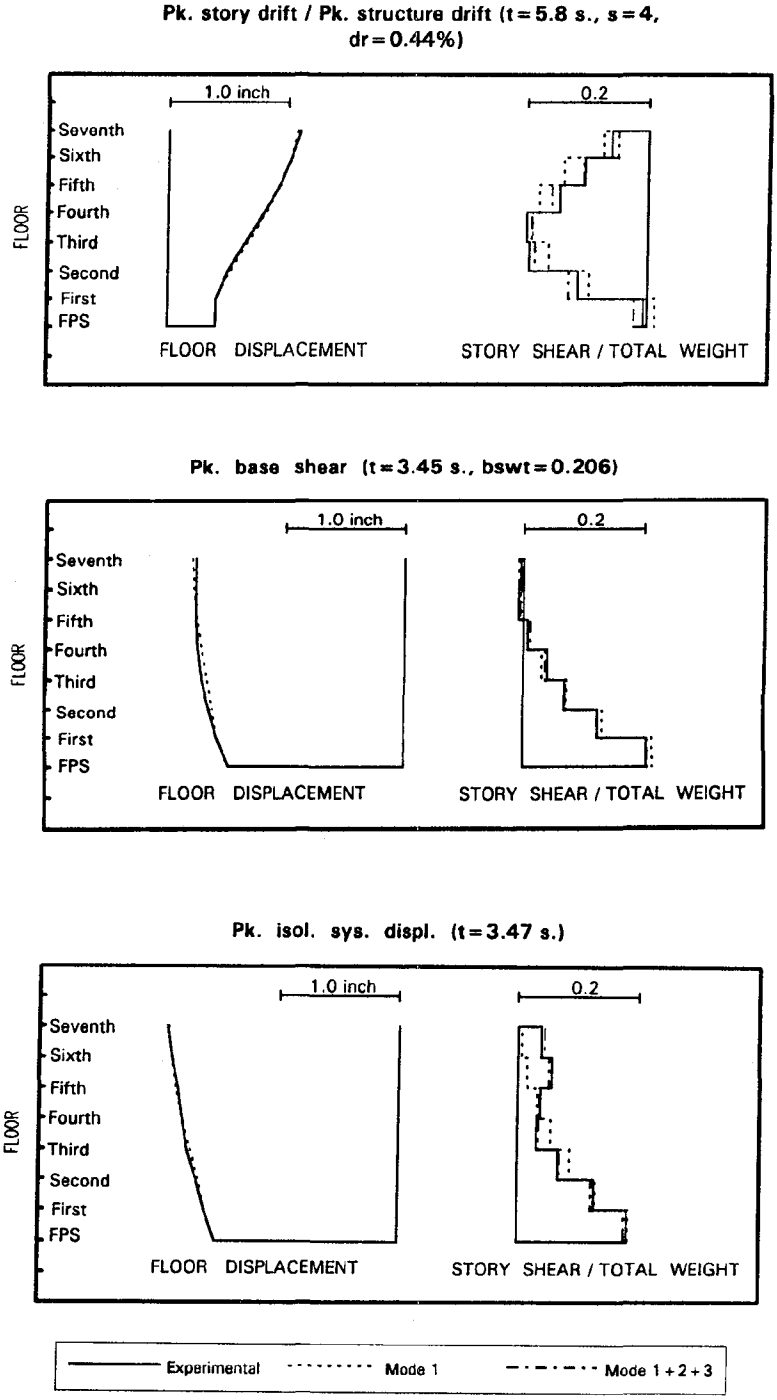

FIGURE 3-31 Modal Participation in Response of Structure MFUIS for Pacoima S74W 100% at Different Instants of Time (t=time, s=story, dr=drift ratio, bswt=base shear/weight)

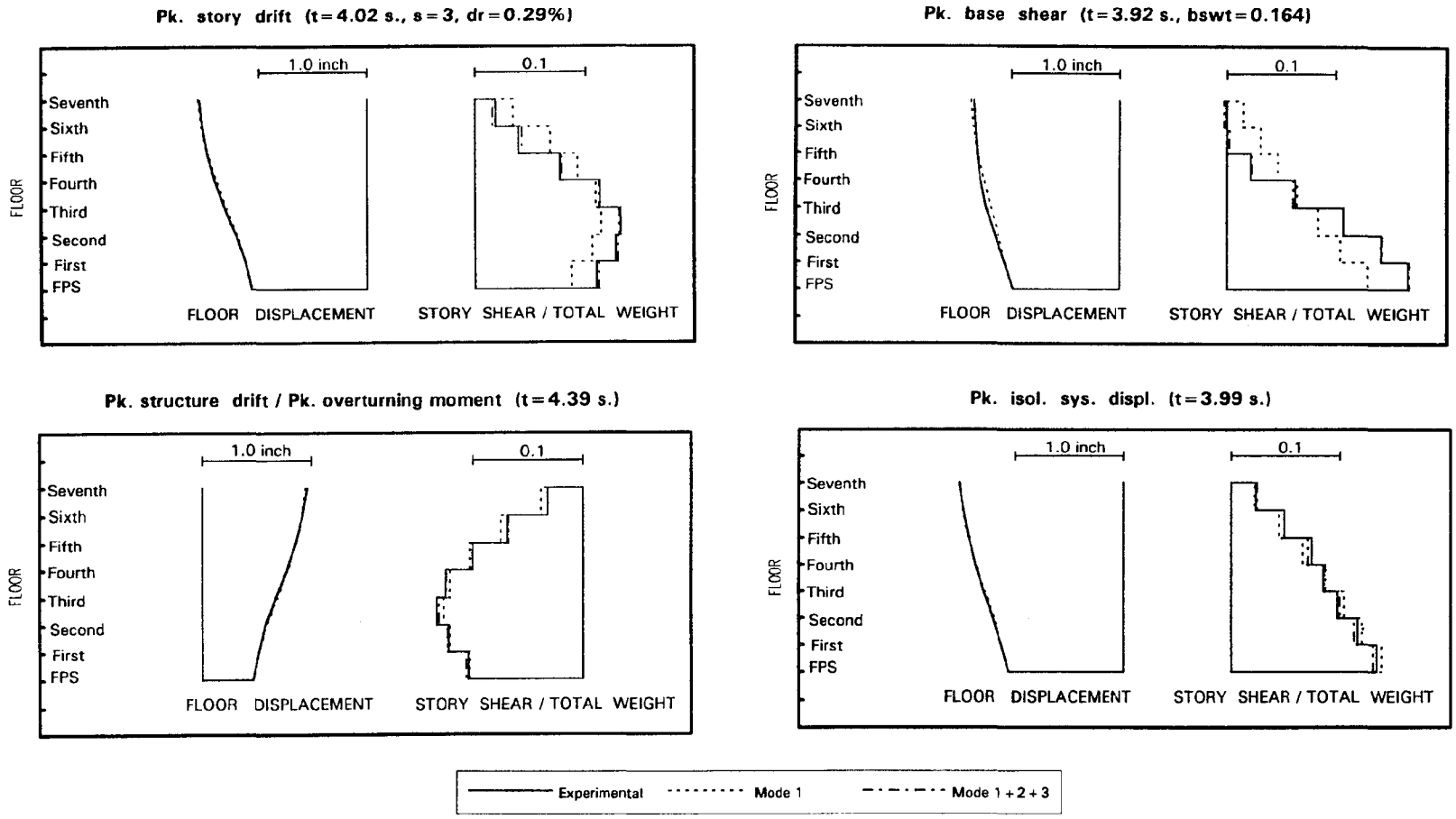

FIGURE 3-32 Modal Participation in Response of Structure MFUIS for Hachinohe NS 150% at Different Instants of Time (t=time, s=story, dr=drift ratio, bswt=base shear/weight)

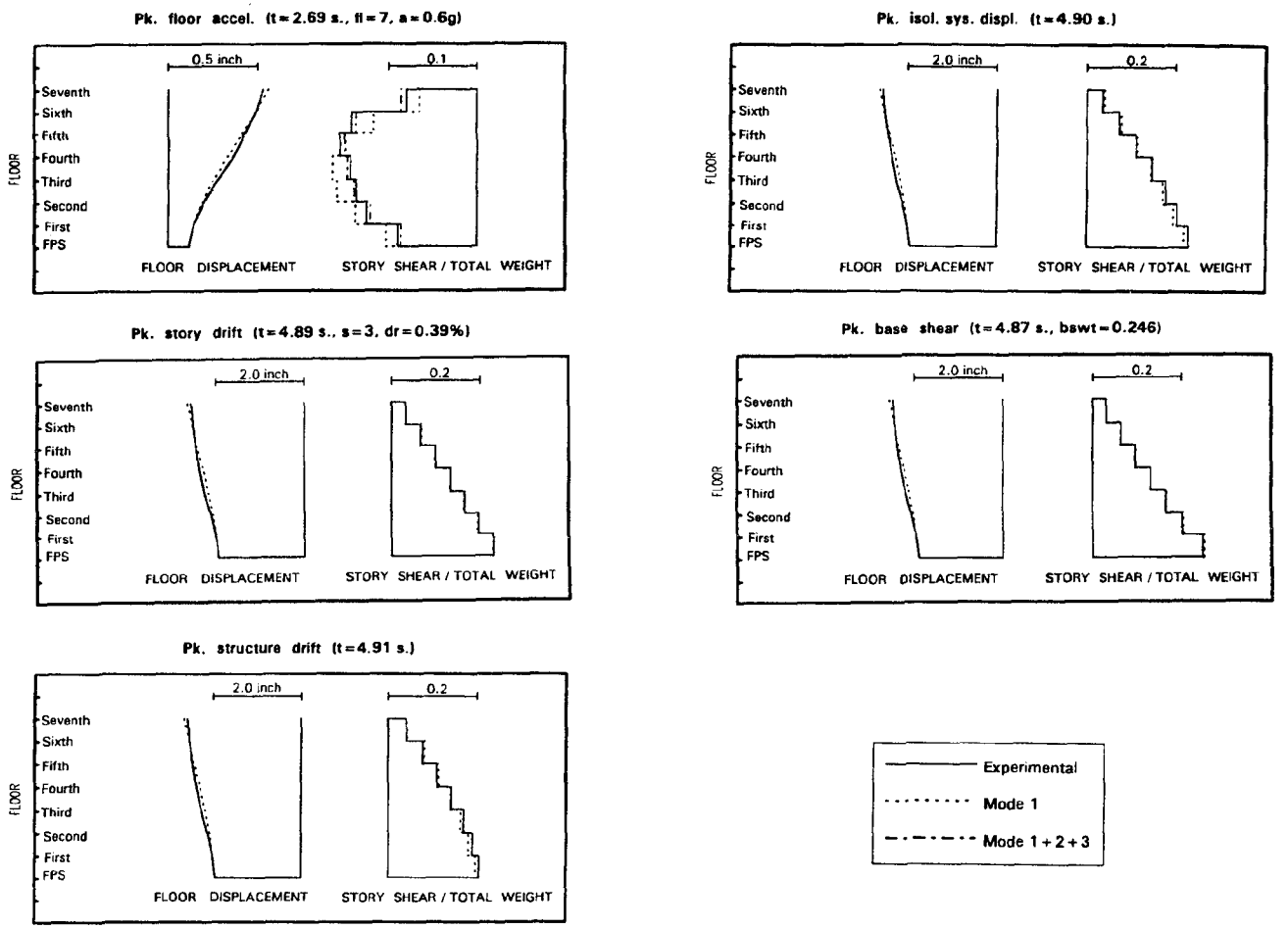

FIGURE 3-33 Modal Participation in Response of Structure BFBIS for El Centro S00E 200% at Different Instants of Time (t=time, s=story, fl=floor, a=acceleration, dr=drift ratio, bswt=base shear/weight)

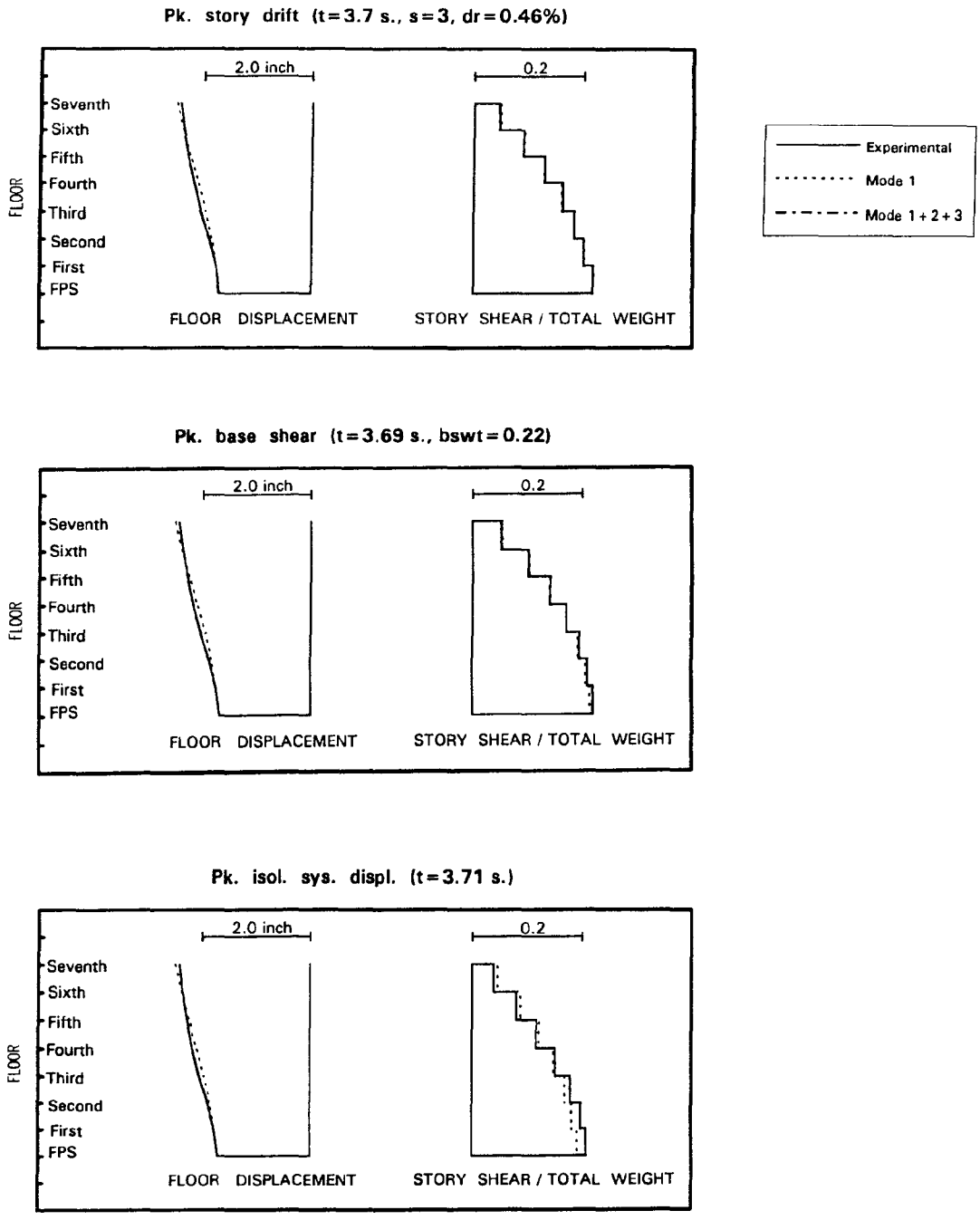

FIGURE 3-34 Modal Participation in Response of Structure BFBIS for Pacoima S74W 100% at Different Instants of Time (t=time, s=story, dr=drift ratio, bswt=base shear/weight)

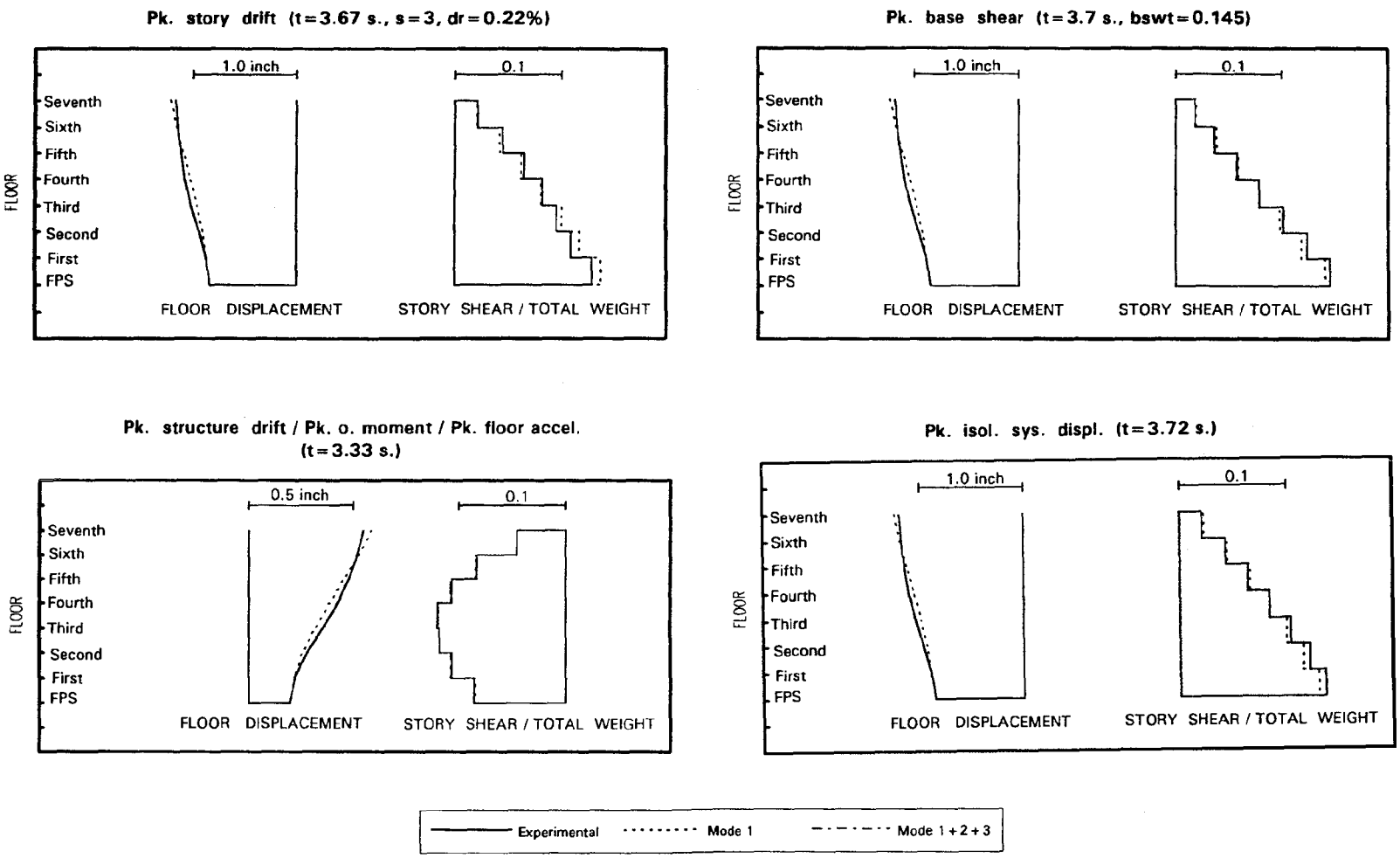

FIGURE 3-35 Modal Participation in Response of Structure BFBIS for Hachinohe NS 150% at Different Instants of Time (t=time, s=story, dr=drift ratio, bswt=base shear/weight)

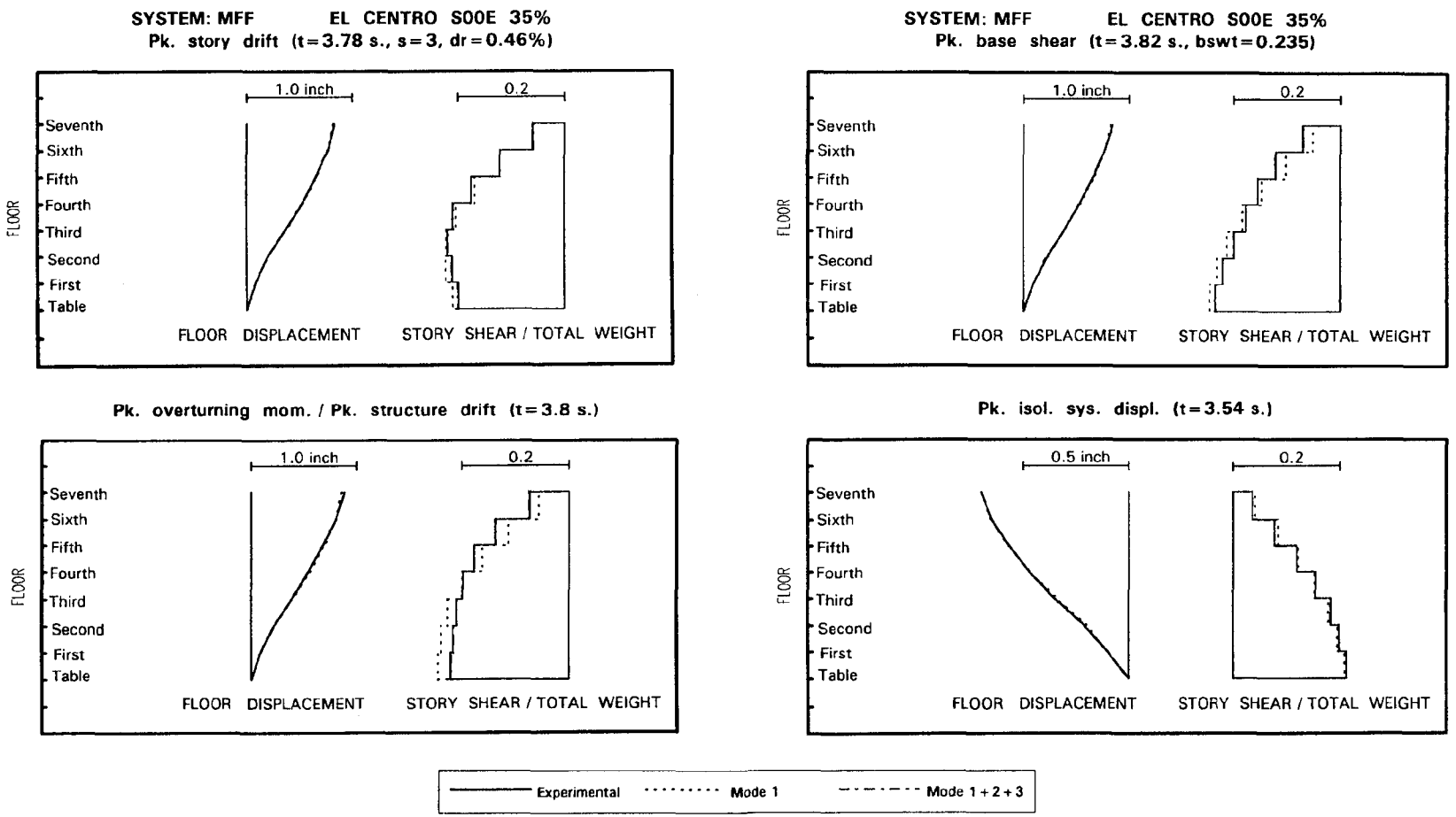

FIGURE 3-36 Modal Participation in Response of Non-Isolated Structure MFF for El Centro S00E 35% at Different Instants of Time (t=time, s=story, dr=drift ratio, bswt=base shear/weight)

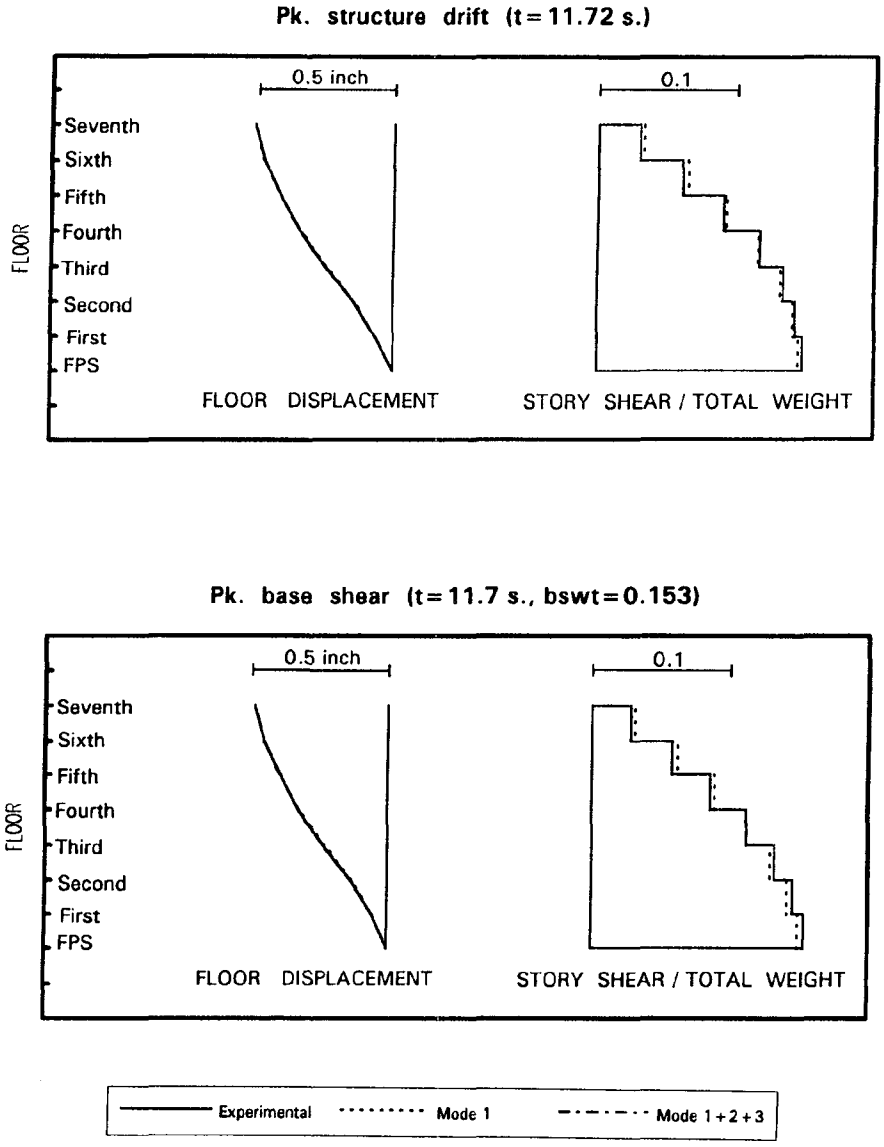

FIGURE 3-37 Modal Participation in Response of Non-Isolated Structure MFF for Hachinohe NS 35% at Different Instants of Time (t=time, bswt=base shear/weight)

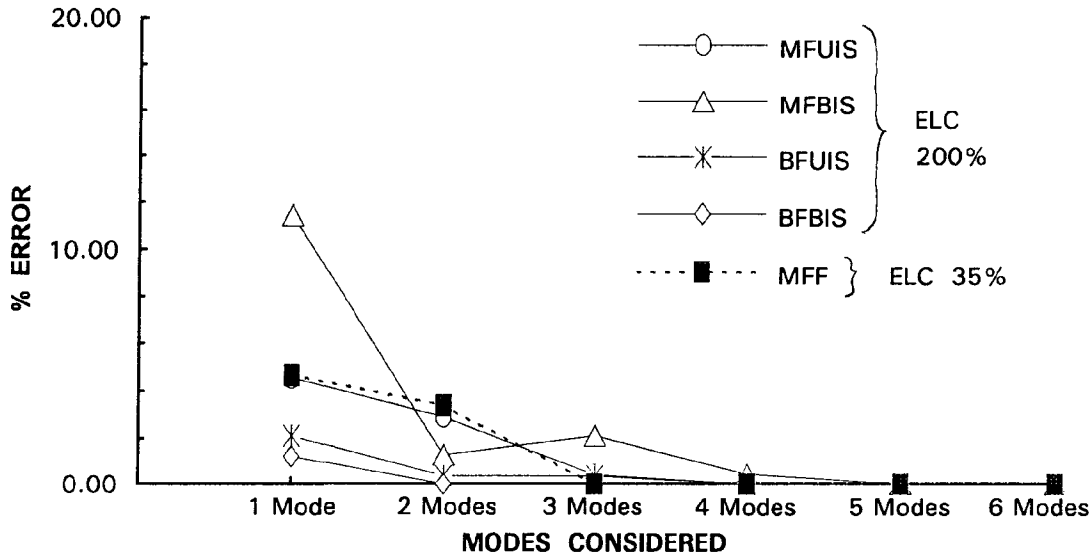

FIGURE 3-38 Percentage Error between Modal Response and Actual Peak Base Shear Response during El Centro S00E Motion

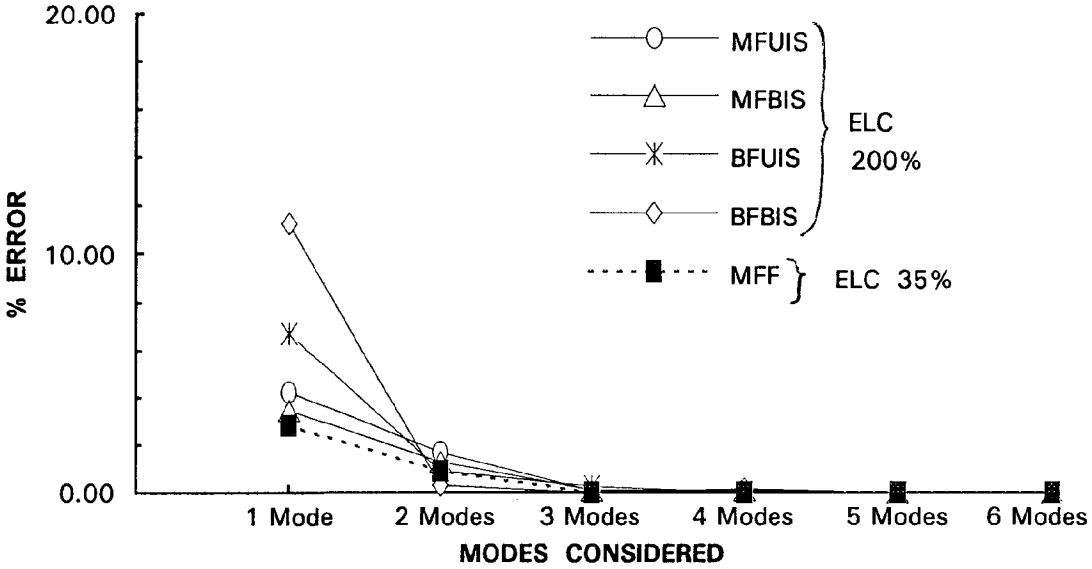

FIGURE 3-39 Percentage Error between Modal Response and Actual Peak Structure Drift Response during El Centro S00E Motion

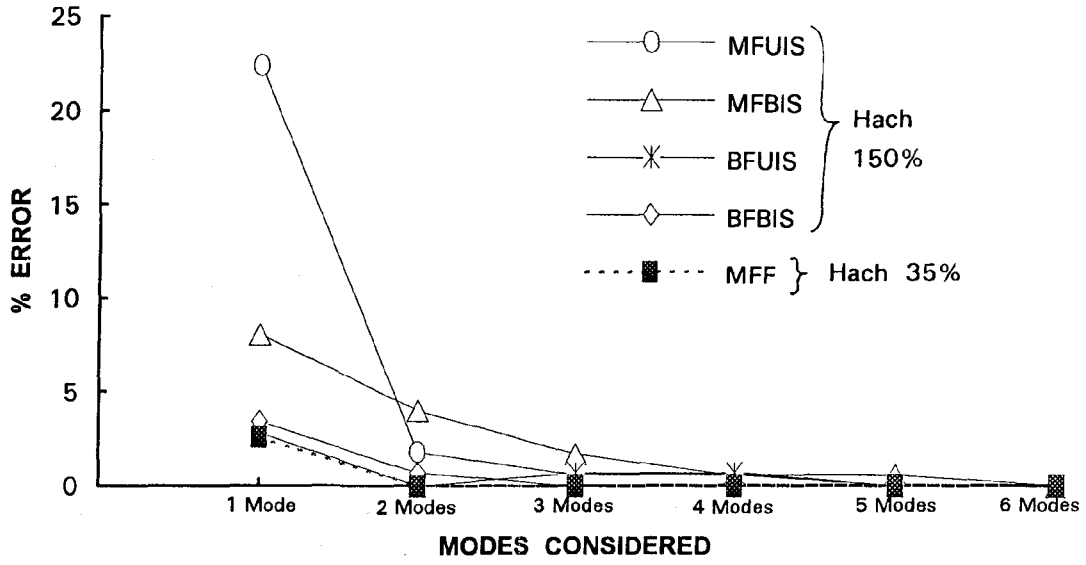

FIGURE 3-40 Percentage Error between Modal Response and Actual Peak Base Shear Response during Hachinohe NS Motion

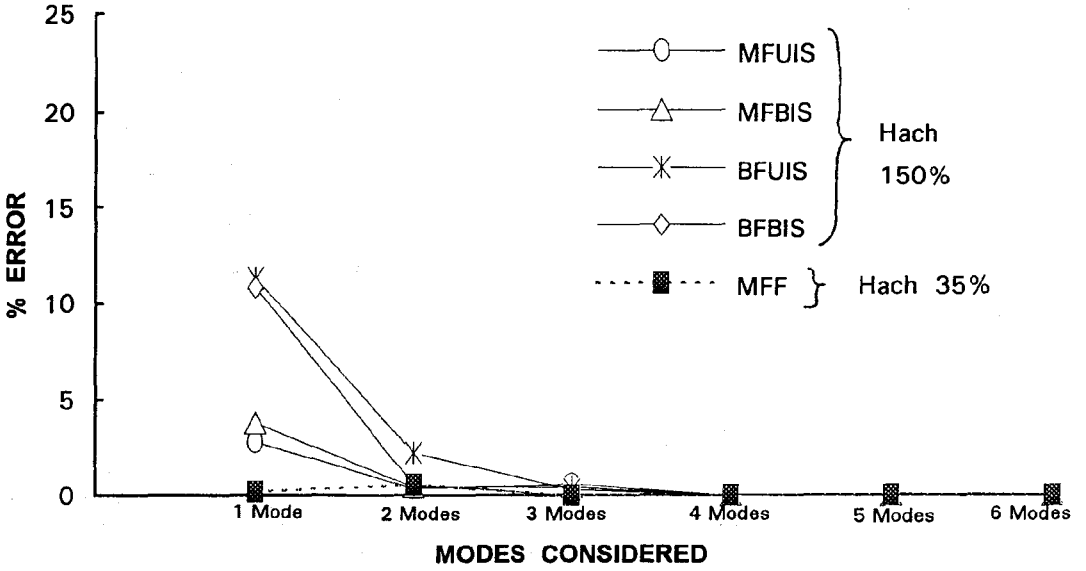

FIGURE 3-41 Percentage Error between Modal Response and Actual Peak Structure Drift Response during Hachinohe NS Motion

SECTION 4

DYNAMIC ANALYSIS PREDICTION OF ISOLATED STRUCTURE RESPONSE

4.1 Time History Dynamic Analysis Formulation

Due to the symmetry of the structure and the application of the excitation in the vertical plane, torsional movements were negligible and a two-dimensional analysis was deemed appropriate for analyzing the 7-story frame structure. As mentioned earlier, the 7-story structure could be modeled as a 6-story upper frame on top of a separately modeled isolation story. The floor levels could be assumed to be rigid in their own plane, resulting in a 7 DOF (lateral) system with the structure masses lumped at the different floor levels. Let these masses be m1, m2, ..., m7 corresponding to floors 1 to 7. The lateral floor displacements are expressed as relative to the 1st floor. Let these relative floor displacements be u2, u3, ..., u7 corresponding to floors 2 to 7. The 2-D model uses four hysteretic elements, representing four column lines in the transverse direction, to model the isolation story. Each hysteretic element, thus, represents the combined effect of two isolation story columns with the FPS isolators beneath. The displacement within the hysteretic element is equal to the bearing displacement plus the isolation story column drift. The element displacement is the isolation system displacement.

Figure 4-1 shows the idealized 7-story structure and the displacement variables (ug and ub represent respectively the ground movement and isolation system displacement) used in the analytical model. The behavior of each hysteretic element is defined by a bi-linear force-displacement relationship, as shown in figure 4-2. The slopes of the bi-linear curve are taken in accordance with the experimentally observed isolation system hysteretic response (see figure 2-4, section 2.2). The initial slope is determined by the stiffness of two columns comprising the hysteretic element. The change of slope is at the onset of sliding, the yield load being equal to the vertical load times the coefficient of sliding friction. The post-yield stiffness may be stated with reasonable accuracy to be equal to the stiffness of the FPS bearings (section 2.2).

The six equations of motion for the six story upper frame may be expressed in matrix form as:

$$[M]\{\ddot{U}_r\} + [C]\{\dot{U}_r\} + [K]\{U_r\} = -\{m\}(\ddot{u}_g + \ddot{u}_b) \tag{4.1}$$

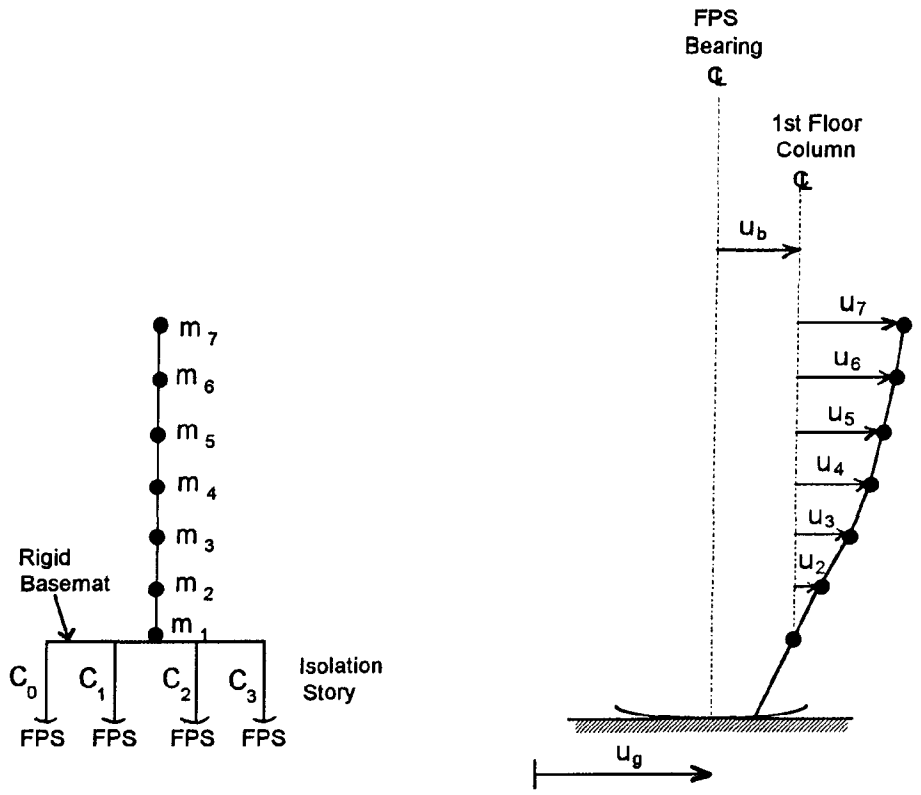

(a) Idealized Structure

(b) Displacement Pattern

FIGURE 4-1 Idealized Model of 7-Story Test Frame

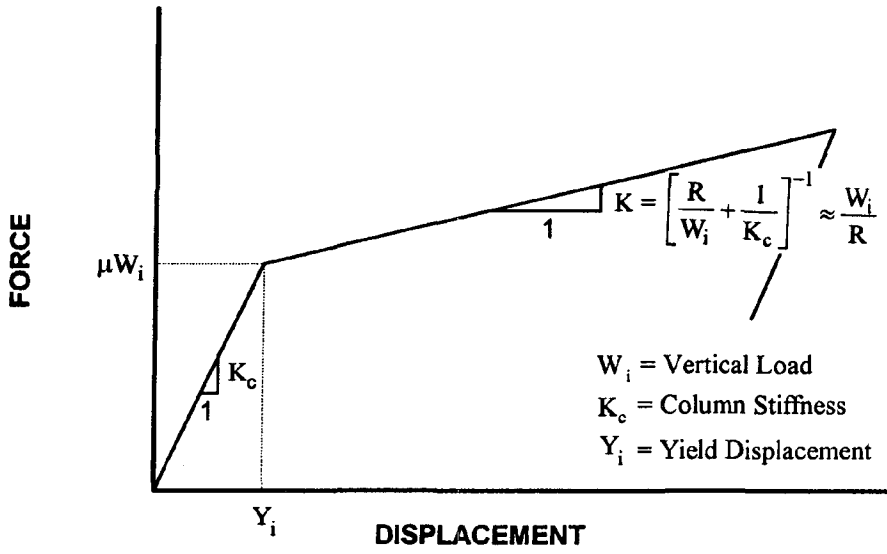

FIGURE 4-2 Idealized Force-Displacement Behavior of Hysteretic Element

where,

$\{U_r\}^T = \lfloor u_7, u_6, u_5, u_4, u_3, u_2 \rfloor$

$[M]$ = Mass matrix (diagonal, comprising of elements m_7, m_6, m_5, m_4, m_3, m_2)

$[C]$ = Damping matrix

$[K]$ = Stiffness matrix

$\{m\}^T = \lfloor m_7, m_6, m_5, m_4, m_3, m_2 \rfloor$

Dot represents differentiation with respect to time.

The stiffness matrix is determined from analytically evaluated frequencies and mode shapes for the fixed-base (base support preventing both translation and rotation) six story upper frame, using a procedure described by Clough and Penzien (1975):

$$[K] = [M]\left(\sum_{i=1}^{L} \frac{\omega_i^2}{m_i^*}\{\varphi_i\}\{\varphi_i\}^T\right)[M] \tag{4.2}$$

where,

m_i^* is given by the following equation:

$$m_i^* = \{\varphi_i\}^T[M]\{\varphi_i\} \tag{4.3}$$

ω_i = *ith* frequency

$\{\varphi_i\}$ = *ith* mode shape vector

L = number of modes included in the analysis

The damping matrix $[C]$ of the six story upper frame is constructed using a similar procedure (Clough and Penzien, 1975) from the analytically determined frequencies and mode shapes, and the experimentally determined (representative of the test frame) damping ratios. The expression for $[C]$ may be given as:

$$[C] = [M]\left(\sum_{i=1}^{L} \frac{2\xi_i\omega_i}{m_i^*}\{\varphi_i\}\{\varphi_i\}^T\right)[M] \tag{4.4}$$

where ξ_i is the damping ratio for *ith* mode.

In order to solve for the seven unknowns (u_b, u_2, u_3, u_4, u_5, u_6, u_7), an additional equation is needed which may be obtained by considering horizontal equilibrium of the entire structure:

$$\sum_{i=2}^{7} m_i\left(\ddot{u}_i + \ddot{u}_b + \ddot{u}_g\right) + m_1\left(\ddot{u}_b + \ddot{u}_g\right) + \sum_{i=1}^{4} F_{b_i} = 0 \tag{4.5}$$

where F_{b_i} is the shear force developed at *ith* hysteretic element (i=1 to 4)

The shear force in the *ith* hysteretic element is expressed as:

$$F_{b_i} = \mu W_i Z_i\left(1 - \frac{W_i}{RK_c}\right) + \left(\frac{W_i}{R}\right)u_b \tag{4.6}$$

where,

W_i = Vertical load on *ith* hysteretic element

Z_i = Dimensionless variable accounting for the conditions of separation and reattachment during sliding motion in the *ith* hysteretic element, its value is bounded by ±1

K_c = Pre-yielding stiffness of each hysteretic element (due to column stiffness)

The new variable Z_i in this equation replaces the signum function of equation (2.1) and is governed by the following differential equation (Constantinou et al., 1990):

$$Y_i\dot{Z}_i + \gamma|\dot{u}_b||Z_i|Z_i|^{\eta-1} + \beta\dot{u}_b|Z_i|^{\eta} - A\dot{u}_b = 0 \tag{4.7}$$

where,

Y_i = yield displacement of *ith* hysteretic element

A, γ, β, η = dimensionless quantities that control shape of the hysteresis loop (Values of A=1, γ=0.9, β=0.1 and η=2 have been used)

The yield displacement is directly obtained from figure 4-2 to be

$$Y_i = \frac{\mu W_i}{K_c} \tag{4.8}$$

It should be noted that equation (4.6) is the same as equation (2.1), which describes the isolator behavior, except for the term $(1 - W_i/RK_c)$ which accounts for the finite initial and

unloading stiffness of the hysteresis loop due to the column flexibility. The quantity W_i/RK_c is actually the ratio of pre-yielding to post-yielding stiffness.

The coefficient of friction μ in equations (4.6) and (4.8) is, in general, dependent on the velocity of sliding and described by equation (2.3) with $\dot{U} = \dot{u}_b$. Here, and in equation (4.7) we used the hysteretic element velocity instead of the true bearing velocity. The former includes the column flexural velocity in addition to the bearing velocity. The error introduced due to this is assumed to be small because of the swift way with which friction varies with velocity.

The fact that the coefficient of friction varies swiftly with velocity and attains its maximum value f_{max} for most of the bearing motion suggests that μ in equations (4.6) and (4.8) may be replaced with f_{max} without any significant error. Indeed analyses with $\mu=f_{max}$ and with μ described by equation (2.3) gave identical results, so that the two-dimensional analysis was performed with $\mu=f_{max}=0.06$. This constant dynamic friction assumption has little effect on the structural responses of the isolation system or the frame as just mentioned, but affects the floor spectra at frequencies higher than the principal modes of the structure.

The solution of equations (4.1) to (4.8) is accomplished by first combining equations (4.1) and (4.5) to yield:

$$[\overline{M}]\{\ddot{U}\}+[\overline{C}]\{\dot{U}\}+[\overline{K}]\{U\}+\{A\}=-\{\overline{m}\}\ddot{u}_g \tag{4.9}$$

$$[\overline{M}]=\begin{bmatrix}[M] & \{m\}\\ \{m\}^T & \sum_{i=1}^{7} m_i\end{bmatrix} \tag{4.10a}$$

$$[\overline{K}]=\begin{bmatrix}[K] & \{0\}\\ \{0\}^T & \dfrac{W}{R}\end{bmatrix} \tag{4.10b}$$

$$[\overline{C}]=\begin{bmatrix}[C] & \{0\}\\ \{0\}^T & 0\end{bmatrix} \tag{4.10c}$$

$$\{U\}^T=\lfloor u_7,u_6,u_5,u_4,u_3,u_2,u_b \rfloor \tag{4.10d}$$

$$\{A\} = \begin{Bmatrix} \{0\} \\ \sum_{i=1}^{4} \mu W_i Z_i \left(1 - \frac{W_i}{RK_c}\right) \end{Bmatrix} \tag{4.10e}$$

$$\{\overline{m}\}^T = \left\lfloor m_7, m_6, m_5, m_4, m_3, m_2, \sum_{i=1}^{7} \frac{W}{g} \right\rfloor \tag{4.10f}$$

where W is the total structure weight $\left(\sum_{i=1}^{4} W_i\right)$.

Equations (4.9) and (4.7) may be reduced to a system of 1st order ordinary differential equations by defining a new vector of variables:

$$\{X\} = \begin{Bmatrix} \{X_1\} \\ \{X_2\} \\ \{Z\} \end{Bmatrix} \tag{4.11}$$

where,

$\{X_1\}^T$ = velocity vector = $\lfloor \dot{u}_7, \dot{u}_6, \dot{u}_5, \dot{u}_4, \dot{u}_3, \dot{u}_2, \dot{u}_b \rfloor$

$\{X_2\}^T$ = displacement vector = $\lfloor u_7, u_6, u_5, u_4, u_3, u_2, u_b \rfloor$

$\{Z\}^T = \lfloor Z_1, Z_2, Z_3, Z_4 \rfloor$

The new system of differential equations is

$$\{\dot{X}_1\} = -[M]^{-1}[C]\{X_1\} - [M]^{-1}[K]\{X_2\} - [M]^{-1}\{A\} - [M]^{-1}\{\overline{m}\}\ddot{u}_g \tag{4.12a}$$

$$\{\dot{X}_2\} = \{X_1\} \tag{4.12b}$$

$$\{\dot{Z}_i\} = \left\{ \frac{1}{Y_i}\left(-0.9|\dot{u}_b|Z_i|Z_i| - 0.1\dot{u}_b Z_i^2 + \dot{u}_b\right) \right\} \tag{4.12c}$$

These equations are numerically integrated using Gear's (1971) predictor-corrector method which is appropriate for stiff differential equations. Once the displacement and velocity values are obtained directly as a solution of these equations, the relative accelerations are calculated

using equation (4.12a). Story shears are then evaluated from the total acceleration time histories, which are obtained by adding to vector $\{\dot{X}_1\}$ the first floor acceleration $\ddot{u}_b$ and ground acceleration $\ddot{u}_g$.

4.2 Constant Load Formulation vs. Variable Load Formulation

The force-displacement relation of each hysteretic element (see equation 4.6) is dependent on the vertical load. The load is not constant but rather it varies as a result of the significant overturning moment in the tested slender model. The effect of the variation is two-fold. First it affects the stiffness (W_i/R) of the bearings, and second it affects the friction force (μW_i). Furthermore, it has an indirect effect on the coefficient of friction, which is dependent on the bearing pressure. All these effects of variation in vertical load were explicitly included in the variable load analytical formulation presented herein.

The FPS bearings were designed such as to achieve a static vertical pressure of about 18 ksi in all the bearings. However, the 7-story frame has a large aspect ratio resulting in large overturning moments during earthquake shaking. Large overturning moments induce large variations in the bearing vertical loading with time. For strong motions, zero vertical loads and local uplift of individual bearings occurred as a result of these overturning moments. It is deemed necessary to study if the local uplifts and zero load states cause significant influence on the isolation system response. Also it is analytically attempted to predict the response of the individual column in the isolation story. For the sake of comparison, two formulations were developed, one with the constant bearing load and the other with the variable bearing load.

In the constant bearing load formulation, the vertical load on all FPS bearings is assumed to be uniform throughout the table motion, as is assumed in the program 3D-BASIS (Nagarajaiah et al., 1989). The bearing load is simply the static dead load coming from the structure above. Hence, for interior column element $W_i = W/3$ and for exterior column element $W_i = W/6$, where W=47.5 kips.

In the variable bearing load formulation, the vertical load on the FPS bearings is calculated based on the local frame column loads caused by the table motion. At each time step of integration, the horizontal inertia forces are calculated from the floor accelerations and multiplied by a coefficient matrix to obtain the corresponding increase or reduction in the

vertical loads on the bearings due to the local frame action. The resulting vertical load may be expressed as:

$$\{W\} = [B]\{FI\} + \{WD\} \tag{4.13}$$

where,

$\{W\}^T = \lfloor W_1, W_2, W_3, W_4 \rfloor$

$[B]$ = Coefficient matrix which upon multiplication by vector $\{FI\}$ gives the bearing forces due to inertia effects.

$\{FI\}$ = Vector containing the horizontal inertia forces at the floor levels

$\{WD\}^T = \left\lfloor \frac{W}{6}, \frac{W}{3}, \frac{W}{3}, \frac{W}{6} \right\rfloor$

The load vector $\{WD\}$ corresponds to the dead load acting on the bearings. The coefficient matrix $[B]$ is evaluated from two dimensional structural analyses of the 7-story frame supported on hinge supports and subjected to horizontally acting static unit loads at the different floor levels. It needs to be noted that the above equation is valid as long as there is no negative bearing reaction.

Negative bearing forces given by equation (4.12) cannot be a reality since there is no uplift restraint provided in the FPS bearings. This means that there will be support uplift due to overturning effects. Accordingly, all vertical bearing loads need to be readjusted as shown below so as to achieve zero bearing reaction at the uplifted support:

$$\{W\} = \{BV\}W_u + [B]\{FI\} + \{WD\} \tag{4.14}$$

where,

$\{BV\}$ = Coefficient vector corresponding to vertical force equal and opposite to the negative bearing reaction

W_u = negative bearing force as calculated from equation (4.13)

The coefficient vector $\{BV\}$ is evaluated from two dimensional structural analysis of the 7-story frame, subjected to static unit upward force at the support of concern, with the other supports remaining unaffected. It may be possible in some extreme cases in the braced frame, the interior columns experience uplift in addition to the exterior columns. That possibility is also taken into account in the analysis following a similar line of action. Using the new bearing

loads, the floor accelerations are recalculated using equation (4.12a) and the bearing loads are reevaluated using the procedure outlined above. Iteration is continued till a convergence is achieved on the bearing loads. These vertical loads are used in the numerical integration process (solution of equations 4.12a,b,c) for the next time step. Furthermore, the friction coefficient is regularly updated according to the new bearing pressure.

The individual bearing displacement is evaluated from the isolation system displacement

$$u_b = u_{bi} + u_{ci} \tag{4.15}$$

where u_{bi} = bearing displacement and u_{ci} = column deformation.
The column deformation equals to the ratio of the bearing shear force to the column stiffness:

$$u_{ci} = \frac{\mu W_i}{K_{ci}} + \frac{W_i}{RK_{ci}} u_{bi} \tag{4.16}$$

Equations (4.14) and (4.15) can be solved for u_{bi}

$$u_{bi} = \frac{u_b - \dfrac{\mu W_i}{K_c}}{1 + \dfrac{W_i}{RK_c}} \tag{4.17}$$

Equation (4.16) is not exact since it assumes first in-phase column deformation and bearing displacement, and second in-phase friction and restoring bearing forces. Furthermore, the calculation of the vertical bearing loads through equations (4.12) and (4.13) is approximate since the equations are based on the assumption of hinged supports. In reality the supports are sliding with frictional and restoring forces acting on them. The implication of this reality is that the matrix $[B]$ and $\{BV\}$ are not constant as assumed, but rather they are dependent on the inertia forces $\{FI\}$ and force W_u.

Analytical results are obtained for the isolated moment frame structure MFUIS for a very strong El Centro S00E 200% earthquake using the two different formulations. Figures 4-4 and 4-5 present comparison of analytical and experimental results for the constant load formulation, while figures 4-6 and 4-7 present the same for the variable load formulation. The shake table acceleration recorded during the test is used as the input ground motion $\ddot{u}_g$ in the

analysis. Figures 4-4 and 4-6 show that both the constant and variable formulations for vertical load modeling demonstrate very good agreement between experimental and analytical results for the isolation system displacement and base shear.

Figures 4-5 and 4-7 present the isolation story column shear force- bearing displacement response for the four columns namely C0, C1, C2, C3 (in the direction of shaking). Experimental results show that the exterior columns (C0, C3) were subjected to zero shear, in other words there was uplift at the exterior bearings. The large aspect ratio of the structure resulted in very large overturning moments under the action of very strong motion. Figure 4-5 demonstrates that the constant load formulation results in a column shear response very different from the experimental results. We observe serious underestimation of the column shears, notably in the exterior columns where the overturning effects are maximum. Figure 4-7 shows that the variable load formulation analysis gives a reasonable representation of the column shear hysteresis response. Analytical column shears in the exterior columns are however somewhat higher (on the conservative side). It may be concluded that the assumption of constant bearing load results in significantly different individual column shears at the isolation story, but the overall behavior of the isolation system is predicted with good accuracy.

4.3 Analytical Verification of Experimental Results

Analytical prediction of experimental results using the variable bearing load formulation are presented in greater detail in this section. Comparison of experimental and analytical results are presented for the moment frame MFUIS and the braced frame BFUIS. The formulation requires the use of the natural frequencies, mode shapes and damping ratios of the upper six story frame on a fixed base. For the moment frame, these dynamic properties are taken from those reported by Mokha et al. (1990) and have been listed in table 2-I. As reported in the previous section, figures 4-6 and 4-7 present results on the isolation system response and the column shear response for earthquake El Centro S00E 200%. Figure 4-8 presents upper story responses (peak story drift / peak story shear). It appears that in addition to the isolation system response, the analytical method also predicts very well the higher mode effects prevailing in the upper structure response. The analytical method is capable of reproducing almost every detail of the experimental results.

Figures 4-9 to 4-14 present similar comparative studies for the moment frame for the earthquakes Pacoima S74W 100% and Taft N21E 400%. It may be noted that the analytical

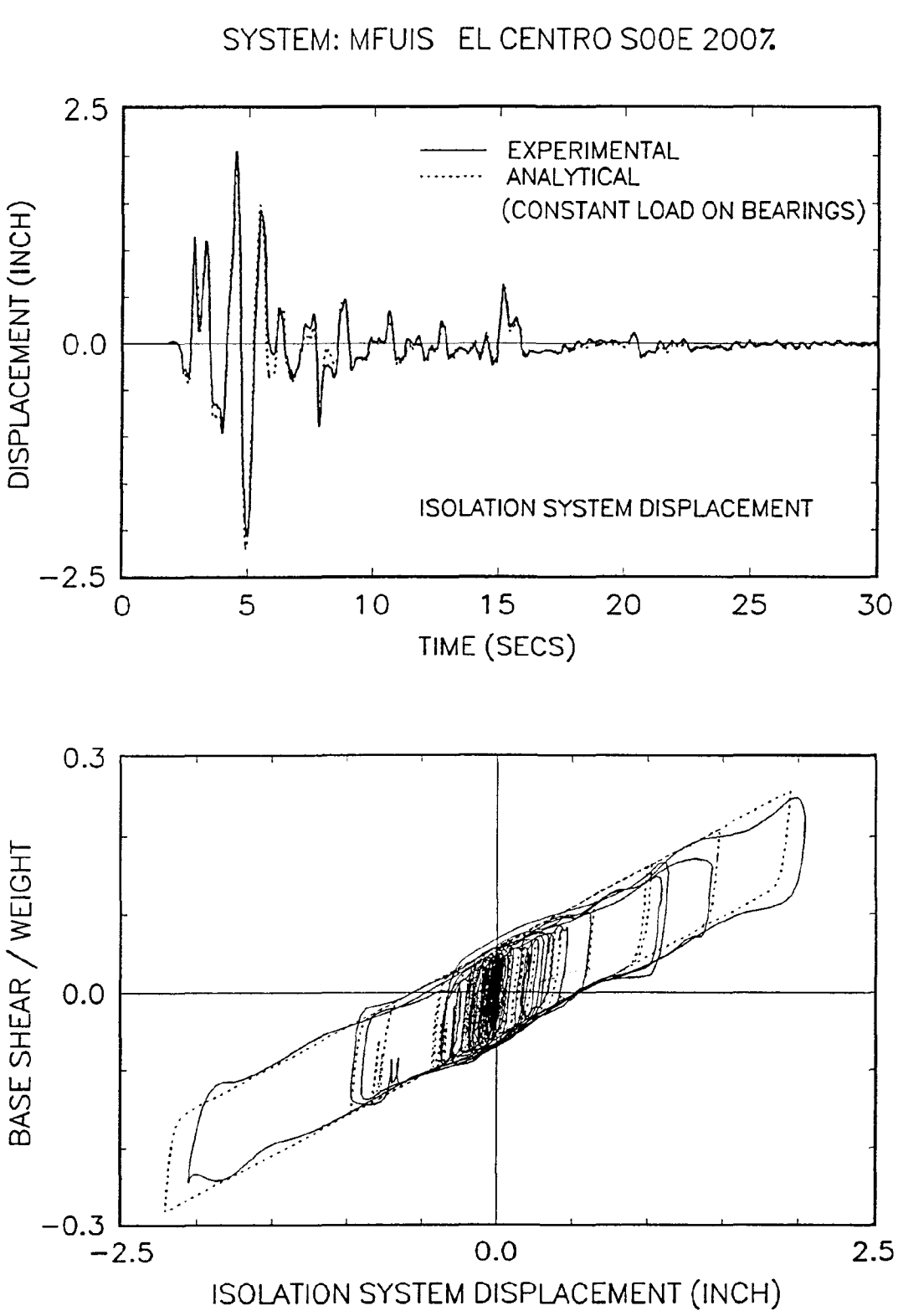

FIGURE 4-4 Comparison between Experimental Results and Analysis (based on constant bearing load): Isolation System Response of MFUIS for El Centro S00E 200%

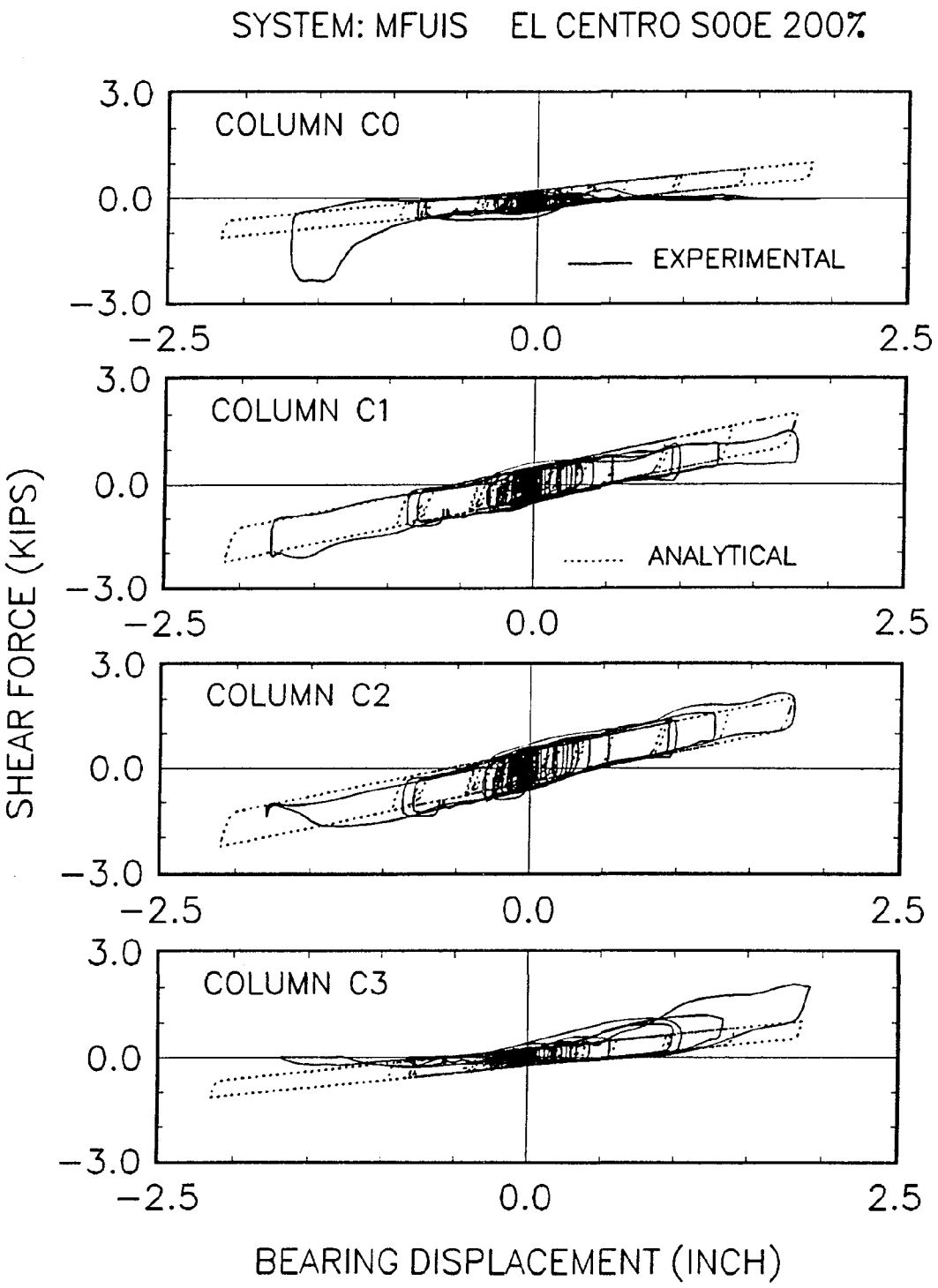

FIGURE 4-5 Comparison between Experimental Results and Analysis (based on constant bearing load): Individual Column Shear Response of MFUIS for El Centro S00E 200%

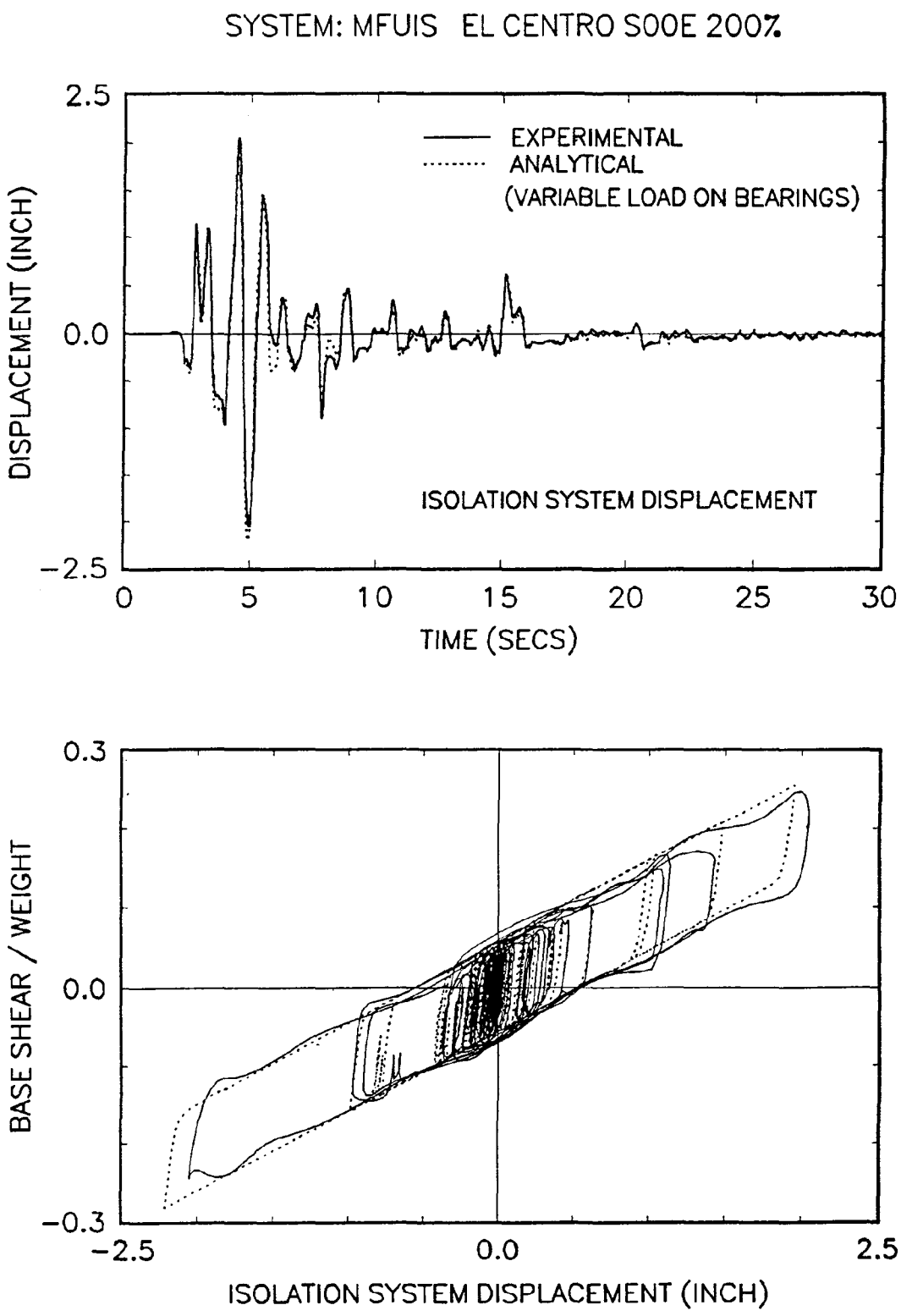

FIGURE 4-6 Comparison between Experimental Results and Analysis (based on variable bearing load): Isolation System Response of MFUIS for El Centro S00E 200%

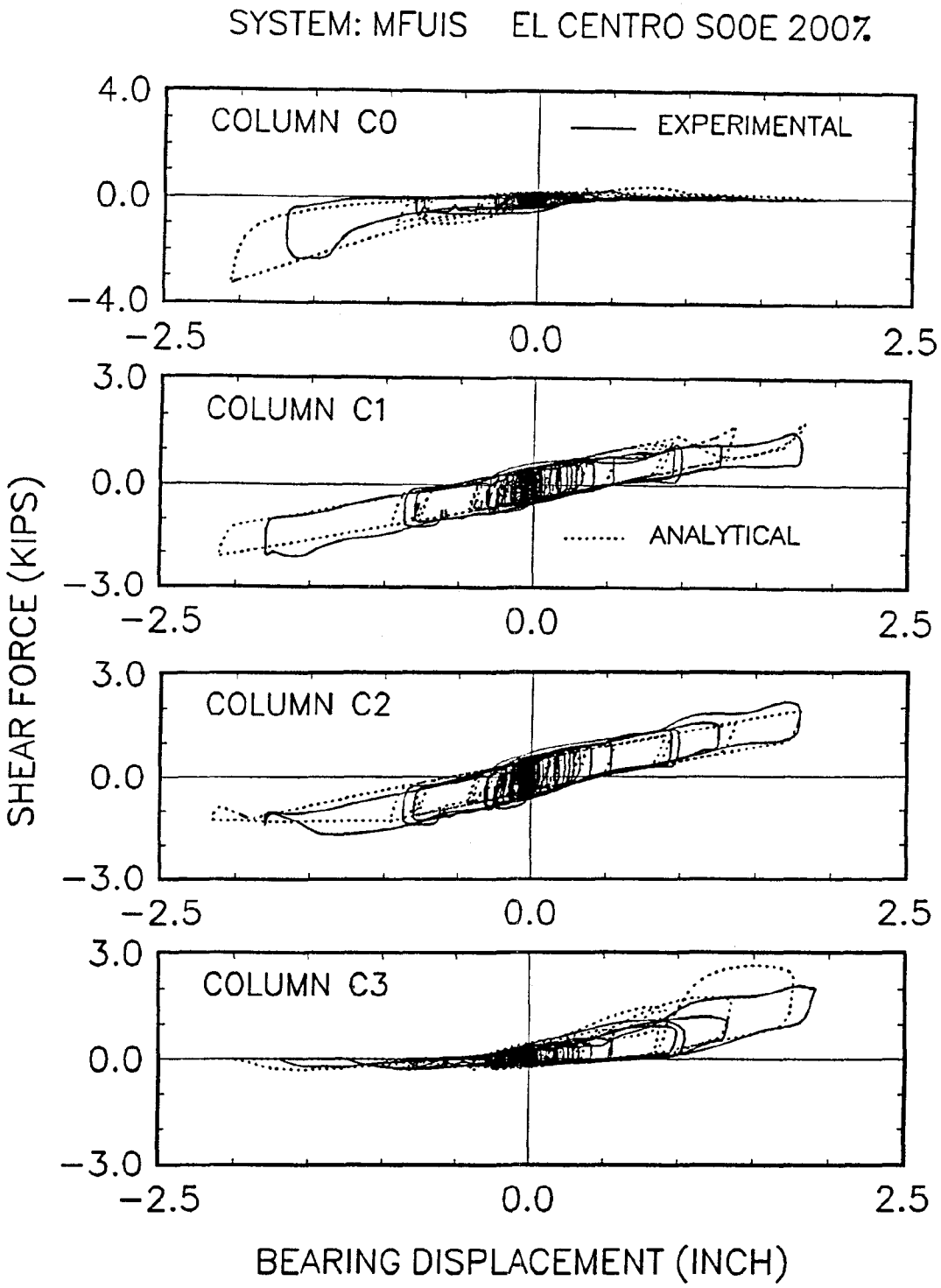

FIGURE 4-7 Comparison between Experimental Results and Analysis (based on variable bearing load): Individual Column Shear Response of MFUIS for El Centro S00E 200%

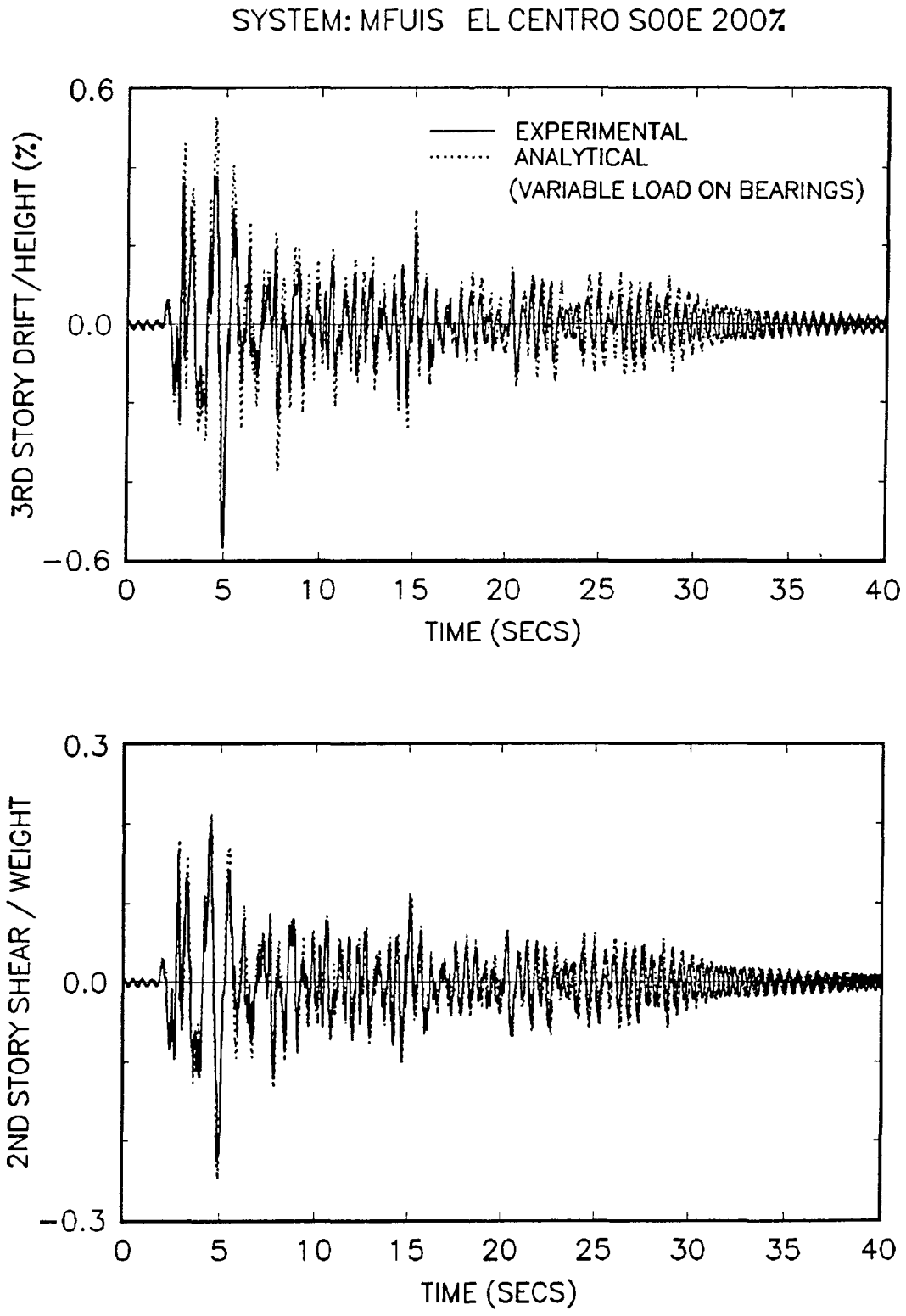

FIGURE 4-8 Comparison between Experimental Results and Analysis (based on variable bearing load): Superstructure Response of MFUIS for El Centro S00E 200%

upper story responses during the final stages (weak part) of the motion are sometimes out of phase with the actual response.

For the seven story braced frame BFUIS, the natural frequency was found to be only 3.0 Hz from white noise tests. The natural frequency of the six story upper frame and the seven story frame is expected to be about the same, as observed in the case of the moment frame (section 2.3.1). However, the upper six story frame was analytically evaluated to have a fundamental frequency of 5.5 Hz. As mentioned earlier in section 2.3.1, this was due to faulty bracing which probably allowed slippage at oversized bolt holes in some of the braces, thus drastically reducing the lateral stiffness of the frame. The fundamental frequency of the upper six story frame was estimated from experimental results considering that structures tend to vibrate (free vibration) in their fundamental mode after the excitation force ceases. From test results of structure vibrations of the seventh floor relative to the first floor after shake table motion stops, a uniform harmonic motion at a frequency of about 3.05 Hz is observed. This value is very close to the white noise test results on the fixed-base braced frame. Keeping all these in mind, all analytically obtained frequencies were scaled down such that the fundamental frequency is about 3.05 Hz. The same mode shapes were, however, used. The same damping ratios as used in the moment frame were used. Table 4-I lists the dynamic characteristics of the six story braced frame that were used in the analysis.

TABLE 4-I Dynamic Properties Used in Analysis of Isolated Braced Frame

Mode	Frequency (Hz)	Damping Ratio	Mode Shapes					
			Floor 2	Floor 3	Floor 4	Floor 5	Floor 6	Floor 7
1	3.05	0.0142	0.105	0.265	0.452	0.645	0.834	1
2	10.86	0.0204	0.578	1	0.994	0.533	-0.217	-0.95
3	20.78	0.0235	0.968	0.881	-0.254	-1	-0.422	0.795
4	29.09	0.0155	1	-0.107	-0.99	0.304	0.882	-0.574
5	35.6	0.0059	0.906	-0.921	0.143	0.792	-1	0.416
6	39.81	0.0086	0.519	-0.86	1	-0.916	0.612	-0.196

Figures 4-15 to 4-20 present comparison of experimental results with analysis results for the braced frame. Two different earthquakes El Centro S00E 200% and Pacoima S74W 100% are presented. Very good agreement is achieved in predicting the overall isolation system response and shear forces. Reasonable prediction of the peak story drift is also possible. If frequencies starting from 5.5 Hz were used in the analysis instead of the 3.05 Hz mark, then a much lower 3rd story drift (than experimentally observed) is obtained. With regards to the individual column shear, there appears to be significant differences between analytical and experimental results, which could be due to improper distribution of the lateral stiffness between the columns caused by faulty bracings.

It may also be noted that analytical results show that the braced frame has a slightly greater base shear than the moment frame (compare Figures 4-6 and 4-15). This is in agreement with experimental observations reported in section 2.3.2.

4.4 3D-BASIS Analysis

The computer program 3D-BASIS (Nagarajaiah, 1990) was also used for predicting the experimental response of the 7-story frame. 3D-BASIS is currently in use by practicing engineers for time history dynamic analysis of three-dimensional base-isolated structures. Currently, the available version of the program employs a constant load formulation for the bearing vertical loads. It also uses a different solution procedure for solving the differential equations of motion from that used in the two dimensional analysis presented in sections 4.1 to 4.3. The algorithm is based on the solution of the equations of motion using a combination of Newmark's integration method and a fourth-order Runge-Kutta scheme, with a Pseudo Load formulation and time marching procedure for accuracy and efficiency. This algorithm has been proven to be very suitable for analyzing highly non-linear sliding isolation systems.

Similar to the structural modeling concept described in section 4.1, the 7-story structure was modeled as a six story three-dimensional frame on top of an isolation story. Each floor mass is lumped into a single point mass having three degrees of freedom (two lateral and one torsional) in the horizontal plane. The isolation story was modeled with eight sliding frictional elements representing the eight columns with a flat sliding interface at their base. The sliding element accounts for the velocity dependency of the friction coefficient given by equation (2.3). The "yield displacement" in the model of friction in 3D-BASIS was selected to be equal to

$$Y_i = \frac{f_{\max} W_i}{K_c} \tag{4.18}$$

where W_i=static load on *ith* bearing, K_c=column stiffness on top of *ith* bearing and f_{max}=0.06. To account for the lateral stiffness of the FPS isolators, a global spring of stiffness $K = W/R$ was used, where W=47.5 kips and R=9.75 inches.

An eigenvalue analysis of the six story upper frame was carried out using 'ETABS' software. These eigenvalues and eigenvectors were then used in the 3D-BASIS input file. Owing to the unidirectional table motion and structural symmetry, only the modes in the direction of motion were considered. A total of nine modes (out of total 18 modes corresponding to six lumped masses) were used in the 3D-BASIS analysis, which included all six modes in the direction of motion. Structural damping were taken corresponding to table 2-I (Mokha et al., 1990) obtained for the six story moment frame.

Comparisons of 3D-BASIS analysis results with the experimental results are given in figures 4-21 to 4-27. Figure 4-21 presents results on the isolation system response of the moment frame with unbraced isolation system (MFUIS) for the very strong level El Centro S00E 200% motion. Figure 4-22 presents comparisons on the 7th, 5th and 2nd story shear time histories (the 2nd story shear is the peak story shear in the upper frame). Figure 4-23 presents results on the 7th, 5th and 3rd story drift time histories (the 3rd story drift is the peak story drift in the upper frame). The comparisons show excellent agreement between the analytical and experimental results for the isolation system shear and displacement, as well as for the upper story structure shears and drifts. However, some difference is observed in the prediction of the story drift response in the top (7th) story level of the test frame. This could be due to various factors such as table rocking effects or inaccurate estimation of modal structure damping.

Figures 4-24 to 4-26 presents similar comparison for a different and a moderate level earthquake of Pacoima S74W 50%. These figures demonstrate excellent agreement regarding the isolation system response and the superstructure responses including the 7th story drift response.

Figure 4-27 presents comparison between analytical and experimental results for the long period motion of Hachinohe NS 150% and for a different moment frame structure MFBIS. The isolation system modeling slightly changes with different stiffness corresponding to the

braced isolation story stiffness. Figure 4-27 shows that the isolation system response is well predicted.

All comparisons indicate that the 3D-BASIS algorithm is a reliable tool for analyzing the response of seismically isolated multi-story frame structures. However, due to the constant load formulation in 3D-BASIS, the individual bearing force prediction are not correct in cases of substantial overturning effects. The excellent agreement, as observed, between the experimental and analytical responses of the isolation system is a result of the consistency and repeatability of the FPS isolation system. The ability to model the isolation system accurately results in excellent predictions of the upper story shears and drifts.

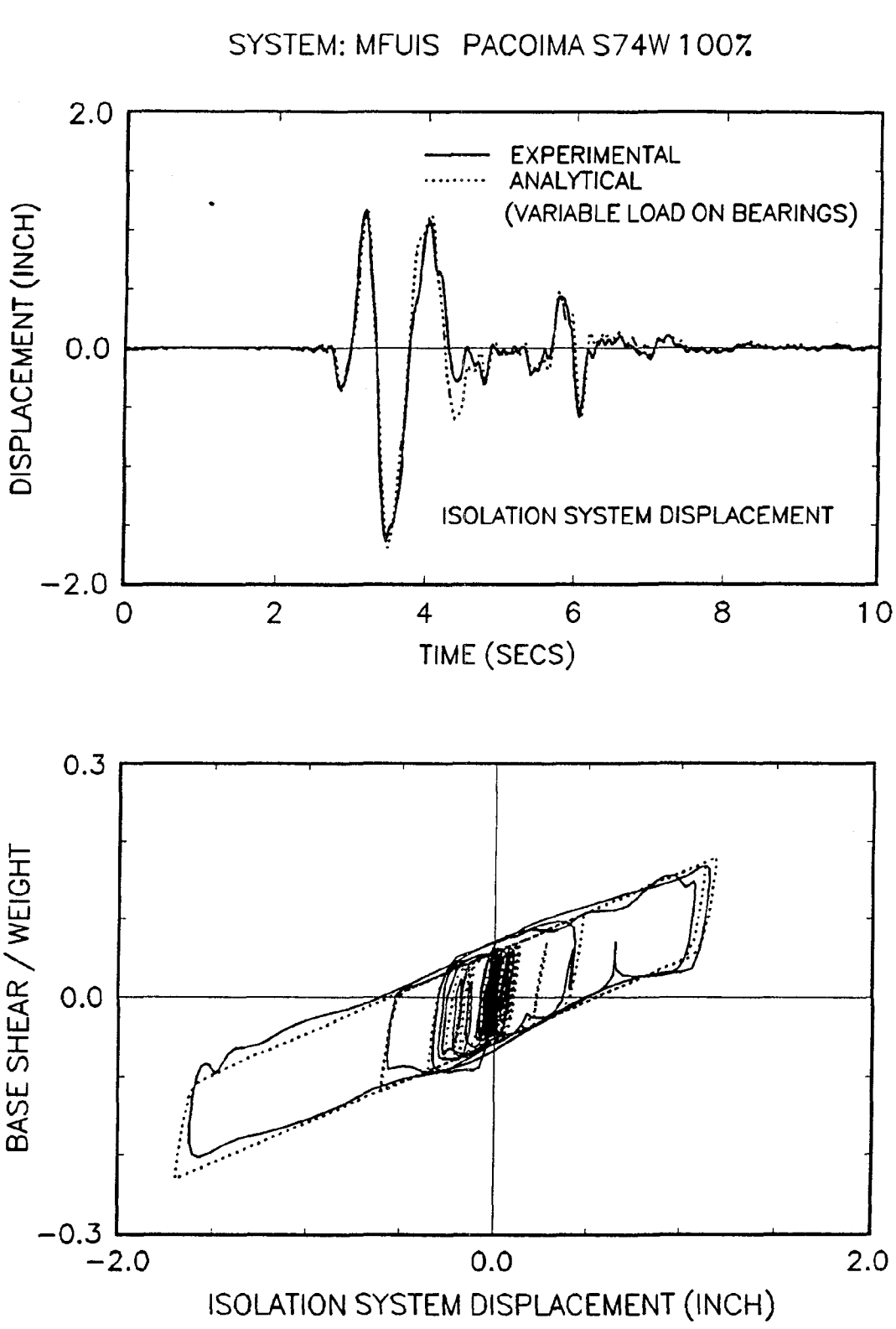

FIGURE 4-9 Comparison between Experimental Results and Analysis: Isolation System Response of MFUIS for Pacoima S74W 100%

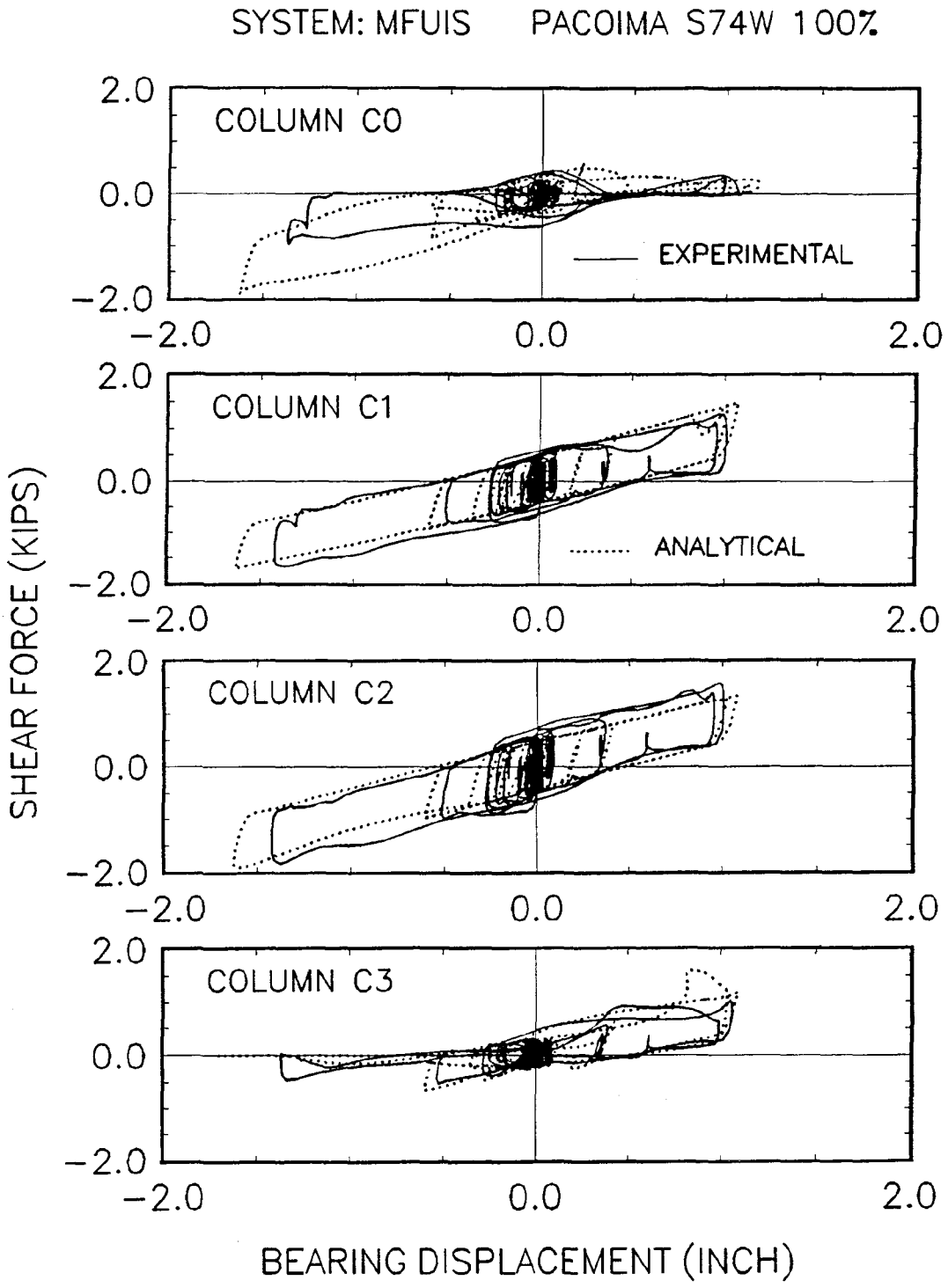

FIGURE 4-10 Comparison between Experimental Results and Analysis: Individual Column Shear Response of MFUIS for Pacoima S74W 100%

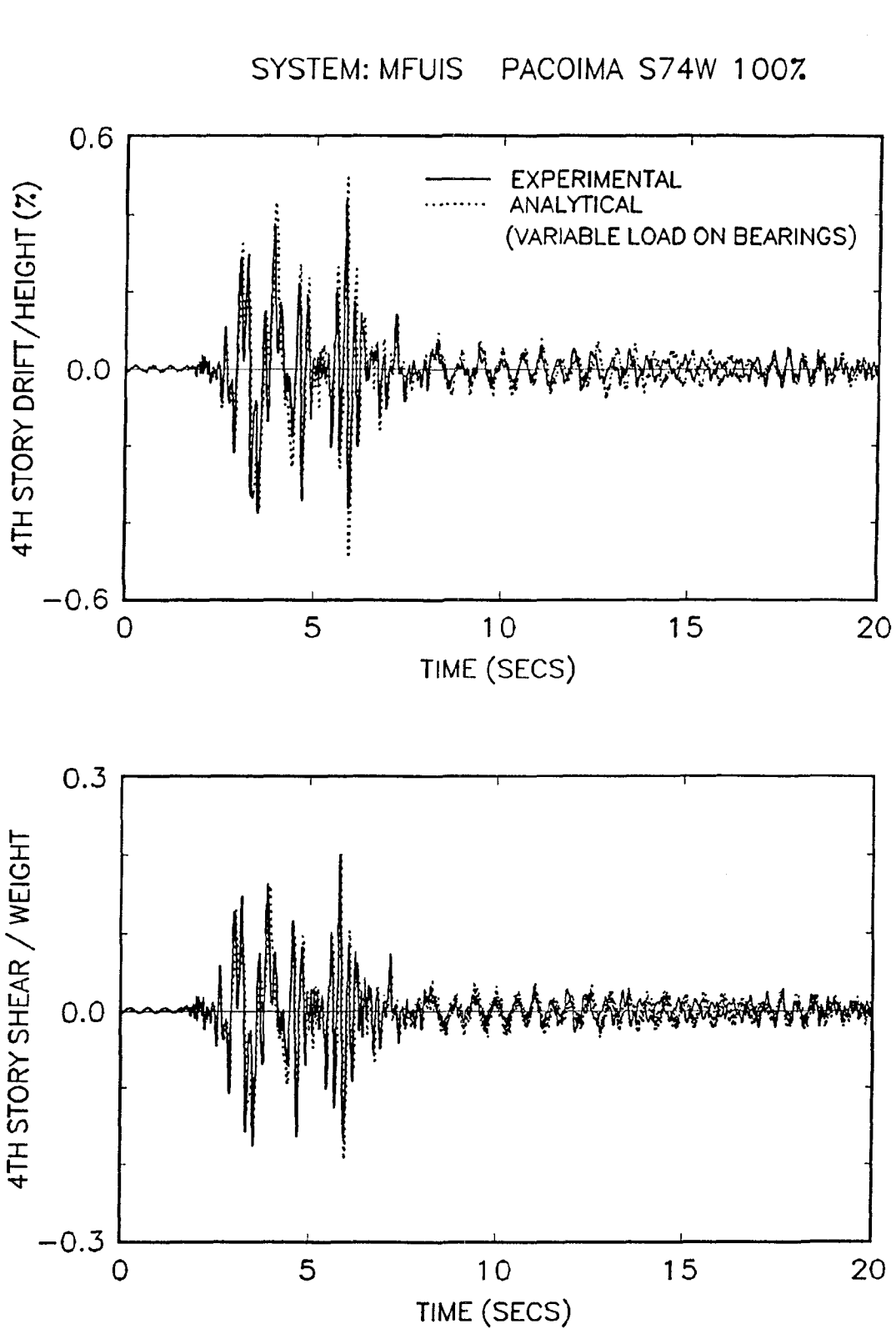

FIGURE 4-11 Comparison between Experimental Results and Analysis: Superstructure Response of MFUIS for Pacoima S74W 100%

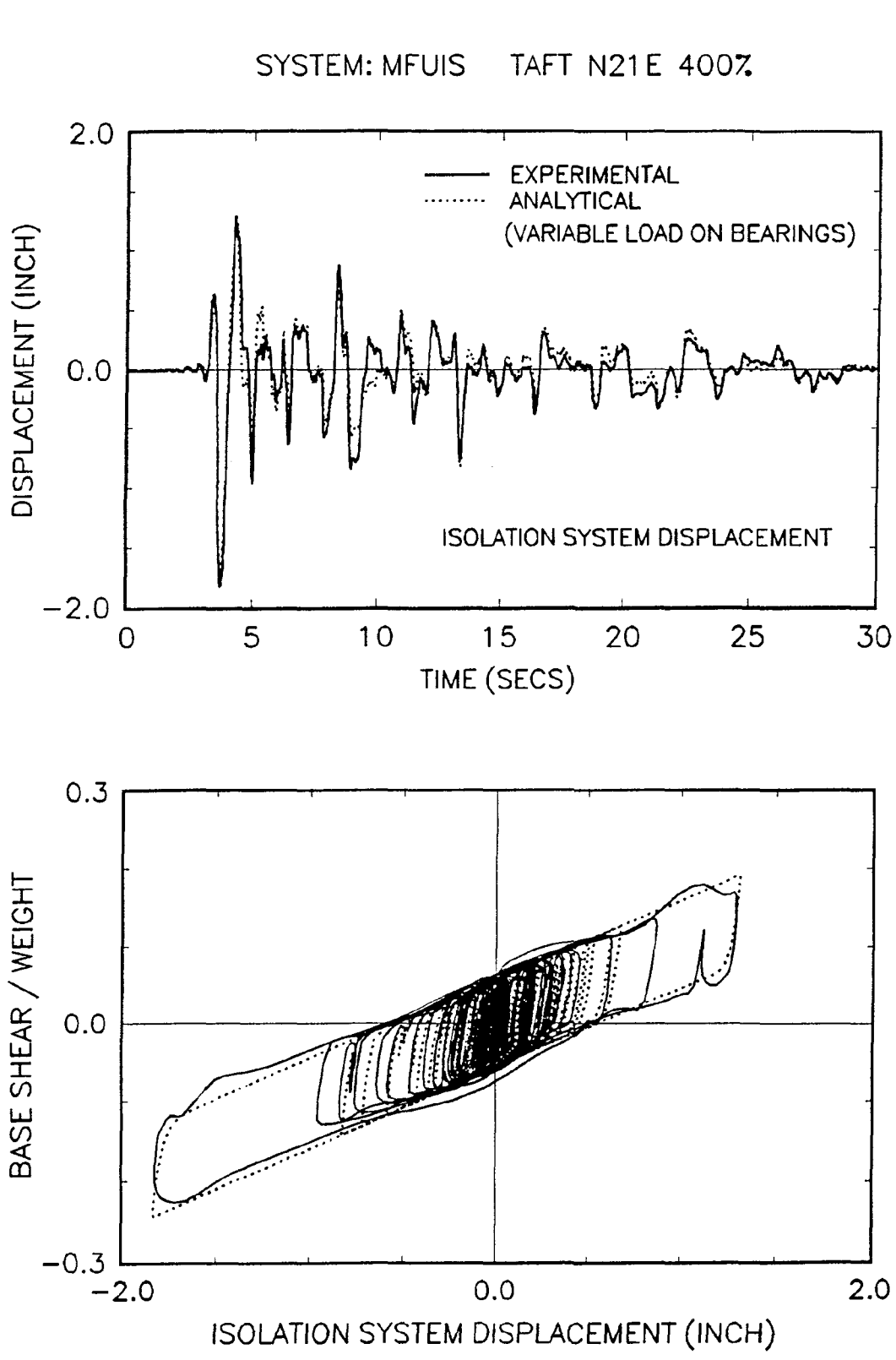

FIGURE 4-12 Comparison between Experimental Results and Analysis: Isolation System Response of MFUIS for Taft N21E 400%

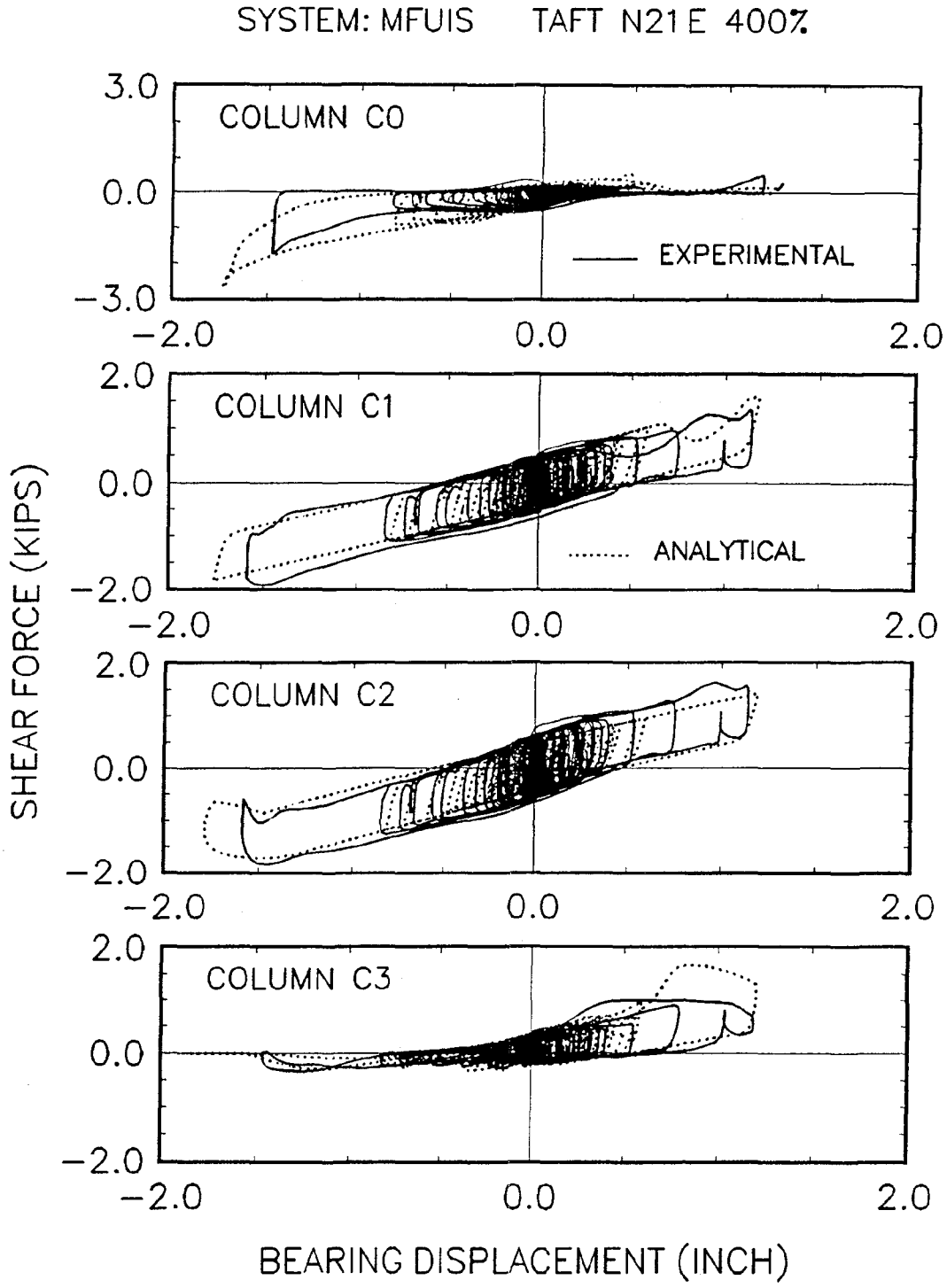

FIGURE 4-13 Comparison between Experimental Results and Analysis: Individual Column Shear Response of MFUIS for Taft N21E 400%

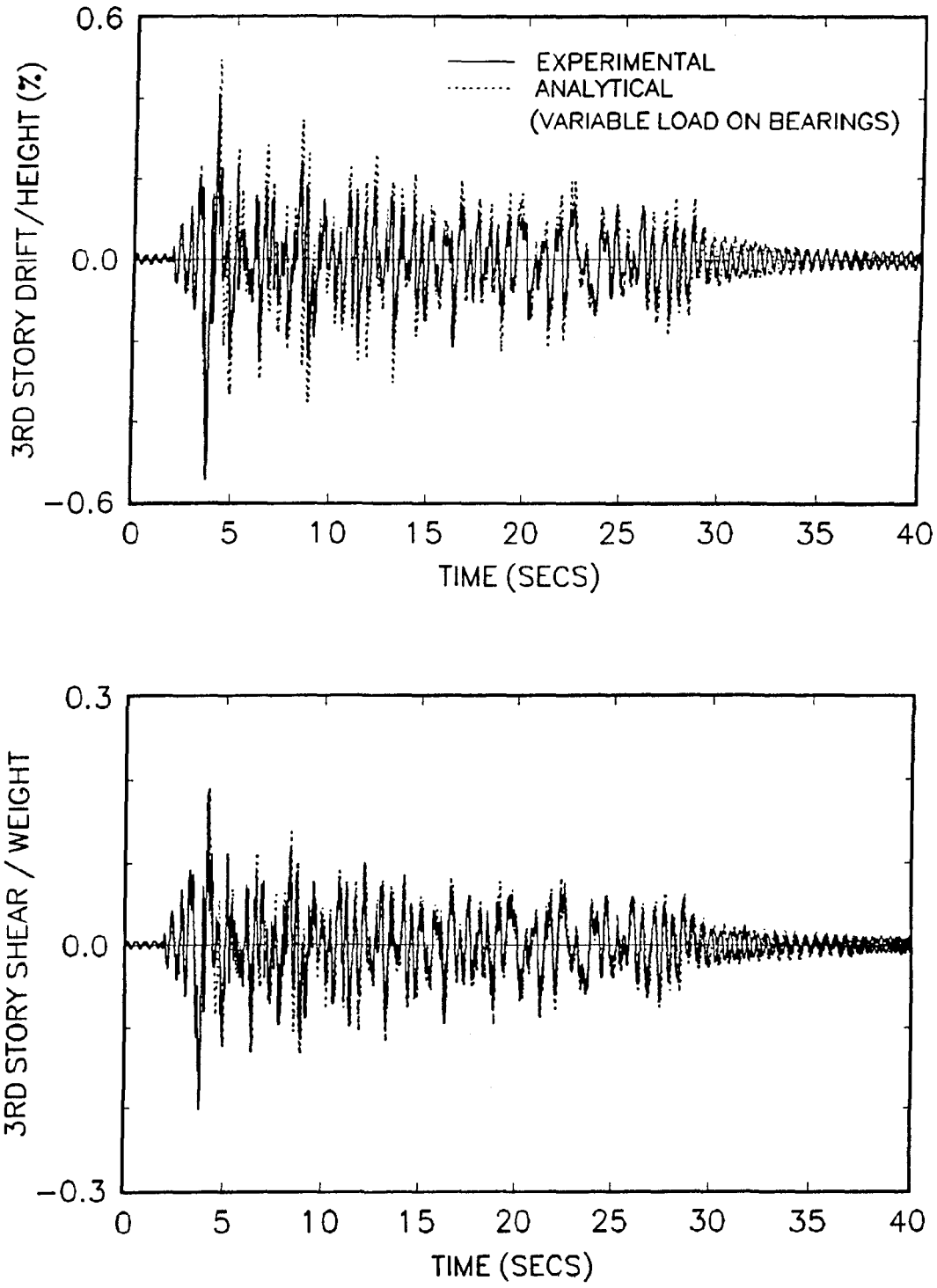

FIGURE 4-14 Comparison between Experimental Results and Analysis: Superstructure Response of MFUIS for Taft N21E 400%

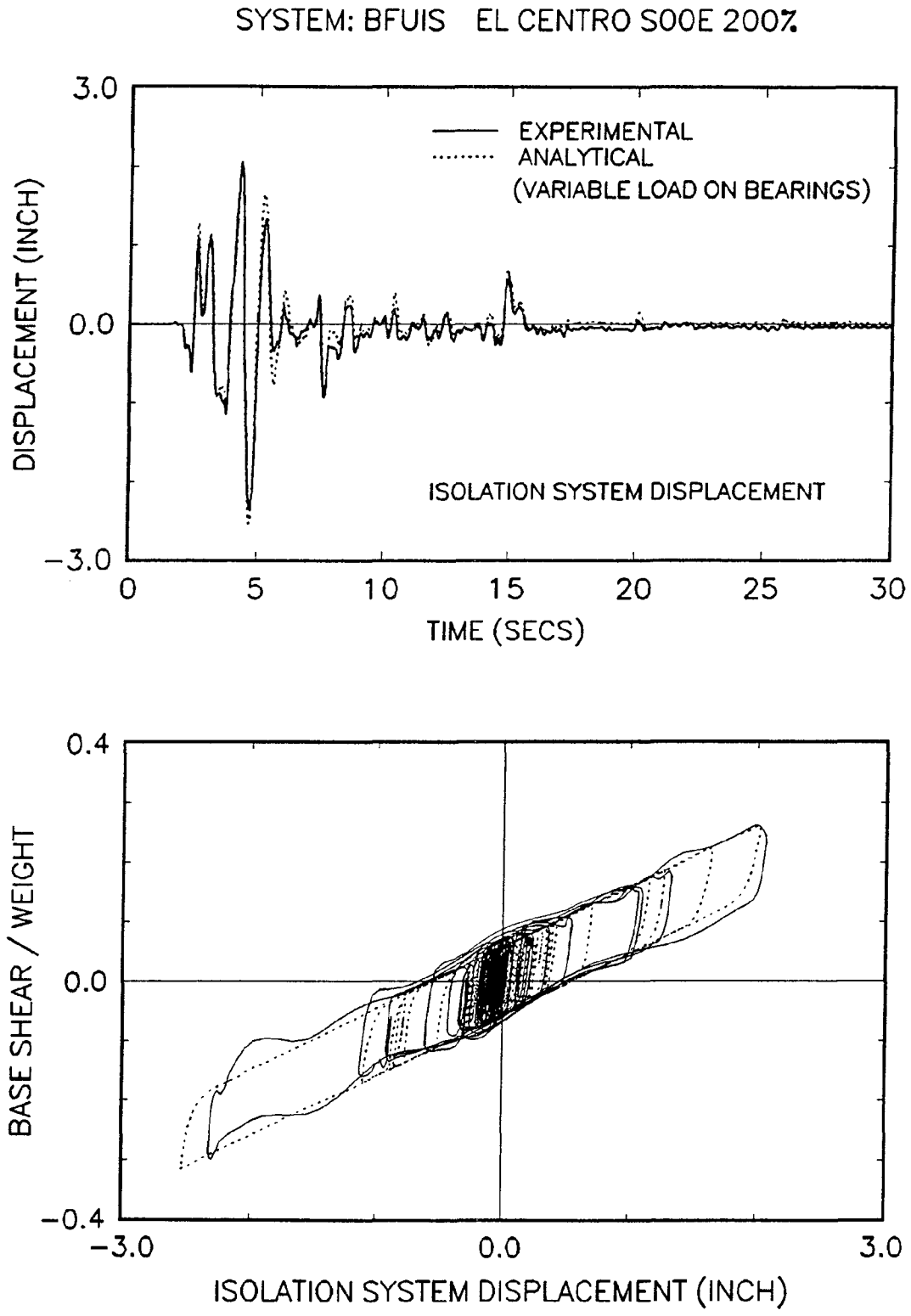

FIGURE 4-15 Comparison between Experimental Results and Analysis: Isolation System Response of BFUIS for El Centro S00E 200%

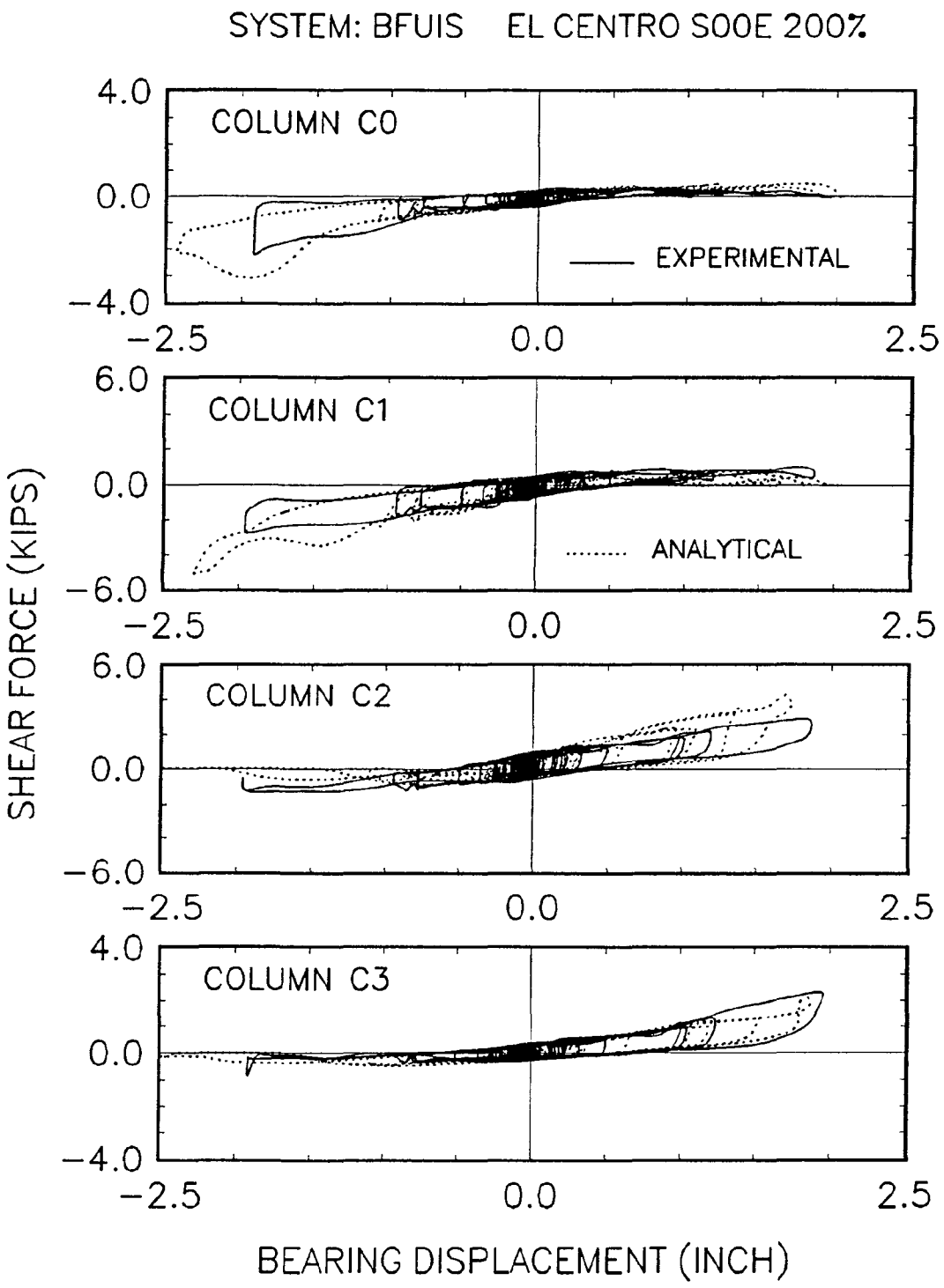

FIGURE 4-16 Comparison between Experimental Results and Analysis: Individual Column Shear Response of BFUIS for El Centro S00E 200%

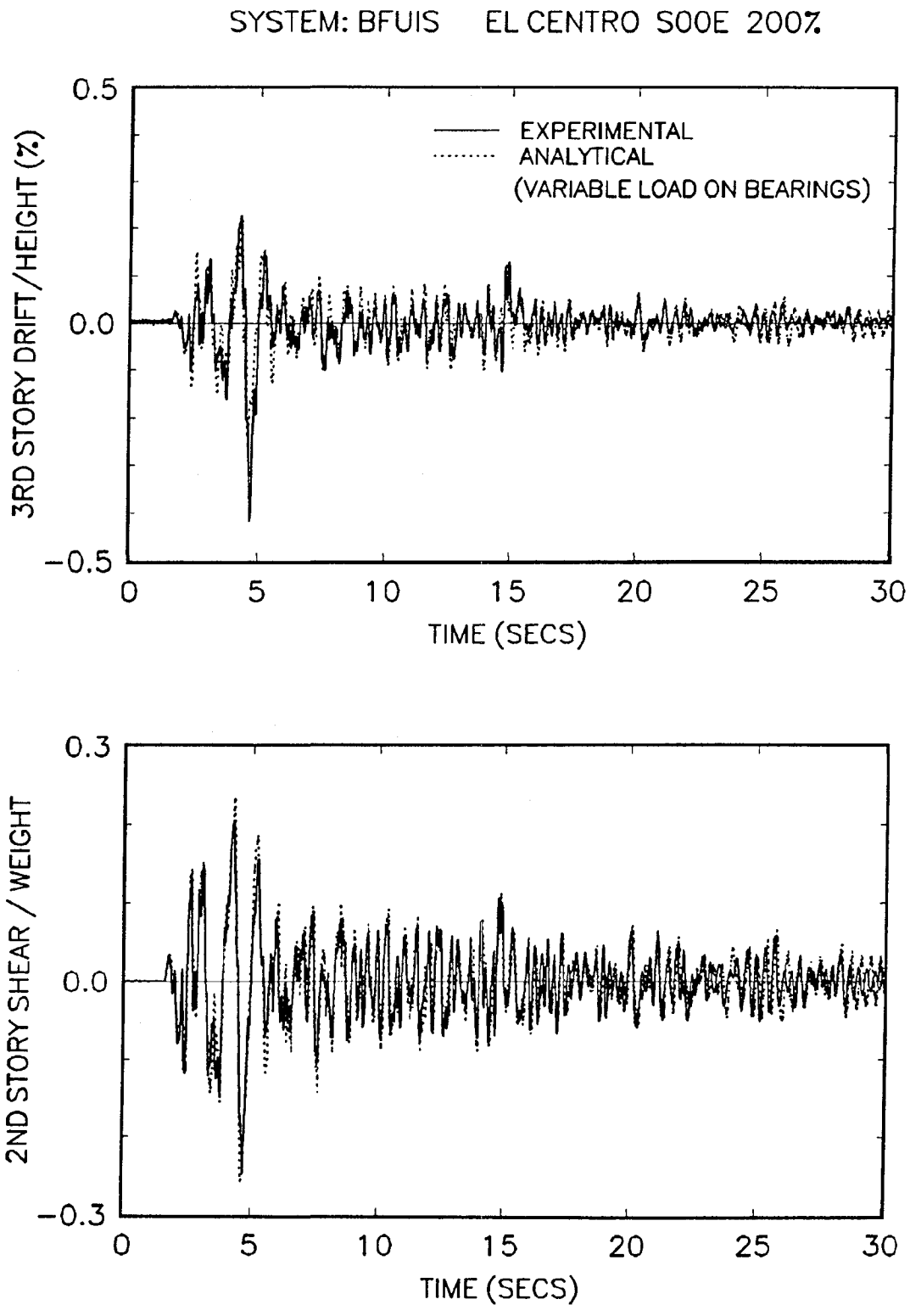

FIGURE 4-17 Comparison between Experimental Results and Analysis: Superstructure Response of BFUIS for El Centro S00E 200%

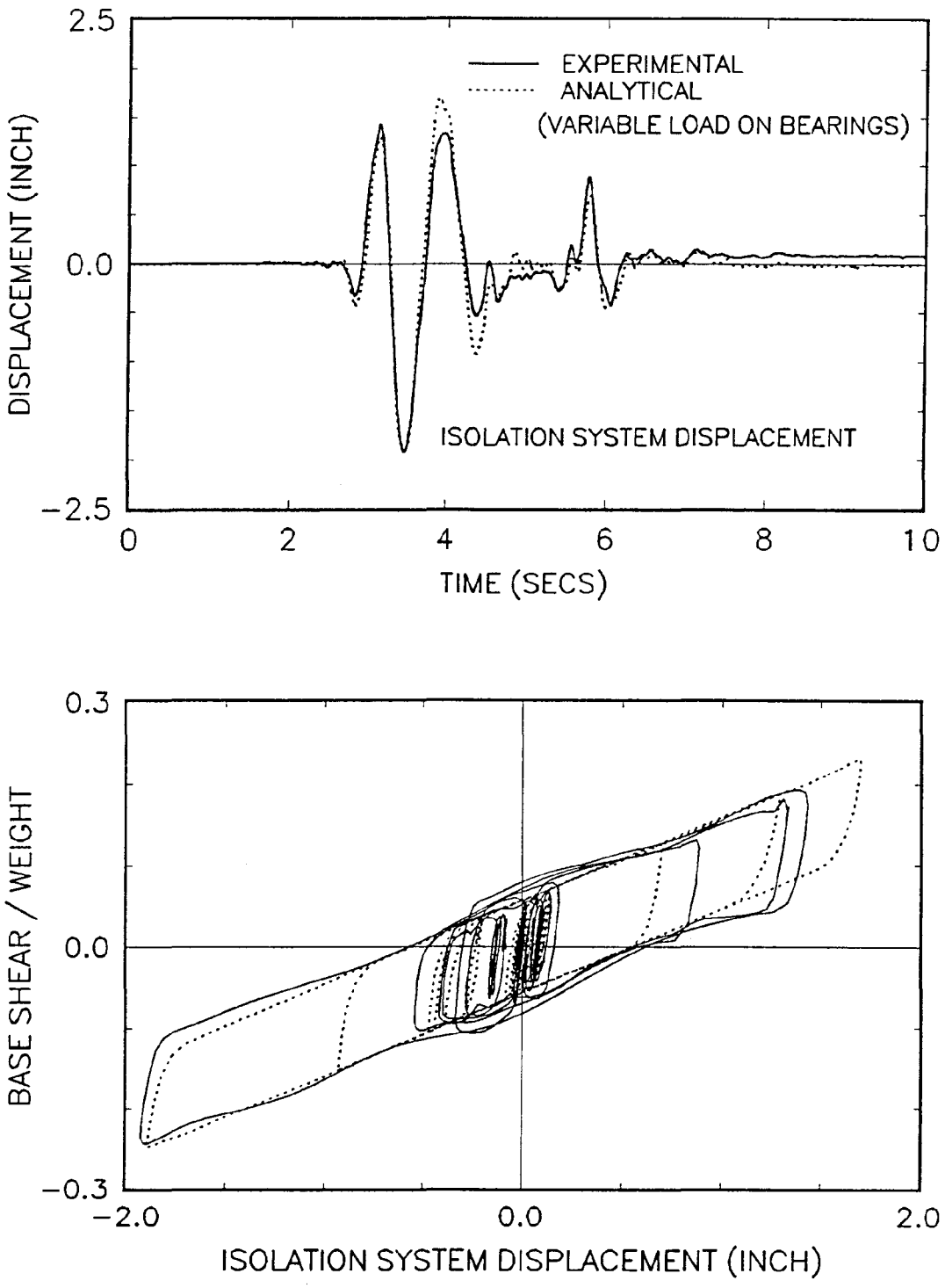

FIGURE 4-18 Comparison between Experimental Results and Analysis: Isolation System Response of BFUIS for Pacoima S74W 100%

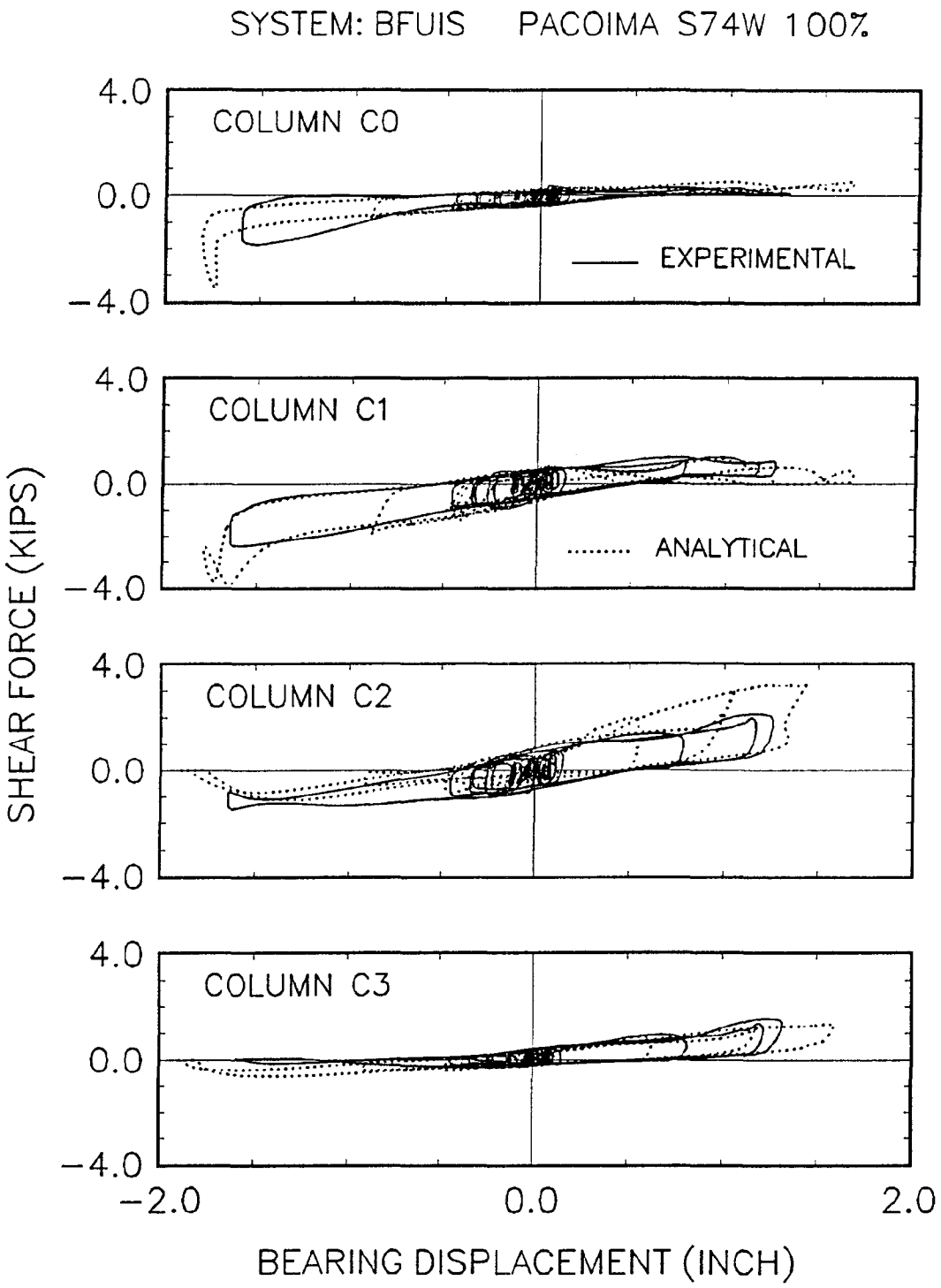

FIGURE 4-19 Comparison between Experimental Results and Analysis: Individual Column Shear Response of BFUIS for Pacoima S74W 100%

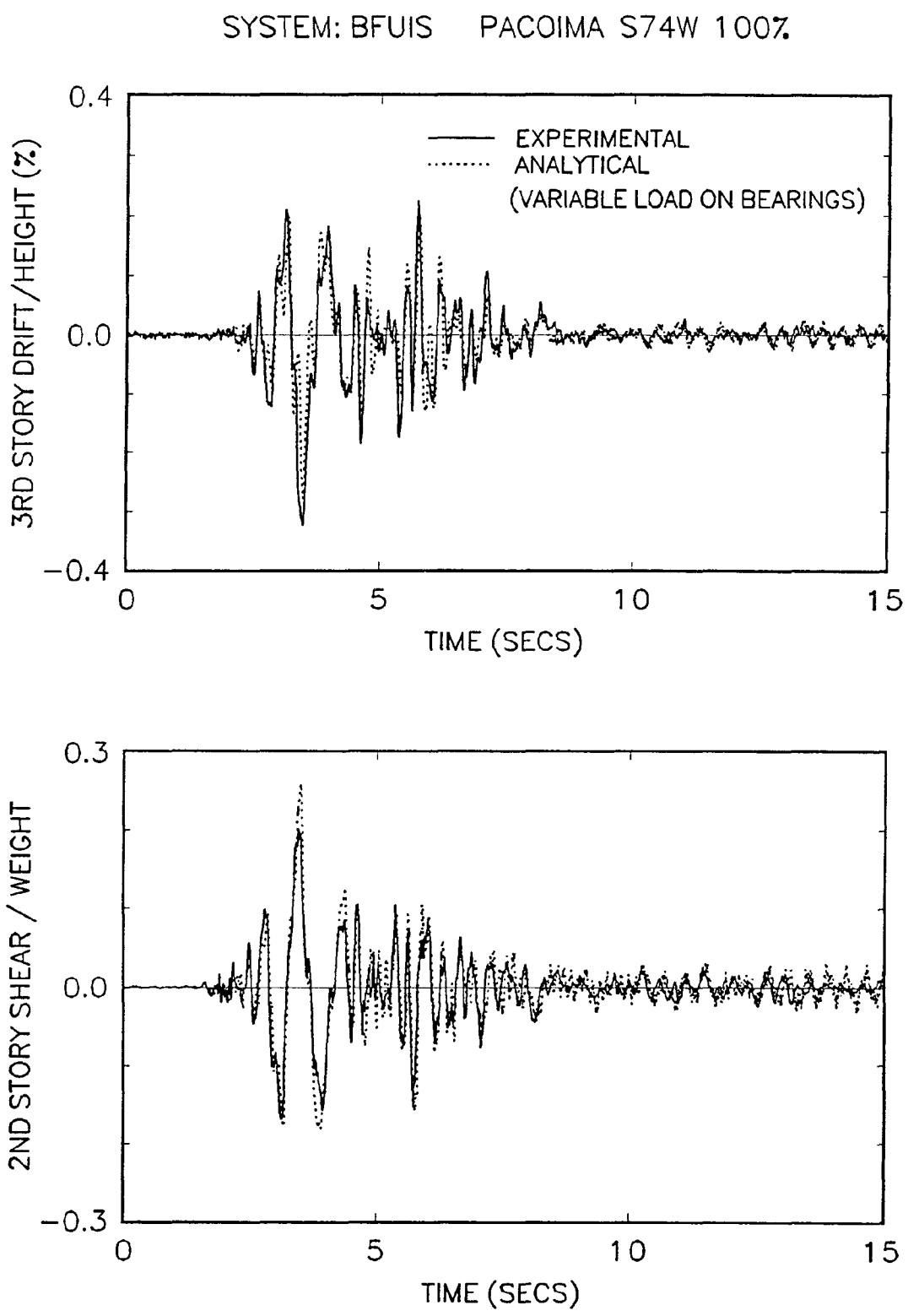

FIGURE 4-20 Comparison between Experimental Results and Analysis: Superstructure Response of BFUIS for Pacoima S74W 100%

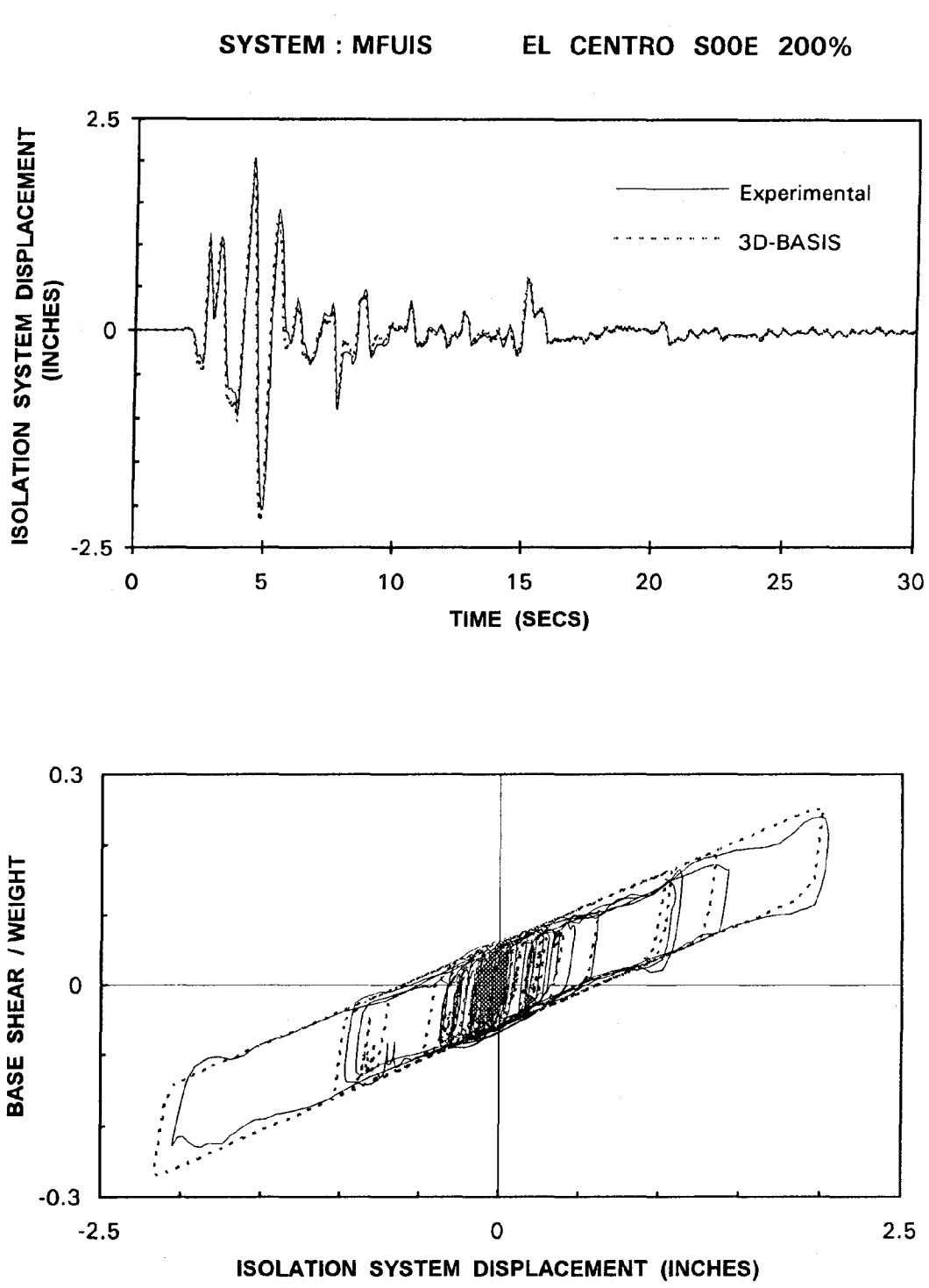

FIGURE 4-21 3D-BASIS Prediction of Isolation System Response in Structure MFUIS for El Centro S00E 200%

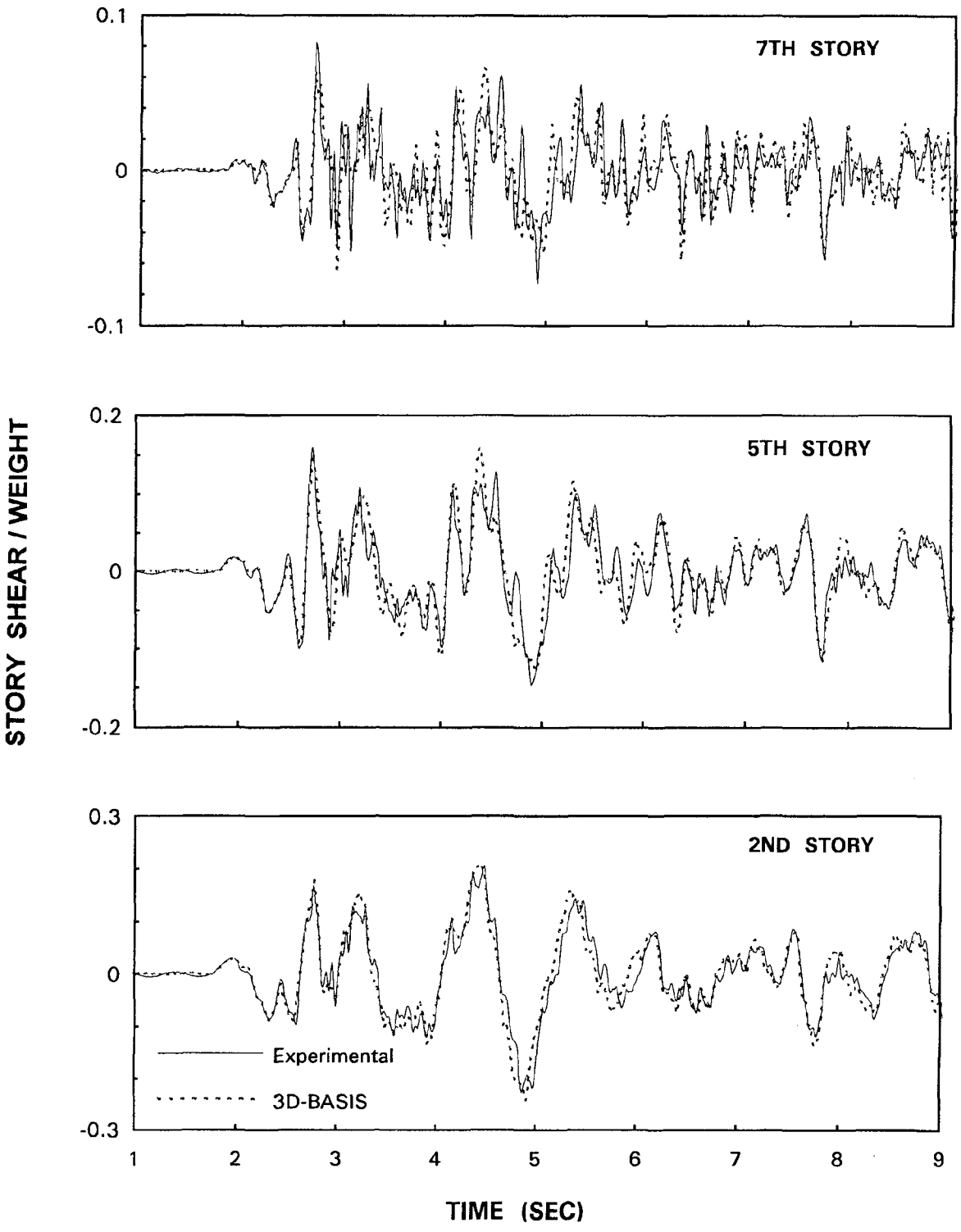

FIGURE 4-22 3D-BASIS Prediction of Story Shear Response in Structure MFUIS for El Centro S00E 200%

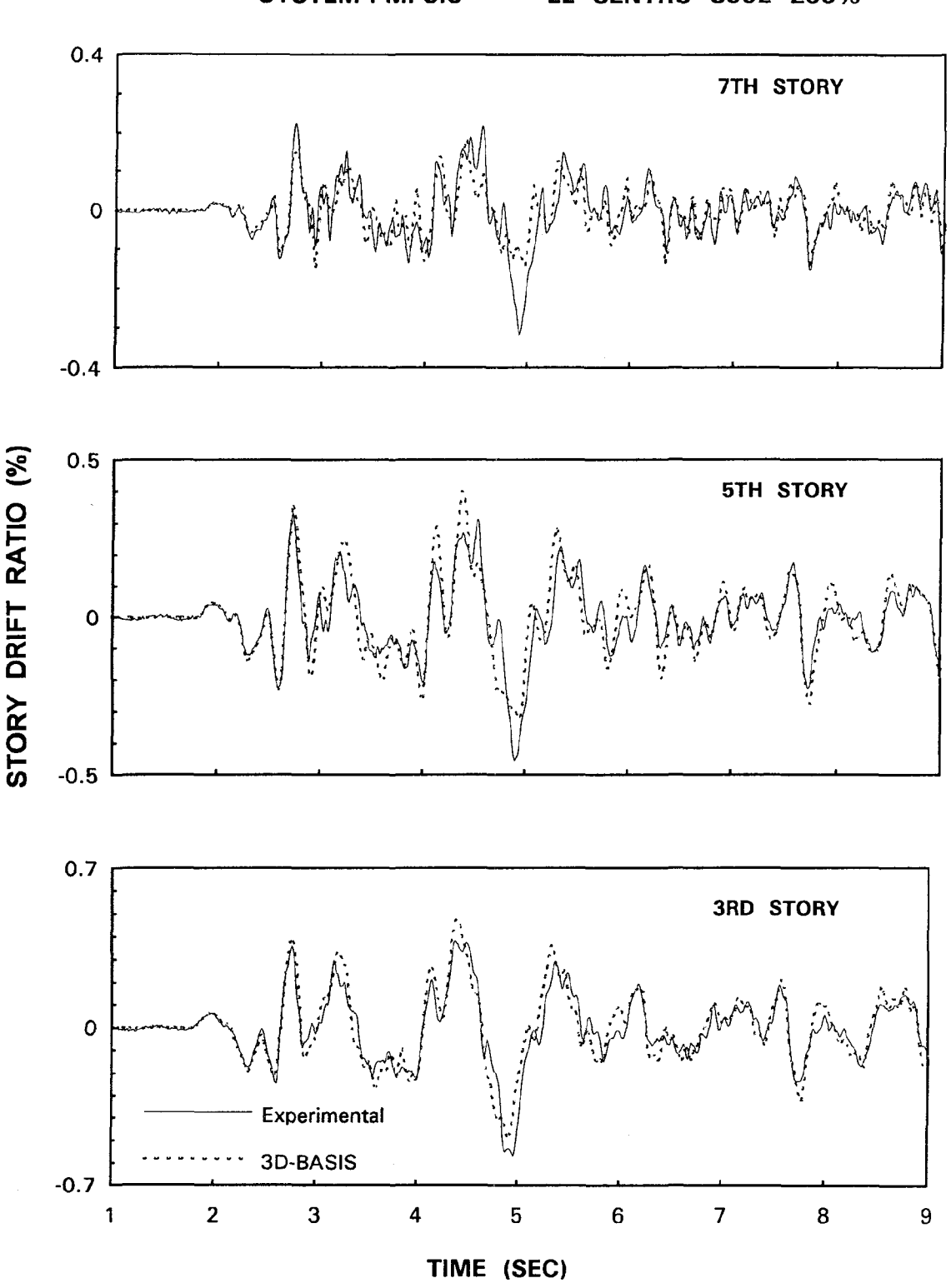

FIGURE 4-23 3D-BASIS Prediction of Inter-Story Drift Response in Structure MFUIS for El Centro S00E 200%

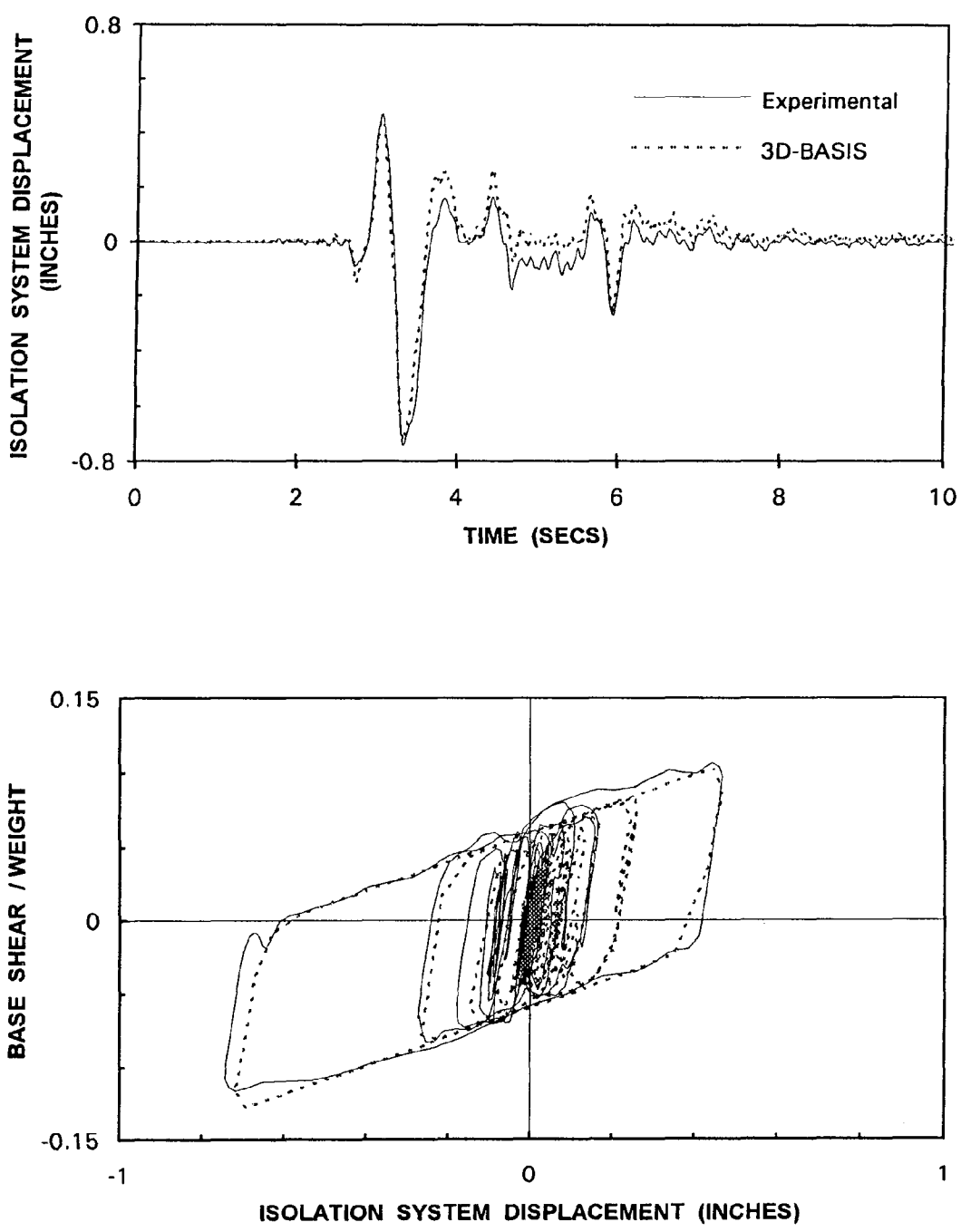

FIGURE 4-24 3D-BASIS Prediction of Isolation System Response in Structure MFUIS for Pacoima S74W 50%

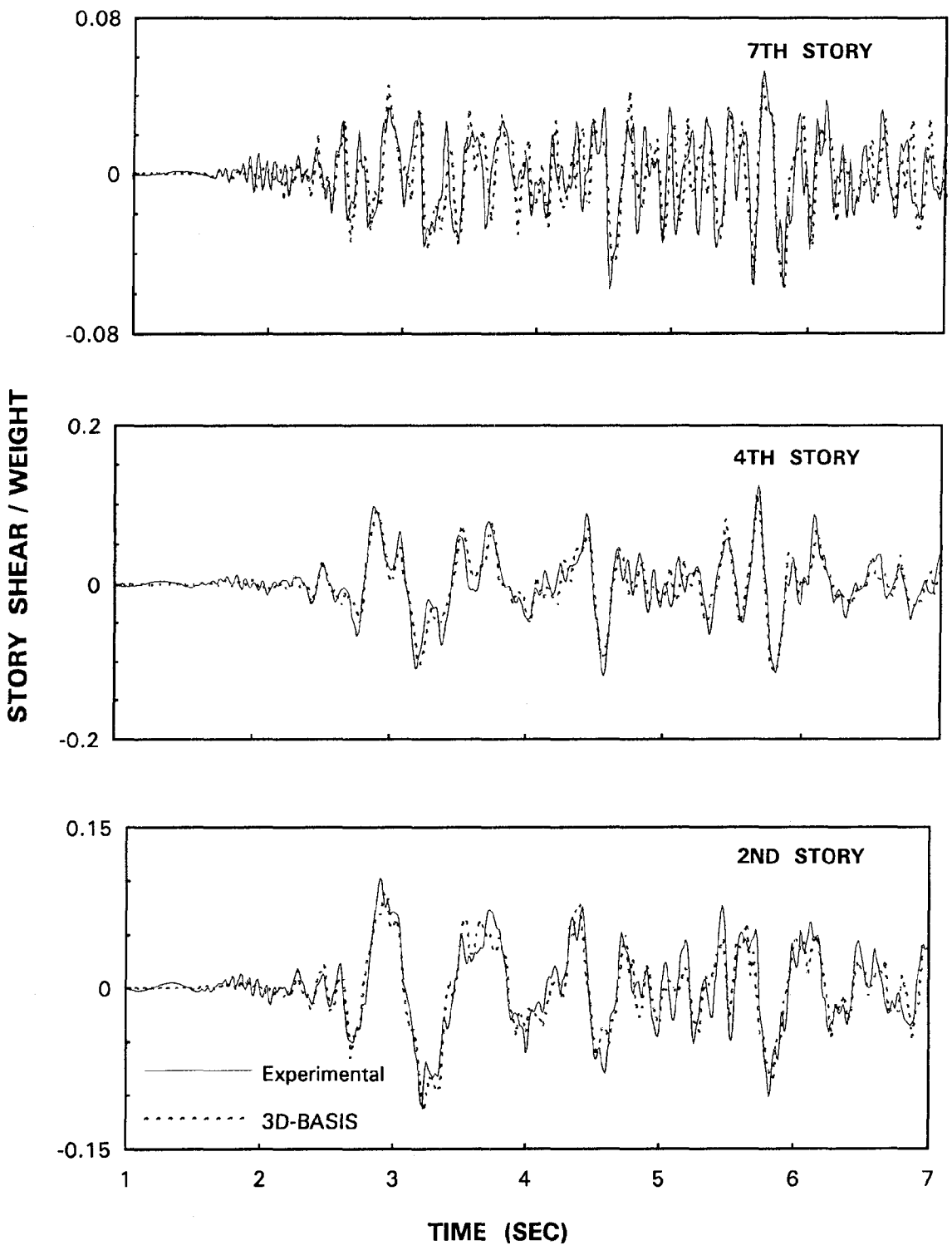

FIGURE 4-25 3D-BASIS Prediction of Story Shear Response in Structure MFUIS for Pacoima S74W 50%

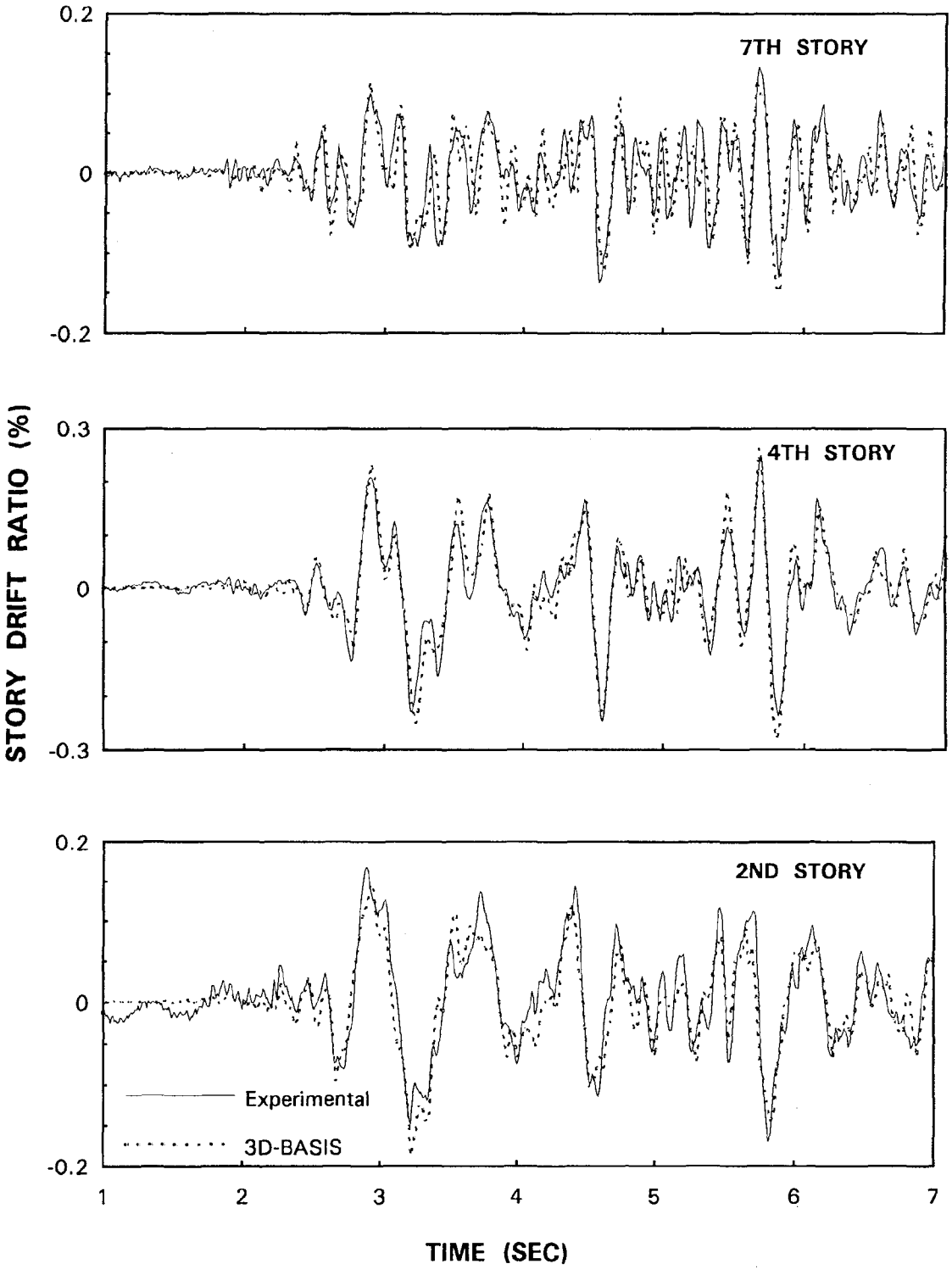

FIGURE 4-26 3D-BASIS Prediction of Inter-Story Drift Response in Structure MFUIS for Pacoima S74W 50%

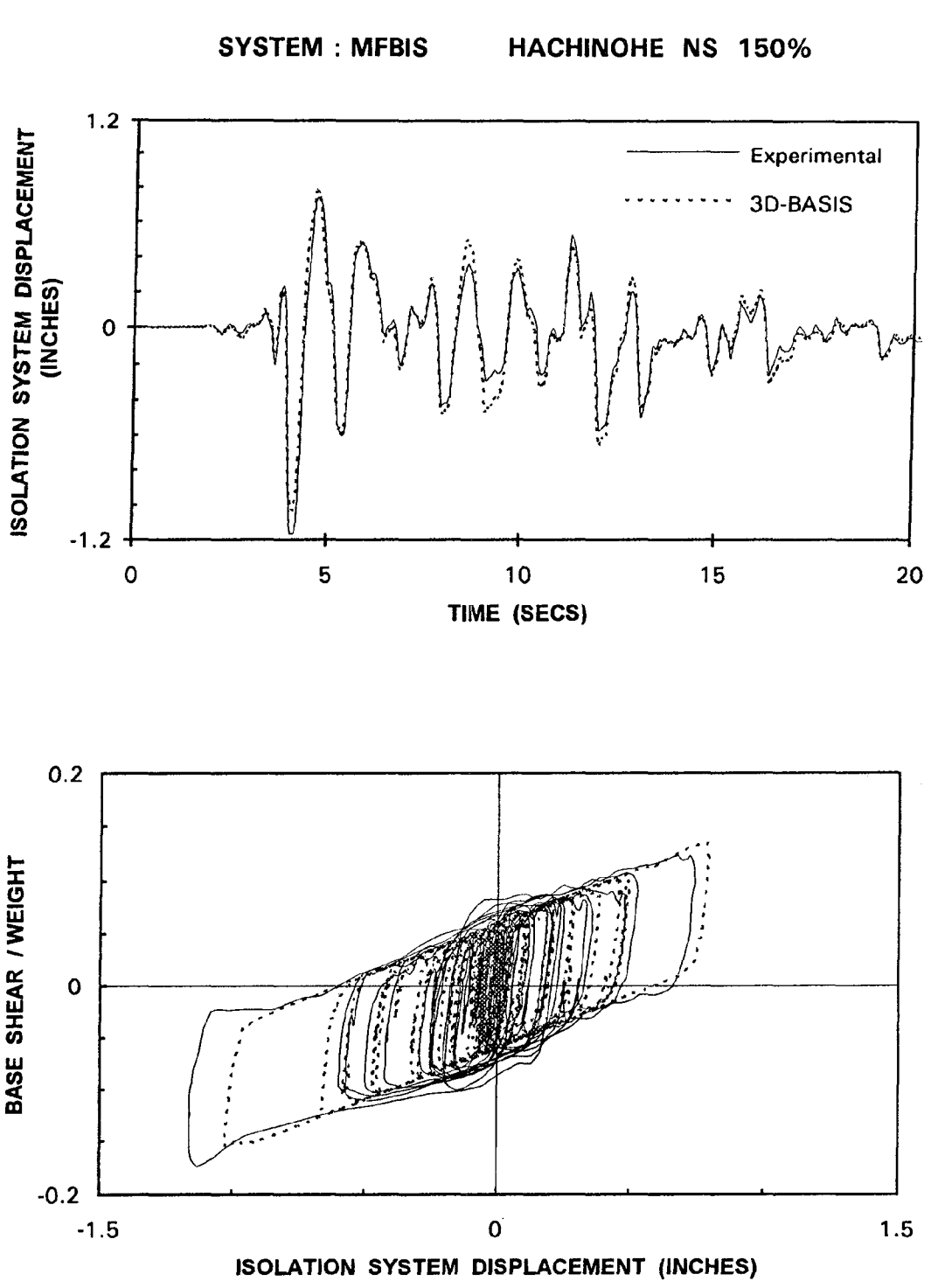

FIGURE 4-27 3D-BASIS Prediction of Isolation System Response in Structure MFBIS for Hachinohe NS 150%

SECTION 5

SPECIAL ISSUES

5.1 Engaging Lateral Restraint of Bearing

The lateral restraint of the friction pendulum isolation bearing is a steel cylinder (figure 2-3) that encloses the concave surface and slider components. It protects the internal components from environmental contamination and serves as a displacement restraint limiting the travel of the slider. For the model bearings tested, the restraint was placed such that the slider slides a distance of two inches before the column housing containing the slider reaches the restraint. For earthquake motions where the shear force developed at the bearing level requires a bearing displacement of more than two inches, the housing engages the lateral restraint and changes the hysteretic response of the isolator. Typical isolation system designs provide bearing displacement capacities which exceed the total displacement demand in the event of a maximum credible earthquake during the lifetime of the structure. Nevertheless, it is valuable to study the effect of engaging the lateral restraints in order to understand the behaviors which occur when the redundant lateral structural system is engaged.

In some of the tests carried out on the seven story frame, earthquake loadings were increased significantly beyond the design earthquake for the isolation system and the isolator displacements reached levels that resulted in engaging the lateral restraints of the FPS bearings (figures 5-1 to 5-4).

Assuming equal lateral displacements occurring in all the bearings, the threshold mark of base shear force for reaching the restraint may be given as:

$$BS = \mu W + \left(\frac{W}{R}\right) u_{bi} \tag{5.1}$$

where u_{bi} is the individual bearing displacement

For values of W=47.5 kips, R=9.75 inches, K_c=95 kip/inch, u_{bi}=2 inches, μ=0.06, this equation gives a base shear coefficient (base shear/structure weight) of 0.265. For the earthquake El Centro S00E 220%, the structure MFUIS attained a base shear coefficient of 0.266, which is equal to the threshold level, assuming equal displacements in all bearings.

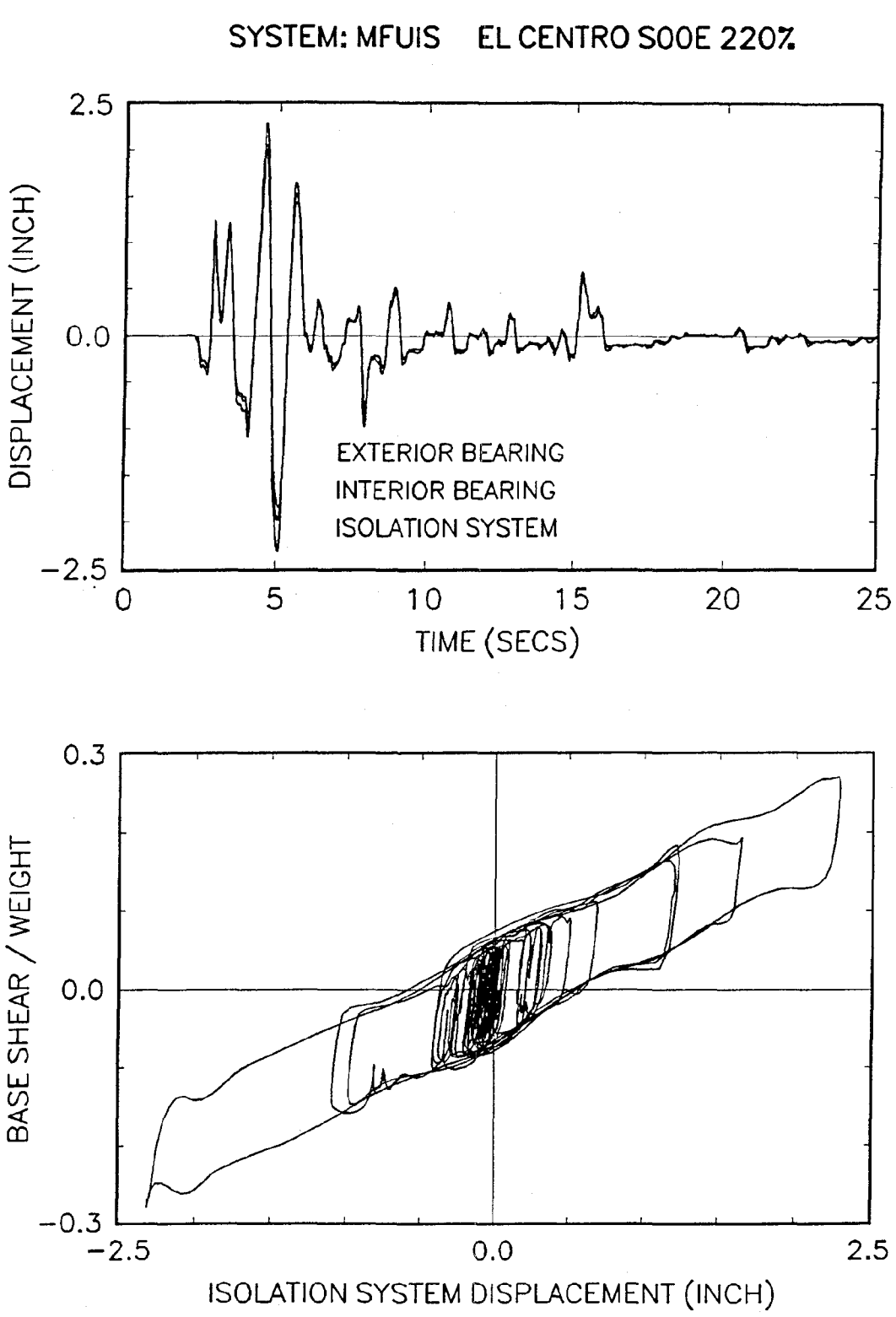

FIGURE 5-1 Isolation System Response of MFUIS for El Centro S00E 220%

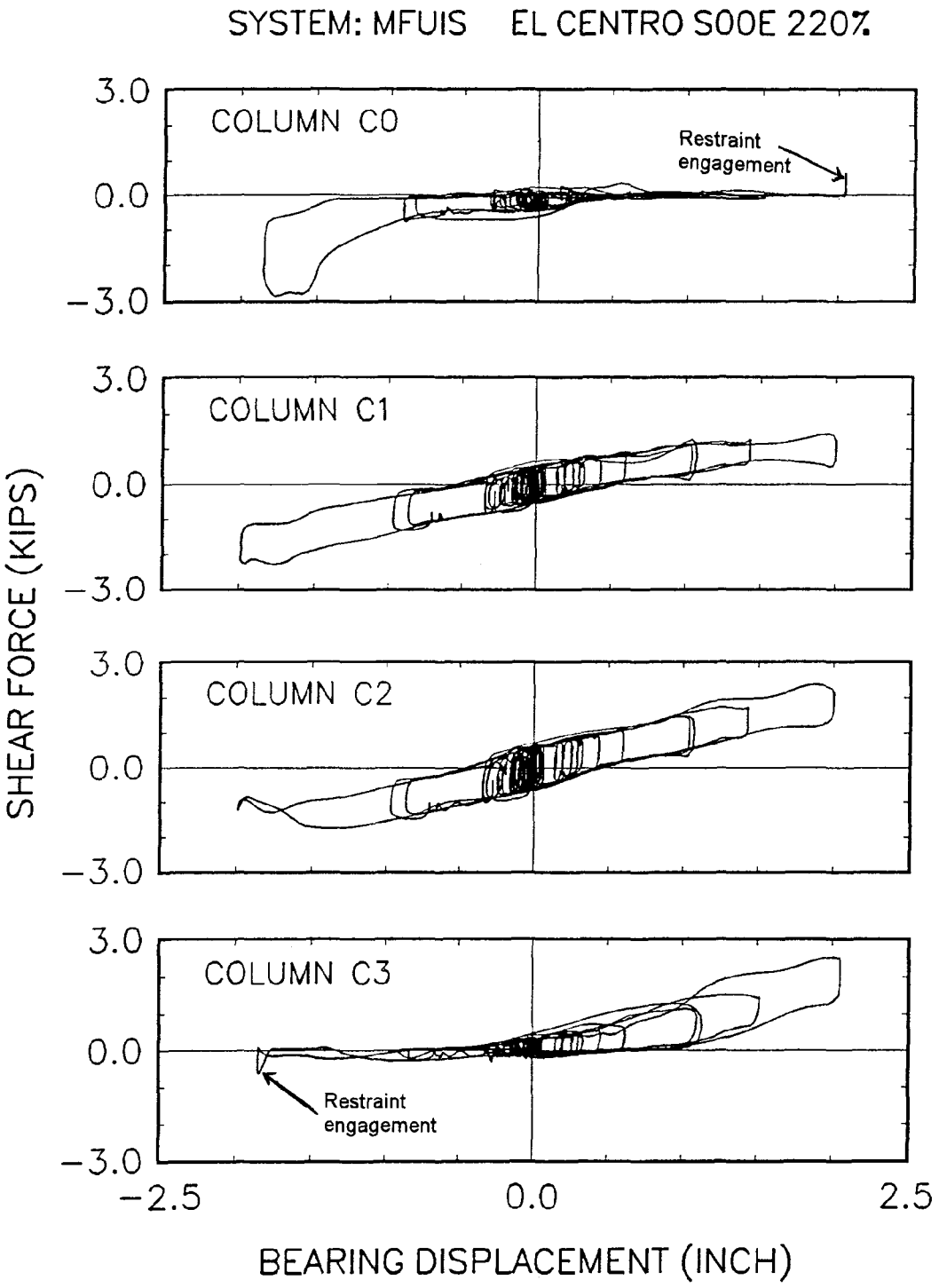

FIGURE 5-2 Individual Bearing Response of MFUIS for El Centro S00E 220%

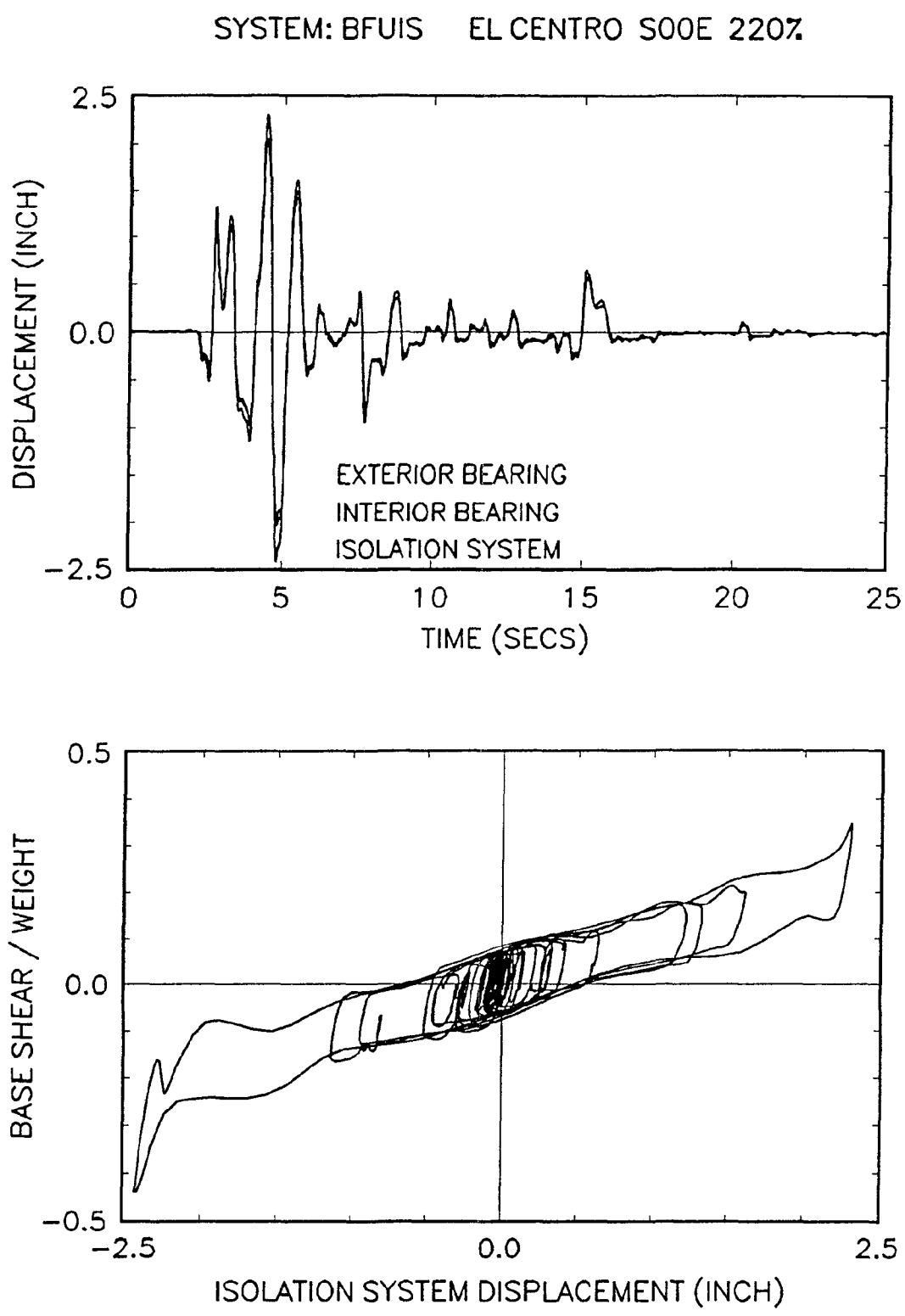

FIGURE 5-3 Isolation System Response of BFUIS for El Centro S00E 220%

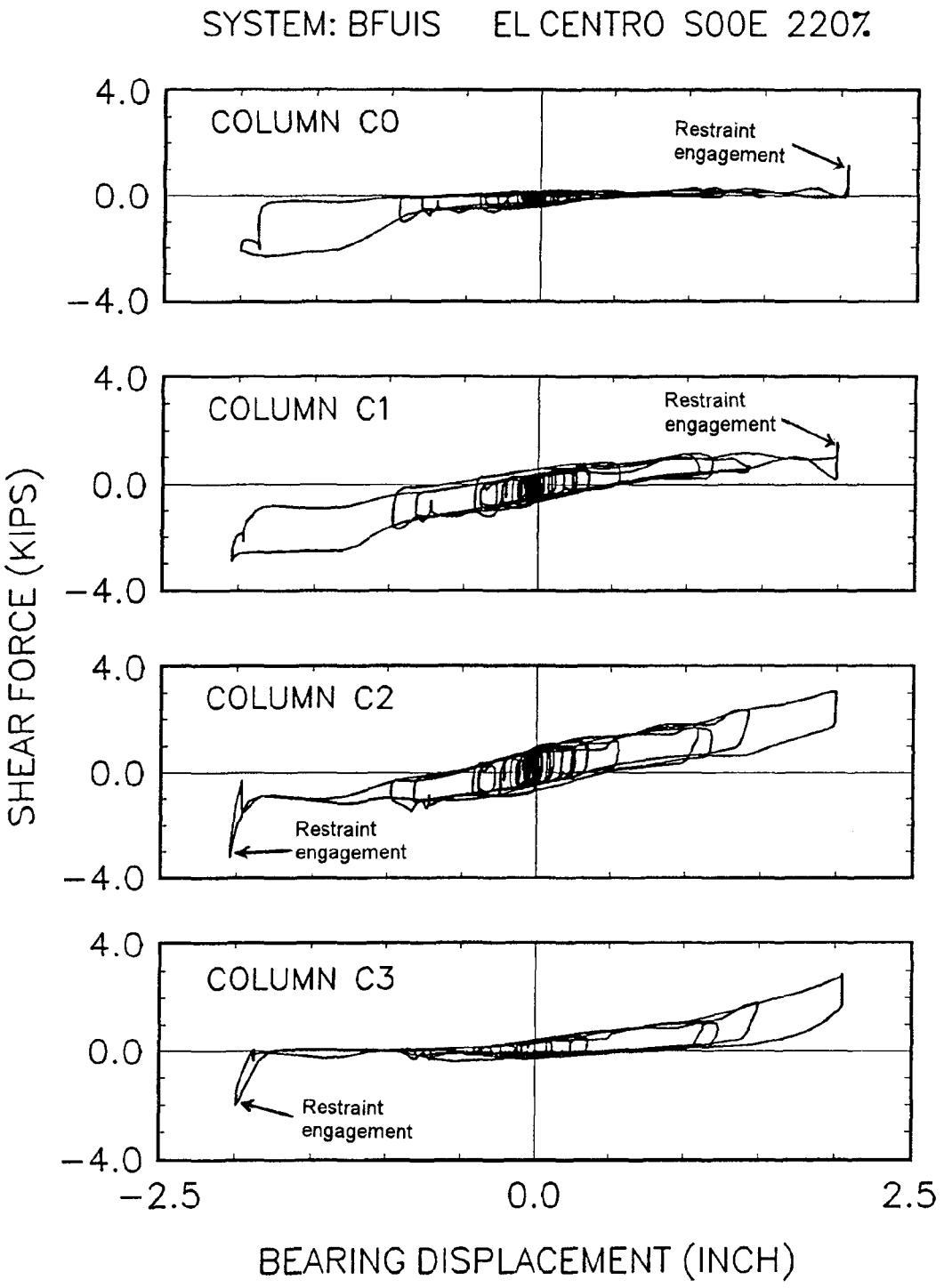

FIGURE 5-4 Individual Bearing Response of BFUIS for El Centro S00E 220%

However, since some bearings have displacements which exceed the average displacement, these bearings engaged the displacement restraint during this earthquake case. Figure 5-1 presents the overall isolation system response, while figure 5-2 shows the individual bearing hysteretic responses. It can be seen from figure 5-1 that the bearing displacement capacity of two inches has been reached, but there is no distinguishable difference as compared to the response of the weaker earthquake of El Centro S00E 200% (compare with figures 4-6 and 4-7). However, in figure 5-2, the effects of engaging the displacement restraint is observed for columns C0 and C3.

We now consider the braced frame structure BFUIS for the El Centro S00E 220% loading, which caused a base shear coefficient of 0.45, about 70% above the threshold value of 0.265. Figures 5-3 and 5-4 present the isolation system response and individual bearing response respectively. As expected, some distinctive features can be noticed in these figures. Figure 5-3 reveals the presence of a newly developed stiffness at the two extreme corners of the hysteresis loop. This stiffness is the result of engaging the lateral restraint and comes from the combined stiffness of the displacement restraint and the isolation story columns. It is much stiffer than the isolation system stiffness and is observed to be about 43% of the initial stiffness of the first story (isolation story) columns. Engaging the restraint resulted in small permanent plastic deformations of the restraint cylinder as well as other energy absorption phenomena that accommodates the excess shear force above the threshold value. Unloading occurs at the initial stiffness of the columns, which is also reflected in the figure. As reported earlier (section 2.3.2), the braced frame is expected to have a base shear exceeding that for the moment frame by a factor of not more than 18%. For El Centro S00E 220%, this means that the base shear coefficient for the braced frame should not generally exceed 0.314 (=1.18*0.266). On the contrary, the base shear is found to be much higher than this. This is due to the effect of engaging the lateral restraint; the bearing needs to slide more and causes deformation along the higher stiffness, until the thrust of the seismic force is met. The higher stiffness of the bearing after engaging the restraint cylinder causes an increase in the base shear. This behavior can be included in analysis by using a tri-linear force-displacement relationship, as described by Zayas et al. (1989).

Figure 5-4 shows the individual bearing hysteresis plots, where it may be observed that the two inch displacement mark was reached on both ends of the FPS bearing. It should, however, be noted that only the bearing displacements for bearings below columns C0 and C1 were actually measured (see Fig. 2.5). The bearing displacements in the other two columns were taken with the assumption that the displacement in both interior column bearings (C1, C2) were the same and so with both exterior column bearings (C0,C3).

Let us now compare the performance of a non-isolated braced frame with the isolated structure BFUIS that result in similar seismic forces in the structure. After several analysis runs, it was found that an earthquake El Centro S00E 60% caused story shears in a non-isolated braced frame that were similar in magnitude to the forces caused in the isolated braced frame BFUIS by the earthquake El Centro S00E 220%. This means that even though the lateral restraint was significantly engaged, resulting in 70% increases in base shear forces, this base shear occurred for an earthquake loading that was 3.7 times greater than the earthquake strength causing similar seismic forces in the non-isolated structure. Therefore, even though the displacement restraint was significantly engaged, the isolation system provided substantially improved performance as compared to a non-isolated structure.

5.2 Local Uplift of Bearings

The local frame action, and the large overturning forces generated by the aspect ratio of the model structure, and the strong motion loadings resulted in large variations in the vertical loads on the bearings. These variations were large enough (compared to the static dead load on the bearing) to reduce the bearing load to zero, and cause local uplift displacements in the bearings. The bearing loads are observed to be zero in the exterior columns. Results from local uplift of bearings were previously presented in sections 4.2 and 4.3. Additional results are shown in figures 5-2 and 5-4. Uplift displacements of the bearings of approximately 1/4 inch were visually observed in the exterior bearings during the performance of the test. This local uplift of the bearings had no effect on the overall response of the isolation system, as may be observed from isolation system responses presented in sections 4.2 and 4.3. Also the uplift did not have any damaging effect on the performance of the FPS bearings, as was evident from the experimental results. The same FPS bearings were used throughout the test program on the 7-story frame and consistent results were achieved for all of over sixty test cases. The FPS isolator properties remained unchanged throughout the test program. The slider bearing material was visually inspected at the end of the test program and showed negligible wear. The FPS bearings remained fully functional with predictable and reliable responses after being subjected to several strong earthquakes, including both bearing uplifts and engagement of lateral restraints.

SECTION 6

CONCLUSIONS

Shake table tests were conducted on six and seven story building models with Friction Pendulum seismic isolators installed at the bases. The building models included moment and braced frames, with different isolator installation configurations, including isolators installed directly at the bases of the first story columns. Realistic framing details representative of full size structures were used. In all cases, the isolators provided the desired and predicted reductions in story shears and drifts. The main conclusions from this study may be summarized as:

1. The Friction Pendulum isolators reduce structure shear forces and inter story drifts in the multi-story building models by factors of 4 to 6, allowing the upper structural system to remain elastic during severe earthquake loadings. The reductions in drifts significantly reduce damage to non-structural and structural building components caused by earthquake ground shaking.

2. The installation of the isolators at the bases of the individual first story columns, as compared to beneath a rigid diaphragm base, does not significantly affect the behavior of the isolation bearings or system. The articulated joint of the Friction Pendulum isolators accommodates the required joint rotations with no affect on the isolator properties.

3. When isolators are installed at the bases of cantilever columns, different isolator displacements are observed at different column locations. The differences in isolator displacements are small in comparison to the total isolator displacements. The relative differences in isolator displacements have no measurable effect on the overall response of the isolation system or the upper story shears and drifts. The differences in displacements can be accounted for in analytical models which include the flexibility of the frame members.

4. Bracing the column bases together achieves equal displacements in the isolators, but does not affect the overall response of the isolation system or the upper structure.

5. The story shears and drifts occurring in the upper structure are affected by the shear stiffness of the framing in the isolation story. The story shear stiffness of the framing in the

isolation story affects the dynamic characteristics of structure, and should be included in the analytical model of the isolated structures. Analytical models which include the flexibility of the framing in the isolation story can fully account for the response of the isolation story and upper structure responses.

6. The response of the first three modes of the upper structure fully accounted for the response of the experimentally observed structure shears and drifts, with differences of typically less than 1% as compared to the experimental results. The inclusion of only two modes resulted in differences as large as 5%, and the inclusion of only 1 mode resulted in differences as large as 23%.

7. Peak floor spectra responses within the isolated structures were reduced by a factor of eight as compared to peak floor spectra responses occurring in the non-isolated structures subjected to equal strength loadings.

8. The response of the isolated structures subjected to severe earthquakes can be accurately predicted by analytical procedures. This is attributed to the well quantified and predictable dynamic response of the Friction Pendulum isolators, and that the upper structural system remaining elastic. The response of non-isolated structures subjected to equivalent strength ground motions is considerably less predictable due to uncertainties associated with the inelastic response of the structures.

9. Local variation of vertical loads on the isolators does not have any measurable effect on the overall response of the isolation system or the upper structure story shears and drifts. Increases in bearing stiffness resulting from increases in vertical load are directly compensated for by equivalent decreases in bearing stiffness resulting from decreases in vertical load.

10. Local uplift of individual isolators within the structural frame does not have any measurable effect on the overall response of the isolation system or the upper structure story shears and drifts. The Friction Pendulum isolator bearings were unaffected and undamaged by the local uplifts.

11. The use of displacement restraints, or displacement limits, were observed to be an effective means to limit isolator displacements, and insure isolator stability, in the event of extreme seismic events significantly exceeding the design event. Engagement of lateral displacement restraint increases the structure shear forces, but maintains a favorable response

in the isolation system and structure. Even in extreme overload cases where engagement of the displacement restraint increased base shear forces by 70%, the resulting structure forces were still only 27% of those occurring in the equivalent non-isolated structure subjected to the same earthquake loading. Without a displacement restraint, isolated structures subjected to equivalent overloads can become unstable and collapse.

12. Consistent results were achieved in the isolation system response throughout the test program which included over 60 seismic tests. The isolator bearings retained their original stiffness and energy dissipation characteristics and needed no repair at the conclusion of testing. Isolator responses observed at the end of the test program were equivalent to those occurring at the beginning of the test program.

SECTION 7

REFERENCES

1. Amin, N., Mokha, A. and Fatehi, H. (1993). "Rehabilitation of the U.S. Court of Appeals Building Using Sliding Isolation System", Proc., ATC-17-1 Seminar on Seismic Isolation, Passive Energy Dissipation and Active Control, Applied Technology Council, San Francisco.

2. Amin, N., Mokha, A., Low, S. and Zayas, V. (1992). "Dynamic Analysis of Sliding Seismic Isolators", Proc., Mechanics Conference, American Society of Civil Engineers, Texas.

3. Clough, R. W. and Penzien, J. (1975)."Dynamics of Structures", McGraw-Hill, Inc., New York, N.Y.

4. Constantinou, M.C. and Kartoum, A. (1993). "Shake Table Testing of Bridge Deck on Friction Pendulum Bearings" (in preparation).

5. Constantinou, M.C., Mokha, A.S. and Reinhorn, A.M. (1990). "Teflon Bearings in Base Isolation. Part 2: Modeling", Journal of Structural Engineering, American Society of Civil Engineers, 116(2), 455-474.

6. Constantinou, M.C., Tsopelas, P., Kim, Y.S. and Okamoto, S. (1993). "NCEER-Taisei Corporation Research Program on Sliding Seismic Isolation Systems for Bridges: Experimental and Analytical Study of Friction Pendulum System", Technical Report No. NCEER-93-0020, National Center for Earthquake Engineering, State University of New York at Buffalo.

7. Gear, C. W. (1971). "The Automatic Integration of Ordinary Differential Equations", Numerical Mathematics, Communications of ACM, 14(3), 176-190.

8. International Conference of Building Officials ICBO (1991). "Uniform Building Code: Earthquake Regulations", Whittier, California.

9. Mokha, A.S., Constantinou, M.C., and Reinhorn, A.M. (1990). "Experimental Study and Analytical Predication of Earthquake Response of a Sliding Isolation System with a Spherical Surface", Technical Report No. NCEER 90-0020, National Center for Earthquake Engineering Research, State University of New York at Buffalo.

10. Mokha, A.S., Constantinou, M.C., Reinhorn, A.M. and Zayas, V.A. (1991). "Experimental Study of Friction-Pendulum Isolation System" Journal of Structural Engineering, American Society of Civil Engineers, 117(4), 1203-1219.

11. Nagarajaiah, S., Reinhorn A.M. and Constantinou, M.C. (1989). "Nonlinear Dynamic Analysis of Three-Dimensional Base-Isolated Structures (3D-BASIS)", Technical Report No. NCEER 89-0019, National Center for Earthquake Engineering Research, State University of New York at Buffalo.

12. Piepenbrock, T.F., Zayas, V.A. and Mahin, S.A. (1993). "Earthquake Simulation Tests of Unreinforced Masonry Structures Using the Friction Pendulum Seismic Isolation System", Earthquake Engineering Reseach Center, University of California, Berkeley (in preparation).

13. Reinhorn A.M. et al. (1989). "1:4 Scale Model Studies of Active Tendons Systems and Active Mass Dampers for Aseismic Protection", Technical Report No. NCEER 89-0026, National Center for Earthquake Engineering Research, State University of New York at Buffalo.

14. Zayas, V. A. and Low, S.S. (1991). "Seismic Isolation Retrofit of an Apartment Building", Proc., Structures Congress, American Society of Civil Engineers, Indianapolis.

15. Zayas, V., Low, S., Bozzo, L. and Mahin S. (1989). "Feasibility and Performance Studies on Improving the Earthquake Resistance of New and Existing Buildings Using the Friction Pendulum System", Report No. UCB/EERC-89/09, Earthquake Engineering Research Center, University of California, Berkeley.

16. Zayas, V.A., Low, S.S., and Mahin S.A. (1987). "The FPS Earthquake Resisting System, Experimental Report", Report No. UCB/EERC 87/01, Earthquake Engineering Research Center, University of California, Berkeley.

17. Zayas, V., Piepenbrock, T. and Al-Hussaini, T. (1993). "Summary of Testing of the Friction Pendulum Seismic Isolation System: 1986-1993", Proc., ATC-17-1 Seminar on Seismic Isolation, Passive Energy Dissipation and Active Control, Applied Technology Council, San Francisco.

18. Zayas, V.A., Low, S. and Mahin, S.A. (1993). "Parameter Studies on the Properties and Response of Friction Pendulum Isolation Bearings", Earthquake Engineering Reseach Center, University of California, Berkeley (under preparation).

NATIONAL CENTER FOR EARTHQUAKE ENGINEERING RESEARCH
LIST OF TECHNICAL REPORTS

The National Center for Earthquake Engineering Research (NCEER) publishes technical reports on a variety of subjects related to earthquake engineering written by authors funded through NCEER. These reports are available from both NCEER's Publications Department and the National Technical Information Service (NTIS). Requests for reports should be directed to the Publications Department, National Center for Earthquake Engineering Research, State University of New York at Buffalo, Red Jacket Quadrangle, Buffalo, New York 14261. Reports can also be requested through NTIS, 5285 Port Royal Road, Springfield, Virginia 22161. NTIS accession numbers are shown in parenthesis, if available.

NCEER-87-0001 "First-Year Program in Research, Education and Technology Transfer," 3/5/87, (PB88-134275).

NCEER-87-0002 "Experimental Evaluation of Instantaneous Optimal Algorithms for Structural Control," by R.C. Lin, T.T. Soong and A.M. Reinhorn, 4/20/87, (PB88-134341).

NCEER-87-0003 "Experimentation Using the Earthquake Simulation Facilities at University at Buffalo," by A.M. Reinhorn and R.L. Ketter, to be published.

NCEER-87-0004 "The System Characteristics and Performance of a Shaking Table," by J.S. Hwang, K.C. Chang and G.C. Lee, 6/1/87, (PB88-134259). This report is available only through NTIS (see address given above).

NCEER-87-0005 "A Finite Element Formulation for Nonlinear Viscoplastic Material Using a Q Model," by O. Gyebi and G. Dasgupta, 11/2/87, (PB88-213764).

NCEER-87-0006 "Symbolic Manipulation Program (SMP) - Algebraic Codes for Two and Three Dimensional Finite Element Formulations," by X. Lee and G. Dasgupta, 11/9/87, (PB88-218522).

NCEER-87-0007 "Instantaneous Optimal Control Laws for Tall Buildings Under Seismic Excitations," by J.N. Yang, A. Akbarpour and P. Ghaemmaghami, 6/10/87, (PB88-134333). This report is only available through NTIS (see address given above).

NCEER-87-0008 "IDARC: Inelastic Damage Analysis of Reinforced Concrete Frame - Shear-Wall Structures," by Y.J. Park, A.M. Reinhorn and S.K. Kunnath, 7/20/87, (PB88-134325).

NCEER-87-0009 "Liquefaction Potential for New York State: A Preliminary Report on Sites in Manhattan and Buffalo," by M. Budhu, V. Vijayakumar, R.F. Giese and L. Baumgras, 8/31/87, (PB88-163704). This report is available only through NTIS (see address given above).

NCEER-87-0010 "Vertical and Torsional Vibration of Foundations in Inhomogeneous Media," by A.S. Veletsos and K.W. Dotson, 6/1/87, (PB88-134291).

NCEER-87-0011 "Seismic Probabilistic Risk Assessment and Seismic Margins Studies for Nuclear Power Plants," by Howard H.M. Hwang, 6/15/87, (PB88-134267).

NCEER-87-0012 "Parametric Studies of Frequency Response of Secondary Systems Under Ground-Acceleration Excitations," by Y. Yong and Y.K. Lin, 6/10/87, (PB88-134309).

NCEER-87-0013 "Frequency Response of Secondary Systems Under Seismic Excitation," by J.A. HoLung, J. Cai and Y.K. Lin, 7/31/87, (PB88-134317).

NCEER-87-0014 "Modelling Earthquake Ground Motions in Seismically Active Regions Using Parametric Time Series Methods," by G.W. Ellis and A.S. Cakmak, 8/25/87, (PB88-134283).

NCEER-87-0015 "Detection and Assessment of Seismic Structural Damage," by E. DiPasquale and A.S. Cakmak, 8/25/87, (PB88-163712).

NCEER-87-0016 "Pipeline Experiment at Parkfield, California," by J. Isenberg and E. Richardson, 9/15/87, (PB88-163720). This report is available only through NTIS (see address given above).

NCEER-87-0017 "Digital Simulation of Seismic Ground Motion," by M. Shinozuka, G. Deodatis and T. Harada, 8/31/87, (PB88-155197). This report is available only through NTIS (see address given above).

NCEER-87-0018 "Practical Considerations for Structural Control: System Uncertainty, System Time Delay and Truncation of Small Control Forces," J.N. Yang and A. Akbarpour, 8/10/87, (PB88-163738).

NCEER-87-0019 "Modal Analysis of Nonclassically Damped Structural Systems Using Canonical Transformation," by J.N. Yang, S. Sarkani and F.X. Long, 9/27/87, (PB88-187851).

NCEER-87-0020 "A Nonstationary Solution in Random Vibration Theory," by J.R. Red-Horse and P.D. Spanos, 11/3/87, (PB88-163746).

NCEER-87-0021 "Horizontal Impedances for Radially Inhomogeneous Viscoelastic Soil Layers," by A.S. Veletsos and K.W. Dotson, 10/15/87, (PB88-150859).

NCEER-87-0022 "Seismic Damage Assessment of Reinforced Concrete Members," by Y.S. Chung, C. Meyer and M. Shinozuka, 10/9/87, (PB88-150867). This report is available only through NTIS (see address given above).

NCEER-87-0023 "Active Structural Control in Civil Engineering," by T.T. Soong, 11/11/87, (PB88-187778).

NCEER-87-0024 "Vertical and Torsional Impedances for Radially Inhomogeneous Viscoelastic Soil Layers," by K.W. Dotson and A.S. Veletsos, 12/87, (PB88-187786).

NCEER-87-0025 "Proceedings from the Symposium on Seismic Hazards, Ground Motions, Soil-Liquefaction and Engineering Practice in Eastern North America," October 20-22, 1987, edited by K.H. Jacob, 12/87, (PB88-188115).

NCEER-87-0026 "Report on the Whittier-Narrows, California, Earthquake of October 1, 1987," by J. Pantelic and A. Reinhorn, 11/87, (PB88-187752). This report is available only through NTIS (see address given above).

NCEER-87-0027 "Design of a Modular Program for Transient Nonlinear Analysis of Large 3-D Building Structures," by S. Srivastav and J.F. Abel, 12/30/87, (PB88-187950).

NCEER-87-0028 "Second-Year Program in Research, Education and Technology Transfer," 3/8/88, (PB88-219480).

NCEER-88-0001 "Workshop on Seismic Computer Analysis and Design of Buildings With Interactive Graphics," by W. McGuire, J.F. Abel and C.H. Conley, 1/18/88, (PB88-187760).

NCEER-88-0002 "Optimal Control of Nonlinear Flexible Structures," by J.N. Yang, F.X. Long and D. Wong, 1/22/88, (PB88-213772).

NCEER-88-0003 "Substructuring Techniques in the Time Domain for Primary-Secondary Structural Systems," by G.D. Manolis and G. Juhn, 2/10/88, (PB88-213780).

NCEER-88-0004 "Iterative Seismic Analysis of Primary-Secondary Systems," by A. Singhal, L.D. Lutes and P.D. Spanos, 2/23/88, (PB88-213798).

NCEER-88-0005 "Stochastic Finite Element Expansion for Random Media," by P.D. Spanos and R. Ghanem, 3/14/88, (PB88-213806).

NCEER-88-0006 "Combining Structural Optimization and Structural Control," by F.Y. Cheng and C.P. Pantelides, 1/10/88, (PB88-213814).

NCEER-88-0007 "Seismic Performance Assessment of Code-Designed Structures," by H.H-M. Hwang, J-W. Jaw and H-J. Shau, 3/20/88, (PB88-219423).

NCEER-88-0008 "Reliability Analysis of Code-Designed Structures Under Natural Hazards," by H.H-M. Hwang, H. Ushiba and M. Shinozuka, 2/29/88, (PB88-229471).

NCEER-88-0009 "Seismic Fragility Analysis of Shear Wall Structures," by J-W Jaw and H.H-M. Hwang, 4/30/88, (PB89-102867).

NCEER-88-0010 "Base Isolation of a Multi-Story Building Under a Harmonic Ground Motion - A Comparison of Performances of Various Systems," by F-G Fan, G. Ahmadi and I.G. Tadjbakhsh, 5/18/88, (PB89-122238).

NCEER-88-0011 "Seismic Floor Response Spectra for a Combined System by Green's Functions," by F.M. Lavelle, L.A. Bergman and P.D. Spanos, 5/1/88, (PB89-102875).

NCEER-88-0012 "A New Solution Technique for Randomly Excited Hysteretic Structures," by G.Q. Cai and Y.K. Lin, 5/16/88, (PB89-102883).

NCEER-88-0013 "A Study of Radiation Damping and Soil-Structure Interaction Effects in the Centrifuge," by K. Weissman, supervised by J.H. Prevost, 5/24/88, (PB89-144703).

NCEER-88-0014 "Parameter Identification and Implementation of a Kinematic Plasticity Model for Frictional Soils," by J.H. Prevost and D.V. Griffiths, to be published.

NCEER-88-0015 "Two- and Three- Dimensional Dynamic Finite Element Analyses of the Long Valley Dam," by D.V. Griffiths and J.H. Prevost, 6/17/88, (PB89-144711).

NCEER-88-0016 "Damage Assessment of Reinforced Concrete Structures in Eastern United States," by A.M. Reinhorn, M.J. Seidel, S.K. Kunnath and Y.J. Park, 6/15/88, (PB89-122220).

NCEER-88-0017 "Dynamic Compliance of Vertically Loaded Strip Foundations in Multilayered Viscoelastic Soils," by S. Ahmad and A.S.M. Israil, 6/17/88, (PB89-102891).

NCEER-88-0018 "An Experimental Study of Seismic Structural Response With Added Viscoelastic Dampers," by R.C. Lin, Z. Liang, T.T. Soong and R.H. Zhang, 6/30/88, (PB89-122212). This report is available only through NTIS (see address given above).

NCEER-88-0019 "Experimental Investigation of Primary - Secondary System Interaction," by G.D. Manolis, G. Juhn and A.M. Reinhorn, 5/27/88, (PB89-122204).

NCEER-88-0020 "A Response Spectrum Approach For Analysis of Nonclassically Damped Structures," by J.N. Yang, S. Sarkani and F.X. Long, 4/22/88, (PB89-102909).

NCEER-88-0021 "Seismic Interaction of Structures and Soils: Stochastic Approach," by A.S. Veletsos and A.M. Prasad, 7/21/88, (PB89-122196).

NCEER-88-0022 "Identification of the Serviceability Limit State and Detection of Seismic Structural Damage," by E. DiPasquale and A.S. Cakmak, 6/15/88, (PB89-122188). This report is available only through NTIS (see address given above).

NCEER-88-0023 "Multi-Hazard Risk Analysis: Case of a Simple Offshore Structure," by B.K. Bhartia and E.H. Vanmarcke, 7/21/88, (PB89-145213).

NCEER-88-0024 "Automated Seismic Design of Reinforced Concrete Buildings," by Y.S. Chung, C. Meyer and M. Shinozuka, 7/5/88, (PB89-122170). This report is available only through NTIS (see address given above).

NCEER-88-0025 "Experimental Study of Active Control of MDOF Structures Under Seismic Excitations," by L.L. Chung, R.C. Lin, T.T. Soong and A.M. Reinhorn, 7/10/88, (PB89-122600).

NCEER-88-0026 "Earthquake Simulation Tests of a Low-Rise Metal Structure," by J.S. Hwang, K.C. Chang, G.C. Lee and R.L. Ketter, 8/1/88, (PB89-102917).

NCEER-88-0027 "Systems Study of Urban Response and Reconstruction Due to Catastrophic Earthquakes," by F. Kozin and H.K. Zhou, 9/22/88, (PB90-162348).

NCEER-88-0028 "Seismic Fragility Analysis of Plane Frame Structures," by H.H-M. Hwang and Y.K. Low, 7/31/88, (PB89-131445).

NCEER-88-0029 "Response Analysis of Stochastic Structures," by A. Kardara, C. Bucher and M. Shinozuka, 9/22/88, (PB89-174429).

NCEER-88-0030 "Nonnormal Accelerations Due to Yielding in a Primary Structure," by D.C.K. Chen and L.D. Lutes, 9/19/88, (PB89-131437).

NCEER-88-0031 "Design Approaches for Soil-Structure Interaction," by A.S. Veletsos, A.M. Prasad and Y. Tang, 12/30/88, (PB89-174437). This report is available only through NTIS (see address given above).

NCEER-88-0032 "A Re-evaluation of Design Spectra for Seismic Damage Control," by C.J. Turkstra and A.G. Tallin, 11/7/88, (PB89-145221).

NCEER-88-0033 "The Behavior and Design of Noncontact Lap Splices Subjected to Repeated Inelastic Tensile Loading," by V.E. Sagan, P. Gergely and R.N. White, 12/8/88, (PB89-163737).

NCEER-88-0034 "Seismic Response of Pile Foundations," by S.M. Mamoon, P.K. Banerjee and S. Ahmad, 11/1/88, (PB89-145239).

NCEER-88-0035 "Modeling of R/C Building Structures With Flexible Floor Diaphragms (IDARC2)," by A.M. Reinhorn, S.K. Kunnath and N. Panahshahi, 9/7/88, (PB89-207153).

NCEER-88-0036 "Solution of the Dam-Reservoir Interaction Problem Using a Combination of FEM, BEM with Particular Integrals, Modal Analysis, and Substructuring," by C-S. Tsai, G.C. Lee and R.L. Ketter, 12/31/88, (PB89-207146).

NCEER-88-0037 "Optimal Placement of Actuators for Structural Control," by F.Y. Cheng and C.P. Pantelides, 8/15/88, (PB89-162846).

NCEER-88-0038 "Teflon Bearings in Aseismic Base Isolation: Experimental Studies and Mathematical Modeling," by A. Mokha, M.C. Constantinou and A.M. Reinhorn, 12/5/88, (PB89-218457). This report is available only through NTIS (see address given above).

NCEER-88-0039 "Seismic Behavior of Flat Slab High-Rise Buildings in the New York City Area," by P. Weidlinger and M. Ettouney, 10/15/88, (PB90-145681).

NCEER-88-0040 "Evaluation of the Earthquake Resistance of Existing Buildings in New York City," by P. Weidlinger and M. Ettouney, 10/15/88, to be published.

NCEER-88-0041 "Small-Scale Modeling Techniques for Reinforced Concrete Structures Subjected to Seismic Loads," by W. Kim, A. El-Attar and R.N. White, 11/22/88, (PB89-189625).

NCEER-88-0042 "Modeling Strong Ground Motion from Multiple Event Earthquakes," by G.W. Ellis and A.S. Cakmak, 10/15/88, (PB89-174445).

NCEER-88-0043 "Nonstationary Models of Seismic Ground Acceleration," by M. Grigoriu, S.E. Ruiz and E. Rosenblueth, 7/15/88, (PB89-189617).

NCEER-88-0044 "SARCF User's Guide: Seismic Analysis of Reinforced Concrete Frames," by Y.S. Chung, C. Meyer and M. Shinozuka, 11/9/88, (PB89-174452).

NCEER-88-0045 "First Expert Panel Meeting on Disaster Research and Planning," edited by J. Pantelic and J. Stoyle, 9/15/88, (PB89-174460).

NCEER-88-0046 "Preliminary Studies of the Effect of Degrading Infill Walls on the Nonlinear Seismic Response of Steel Frames," by C.Z. Chrysostomou, P. Gergely and J.F. Abel, 12/19/88, (PB89-208383).

NCEER-88-0047 "Reinforced Concrete Frame Component Testing Facility - Design, Construction, Instrumentation and Operation," by S.P. Pessiki, C. Conley, T. Bond, P. Gergely and R.N. White, 12/16/88, (PB89-174478).

NCEER-89-0001 "Effects of Protective Cushion and Soil Compliancy on the Response of Equipment Within a Seismically Excited Building," by J.A. HoLung, 2/16/89, (PB89-207179).

NCEER-89-0002 "Statistical Evaluation of Response Modification Factors for Reinforced Concrete Structures," by H.H-M. Hwang and J-W. Jaw, 2/17/89, (PB89-207187).

NCEER-89-0003 "Hysteretic Columns Under Random Excitation," by G-Q. Cai and Y.K. Lin, 1/9/89, (PB89-196513).

NCEER-89-0004 "Experimental Study of 'Elephant Foot Bulge' Instability of Thin-Walled Metal Tanks," by Z-H. Jia and R.L. Ketter, 2/22/89, (PB89-207195).

NCEER-89-0005 "Experiment on Performance of Buried Pipelines Across San Andreas Fault," by J. Isenberg, E. Richardson and T.D. O'Rourke, 3/10/89, (PB89-218440). This report is available only through NTIS (see address given above).

NCEER-89-0006 "A Knowledge-Based Approach to Structural Design of Earthquake-Resistant Buildings," by M. Subramani, P. Gergely, C.H. Conley, J.F. Abel and A.H. Zaghw, 1/15/89, (PB89-218465).

NCEER-89-0007 "Liquefaction Hazards and Their Effects on Buried Pipelines," by T.D. O'Rourke and P.A. Lane, 2/1/89, (PB89-218481).

NCEER-89-0008 "Fundamentals of System Identification in Structural Dynamics," by H. Imai, C-B. Yun, O. Maruyama and M. Shinozuka, 1/26/89, (PB89-207211).

NCEER-89-0009 "Effects of the 1985 Michoacan Earthquake on Water Systems and Other Buried Lifelines in Mexico," by A.G. Ayala and M.J. O'Rourke, 3/8/89, (PB89-207229).

NCEER-89-R010 "NCEER Bibliography of Earthquake Education Materials," by K.E.K. Ross, Second Revision, 9/1/89, (PB90-125352).

NCEER-89-0011 "Inelastic Three-Dimensional Response Analysis of Reinforced Concrete Building Structures (IDARC-3D), Part I - Modeling," by S.K. Kunnath and A.M. Reinhorn, 4/17/89, (PB90-114612).

NCEER-89-0012 "Recommended Modifications to ATC-14," by C.D. Poland and J.O. Malley, 4/12/89, (PB90-108648).

NCEER-89-0013 "Repair and Strengthening of Beam-to-Column Connections Subjected to Earthquake Loading," by M. Corazao and A.J. Durrani, 2/28/89, (PB90-109885).

NCEER-89-0014 "Program EXKAL2 for Identification of Structural Dynamic Systems," by O. Maruyama, C-B. Yun, M. Hoshiya and M. Shinozuka, 5/19/89, (PB90-109877).

NCEER-89-0015 "Response of Frames With Bolted Semi-Rigid Connections, Part I - Experimental Study and Analytical Predictions," by P.J. DiCorso, A.M. Reinhorn, J.R. Dickerson, J.B. Radziminski and W.L. Harper, 6/1/89, to be published.

NCEER-89-0016 "ARMA Monte Carlo Simulation in Probabilistic Structural Analysis," by P.D. Spanos and M.P. Mignolet, 7/10/89, (PB90-109893).

NCEER-89-P017 "Preliminary Proceedings from the Conference on Disaster Preparedness - The Place of Earthquake Education in Our Schools," Edited by K.E.K. Ross, 6/23/89, (PB90-108606).

NCEER-89-0017 "Proceedings from the Conference on Disaster Preparedness - The Place of Earthquake Education in Our Schools," Edited by K.E.K. Ross, 12/31/89, (PB90-207895). This report is available only through NTIS (see address given above).

NCEER-89-0018 "Multidimensional Models of Hysteretic Material Behavior for Vibration Analysis of Shape Memory Energy Absorbing Devices, by E.J. Graesser and F.A. Cozzarelli, 6/7/89, (PB90-164146).

NCEER-89-0019 "Nonlinear Dynamic Analysis of Three-Dimensional Base Isolated Structures (3D-BASIS)," by S. Nagarajaiah, A.M. Reinhorn and M.C. Constantinou, 8/3/89, (PB90-161936). This report is available only through NTIS (see address given above).

NCEER-89-0020 "Structural Control Considering Time-Rate of Control Forces and Control Rate Constraints," by F.Y. Cheng and C.P. Pantelides, 8/3/89, (PB90-120445).

NCEER-89-0021 "Subsurface Conditions of Memphis and Shelby County," by K.W. Ng, T-S. Chang and H-H.M. Hwang, 7/26/89, (PB90-120437).

NCEER-89-0022 "Seismic Wave Propagation Effects on Straight Jointed Buried Pipelines," by K. Elhmadi and M.J. O'Rourke, 8/24/89, (PB90-162322).

NCEER-89-0023 "Workshop on Serviceability Analysis of Water Delivery Systems," edited by M. Grigoriu, 3/6/89, (PB90-127424).

NCEER-89-0024 "Shaking Table Study of a 1/5 Scale Steel Frame Composed of Tapered Members," by K.C. Chang, J.S. Hwang and G.C. Lee, 9/18/89, (PB90-160169).

NCEER-89-0025 "DYNA1D: A Computer Program for Nonlinear Seismic Site Response Analysis - Technical Documentation," by Jean H. Prevost, 9/14/89, (PB90-161944). This report is available only through NTIS (see address given above).

NCEER-89-0026 "1:4 Scale Model Studies of Active Tendon Systems and Active Mass Dampers for Aseismic Protection," by A.M. Reinhorn, T.T. Soong, R.C. Lin, Y.P. Yang, Y. Fukao, H. Abe and M. Nakai, 9/15/89, (PB90-173246).

NCEER-89-0027 "Scattering of Waves by Inclusions in a Nonhomogeneous Elastic Half Space Solved by Boundary Element Methods," by P.K. Hadley, A. Askar and A.S. Cakmak, 6/15/89, (PB90-145699).

NCEER-89-0028 "Statistical Evaluation of Deflection Amplification Factors for Reinforced Concrete Structures," by H.H.M. Hwang, J-W. Jaw and A.L. Ch'ng, 8/31/89, (PB90-164633).

NCEER-89-0029 "Bedrock Accelerations in Memphis Area Due to Large New Madrid Earthquakes," by H.H.M. Hwang, C.H.S. Chen and G. Yu, 11/7/89, (PB90-162330).

NCEER-89-0030 "Seismic Behavior and Response Sensitivity of Secondary Structural Systems," by Y.Q. Chen and T.T. Soong, 10/23/89, (PB90-164658).

NCEER-89-0031 "Random Vibration and Reliability Analysis of Primary-Secondary Structural Systems," by Y. Ibrahim, M. Grigoriu and T.T. Soong, 11/10/89, (PB90-161951).

NCEER-89-0032 "Proceedings from the Second U.S. - Japan Workshop on Liquefaction, Large Ground Deformation and Their Effects on Lifelines, September 26-29, 1989," Edited by T.D. O'Rourke and M. Hamada, 12/1/89, (PB90-209388).

NCEER-89-0033 "Deterministic Model for Seismic Damage Evaluation of Reinforced Concrete Structures," by J.M. Bracci, A.M. Reinhorn, J.B. Mander and S.K. Kunnath, 9/27/89.

NCEER-89-0034 "On the Relation Between Local and Global Damage Indices," by E. DiPasquale and A.S. Cakmak, 8/15/89, (PB90-173865).

NCEER-89-0035 "Cyclic Undrained Behavior of Nonplastic and Low Plasticity Silts," by A.J. Walker and H.E. Stewart, 7/26/89, (PB90-183518).

NCEER-89-0036 "Liquefaction Potential of Surficial Deposits in the City of Buffalo, New York," by M. Budhu, R. Giese and L. Baumgrass, 1/17/89, (PB90-208455).

NCEER-89-0037 "A Deterministic Assessment of Effects of Ground Motion Incoherence," by A.S. Veletsos and Y. Tang, 7/15/89, (PB90-164294).

NCEER-89-0038 "Workshop on Ground Motion Parameters for Seismic Hazard Mapping," July 17-18, 1989, edited by R.V. Whitman, 12/1/89, (PB90-173923).

NCEER-89-0039 "Seismic Effects on Elevated Transit Lines of the New York City Transit Authority," by C.J. Costantino, C.A. Miller and E. Heymsfield, 12/26/89, (PB90-207887).

NCEER-89-0040 "Centrifugal Modeling of Dynamic Soil-Structure Interaction," by K. Weissman, Supervised by J.H. Prevost, 5/10/89, (PB90-207879).

NCEER-89-0041 "Linearized Identification of Buildings With Cores for Seismic Vulnerability Assessment," by I-K. Ho and A.E. Aktan, 11/1/89, (PB90-251943).

NCEER-90-0001 "Geotechnical and Lifeline Aspects of the October 17, 1989 Loma Prieta Earthquake in San Francisco," by T.D. O'Rourke, H.E. Stewart, F.T. Blackburn and T.S. Dickerman, 1/90, (PB90-208596).

NCEER-90-0002 "Nonnormal Secondary Response Due to Yielding in a Primary Structure," by D.C.K. Chen and L.D. Lutes, 2/28/90, (PB90-251976).

NCEER-90-0003 "Earthquake Education Materials for Grades K-12," by K.E.K. Ross, 4/16/90, (PB91-251984).

NCEER-90-0004 "Catalog of Strong Motion Stations in Eastern North America," by R.W. Busby, 4/3/90, (PB90-251984).

NCEER-90-0005 "NCEER Strong-Motion Data Base: A User Manual for the GeoBase Release (Version 1.0 for the Sun3)," by P. Friberg and K. Jacob, 3/31/90 (PB90-258062).

NCEER-90-0006 "Seismic Hazard Along a Crude Oil Pipeline in the Event of an 1811-1812 Type New Madrid Earthquake," by H.H.M. Hwang and C-H.S. Chen, 4/16/90(PB90-258054).

NCEER-90-0007 "Site-Specific Response Spectra for Memphis Sheahan Pumping Station," by H.H.M. Hwang and C.S. Lee, 5/15/90, (PB91-108811).

NCEER-90-0008 "Pilot Study on Seismic Vulnerability of Crude Oil Transmission Systems," by T. Ariman, R. Dobry, M. Grigoriu, F. Kozin, M. O'Rourke, T. O'Rourke and M. Shinozuka, 5/25/90, (PB91-108837).

NCEER-90-0009 "A Program to Generate Site Dependent Time Histories: EQGEN," by G.W. Ellis, M. Srinivasan and A.S. Cakmak, 1/30/90, (PB91-108829).

NCEER-90-0010 "Active Isolation for Seismic Protection of Operating Rooms," by M.E. Talbott, Supervised by M. Shinozuka, 6/8/9, (PB91-110205).

NCEER-90-0011 "Program LINEARID for Identification of Linear Structural Dynamic Systems," by C-B. Yun and M. Shinozuka, 6/25/90, (PB91-110312).

NCEER-90-0012 "Two-Dimensional Two-Phase Elasto-Plastic Seismic Response of Earth Dams," by A.N. Yiagos, Supervised by J.H. Prevost, 6/20/90, (PB91-110197).

NCEER-90-0013 "Secondary Systems in Base-Isolated Structures: Experimental Investigation, Stochastic Response and Stochastic Sensitivity," by G.D. Manolis, G. Juhn, M.C. Constantinou and A.M. Reinhorn, 7/1/90, (PB91-110320).

NCEER-90-0014 "Seismic Behavior of Lightly-Reinforced Concrete Column and Beam-Column Joint Details," by S.P. Pessiki, C.H. Conley, P. Gergely and R.N. White, 8/22/90, (PB91-108795).

NCEER-90-0015 "Two Hybrid Control Systems for Building Structures Under Strong Earthquakes," by J.N. Yang and A. Danielians, 6/29/90, (PB91-125393).

NCEER-90-0016 "Instantaneous Optimal Control with Acceleration and Velocity Feedback," by J.N. Yang and Z. Li, 6/29/90, (PB91-125401).

NCEER-90-0017 "Reconnaissance Report on the Northern Iran Earthquake of June 21, 1990," by M. Mehrain, 10/4/90, (PB91-125377).

NCEER-90-0018 "Evaluation of Liquefaction Potential in Memphis and Shelby County," by T.S. Chang, P.S. Tang, C.S. Lee and H. Hwang, 8/10/90, (PB91-125427).

NCEER-90-0019 "Experimental and Analytical Study of a Combined Sliding Disc Bearing and Helical Steel Spring Isolation System," by M.C. Constantinou, A.S. Mokha and A.M. Reinhorn, 10/4/90, (PB91-125385).

NCEER-90-0020 "Experimental Study and Analytical Prediction of Earthquake Response of a Sliding Isolation System with a Spherical Surface," by A.S. Mokha, M.C. Constantinou and A.M. Reinhorn, 10/11/90, (PB91-125419).

NCEER-90-0021 "Dynamic Interaction Factors for Floating Pile Groups," by G. Gazetas, K. Fan, A. Kaynia and E. Kausel, 9/10/90, (PB91-170381).

NCEER-90-0022 "Evaluation of Seismic Damage Indices for Reinforced Concrete Structures," by S. Rodriguez-Gomez and A.S. Cakmak, 9/30/90, PB91-171322).

NCEER-90-0023 "Study of Site Response at a Selected Memphis Site," by H. Desai, S. Ahmad, E.S. Gazetas and M.R. Oh, 10/11/90, (PB91-196857).

NCEER-90-0024 "A User's Guide to Strongmo: Version 1.0 of NCEER's Strong-Motion Data Access Tool for PCs and Terminals," by P.A. Friberg and C.A.T. Susch, 11/15/90, (PB91-171272).

NCEER-90-0025 "A Three-Dimensional Analytical Study of Spatial Variability of Seismic Ground Motions," by L-L. Hong and A.H.-S. Ang, 10/30/90, (PB91-170399).

NCEER-90-0026 "MUMOID User's Guide - A Program for the Identification of Modal Parameters," by S. Rodri guez-Go mez and E. DiPasquale, 9/30/90, (PB91-171298).

NCEER-90-0027 "SARCF-II User's Guide - Seismic Analysis of Reinforced Concrete Frames," by S. Rodri guez-Go mez, Y.S. Chung and C. Meyer, 9/30/90, (PB91-171280).

NCEER-90-0028 "Viscous Dampers: Testing, Modeling and Application in Vibration and Seismic Isolation," by N. Makris and M.C. Constantinou, 12/20/90 (PB91-190561).

NCEER-90-0029 "Soil Effects on Earthquake Ground Motions in the Memphis Area," by H. Hwang, C.S. Lee, K.W. Ng and T.S. Chang, 8/2/90, (PB91-190751).

NCEER-91-0001 "Proceedings from the Third Japan-U.S. Workshop on Earthquake Resistant Design of Lifeline Facilities and Countermeasures for Soil Liquefaction, December 17-19, 1990," edited by T.D. O'Rourke and M. Hamada, 2/1/91, (PB91-179259).

NCEER-91-0002 "Physical Space Solutions of Non-Proportionally Damped Systems," by M. Tong, Z. Liang and G.C. Lee, 1/15/91, (PB91-179242).

NCEER-91-0003 "Seismic Response of Single Piles and Pile Groups," by K. Fan and G. Gazetas, 1/10/91, (PB92-174994).

NCEER-91-0004 "Damping of Structures: Part 1 - Theory of Complex Damping," by Z. Liang and G. Lee, 10/10/91, (PB92-197235).

NCEER-91-0005 "3D-BASIS - Nonlinear Dynamic Analysis of Three Dimensional Base Isolated Structures: Part II," by S. Nagarajaiah, A.M. Reinhorn and M.C. Constantinou, 2/28/91, (PB91-190553).

NCEER-91-0006 "A Multidimensional Hysteretic Model for Plasticity Deforming Metals in Energy Absorbing Devices," by E.J. Graesser and F.A. Cozzarelli, 4/9/91, (PB92-108364).

NCEER-91-0007 "A Framework for Customizable Knowledge-Based Expert Systems with an Application to a KBES for Evaluating the Seismic Resistance of Existing Buildings," by E.G. Ibarra-Anaya and S.J. Fenves, 4/9/91, (PB91-210930).

NCEER-91-0008 "Nonlinear Analysis of Steel Frames with Semi-Rigid Connections Using the Capacity Spectrum Method," by G.G. Deierlein, S-H. Hsieh, Y-J. Shen and J.F. Abel, 7/2/91, (PB92-113828).

NCEER-91-0009 "Earthquake Education Materials for Grades K-12," by K.E.K. Ross, 4/30/91, (PB91-212142).

NCEER-91-0010 "Phase Wave Velocities and Displacement Phase Differences in a Harmonically Oscillating Pile," by N. Makris and G. Gazetas, 7/8/91, (PB92-108356).

NCEER-91-0011 "Dynamic Characteristics of a Full-Size Five-Story Steel Structure and a 2/5 Scale Model," by K.C. Chang, G.C. Yao, G.C. Lee, D.S. Hao and Y.C. Yeh," 7/2/91, (PB93-116648).

NCEER-91-0012 "Seismic Response of a 2/5 Scale Steel Structure with Added Viscoelastic Dampers," by K.C. Chang, T.T. Soong, S-T. Oh and M.L. Lai, 5/17/91, (PB92-110816).

NCEER-91-0013 "Earthquake Response of Retaining Walls; Full-Scale Testing and Computational Modeling," by S. Alampalli and A-W.M. Elgamal, 6/20/91, to be published.

NCEER-91-0014 "3D-BASIS-M: Nonlinear Dynamic Analysis of Multiple Building Base Isolated Structures," by P.C. Tsopelas, S. Nagarajaiah, M.C. Constantinou and A.M. Reinhorn, 5/28/91, (PB92-113885).

NCEER-91-0015 "Evaluation of SEAOC Design Requirements for Sliding Isolated Structures," by D. Theodossiou and M.C. Constantinou, 6/10/91, (PB92-114602).

NCEER-91-0016 "Closed-Loop Modal Testing of a 27-Story Reinforced Concrete Flat Plate-Core Building," by H.R. Somaprasad, T. Toksoy, H. Yoshiyuki and A.E. Aktan, 7/15/91, (PB92-129980).

NCEER-91-0017 "Shake Table Test of a 1/6 Scale Two-Story Lightly Reinforced Concrete Building," by A.G. El-Attar, R.N. White and P. Gergely, 2/28/91, (PB92-222447).

NCEER-91-0018 "Shake Table Test of a 1/8 Scale Three-Story Lightly Reinforced Concrete Building," by A.G. El-Attar, R.N. White and P. Gergely, 2/28/91, (PB93-116630).

NCEER-91-0019 "Transfer Functions for Rigid Rectangular Foundations," by A.S. Veletsos, A.M. Prasad and W.H. Wu, 7/31/91.

NCEER-91-0020 "Hybrid Control of Seismic-Excited Nonlinear and Inelastic Structural Systems," by J.N. Yang, Z. Li and A. Danielians, 8/1/91, (PB92-143171).

NCEER-91-0021 "The NCEER-91 Earthquake Catalog: Improved Intensity-Based Magnitudes and Recurrence Relations for U.S. Earthquakes East of New Madrid," by L. Seeber and J.G. Armbruster, 8/28/91, (PB92-176742).

NCEER-91-0022 "Proceedings from the Implementation of Earthquake Planning and Education in Schools: The Need for Change - The Roles of the Changemakers," by K.E.K. Ross and F. Winslow, 7/23/91, (PB92-129998).

NCEER-91-0023 "A Study of Reliability-Based Criteria for Seismic Design of Reinforced Concrete Frame Buildings," by H.H.M. Hwang and H-M. Hsu, 8/10/91, (PB92-140235).

NCEER-91-0024 "Experimental Verification of a Number of Structural System Identification Algorithms," by R.G. Ghanem, H. Gavin and M. Shinozuka, 9/18/91, (PB92-176577).

NCEER-91-0025 "Probabilistic Evaluation of Liquefaction Potential," by H.H.M. Hwang and C.S. Lee," 11/25/91, (PB92-143429).

NCEER-91-0026 "Instantaneous Optimal Control for Linear, Nonlinear and Hysteretic Structures - Stable Controllers," by J.N. Yang and Z. Li, 11/15/91, (PB92-163807).

NCEER-91-0027 "Experimental and Theoretical Study of a Sliding Isolation System for Bridges," by M.C. Constantinou, A. Kartoum, A.M. Reinhorn and P. Bradford, 11/15/91, (PB92-176973).

NCEER-92-0001 "Case Studies of Liquefaction and Lifeline Performance During Past Earthquakes, Volume 1: Japanese Case Studies," Edited by M. Hamada and T. O'Rourke, 2/17/92, (PB92-197243).

NCEER-92-0002 "Case Studies of Liquefaction and Lifeline Performance During Past Earthquakes, Volume 2: United States Case Studies," Edited by T. O'Rourke and M. Hamada, 2/17/92, (PB92-197250).

NCEER-92-0003 "Issues in Earthquake Education," Edited by K. Ross, 2/3/92, (PB92-222389).

NCEER-92-0004 "Proceedings from the First U.S. - Japan Workshop on Earthquake Protective Systems for Bridges," Edited by I.G. Buckle, 2/4/92, (PB94-142239, A99, MF-A06).

NCEER-92-0005 "Seismic Ground Motion from a Haskell-Type Source in a Multiple-Layered Half-Space," A.P. Theoharis, G. Deodatis and M. Shinozuka, 1/2/92, to be published.

NCEER-92-0006 "Proceedings from the Site Effects Workshop," Edited by R. Whitman, 2/29/92, (PB92-197201).

NCEER-92-0007 "Engineering Evaluation of Permanent Ground Deformations Due to Seismically-Induced Liquefaction," by M.H. Baziar, R. Dobry and A-W.M. Elgamal, 3/24/92, (PB92-222421).

NCEER-92-0008 "A Procedure for the Seismic Evaluation of Buildings in the Central and Eastern United States," by C.D. Poland and J.O. Malley, 4/2/92, (PB92-222439).

NCEER-92-0009 "Experimental and Analytical Study of a Hybrid Isolation System Using Friction Controllable Sliding Bearings," by M.Q. Feng, S. Fujii and M. Shinozuka, 5/15/92, (PB93-150282).

NCEER-92-0010 "Seismic Resistance of Slab-Column Connections in Existing Non-Ductile Flat-Plate Buildings," by A.J. Durrani and Y. Du, 5/18/92.

NCEER-92-0011 "The Hysteretic and Dynamic Behavior of Brick Masonry Walls Upgraded by Ferrocement Coatings Under Cyclic Loading and Strong Simulated Ground Motion," by H. Lee and S.P. Prawel, 5/11/92, to be published.

NCEER-92-0012 "Study of Wire Rope Systems for Seismic Protection of Equipment in Buildings," by G.F. Demetriades, M.C. Constantinou and A.M. Reinhorn, 5/20/92.

NCEER-92-0013 "Shape Memory Structural Dampers: Material Properties, Design and Seismic Testing," by P.R. Witting and F.A. Cozzarelli, 5/26/92.

NCEER-92-0014 "Longitudinal Permanent Ground Deformation Effects on Buried Continuous Pipelines," by M.J. O'Rourke, and C. Nordberg, 6/15/92.

NCEER-92-0015 "A Simulation Method for Stationary Gaussian Random Functions Based on the Sampling Theorem," by M. Grigoriu and S. Balopoulou, 6/11/92, (PB93-127496).

NCEER-92-0016 "Gravity-Load-Designed Reinforced Concrete Buildings: Seismic Evaluation of Existing Construction and Detailing Strategies for Improved Seismic Resistance," by G.W. Hoffmann, S.K. Kunnath, A.M. Reinhorn and J.B. Mander, 7/15/92, (PB94-142007, A08, MF-A02).

NCEER-92-0017 "Observations on Water System and Pipeline Performance in the Limón Area of Costa Rica Due to the April 22, 1991 Earthquake," by M. O'Rourke and D. Ballantyne, 6/30/92, (PB93-126811).

NCEER-92-0018 "Fourth Edition of Earthquake Education Materials for Grades K-12," Edited by K.E.K. Ross, 8/10/92.

NCEER-92-0019 "Proceedings from the Fourth Japan-U.S. Workshop on Earthquake Resistant Design of Lifeline Facilities and Countermeasures for Soil Liquefaction," Edited by M. Hamada and T.D. O'Rourke, 8/12/92, (PB93-163939).

NCEER-92-0020 "Active Bracing System: A Full Scale Implementation of Active Control," by A.M. Reinhorn, T.T. Soong, R.C. Lin, M.A. Riley, Y.P. Wang, S. Aizawa and M. Higashino, 8/14/92, (PB93-127512).

NCEER-92-0021 "Empirical Analysis of Horizontal Ground Displacement Generated by Liquefaction-Induced Lateral Spreads," by S.F. Bartlett and T.L. Youd, 8/17/92, (PB93-188241).

NCEER-92-0022 "IDARC Version 3.0: Inelastic Damage Analysis of Reinforced Concrete Structures," by S.K. Kunnath, A.M. Reinhorn and R.F. Lobo, 8/31/92, (PB93-227502, A07, MF-A02).

NCEER-92-0023 "A Semi-Empirical Analysis of Strong-Motion Peaks in Terms of Seismic Source, Propagation Path and Local Site Conditions, by M. Kamiyama, M.J. O'Rourke and R. Flores-Berrones, 9/9/92, (PB93-150266).

NCEER-92-0024 "Seismic Behavior of Reinforced Concrete Frame Structures with Nonductile Details, Part I: Summary of Experimental Findings of Full Scale Beam-Column Joint Tests," by A. Beres, R.N. White and P. Gergely, 9/30/92, (PB93-227783, A05, MF-A01).

NCEER-92-0025 "Experimental Results of Repaired and Retrofitted Beam-Column Joint Tests in Lightly Reinforced Concrete Frame Buildings," by A. Beres, S. El-Borgi, R.N. White and P. Gergely, 10/29/92, (PB93-227791, A05, MF-A01).

NCEER-92-0026 "A Generalization of Optimal Control Theory: Linear and Nonlinear Structures," by J.N. Yang, Z. Li and S. Vongchavalitkul, 11/2/92, (PB93-188621).

NCEER-92-0027 "Seismic Resistance of Reinforced Concrete Frame Structures Designed Only for Gravity Loads: Part I - Design and Properties of a One-Third Scale Model Structure," by J.M. Bracci, A.M. Reinhorn and J.B. Mander, 12/1/92, (PB94-104502, A08, MF-A02).

NCEER-92-0028 "Seismic Resistance of Reinforced Concrete Frame Structures Designed Only for Gravity Loads: Part II - Experimental Performance of Subassemblages," by L.E. Aycardi, J.B. Mander and A.M. Reinhorn, 12/1/92, (PB94-104510, A08, MF-A02).

NCEER-92-0029 "Seismic Resistance of Reinforced Concrete Frame Structures Designed Only for Gravity Loads: Part III - Experimental Performance and Analytical Study of a Structural Model," by J.M. Bracci, A.M. Reinhorn and J.B. Mander, 12/1/92, (PB93-227528, A09, MF-A01).

NCEER-92-0030 "Evaluation of Seismic Retrofit of Reinforced Concrete Frame Structures: Part I - Experimental Performance of Retrofitted Subassemblages," by D. Choudhuri, J.B. Mander and A.M. Reinhorn, 12/8/92, (PB93-198307, A07, MF-A02).

NCEER-92-0031 "Evaluation of Seismic Retrofit of Reinforced Concrete Frame Structures: Part II - Experimental Performance and Analytical Study of a Retrofitted Structural Model," by J.M. Bracci, A.M. Reinhorn and J.B. Mander, 12/8/92, (PB93-198315, A09, MF-A03).

NCEER-92-0032 "Experimental and Analytical Investigation of Seismic Response of Structures with Supplemental Fluid Viscous Dampers," by M.C. Constantinou and M.D. Symans, 12/21/92, (PB93-191435).

NCEER-92-0033 "Reconnaissance Report on the Cairo, Egypt Earthquake of October 12, 1992," by M. Khater, 12/23/92, (PB93-188621).

NCEER-92-0034 "Low-Level Dynamic Characteristics of Four Tall Flat-Plate Buildings in New York City," by H. Gavin, S. Yuan, J. Grossman, E. Pekelis and K. Jacob, 12/28/92, (PB93-188217).

NCEER-93-0001 "An Experimental Study on the Seismic Performance of Brick-Infilled Steel Frames With and Without Retrofit," by J.B. Mander, B. Nair, K. Wojtkowski and J. Ma, 1/29/93, (PB93-227510, A07, MF-A02).

NCEER-93-0002 "Social Accounting for Disaster Preparedness and Recovery Planning," by S. Cole, E. Pantoja and V. Razak, 2/22/93, to be published.

NCEER-93-0003 "Assessment of 1991 NEHRP Provisions for Nonstructural Components and Recommended Revisions," by T.T. Soong, G. Chen, Z. Wu, R-H. Zhang and M. Grigoriu, 3/1/93, (PB93-188639).

NCEER-93-0004 "Evaluation of Static and Response Spectrum Analysis Procedures of SEAOC/UBC for Seismic Isolated Structures," by C.W. Winters and M.C. Constantinou, 3/23/93, (PB93-198299).

NCEER-93-0005 "Earthquakes in the Northeast - Are We Ignoring the Hazard? A Workshop on Earthquake Science and Safety for Educators," edited by K.E.K. Ross, 4/2/93, (PB94-103066, A09, MF-A02).

NCEER-93-0006 "Inelastic Response of Reinforced Concrete Structures with Viscoelastic Braces," by R.F. Lobo, J.M. Bracci, K.L. Shen, A.M. Reinhorn and T.T. Soong, 4/5/93, (PB93-227486, A05, MF-A02).

NCEER-93-0007 "Seismic Testing of Installation Methods for Computers and Data Processing Equipment," by K. Kosar, T.T. Soong, K.L. Shen, J.A. HoLung and Y.K. Lin, 4/12/93, (PB93-198299).

NCEER-93-0008 "Retrofit of Reinforced Concrete Frames Using Added Dampers," by A. Reinhorn, M. Constantinou and C. Li, to be published.

NCEER-93-0009 "Seismic Behavior and Design Guidelines for Steel Frame Structures with Added Viscoelastic Dampers," by K.C. Chang, M.L. Lai, T.T. Soong, D.S. Hao and Y.C. Yeh, 5/1/93, (PB94-141959, A07, MF-A02).

NCEER-93-0010 "Seismic Performance of Shear-Critical Reinforced Concrete Bridge Piers," by J.B. Mander, S.M. Waheed, M.T.A. Chaudhary and S.S. Chen, 5/12/93, (PB93-227494, A08, MF-A02).

NCEER-93-0011 "3D-BASIS-TABS: Computer Program for Nonlinear Dynamic Analysis of Three Dimensional Base Isolated Structures," by S. Nagarajaiah, C. Li, A.M. Reinhorn and M.C. Constantinou, 8/2/93, (PB94-141819, A09, MF-A02).

NCEER-93-0012 "Effects of Hydrocarbon Spills from an Oil Pipeline Break on Ground Water," by O.J. Helweg and H.H.M. Hwang, 8/3/93, (PB94-141942, A06, MF-A02).

NCEER-93-0013 "Simplified Procedures for Seismic Design of Nonstructural Components and Assessment of Current Code Provisions," by M.P. Singh, L.E. Suarez, E.E. Matheu and G.O. Maldonado, 8/4/93, (PB94-141827, A09, MF-A02).

NCEER-93-0014 "An Energy Approach to Seismic Analysis and Design of Secondary Systems," by G. Chen and T.T. Soong, 8/6/93, (PB94-142767, A11, MF-A03).

NCEER-93-0015 "Proceedings from School Sites: Becoming Prepared for Earthquakes - Commemorating the Third Anniversary of the Loma Prieta Earthquake," Edited by F.E. Winslow and K.E.K. Ross, 8/16/93.

NCEER-93-0016 "Reconnaissance Report of Damage to Historic Monuments in Cairo, Egypt Following the October 12, 1992 Dahshur Earthquake," by D. Sykora, D. Look, G. Croci, E. Karaesmen and E. Karaesmen, 8/19/93, (PB94-142221, A08, MF-A02).

NCEER-93-0017 "The Island of Guam Earthquake of August 8, 1993," by S.W. Swan and S.K. Harris, 9/30/93, (PB94-141843, A04, MF-A01).

NCEER-93-0018 "Engineering Aspects of the October 12, 1992 Egyptian Earthquake," by A.W. Elgamal, M. Amer, K. Adalier and A. Abul-Fadl, 10/7/93, (PB94-141983, A05, MF-A01).

NCEER-93-0019 "Development of an Earthquake Motion Simulator and its Application in Dynamic Centrifuge Testing," by I. Krstelj, Supervised by J.H. Prevost, 10/23/93.

NCEER-93-0020 "NCEER-Taisei Corporation Research Program on Sliding Seismic Isolation Systems for Bridges: Experimental and Analytical Study of a Friction Pendulum System (FPS)," by M.C. Constantinou, P. Tsopelas, Y-S. Kim and S. Okamoto, 11/1/93, (PB94-142775, A08, MF-A02).

NCEER-93-0021 "Finite Element Modeling of Elastomeric Seismic Isolation Bearings," by L.J. Billings, Supervised by R. Shepherd, 11/8/93, to be published.

NCEER-93-0022 "Seismic Vulnerability of Equipment in Critical Facilities: Life-Safety and Operational Consequences," by K. Porter, G.S. Johnson, M.M. Zadeh, C. Scawthorn and S. Eder, 11/24/93.

NCEER-93-0023 "Hokkaido Nansei-oki, Japan Earthquake of July 12, 1993, by P.I. Yanev and C.R. Scawthorn, 12/23/93.

NCEER-94-0001 "Seismic Serviceability of Water Supply Networks with Application to San Francisco Auxiliary Water Supply System," by I. Markov, Supervised by M. Grigoriu and T. O'Rourke, 1/21/94, to be published.

NCEER-94-0002 "NCEER-Taisei Corporation Research Program on Sliding Seismic Isolation Systems for Bridges: Experimental and Analytical Study of Systems Consisting of Sliding Bearings, Rubber Restoring Force Devices and Fluid Dampers," Volumes I and II, by P. Tsopelas, S. Okamoto, M.C. Constantinou, D. Ozaki and S. Fujii, 2/4/94.

NCEER-94-0003 "A Markov Model for Local and Global Damage Indices in Seismic Analysis," by S. Rahman and M. Grigoriu, 2/18/94, to be published.

NCEER-94-0004 "Proceedings from the NCEER Workshop on Seismic Response of Masonry Infills," edited by D.P. Abrams, 3/1/94.

NCEER-94-0005 "The Northridge, California Earthquake of January 17, 1994: General Overview," edited by J.D. Goltz, 3/11/94.

NCEER-94-0006 "Seismic Energy Based Fatigue Damage Analysis of Bridge Columns: Part I - Evaluation of Seismic Capacity," by G.A. Chang and J.B. Mander, 3/14/94, to be published.

NCEER-94-0007 "Seismic Isolation of Multi-Story Frame Structures Using Spherical Sliding Isolation Systems," by T.M. Al-Hussaini, V.A. Zayas and M.C. Constantinou, 3/17/94.